Title

Reaction Development and Mechanistic Elucidation in Nickel Catalysis

Permalink

https://escholarship.org/uc/item/5tg8c0qg

Author

Bradley, Robert Dennis

Publication Date

2024

Peer reviewed|Thesis/dissertation

UNIVERSITY OF CALIFORNIA
RIVERSIDE

Reaction Development and Mechanistic Elucidation in Nickel Catalysis

A Dissertation submitted in partial satisfaction
of the requirements for the degree of

Doctor of Philosophy

in

Chemistry

by

Robert D. Bradley

September 2024

Dissertation Committee:
     Dr. Ana Bahamonde, Chairperson
     Dr. Michael C. Pirrung
     Dr. Kevin Kou

The Dissertation of Robert D. Bradley is approved:

_____

_____

_____

Committee Chairperson

University of California, Riverside

jokes were getting stale. To Oscar Hung, thank you for being a good friend and for reminding me that we should thank Taiwan for boba tea.

To all of the newer graduate students—Yvette, Harsh, and RJ—thank you for making the Bahamonde lab a positive and fun environment to work in. I would also like to thank our current and former undergraduate student researchers for supporting my projects and for boosting our morale with their youthful positivity. Thank you Jessalyn, Angie, Madison, Nick, both Pauls, Alfredo, and Eyad. I would also like to thank my former coworkers Jason Hibbard and Kyle Arriola for their camaraderie when our group was still very small.

I am grateful for friends from a variety of research groups on the fourth floor of Chemical Sciences that have made it a great place to do research. Thank you for all the excellent lunchtime conversations, the happy hours, and the early morning surf sessions. A special thanks to the Harman and Lavallo groups for going out of their way to help fix broken vacuum pumps and troubleshoot glovebox errors. I am also grateful for assistance from the Kou lab students whenever I had a question regarding synthesis.

A variety of faculty members were also key to the success of my research and my development as a scientist. I am thankful to Dr. Pirrung and Dr. Kou for organizing weekly problem sessions and for teaching me how to think like an organic chemist. I am also thankful to Veronica Carta and Lingchao Zhu for their expertise and assistance with X-ray crystallography, NMR, and EPR experiments.

None of this would have been possible without the unconditional support of my fiancée, Sara Newstein. Despite the failures, uncertainty, and long hours of research, Sara was invariably a source of positivity. Thank you for always brightening my day and for forcing me to do things that are not science-related. The challenges we have faced together over the years have only made our love stronger. Lastly, to my parents and to all of my east coast family and friends, thank you for your continued support from 3,000 miles away and for making every trip home something I look forward to.

List of publications

The text of this dissertation is in part a reprint of the material as they appear in the following publications:

Chapter 2: Bradley, R. D. and Bahamonde, A. *Org. Lett.* **2022,** 24 *(39)*, 7134-7139.

Chapter 3: Bradley, R. D., McManus, B. D., Yam, Y. G., Carta, V., Bahamonde, A. *Angew. Chem. Int. Ed.* **2023,** 62 *(43),* e202310753.

Chapter 4: unpublished work, in collaboration with Nathan Coddington and Madison Loper.

ABSTRACT OF THE DISSERTATION

Reaction Development and Mechanistic Elucidation in Nickel Catalysis

by

Robert D. Bradley

Doctor of Philosophy, Graduate Program in Chemistry
University of California, Riverside, September 2024
Dr. Ana Bahamonde, Chairperson

This thesis highlights the versatility of nickel as a transition metal that enables the activation of relatively inert chemical bonds and offers lower energy pathways to challenging bond formations. In this work, reaction development and mechanistic inquiry inform one another, enhancing our understanding of nickel catalysis.

Despite major advancements in C-heteroatom cross-coupling enabled by Ni-photoredox catalysis, the mechanisms of this form of catalysis are not well understood and are highly debated. Although mild Ni-photoredox C-N cross-coupling had been reported for strong *N*-nucleophiles like alkylamines, such a reaction involving weak *N*-nucleophiles such as amides had not been reported. This work describes the development of an unprecedented Ni-photoredox-catalyzed amide arylation reaction that proceeds under mild conditions. These mild

conditions enable access to a broad scope including base-sensitive functional groups and excellent preservation of epimerizable stereocenters.

We hypothesized that this amide arylation reaction might proceed via an alternative mechanism to the self-sustaining Ni(I/III) cycle that is usually reported for Ni-photoredox C-N coupling. This is because our reaction utilizes a redox-inactive base and weak *N*-nucleophiles, whereas the prior published methods in this arena couple strong *N*-nucleophiles and require redox-active bases as electron shuttles. A combined approach involving stoichiometric experiments with synthesized Ni complexes and the measurement of kinetic profiles of the catalytic reaction led us to propose an unusual Ni(0/II/III) cycle, which has a profound consequence for the rate-limiting step and the overall reaction kinetics. Kinetic studies probing the effect of nickel precatalysts of various oxidation states revealed a marked induction period with Ni(II) precatalysts, providing insight into the photochemical process that generates the active Ni(0) species.

This thesis will also discuss the optimization and mechanistic investigation of a dual nickel/Lewis acid catalyst system that is capable of breaking carbon-carbon bonds in cyclopropanes and benzonitriles in a catalytic cyanide transfer reaction. The mechanism by which the catalyst is able to activate nitriles as relatively nontoxic cyanide surrogates is explored. Extensive efforts towards the design of an optimal ligand for regioselective ring-opening cyanation utilizing the modular phosphinooxazoline (PHOX) platform are described herein. Ligand

optimization, mechanistic investigation, and determination of scope for this chemistry are ongoing.

TABLE OF CONTENTS

Chapter 1: Nickel catalysis as a versatile addition to the synthetic toolkit

Chapter 2: Nickel-photoredox catalysis enables amide *N*-arylation under mild conditions

Chapter 3: Mechanistic investigation of the catalytic mechanism of Ni-photoredox amide *N*-arylation

Chapter 4: Nickel-catalyzed activation of benzonitriles as low-toxicity cyanide surrogates for cyclopropyl ketone ring-opening cyanation

List of Figures

Chapter 1

Chapter 2

Chapter 3

Chapter 4

List of Schemes

List of Tables

Chapter 1

Chapter 2

Chapter 3

Chapter 4

Chapter 1: Nickel catalysis as a versatile addition to the synthetic toolkit

1.1   Nickel: not just a palladium surrogate

Palladium (Pd) is a privileged transition metal in catalysis and is especially valued for its ability to catalyze a variety of cross-coupling reactions. Pd-catalyzed cross-coupling reactions are among the most commonly used reactions in synthetic chemistry, providing robust methodologies for the formation of C-C and C-heteroatom bonds[1–5]. Nickel (Ni), a first-row transition metal, is situated directly above Pd in group 10 of the periodic table and is often touted as a cheaper, Earth-abundant replacement for Pd because both metals display similar cross-coupling reactivity[1]. Ni is able to catalyze a variety of classic Pd-catalyzed cross-coupling reactions including Suzuki[6–23], Buchwald-Hartwig[24–27], Heck[28–33], Kumada[34–40], Negishi[41,42], Hiyama[43–45], Stille[46–49], and Sonogashira[50–54] reactions. Although this Pd-like behavior is an attractive feature of Ni catalysis, recent advances in the field have revealed an abundance of catalytic transformations that are accessible to Ni catalysis but difficult or inaccessible with Pd catalysis. Some examples of these unique Ni-catalyzed transformations are $C(sp^3)$ cross-coupling[1,55,56], cross-electrophile coupling[57], photoredox catalysis[58], electrochemically-enabled catalysis[27,59], difficult bond activations in cross-coupling[1,9,55,60–64], ring-opening cross-coupling[1,55], and intermolecular alkene difunctionalization reactions[65,66]. This is not an exhaustive list of the impressive and diverse chemistry that is accessible

with Ni catalysis. These modes of reactivity are afforded to Ni due to its unique set of fundamental properties[1,55,67–69], which will be discussed in this chapter.

The aim of this thesis is to underscore how Ni catalysis enables access to novel catalytic mechanisms for making and breaking chemical bonds, providing synthetic utility that is complementary to the classic Pd-catalyzed transformations. Despite the widespread adoption of diverse Ni-catalyzed methodologies, there is still much to be uncovered regarding the mechanisms of Ni catalysis, which are more poorly understood and often more complex than the mechanisms of Pd catalysis. Efforts to control and understand Ni-catalyzed reactions are complicated by the diverse reaction pathways accessible to Ni catalysts[1,55]. Advances in our understanding of the behavior of Ni complexes from both stoichiometric and catalytic experiments have proven to be crucial to the development of novel transformations in this field[27,55,67,70–100]. As such, Chapters 2-4 of this thesis will discuss the novel Ni-catalyzed methodologies developed by our group and our efforts to elucidate their mechanisms.

1.2   Comparing the fundamental properties of nickel and palladium

Ni can access a variety of closed- and open-shell electronic configurations[55]. As such, Ni catalytic cycles routinely go through oxidation states of 0, I, II, and III, whereas those of Pd are almost always limited to oxidation states of 0, II, and IV [1] (although rare exceptions involving oxidation states of I and III in Pd do exist[101–105]). Ni can cycle between its various oxidation states through either

1- or 2-electron processes, whereas Pd is almost always limited to 2-electron redox pathways[1] **(Table 1)**. An often invoked explanation for the higher stability of Ni(I) and Ni(III) relative to Pd(I) and Pd(III) is that valence electrons in first-row transition metals have a higher pairing energy than valence electrons in second- and third-row transition metals[106]. The release of this pairing energy provides a thermodynamic incentive for the formation of open-shell species[67]. Pairing energy can also be understood as a consequence of atomic radius: because Ni has a smaller atomic radius than Pd[107], it contains greater electron density near its nucleus, whereas Pd has a more diffuse electron cloud. This causes more repulsion between electrons occupying the same valence orbital in Ni, destabilizing closed-shell species[67].

Table 1. Fundamental properties of Ni and Pd		
	Ni	Pd
atomic number:	28	46
typical oxidation states:	0, I, II, III	0, II, IV
redox behavior:	1- or 2-electron	usually 2-electron
vdW radius:	1.92 Å	2.05 Å
electronegativity (Pauling):	1.91	2.20
oxidative addition:	fast	slow
reductive elimination:	slow	fast
β-hydride elimination:	slow	fast

The ability of Ni to cycle through a variety of oxidation states via either 1- or 2-electron redox pathways provides access to a variety of unique reaction mechanisms. Both Ni and Pd can oxidatively add into electrophiles via a concerted, 2-electron pathway. Additionally, Ni has access to a radical pathway of oxidative addition that involves a Ni(I) intermediate and mesolysis of the electrophile[99,100]. This radical oxidative addition provides an alternative pathway for Ni to engage alkyl halides[11], which have higher kinetic barriers to oxidative addition than the corresponding aryl halides[1]. Ni's access to radical pathways and open-shell configurations also renders it an effective radical trap for carbon-centered radicals[55] **(Figure 1a)**. Ni's ability to trap alkyl radicals and react with alkyl halides is complemented by the relative stability of alkyl ligands on Ni. These Ni-alkyl species are less prone to β-hydride elimination than Pd-alkyl species[55] **(Table 1)**. β-hydride elimination is less kinetically favorable with Ni than with Pd due to a weaker agostic interaction, since Ni is smaller and relatively electropositive[55,107,108]. This enables Ni catalysis to be used in the cross-coupling of alkyl groups with an expansive chemical space of coupling partners[6,10,11,40,41,43,46,47,50,56,57,59,109–122].

Another consequence of the 1-electron chemistry accessible to Ni is the involvement of Ni(III) intermediates in many catalytic cycles. Reductive elimination from open-shell Ni(III) to form C-C and C-heteroatom bonds is known to have a relatively low kinetic barrier, enabling these

Figure 1. Unique reactivity available to Ni

a) radical trapping

$$Ni(0) \ + \ R\cdot \ \longrightarrow \ Ni(I){-}R$$
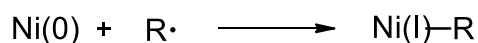
b) challenging bond activations

$$Ni(0) \ + \ C{-}X \ \longrightarrow \ Ni(II){\diagup}^{C}_{X}$$
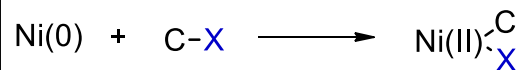
$C = C(sp^2), C(sp^3)$
$X = F, OR, CN, H \text{ (aldehyde)}, NR_2 \text{ (amide)}, etc.$

c) 1-electron redox

$$Ni(n{-}1) \ \underset{}{\overset{+1 \ e^-}{\longleftarrow}} \ Ni(n) \ \overset{-1 \ e^-}{\longrightarrow} \ Ni(n{+}1)$$
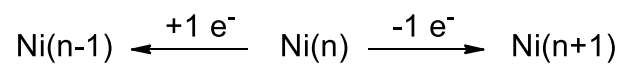
redox pathways: chemical (stoichiometric)
photocatalytic
electrochemically-mediated

bond formations to occur at room temperature[72,73,88,123]. These highly reactive Ni(III) intermediates can be accessed via 1- or 2-electron redox pathways. In contrast, reductive elimination from Ni(II), isoelectronic Cu(III), or Pd(II) often require elevated temperatures to overcome their kinetic barriers to reductive elimination[123,124]. Additionally, Ni(I) catalytic intermediates provide access to a 2-electron redox cycle involving Ni(III)[83,86].

Ni's access to 1-electron redox pathways **(Figure 1c)** has also enabled the emergence of cooperative Ni catalysis. Ni-photoredox catalysis has received a great deal of attention over the past decade due to its ability to enable impressive transformations such as mild C-heteroatom cross-coupling[25,92,123–126], catalytic $C(sp^3)$-H activation[56,116–122], and the cross-coupling of in situ-generated radical species from radical precursor substrates which can be activated by single-

electron reduction or oxidation[47,56,109–115]. This field will be discussed in greater detail in Chapters 2 and 3 of this thesis. Similarly to photoredox catalysis, electrochemistry can be combined with Ni catalysis to leverage the 1-electron redox reactivity of Ni[27,59].

Ni's redox promiscuity is a double-edged sword. Although it opens new avenues of reactivity, it also introduces a variety of catalyst deactivation pathways that one does not usually have to consider when studying Pd-catalyzed reactions **(Figure 2)**. These deactivation pathways can involve any of the oxidation states available to Ni. Due to Ni's ability to engage in 1-electron redox events, catalyst speciation can occur via comproportionation **(Figure 2a)** or disproportionation[27,84,86,90,127,128] **(Figure 2b)**. Ni(0) is also much more prone to catalyst deactivation via oxidation than Pd(0) due to its low reduction potential[69] **(Figure 2c)**, which is problematic since a variety of Ni-catalyzed reactions require Ni(0) sources or Ni(0) active catalysts generated in situ from the

Figure 2. Challenges of Ni catalysis

a) comproportionation

A + B

Ni(I) Ni(II) Ni(III)

A-B

b) disproportionation

A + B

Ni(0)

Ni(I)   Ni(III)

Ni(II)

A-B

c) air sensitivity

$$Ni(0) \xrightarrow[fast]{O_2} Ni(II)$$

d) aggregation

$$L \cdot Ni(0) \xrightarrow{ligand\ dissociation} L + Ni(0)_n$$

e) formation of inactive dimers

$$Ni(I/II)-X \longrightarrow Ni(I/II)\underset{X}{\overset{X}{\diamond}}Ni(I/II)$$

catalytically inactive
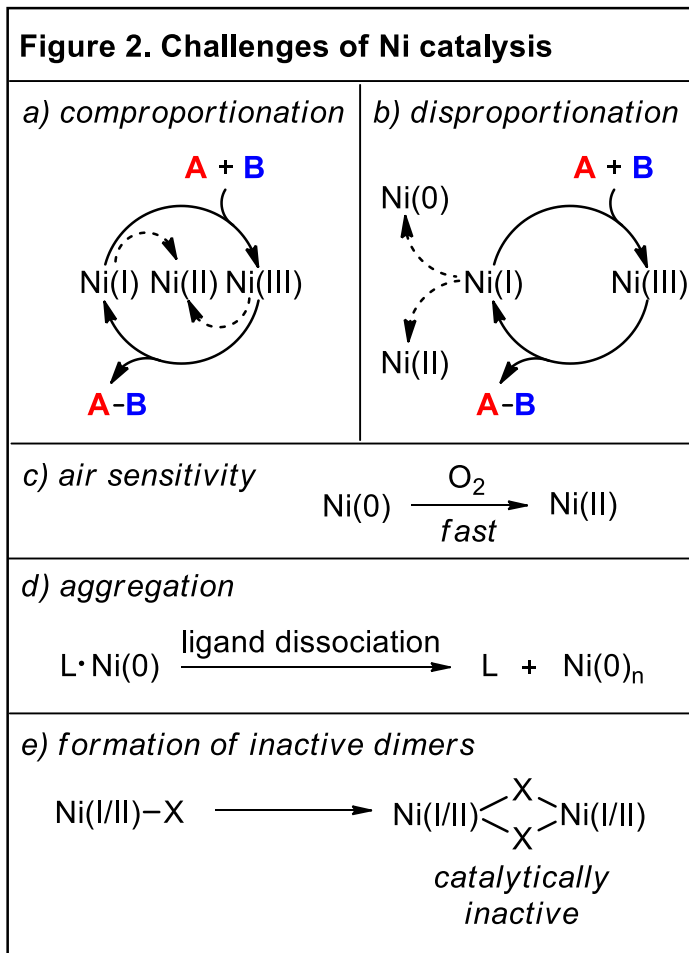
reduction of Ni(II) precatalysts[1]. Ni(0) sources are typically less stable to oxygen than Pd(0) sources and their use is complicated by the need for gloveboxes[129–131]. Aggregation of Ni is a frequently encountered mode of catalyst deactivation and can be observed with Ni(0), Ni(I), and Ni(II) **(Figure 2d-e)**. Ligand dissociation from active Ni(0) complexes can lead to the irreversible precipitation of "nickel black" aggregates[69]. Ni(I) dimers with bridging X-type ligands are remarkably stable[89] and have been proposed as off-cycle species in Ni-catalyzed reactions[84]. Ni-catalyzed Suzuki cross-coupling is complicated by the formation of inactive hydroxo-bridging Ni(II) dimers since hydroxide is used as a base[23]. These dimers are not problematic for Pd-catalyzed Suzuki cross-coupling reactions because Pd is significantly less oxophilic than Ni[23,132,133]. All of the aforementioned factors are disadvantageous to Ni catalysis, leading to the formation of off-cycle species that limit catalytic turnover. The ease of catalyst deactivation in Ni-catalyzed reactions often necessitates relatively high catalyst loadings compared to Pd-catalyzed reactions[69]. These high loadings in Ni-catalyzed reactions can limit the practicality of using ligands that are expensive or synthetically challenging to access, thus negating the economic benefit of using an Earth-abundant metal like Ni for catalysis.

A defining feature of Ni is that it is relatively electropositive compared to Pd and other late transition metals[1,108]. Consequently, Ni also has a lower reduction potential than Pd[55]. These fundamental properties affect the relative abilities of these two transition metals to activate chemical bonds towards oxidative addition

and reductive elimination. Ni(0) is able to engage aryl and alkyl halides in oxidative addition with faster rates than those observed with Pd(0)[55,99] **(Table 1)**. Additionally, low-valent Ni can undergo oxidative addition with these substrates at lower temperatures than are required with Pd[1,6,134], which is useful for cross-coupling thermally sensitive substrates[7]. Ni can oxidatively add into a variety of covalent bonds that are relatively inert such as C-F bonds[9,37,38], C-CN bonds[36,39,61,135], C-H bonds in aldehydes[64,136], C-O bonds in esters and ethers[137–142], C-N bonds in amides[141], and strained rings[42,62,75,143–148] **(Figure 1b)**. Although Ni is better suited for oxidative addition than Pd, reductive elimination from Ni(II) is more difficult than from Pd(II)[1,149] **(Table 1)**. The difficult reductive elimination from Ni can be enabled via access to Ni(III) [73,123,127] or it can be promoted by ligands with finely tuned steric and electronic parameters[26,127].
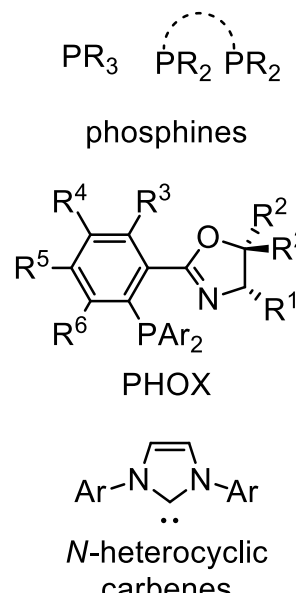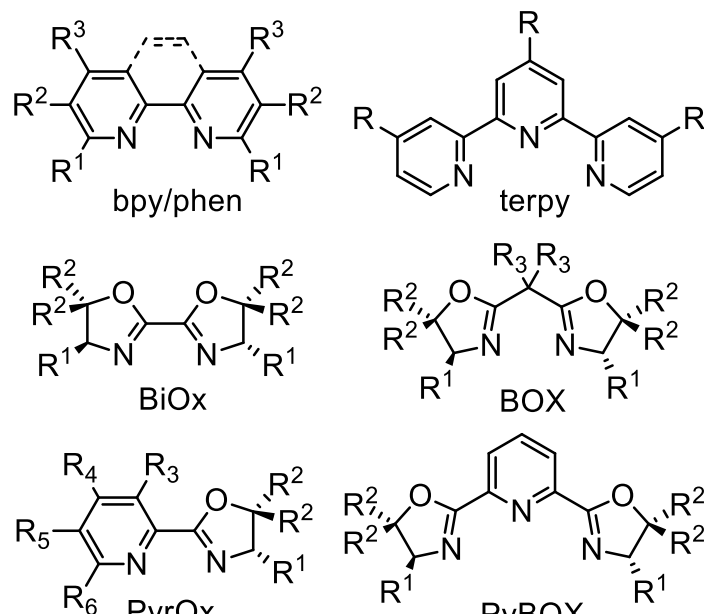
1.3   Comparing ligand effects in nickel and palladium catalysis

Ligand choice is an important consideration in homogeneous transition metal catalysis. Because of Ni's redox promiscuity, a variety of accessible reaction pathways may exist[68,127]. Characteristics like steric parameters and redox potentials can be tuned via minor changes to the structure and electronics of the ligand bound to Ni. Thus, ligand choice has a great influence on which reaction pathways are predominant when multiple pathways are available. This is crucial because some of these feasible reaction pathways may lead to undesired side products or unproductive off-cycle species which must be suppressed in order to

achieve efficient Ni catalysis. The diversity of reaction pathways available to Ni has been exploited in Ni-catalyzed systems that utilize ligand combinations wherein separate Ni-ligand complexes serve separate functions in intertwined catalytic cycles. In this manner, cross-selectivity in cross-electrophile couplings can be achieved in which each Ni-ligand complex selectively activates one of the two coupling partners[59].

In contrast to Ni-catalyzed reactions, Pd-catalyzed reactions often tolerate a variety of ligands with only minor differences in yield and product selectivity since they are not complicated by the same set of limiting factors that are associated with Ni catalysis[68]. Because Pd is typically limited to even-numbered oxidation states, redox-active N-containing ligands like polypyridines are not commonly

Figure 3. Commonly used ligand classes in Ni and Pd catalysis

phosphines

PHOX

N-heterocyclic carbenes

bpy/phen

terpy

BiOx

BOX

PyrOx

PyBOX

electron-rich ligands common with both Ni and Pd promote 2-electron processes	electron-poor ligands common with Ni, not Pd promote 1-electron processes, often redox-active

paired with it. A variety of ligands, ligand-free Pd, and Pd aggregates of varying nuclearity can catalyze cross-coupling reactions[150].

Phosphines and N-heterocyclic carbenes (NHCs) are common to both Pd and Ni catalysis, although Ni catalysts are often found paired with polypyridine or other N-containing polydentate ligands[127] **(Figure 3)**. Pd- and Ni-catalyzed reactions that involve 2-electron redox pathways often rely on more strongly σ-donating ligands (i.e., phosphines and NHCs)[55]. Phosphine ligands are not always effective for Ni catalysis due to Ni's relatively small atomic radius, low electronegativity, and redox promiscuity[127]. Since low-valent Ni is better-suited for oxidative addition than Pd, ligands that promote reductive elimination are more

important for Ni catalysis, whereas ligands that promote oxidative addition are often more important for Pd catalysis. In order to promote the challenging reductive elimination, Ni catalysts are often paired with sterically bulky or electron-poor ligands[24,26].

Ni-catalyzed reactions that involve 1-electron redox pathways often use polypyridine ligands such as bipyridine (bpy) and terpyridine (terpy) derivatives, as well as other N-containing polydentate ligands such as bisoxazoline (BOX), bioxazoline (biOx), pyridyl oxazoline (PyrOx), and pyridine bisoxazoline (PyBOX) **(Figure 3)**. These weaker N-containing ligands cause less ligand field-splitting relative to phosphines and NHCs, stabilizing open-shell electron configurations of catalytic intermediates[55]. This weaker field-splitting is also responsible for the redox activity often observed in these Ni-ligand complexes, leading to open-shell species that are stabilized by ligand-centered radicals, enabling facile access to radical mechanisms[89,146,151,152].

This dissertation will demonstrate how our group has used various classes of ligands with Ni to enable catalysis. Namely, we have employed bipyridine-type ligands for Ni-photoredox-catalyzed C-N cross-coupling (Chapters 2-3), and we have leveraged bisphosphine and phosphinooxazoline (PHOX) ligands for the activation of C-C bonds in Ni-catalyzed Lewis acid-assisted cross-coupling (Chapter 4).

1.4   Thesis overview

Chapters 2-4 of this thesis will discuss our contributions to the field of Ni catalysis during my doctoral studies under the supervision of Dr. Ana Bahamonde. This work encompasses both method development and mechanistic investigation. Chapter 2 will discuss our development of a remarkably mild C-N cross-coupling method that enables the arylation of poorly nucleophilic amides via Ni-photoredox catalysis. Chapter 3 will delve further into this chemistry with a thorough mechanistic investigation involving kinetic studies and stoichiometric experiments on Ni complexes that are proposed catalytic intermediates. Our investigation unveiled a previously undescribed mechanism involving a prolonged induction period before rapid product formation. Chapter 4 will discuss a different area of Ni catalysis that we have been exploring: Lewis acid-assisted activation of benzonitriles as cyanide sources for Ni-catalyzed cyanation reactions. Ligand optimization and mechanistic inquiry related to this project are ongoing, although great strides have been made towards taming and understanding this chemistry.

1.5   References

(1)   Tasker, S. Z.; Standley, E. A.; Jamison, T. F. Recent Advances in Homogeneous Nickel Catalysis. *Nature* **2014**, *509* (7500), 299–309. https://doi.org/10.1038/nature13274.

(2)   Ruiz-Castillo, P.; Buchwald, S. L. Applications of Palladium-Catalyzed C−N Cross-Coupling Reactions. *Chem. Rev.* **2016**, *116* (19), 12564–12649. https://doi.org/10.1021/acs.chemrev.6b00512.

(3)   Johansson Seechurn, C. C. C.; Kitching, M. O.; Colacot, T. J.; Snieckus, V. Palladium-Catalyzed Cross-Coupling: A Historical Contextual Perspective to the 2010 Nobel Prize. *Angew. Chem. Int. Ed.* **2012**, *51* (21), 5062–5085. https://doi.org/10.1002/anie.201107017.

(4)   Miyaura, N.; Suzuki, A. Palladium-Catalyzed Cross-Coupling Reactions of Organoboron Compounds. *Chem. Rev.* **1995**, *95*, 2457–2483.

(5)   Nicolaou, K. C.; Bulger, P. G.; Sarlah, D. Palladium-Catalyzed Cross-Coupling Reactions in Total Synthesis. *Angew. Chem. Int. Ed.* **2005**, *44* (29), 4442–4489. https://doi.org/10.1002/anie.200500368.

(6)   Saito, B.; Fu, G. C. Alkyl-Alkyl Suzuki Cross-Couplings of Unactivated Secondary Alkyl Halides at Room Temperature. *J. Am. Chem. Soc.* **2007**, *129* (31), 9602–9603. https://doi.org/10.1021/ja074008l.

(7)   Ge, S.; Hartwig, J. F. Highly Reactive, Single-Component Nickel Catalyst Precursor for Suzuki-Miyuara Cross-Coupling of Heteroaryl Boronic Acids with Heteroaryl Halides. *Angew. Chem. Int. Ed.* **2012**, *51* (51), 12837–12841. https://doi.org/10.1002/anie.201207428.

(8)   Hie, L.; Chang, J. J.; Garg, N. K. Nickel-Catalyzed Suzuki-Miyaura Cross-Coupling in a Green Alcohol Solvent for an Undergraduate Organic Chemistry Laboratory. *J. Chem. Educ.* **2015**, *92* (3), 571–574. https://doi.org/10.1021/ed500158p.

(9)   Tobisu, M.; Xu, T.; Shimasaki, T.; Chatani, N. Nickel-Catalyzed Suzuki-Miyaura Reaction of Aryl Fluorides. *J. Am. Chem. Soc.* **2011**, *133* (48), 19505–19511. https://doi.org/10.1021/ja207759e.

(10)   Zhou, J.; Fu, G. C. Suzuki Cross-Couplings of Unactivated Secondary Alkyl Bromides and Iodides. *J. Am. Chem. Soc.* **2004**, *126* (5), 1340–1341. https://doi.org/10.1021/ja039889k.

(11)   Zultanski, S. L.; Fu, G. C. Nickel-Catalyzed Carbon-Carbon Bond-Forming Reactions of Unactivated Tertiary Alkyl Halides: Suzuki Arylations. *J. Am. Chem. Soc.* **2013**, *135* (2), 624–627. https://doi.org/10.1021/ja311669p.

(12)   Zim, D.; Lando, V. R.; Dupont, J.; Monteiro, A. L. NiCl2(PCy3)2: A Simple and Efficient Catalyst Precursor for the Suzuki Cross-Coupling of Aryl Tosylates and Arylboronic Acids. *Org. Lett.* **2001**, *3* (19), 3049–3051. https://doi.org/10.1021/ol016526l.

(13)   Tang, Z. Y.; Hu, Q. S. Room-Temperature Ni(0)-Catalyzed Cross-Coupling Reactions of Aryl Arenesulfonates with Arylboronic Acids. *J. Am. Chem. Soc.* **2004**, *126* (10), 3058–3059. https://doi.org/10.1021/ja038752r.

(14)   Zim, D.; Monteiro, A. L. Suzuki Cross-Coupling of Aryl Halides with Aryl Boronic Acids Catalyzed by Phosphine-Free NiCl 2 ·6H 2 O. *Tetrahedron Lett.* **2002**, *43*, 4009–4011.

(15)   Ueda, M.; Saitoh, A.; Saori, O.-T.; Miyaura, N. Synthesis of Biaryls via Nickel-Catalyzed Cross-Coupling Reaction of Arylboronic Acids and Aryi Mesylates. *Tetrahedron* **1998**, *54*, 13079–13086.

(16)   Kobayashi, Y.; Mizojiri, R. Nickel-Catalyzed Coupling Reaction of Lithium Organoborates and Aryl Mesylates Possessing An Electron Withdrawing Group. *Tetrahedron Lett.* **1996**, *37* (47), 8531–8534.

(17)   Inada, K.; Miyaura, N. Synthesis of Biaryls via Cross-Coupling Reaction of Arylboronic Acids with Aryl Chlorides Catalyzed by NiCl 2 /Triphenylphosphine Complexes. *Tetrahedron* **2000**, *56*, 8657–8660.

(18)   Galland, J.-C.; Savignac, M.; Gentt, J.-P. Cross-Coupling of Chloroarenes with Boronic Acids Using a Water-Soluble Nickel Catalyst. *Tetrahedron Lett.* **1999**, *40*, 2323–2326.

(19)   Percec, V.; Bae, J.-Y.; Hill, D. H. Aryl Mesylates in Metal Catalyzed Homocoupling and Cross-Coupling Reactions. 2. Suzuki-Type Nickel-Catalyzed Cross-Coupling of Aryl Arenesulfonates and Aryl Mesylates with Arylboronic Acids. *J. Org. Chem.* **1995**, *60*, 1060–1065.

(20)   Saito, S.; Sakai, M.; Miyaura, N. A Synthesis of Biaryls v/a Nickei(0).Catalyzed Cross-Coupling Reaction of Chloroarenes with Phenylboronic Acids. *Tetrahedron Lett.* **1996**, *37* (17), 2993–2996.

(21)   Saito, S.; Oh-Tani, S.; Miyaura, N. Synthesis of Biaryls via a Nickel(0)-Catalyzed Cross-Coupling Reaction of Chloroarenes with Arylboronic Acids. *J. Org. Chem.* **1997**, *62* (23), 8024–8030.

(22) Indolese, A. F. Suzuki-Type Coupling of Chloroarenes with Arylboronic Acids Catalysed by Nickel Complexes. *Tetrahedron Lett.* **1997**, *38* (20), 3513–3516.

(23) Payard, P. A.; Perego, L. A.; Ciofini, I.; Grimaud, L. Taming Nickel-Catalyzed Suzuki-Miyaura Coupling: A Mechanistic Focus on Boron-to-Nickel Transmetalation. *ACS Catal.* **2018**, *8* (6), 4812–4823. https://doi.org/10.1021/acscatal.8b00933.

(24) Wolfe, J. P.; Buchwald, S. L. Nickel-Catalyzed Amination of Aryl Chlorides. *J. Am. Chem. Soc.* **1997**, *119* (26), 6054–6058.

(25) Corcoran, E. B.; Pirnot, M. T.; Lin, S.; Dreher, S. D.; Dirocco, D. A.; Davies, I. W.; Buchwald, S. L.; Macmillan, D. W. C. Aryl Amination Using Ligand-Free Ni(II) Salts and Photoredox Catalysis. *Science* **2016**, *353* (6296), 279–283.

(26) Lavoie, C. M.; Macqueen, P. M.; Rotta-Loria, N. L.; Sawatzky, R. S.; Borzenko, A.; Chisholm, A. J.; Hargreaves, B. K. V.; McDonald, R.; Ferguson, M. J.; Stradiotto, M. Challenging Nickel-Catalysed Amine Arylations Enabled by Tailored Ancillary Ligand Design. *Nat. Commun.* **2016**, *7:11073*. https://doi.org/10.1038/ncomms11073.

(27) Kawamata, Y.; Vantourout, J. C.; Hickey, D. P.; Bai, P.; Chen, L.; Hou, Q.; Qiao, W.; Barman, K.; Edwards, M. A.; Garrido-Castro, A. F.; Degruyter, J. N.; Nakamura, H.; Knouse, K.; Qin, C.; Clay, K. J.; Bao, D.; Li, C.; Starr, J. T.; Garcia-Irizarry, C.; Sach, N.; White, H. S.; Neurock, M.; Minteer, S. D.; Baran, P. S. Electrochemically Driven, Ni-Catalyzed Aryl Amination: Scope, Mechanism, and Applications. *J. Am. Chem. Soc.* **2019**, *141* (15), 6392–6402. https://doi.org/10.1021/jacs.9b01886.

(28) Standley, E. A.; Jamison, T. F. Simplifying Nickel(0) Catalysis: An Air-Stable Nickel Precatalyst for the Internally Selective Benzylation of Terminal Alkenes. *J. Am. Chem. Soc.* **2013**, *135* (4), 1585–1592. https://doi.org/10.1021/ja3116718.

(29) Wang, Z. X.; Chai, Z. Y. Palladium(II) and Nickel(II) Complexes Bearing N,N,O-Chelate Ligands: Syntheses, Characterization and Catalysis in Heck and Kumada Coupling Reactions. *Eur. J. Inorg. Chem.* **2007**, No. 28, 4492–4499. https://doi.org/10.1002/ejic.200700347.

(30) Kwiatkowski, M. R.; Alexanian, E. J. Nickel-Catalyzed Mizoroki–Heck-Type Reactions of Unactivated Alkyl Bromides. *Angew. Chem. Int. Ed.* **2018**, *130* (51), 17099–17102. https://doi.org/10.1002/ange.201810757.

(31) Lv, H.; Kang, H.; Zhou, B.; Xue, X.; Engle, K. M.; Zhao, D. Nickel-Catalyzed Intermolecular Oxidative Heck Arylation Driven by Transfer Hydrogenation. *Nat. Commun.* **2019**, *10* (1). https://doi.org/10.1038/s41467-019-12949-1.

(32) Zhang, W. S.; Ji, D. W.; Li, Y.; Zhang, X. X.; Mei, Y. K.; Chen, B. Z.; Chen, Q. A. Nickel-Catalyzed Divergent Mizoroki–Heck Reaction of 1,3-Dienes. *Nat Commun* **2023**, *14* (1). https://doi.org/10.1038/s41467-023-36237-1.

(33) Gøgsig, T. M.; Kleimark, J.; Nilsson Lill, S. O.; Korsager, S.; Lindhardt, A. T.; Norrby, P. O.; Skrydstrup, T. Mild and Efficient Nickel-Catalyzed Heck Reactions with Electron-Rich Olefins. *J. Am. Chem. Soc.* **2012**, *134* (1), 443–452. https://doi.org/10.1021/ja2084509.

(34) Li, G. Y.; Marshall, W. J. Applied Homogeneous Catalysis with Organometallic Compounds. *Organometallics* **2002**, *21* (4), 590–591. https://doi.org/10.1021/om010828.

(35) Böhm, V. P. W.; Weskamp, T.; Gstöttmayr, C. W. K.; Herrmann, W. A. Nickel-Catalyzed Cross-Coupling of Aryl Chlorides with Aryl Grignard Reagents. *Angew. Chem. Int. Ed.* **2000**, *39* (9), 1602–1604. https://doi.org/10.1002/(SICI)1521-3773(20000502)39:9<1602::AID-ANIE1602>3.0.CO;2-N.

(36) Miller, J. A.; Dankwardt, J. W. Nickel Catalyzed Cross-Coupling of Modified Alkyl and Alkenyl Grignard Reagents with Aryl-and Heteroaryl Nitriles: Activation of the CCN Bond. *Tetrahedron Lett.* **2003**, *44*, 1907–1910.

(37) Böhm, V. P. W.; Gstöttmayr, C. W. K.; Weskamp, T.; Herrmann, W. A. Catalytic C-C Bond Formation through Selective Activation of C-F Bonds. *Angew. Chem. Int. Ed.* **2001**, *40* (18), 3387–3389. https://doi.org/10.1002/1521-3773(20010917)40:18<3387::AID-ANIE3387>3.0.CO;2-6.

(38) Mongin, F.; Mojovic, L.; Guillamet, B.; Trécourt, F.; Quéguiner, G. Cross-Coupling Reactions of Phenylmagnesium Halides with Fluoroazines and Fluorodiazines. *J. Org. Chem.* **2002**, *67* (25), 8991–8994. https://doi.org/10.1021/jo026136s.

(39) Miller, J. A. CC Bond Activation with Selective Functionalization: Preparation of Unsymmetrical Biaryls from Benzonitriles. *Tetrahedron Lett.* **2001**, *42*, 6991–6993.

(40) Vechorkin, O.; Hu, X. Nickel-Catalyzed Cross-Coupling of Non-Activated and Functionalized Alkyl Halides with Alkyl Grignard Reagents. *Angew.*

Chem. Int. Ed. **2009**, *48* (16), 2937–2940.
https://doi.org/10.1002/anie.200806138.

(41) Zhou, J.; Fu, G. C. Cross-Couplings of Unactivated Secondary Alkyl Halides: Room-Temperature Nickel-Catalyzed Negishi Reactions of Alkyl Bromides and Iodides. *J. Am. Chem. Soc.* **2003**, *125* (48), 14726–14727. https://doi.org/10.1021/ja0389366.

(42) Huang, C. Y.; Doyle, A. G. Nickel-Catalyzed Negishi Alkylations of Styrenyl Aziridines. *J. Am. Chem. Soc.* **2012**, *134* (23), 9541–9544. https://doi.org/10.1021/ja3013825.

(43) Powell, D. A.; Fu, G. C. Nickel-Catalyzed Cross-Couplings of Organosilicon Reagents with Unactivated Secondary Alkyl Bromides. *J. Am. Chem. Soc.* **2004**, *126* (25), 7788–7789. https://doi.org/10.1021/ja047433c.

(44) Strotman, N. A.; Sommer, S.; Fu, G. C. Hiyama Reactions of Activated and Unactivated Secondary Alkyl Halides Catalyzed by a Nickel/Norephedrine Complex. *Angew. Chem. Int. Ed.* **2007**, *46* (19), 3556–3558. https://doi.org/10.1002/anie.200700440.

(45) Dai, X.; Strotman, N. A.; Fu, G. C. Catalytic Asymmetric Hiyama Cross-Couplings of Racemic α-Bromo Esters. *J. Am. Chem. Soc.* **2008**, *130* (11), 3302–3303. https://doi.org/10.1021/ja8009428.

(46) Powell, D. A.; Maki, T.; Fu, G. C. Stille Cross-Couplings of Unactivated Secondary Alkyl Halides Using Monoorganotin Reagents. *J. Am. Chem. Soc.* **2005**, *127* (2), 510–511. https://doi.org/10.1021/ja0436300.

(47) Zhou, Z.; Yang, J.; Yang, B.; Han, Y.; Zhu, L.; Xue, X. S.; Zhu, F. Photoredox Nickel-Catalysed Stille Cross-Coupling Reactions. *Angew. Chem. Int. Ed.* **2023**, *62* (52). https://doi.org/10.1002/anie.202314832.

(48) Russell, J. E. A.; Entz, E. D.; Joyce, I. M.; Neufeldt, S. R. Nickel-Catalyzed Stille Cross Coupling of C-O Electrophiles. *ACS Catal.* **2019**, *9* (4), 3304–3310. https://doi.org/10.1021/acscatal.9b00744.

(49) Wang, D. Y.; Kawahata, M.; Yang, Z. K.; Miyamoto, K.; Komagawa, S.; Yamaguchi, K.; Wang, C.; Uchiyama, M. Stille Coupling via C-N Bond Cleavage. *Nat. Commun.* **2016**, *7*. https://doi.org/10.1038/ncomms12937.

(50) Vechorkin, O.; Barmaz, D.; Proust, V.; Hu, X. Ni-Catalyzed Sonogashira Coupling of Nonactivated Alkyl Halides: Orthogonal Functionalization of Alkyl Iodides, Bromides, and Chlorides. *J. Am. Chem. Soc.* **2009**, *131* (34), 12078–12079. https://doi.org/10.1021/ja906040t.

(51) Pérez García, P. M.; Ren, P.; Scopelliti, R.; Hu, X. Nickel-Catalyzed Direct Alkylation of Terminal Alkynes at Room Temperature: A Hemilabile Pincer Ligand Enhances Catalytic Activity. *ACS Catal.* **2015**, *5* (2), 1164–1171. https://doi.org/10.1021/cs501502u.

(52) Zhang, X.; Qi, D.; Jiao, C.; Liu, X.; Zhang, G. Nickel-Catalyzed Deaminative Sonogashira Coupling of Alkylpyridinium Salts Enabled by NN2 Pincer Ligand. *Nat. Commun.* **2021**, *12* (1). https://doi.org/10.1038/s41467-021-25222-1.

(53) Yi, J.; Lu, X.; Sun, Y. Y.; Xiao, B.; Liu, L. Nickel-Catalyzed Sonogashira Reactions of Non-Activated Secondary Alkyl Bromides and Iodides. *Angew. Chem. Int. Ed.* **2013**, *52* (47), 12409–12413. https://doi.org/10.1002/anie.201307069.

(54) Beletskaya, I. P.; Latyshev, G. V.; Tsvetkov, A. V.; Lukashev, N. V. The Nickel-Catalyzed Sonogashira-Hagihara Reaction. *Tetrahedron Lett.* **2003**, *44* (27), 5011–5013. https://doi.org/10.1016/S0040-4039(03)01174-2.

(55) Diccianni, J. B.; Diao, T. Mechanisms of Nickel-Catalyzed Cross-Coupling Reactions. *Trends Chem.* **2019**, *1* (9), 830–844. https://doi.org/10.1016/j.trechm.2019.08.004.

(56) Milligan, J. A.; Phelan, J. P.; Badir, S. O.; Molander, G. A. Alkyl Carbon-Carbon Bond Formation by Nickel/Photoredox Cross-Coupling. *Angew. Chem. Int. Ed.* **2019**, *131* (19), 6212–6224. https://doi.org/10.1002/ANGE.201809431.

(57) Weix, D. J. Methods and Mechanisms for Cross-Electrophile Coupling of Csp2 Halides with Alkyl Electrophiles. *Acc. Chem. Res.* **2015**, *48* (6), 1767–1775. https://doi.org/10.1021/acs.accounts.5b00057.

(58) Chan, A. Y.; Perry, I. B.; Bissonnette, N. B.; Buksh, B. F.; Edwards, G. A.; Frye, L. I.; Garry, O. L.; Lavagnino, M. N.; Li, B. X.; Liang, Y.; Mao, E.; Millet, A.; Oakley, J. V.; Reed, N. L.; Sakai, H. A.; Seath, C. P.; MacMillan, D. W. C. Metallaphotoredox: The Merger of Photoredox and Transition Metal Catalysis. *Chem. Rev.* **2022**, *122* (2), 1485–1542. https://doi.org/10.1021/acs.chemrev.1c00383.

(59) Franke, M. C.; Longley, V. R.; Rafiee, M.; Stahl, S. S.; Hansen, E. C.; Weix, D. J. Zinc-Free, Scalable Reductive Cross-Electrophile Coupling Driven by Electrochemistry in an Undivided Cell. *ACS Catal.* **2022**, *12* (20), 12617–12626. https://doi.org/10.1021/acscatal.2c03033.

(60) Boit, T. B.; Bulger, A. S.; Dander, J. E.; Garg, N. K. Activation of C-O and C-N Bonds Using Non-Precious-Metal Catalysis. *ACS Catal.* **2020**, *10* (20), 12109–12126. https://doi.org/10.1021/acscatal.0c03334.

(61) Nakao, Y. Metal-Mediated C-CN Bond Activation in Organic Synthesis. *Chem. Rev.* **2021**, *121* (1), 327–344. https://doi.org/10.1021/acs.chemrev.0c00301.

(62) Chen, P. H.; Billett, B. A.; Tsukamoto, T.; Dong, G. Cut and Sew Transformations via Transition-Metal-Catalyzed Carbon-Carbon Bond Activation. *ACS Catal.* **2017**, *7* (2), 1340–1360. https://doi.org/10.1021/acscatal.6b03210.

(63) Khake, S. M.; Chatani, N. Nickel-Catalyzed C−H Functionalization Using a Non-Directed Strategy. *Chem* **2020**, *6* (5), 1056–1081. https://doi.org/10.1016/j.chempr.2020.04.005.

(64) Guo, L.; Srimontree, W.; Zhu, C.; Maity, B.; Liu, X.; Cavallo, L.; Rueping, M. Nickel-Catalyzed Suzuki–Miyaura Cross-Couplings of Aldehydes. *Nat. Commun.* **2019**, *10* (1). https://doi.org/10.1038/s41467-019-09766-x.

(65) Derosa, J.; Apolinar, O.; Kang, T.; Tran, V. T.; Engle, K. M. Recent Developments in Nickel-Catalyzed Intermolecular Dicarbofunctionalization of Alkenes. *Chem. Sci.* **2020**, *11* (17), 4287–4296. https://doi.org/10.1039/c9sc06006e.

(66) Badir, S. O.; Molander, G. A. Developments in Photoredox/Nickel Dual-Catalyzed 1,2-Difunctionalizations. *Chem* **2020**, *6* (6), 1327–1339. https://doi.org/10.1016/j.chempr.2020.05.013.

(67) Diccianni, J.; Lin, Q.; Diao, T. Mechanisms of Nickel-Catalyzed Coupling Reactions and Applications in Alkene Functionalization. *Acc. Chem. Res.* **2020**, *53* (4), 906–919. https://doi.org/10.1021/acs.accounts.0c00032.

(68) Ananikov, V. P. Nickel: The "Spirited Horse" of Transition Metal Catalysis. *ACS Catal.* **2015**, *5* (3), 1964–1971. https://doi.org/10.1021/acscatal.5b00072.

(69) Chernyshev, V. M.; Ananikov, V. P. Nickel and Palladium Catalysis: Stronger Demand than Ever. *ACS Catal.* **2022**, *12* (2), 1180–1200. https://doi.org/10.1021/acscatal.1c04705.

(70) Koo, K.; Hillhouse, G. L. Indoline Synthesis via Coupling of Phenethyl Grignard Reagents with Organoazides Mediated by

(Alkylphosphine)Nickel(II) Complexes. *Organometallics* **1996**, *15* (12), 2669–2671.

(71)　Han, R.; Hillhouse, G. L. Sulfur-Atom Transfer from Elemental Sulfur to Nickel-Carbon Bonds as a New Route to Reactive Nickel(II) Thiolates. *J. Am. Chem. Soc.* **1998**, *120*, 7657–7658.

(72)　Han, R.; Hillhouse, G. L. Carbon-Oxygen Reductive-Elimination from Nickel(II) Oxametallacycles and Factors That Control Formation of Ether, Aldehyde, Alcohol, or Ester Products. *J. Am. Chem. Soc.* **1997**, *119*, 8135–8136.

(73)　Koo, K.; Hillhouse, G. L. Carbon-Nitrogen Bond Formation by Reductive Elimination from Nickel(II) Amido Alkyl Complexes. *Organometallics* **1995**, *14*, 4421–4423.

(74)　Matsunaga, P. T.; Hillhouse, G. L. Oxygen-Atom Transfer from Nitrous Oxide to a Nickel Metallacycle. Synthesis, Structure, and Reactions of (2,2'-Bipyridine)Ni(OCH2CH2CH2CH2). *J. Am. Chem. Soc.* **1993**, *115*, 2075–2077.

(75)　Lin, B. L.; Clough, C. R.; Hillhouse, G. L. Interactions of Aziridines with Nickel Complexes: Oxidative-Addition and Reductive-Elimination Reactions That Break and Make C-N Bonds. *J. Am. Chem. Soc.* **2002**, *124* (12), 2890–2891. https://doi.org/10.1021/ja017652n.

(76)　Camasso, N. M.; Sanford, M. S. Design, Synthesis, and Carbon-Heteroatom Coupling Reactions of Organometallic Nickel(IV) Complexes. *Science* **2015**, *347* (6227), 1218–1220. https://doi.org/10.1126/science.aaa4526.

(77)　Camasso, N. M.; Canty, A. J.; Ariafard, A.; Sanford, M. S. Experimental and Computational Studies of High-Valent Nickel and Palladium Complexes. *Organometallics* **2017**, *36* (22), 4382–4393. https://doi.org/10.1021/acs.organomet.7b00613.

(78)　Roberts, C. C.; Camasso, N. M.; Bowes, E. G.; Sanford, M. S. Impact of Oxidation State on Reactivity and Selectivity Differences between Nickel(III) and Nickel(IV) Alkyl Complexes. *Angew. Chem. Int. Ed.* **2019**, *131* (27), 9202–9206. https://doi.org/10.1002/ange.201903638.

(79)　Bour, J. R.; Ferguson, D. M.; McClain, E. J.; Kampf, J. W.; Sanford, M. S. Connecting Organometallic Ni(III) and Ni(IV): Reactions of Carbon-Centered Radicals with High-Valent Organonickel Complexes. *J. Am.*

Chem. Soc. **2019**, *141* (22), 8914–8920.
https://doi.org/10.1021/jacs.9b02411.

(80) Bour, J. R.; Camasso, N. M.; Meucci, E. A.; Kampf, J. W.; Canty, A. J.;
Sanford, M. S. Carbon-Carbon Bond-Forming Reductive Elimination from
Isolated Nickel(III) Complexes. *J. Am. Chem. Soc.* **2016**, *138* (49), 16105–
16111. https://doi.org/10.1021/jacs.6b10350.

(81) Na, H.; Mirica, L. M. Deciphering the Mechanism of the Ni-Photocatalyzed
C–O Cross-Coupling Reaction Using a Tridentate Pyridinophane Ligand.
Nat. Commun. **2022**, *13* (1). https://doi.org/10.1038/s41467-022-28948-8.

(82) Schultz, J. W.; Fuchigami, K.; Zheng, B.; Rath, N. P.; Mirica, L. M. Isolated
Organometallic Nickel(III) and Nickel(IV) Complexes Relevant to Carbon-
Carbon Bond Formation Reactions. *J. Am. Chem. Soc.* **2016**, *138* (39),
12928–12934. https://doi.org/10.1021/jacs.6b06862.

(83) Sun, R.; Qin, Y.; Nocera, D. G. General Paradigm in Photoredox Nickel-
Catalyzed Cross-Coupling Allows for Light-Free Access to Reactivity.
Angew. Chem. Int. Ed. **2020**, *59* (24), 9527–9533.
https://doi.org/10.1002/anie.201916398.

(84) Sun, R.; Qin, Y.; Ruccolo, S.; Schnedermann, C.; Costentin, C.; Nocera, D.
G. Elucidation of a Redox-Mediated Reaction Cycle for Nickel-Catalyzed
Cross Coupling. *J. Am. Chem. Soc.* **2019**, *141* (1), 89–93.
https://doi.org/10.1021/jacs.8b11262.

(85) Hwang, S. J.; Anderson, B. L.; Powers, D. C.; Maher, A. G.; Hadt, R. G.;
Nocera, D. G. Halogen Photoelimination from Monomeric Nickel(III)
Complexes Enabled by the Secondary Coordination Sphere.
Organometallics **2015**, *34* (19), 4766–4774.
https://doi.org/10.1021/acs.organomet.5b00568.

(86) Till, N. A.; Tian, L.; Dong, Z.; Scholes, G. D.; MacMillan, D. W. C.
Mechanistic Analysis of Metallaphotoredox C-N Coupling: Photocatalysis
Initiates and Perpetuates Ni(I)/Ni(III) Coupling Activity. *J. Am. Chem. Soc.*
2020, *142* (37), 15830–15841. https://doi.org/10.1021/jacs.0c05901.

(87) Kariofillis, S. K.; Doyle, A. G. Synthetic and Mechanistic Implications of
Chlorine Photoelimination in Nickel/Photoredox C(Sp3)-H Cross-Coupling.
Acc. Chem. Res. **2021**, *54* (4), 988–1000.
https://doi.org/10.1021/acs.accounts.0c00694.

(88) Cloutier, J. P.; Zargarian, D. Functionalization of the Aryl Moiety in the
Pincer Complex (NCN)NiIIIBr2: Insights on NiIII-Promoted Carbon-

Heteroatom Coupling. *Organometallics* **2018**, *37* (9), 1446–1455. https://doi.org/10.1021/acs.organomet.8b00103.

(89) Mohadjer Beromi, M.; Brudvig, G. W.; Hazari, N.; Lant, H. M. C.; Mercado, B. Q. Synthesis and Reactivity of Paramagnetic Nickel Polypyridyl Complexes Relevant to C(Sp 2)–C(Sp 3)Coupling Reactions . *Angew. Chem. Int. Ed.* **2019**, *131* (18), 6155–6159. https://doi.org/10.1002/ange.201901866.

(90) Bradley, R. D.; McManus, B. D.; Yam, J. G.; Carta, V.; Bahamonde, A. Mechanistic Evidence of a Ni(0/II/III) Cycle for Nickel Photoredox Amide Arylation. *Angew. Chem. Int. Ed.* **2023**, *62* (43), e202310753. https://doi.org/10.1002/anie.202310753.

(91) Dawson, G. A.; Spielvogel, E. H.; Diao, T. Nickel-Catalyzed Radical Mechanisms: Informing Cross-Coupling for Synthesizing Non-Canonical Biomolecules. *Acc. Chem. Res.* **2023**, *56* (24), 3640–3653. https://doi.org/10.1021/acs.accounts.3c00588.

(92) Welin, E. R.; Le, C.; Arias-Rotondo, D. M.; Mccusker, J. K.; Macmillan, D. W. C. Photosensitized, Energy Transfer-Mediated Organometallic Catalysis through Electronically Excited Nickel(II). *Science* **2017**, *355* (6323), 380–385.

(93) Ting, S. I.; Williams, W. L.; Doyle, A. G. Oxidative Addition of Aryl Halides to a Ni(I)-Bipyridine Complex. *J. Am. Chem. Soc.* **2022**, *144* (12), 5575–5582. https://doi.org/10.1021/jacs.2c00462.

(94) Shields, B. J.; Kudisch, B.; Scholes, G. D.; Doyle, A. G. Long-Lived Charge-Transfer States of Nickel(II) Aryl Halide Complexes Facilitate Bimolecular Photoinduced Electron Transfer. *J. Am. Chem. Soc.* **2018**, *140* (8), 3035–3039. https://doi.org/10.1021/jacs.7b13281.

(95) Ting, S. I.; Garakyaraghi, S.; Taliaferro, C. M.; Shields, B. J.; Scholes, G. D.; Castellano, F. N.; Doyle, A. G. 3d-d Excited States of Ni(II) Complexes Relevant to Photoredox Catalysis: Spectroscopic Identification and Mechanistic Implications. *J. Am. Chem. Soc.* **2020**, *142* (12), 5800–5810. https://doi.org/10.1021/jacs.0c00781.

(96) Gutierrez, O.; Tellis, J. C.; Primer, D. N.; Molander, G. A.; Kozlowski, M. C. Nickel-Catalyzed Cross-Coupling of Photoredox-Generated Radicals: Uncovering a General Manifold for Stereoconvergence in Nickel-Catalyzed Cross-Couplings. *J. Am. Chem. Soc.* **2015**, *137* (15), 4896–4899. https://doi.org/10.1021/ja513079r.

(97) Cornella, J.; Gómez-Bengoa, E.; Martin, R. Combined Experimental and Theoretical Study on the Reductive Cleavage of Inert C-O Bonds with Silanes: Ruling out a Classical Ni(0)/Ni(II) Catalytic Couple and Evidence for Ni(I) Intermediates. *J. Am. Chem. Soc.* **2013**, *135* (5), 1997–2009. https://doi.org/10.1021/ja311940s.

(98) Lipschutz, M. I.; Yang, X.; Chatterjee, R.; Tilley, T. D. A Structurally Rigid Bis(Amido) Ligand Framework in Low-Coordinate Ni(I), Ni(II), and Ni(III) Analogues Provides Access to a Ni(III) Methyl Complex via Oxidative Addition. *J. Am. Chem. Soc.* **2013**, *135* (41), 15298–15301. https://doi.org/10.1021/ja408151h.

(99) Tsou, T. T.; Kochi, J. K. Mechanism of Oxidative Addition. Reaction of Nickel(0) Complexes with Aromatic Halides. *J. Am. Chem. Soc.* **1979**, *101* (21), 6319–6332.

(100) Pierson, C. N.; Hartwig, J. F. Mapping the Mechanisms of Oxidative Addition in Cross-Coupling Reactions Catalysed by Phosphine-Ligated Ni(0). *Nat. Chem.* **2024**. https://doi.org/10.1038/s41557-024-01451-x.

(101) Powers, D. C.; Ritter, T. Bimetallic Pd(III) Complexes in Palladium-Catalysed Carbon-Heteroatom Bond Formation. *Nat. Chem.* **2009**, *1* (4), 302–309. https://doi.org/10.1038/nchem.246.

(102) Powers, D. C.; Geibel, M. A. L.; Klein, J. E. M. N.; Ritter, T. Bimetallic Palladium Catalysis: Direct Observation of Pd(III)-Pd(III) Intermediates. *J. Am. Chem. Soc.* **2009**, *131* (47), 17050–17051. https://doi.org/10.1021/ja906935c.

(103) Canty, A. J.; Bercaw, J. E.; Goldberg, K. I.; Grice, K. A.; Labinger, J. A.; Malinakova, H. C.; Moret, M.-E.; Powers, D. C.; Racowski, J. M.; Ritter, T.; Sanford, M. S.; Scheuermann, M. L.; Sharma, M. Palladium(III) in Synthesis and Catalysis. In *Topics in Organometallic Chemistry: Higher Oxidation State Organopalladium and Platinum Chemistry*; Springer, 2011; Vol. 35, pp 129–156.

(104) Kancherla, R.; Muralirajan, K.; Maity, B.; Zhu, C.; Krach, P. E.; Cavallo, L.; Rueping, M. Oxidative Addition to Palladium(0) Made Easy through Photoexcited-State Metal Catalysis: Experiment and Computation. *Angew. Chem. Int. Ed.* **2019**, *58* (11), 3412–3416. https://doi.org/10.1002/anie.201811439.

(105) Fang, H.; Empel, C.; Atodiresei, I.; Koenigs, R. M. Photoinduced Palladium-Catalyzed 1,2-Difunctionalization of Electron-Rich Olefins via a

Reductive Radical-Polar Crossover Reaction. *ACS Catal.* **2023**, *13* (9), 6445–6451. https://doi.org/10.1021/acscatal.3c00938.

(106) Poli, R.; Cacelli, I. Orbital Splitting and Pairing Energy in Open-Shell Organometallics: A Study of Two Families of 16-Electron Complexes [Cp2M] (M = Cr, Mo, W) and [CpM(PH3)] (M = Co, Rh, Ir). *Eur. J. Inorg. Chem.* **2005**, No. 12, 2324–2331. https://doi.org/10.1002/ejic.200400839.

(107) Batsanov, S. S. Van Der Waals Radii of Elements. *Inorg. Mater.* **2001**, *37*, 871–885.

(108) Mann, J. B.; Meek, T. L.; Knight, E. T.; Capitani, J. F.; Allen, L. C. Configuration Energies of the D-Block Elements. *J. Am. Chem. Soc.* **2000**, *122* (21), 5132–5137. https://doi.org/10.1021/ja9928677.

(109) Tellis, J. C.; Primer, D. N.; Molander, G. A. Single-Electron Transmetalation in Organoboron Cross-Coupling by Photoredox/Nickel Dual Catalysis. *Science* **2014**, *345* (6195), 430–433. https://doi.org/10.1126/science.1251422.

(110) Vara, B. A.; Patel, N. R.; Molander, G. A. O-Benzyl Xanthate Esters under Ni/Photoredox Dual Catalysis: Selective Radical Generation and Csp3-Csp2 Cross-Coupling. *ACS Catal.* **2017**, *7* (6), 3955–3959. https://doi.org/10.1021/acscatal.7b00772.

(111) Yi, J.; Badir, S. O.; Kammer, L. M.; Ribagorda, M.; Molander, G. A. Deaminative Reductive Arylation Enabled by Nickel/Photoredox Dual Catalysis. *Org. Lett.* **2019**, *21* (9), 3346–3351. https://doi.org/10.1021/acs.orglett.9b01097.

(112) Remeur, C.; Kelly, C. B.; Patel, N. R.; Molander, G. A. Aminomethylation of Aryl Halides Using α-Silylamines Enabled by Ni/Photoredox Dual Catalysis. *ACS Catal.* **2017**, *7* (9), 6065–6069. https://doi.org/10.1021/acscatal.7b01973.

(113) Zuo, Z.; Ahneman, D. T.; Chu, L.; Terrett, J. A.; Doyle, A. G.; Macmillan, D. W. C. Merging Photoredox with Nickel Catalysis: Coupling of α-Carboxyl Sp 3-Carbons with Aryl Halides. *Science* **2014**, *345* (6195), 437–440.

(114) Dongbang, S.; Doyle, A. G. Ni/Photoredox-Catalyzed C(Sp3)-C(Sp3) Coupling between Aziridines and Acetals as Alcohol-Derived Alkyl Radical Precursors. *J. Am. Chem. Soc.* **2022**, *144* (43), 20067–20077. https://doi.org/10.1021/jacs.2c09294.

(115) Kariofillis, S. K.; Shields, B. J.; Tekle-Smith, M. A.; Zacuto, M. J.; Doyle, A. G. Nickel/Photoredox-Catalyzed Methylation of (Hetero)Aryl Chlorides Using Trimethyl Orthoformate as a Methyl Radical Source. *J. Am. Chem. Soc.* **2020**, *142* (16), 7683–7689. https://doi.org/10.1021/jacs.0c02805.

(116) Zheng, S.; Gutiérrez-Bonet, Á.; Molander, G. A. Merging Photoredox PCET with Ni-Catalyzed Cross-Coupling: Cascade Amidoarylation of Unactivated Olefins. *Chem* **2019**, *5* (2), 339–352. https://doi.org/10.1016/j.chempr.2018.11.014.

(117) Shields, B. J.; Doyle, A. G. Direct C(Sp3)-H Cross Coupling Enabled by Catalytic Generation of Chlorine Radicals. *J. Am. Chem. Soc.* **2016**, *138* (39), 12719–12722. https://doi.org/10.1021/jacs.6b08397.

(118) Perry, I. B.; Brewer, T. F.; Sarver, P. J.; Schultz, D. M.; DiRocco, D. A.; MacMillan, D. W. C. Direct Arylation of Strong Aliphatic C–H Bonds. *Nature* **2018**, *560* (7716), 70–75. https://doi.org/10.1038/s41586-018-0366-x.

(119) Joe, C. L.; Doyle, A. G. Direct Acylation of C(Sp 3)−H Bonds Enabled by Nickel and Photoredox Catalysis . *Angew. Chem. Int. Ed.* **2016**, *128* (12), 4108–4111. https://doi.org/10.1002/ange.201511438.

(120) Ahneman, D. T.; Doyle, A. G. C-H Functionalization of Amines with Aryl Halides by Nickel-Photoredox Catalysis. *Chem. Sci.* **2016**, *7* (12), 7002–7006. https://doi.org/10.1039/c6sc02815b.

(121) Nielsen, M. K.; Shields, B. J.; Liu, J.; Williams, M. J.; Zacuto, M. J.; Doyle, A. G. Mild, Redox-Neutral Formylation of Aryl Chlorides through the Photocatalytic Generation of Chlorine Radicals. *Angew. Chem. Int. Ed.* **2017**, *56* (25), 7191–7194. https://doi.org/10.1002/anie.201702079.

(122) Leibler, I. N. M.; Tekle-Smith, M. A.; Doyle, A. G. A General Strategy for C(Sp3)–H Functionalization with Nucleophiles Using Methyl Radical as a Hydrogen Atom Abstractor. *Nat. Commun.* **2021**, *12* (1). https://doi.org/10.1038/s41467-021-27165-z.

(123) Zhu, C.; Uifeng Yue, H.; Jia, J.; Rueping, M. Cross-Coupling Nickel-Catalyzed C-Heteroatom Cross-Coupling Reactions under Mild Conditions via Facilitated Reductive Elimination. *Angew. Chem. Int. Ed.* **2021**, *60*, 17810–17831. https://doi.org/10.1002/anie.202013852.

(124) Bradley, R. D.; Bahamonde, A. Mild Amide N-Arylation Enabled by Nickel-Photoredox Catalysis. *Org. Lett.* **2022**, *24* (39), 7134–7139. https://doi.org/10.1021/acs.orglett.2c02808.

(125) Terrett, J. A.; Cuthbertson, J. D.; Shurtleff, V. W.; MacMillan, D. W. C. Switching on Elusive Organometallic Mechanisms with Photoredox Catalysis. *Nature* **2015**, *524* (7565), 330–334. https://doi.org/10.1038/nature14875.

(126) Jouffroy, M.; Kelly, C. B.; Molander, G. A. Thioetherification via Photoredox/Nickel Dual Catalysis. *Org. Lett.* **2016**, *18* (4), 876–879. https://doi.org/10.1021/acs.orglett.6b00208.

(127) Taylor, O. R.; Saucedo, P. J.; Bahamonde, A. Leveraging the Redox Promiscuity of Nickel To Catalyze C-N Coupling Reactions. *J. Org. Chem.* **2024**. https://doi.org/10.1021/acs.joc.3c02353.

(128) Day, C. S.; Martin, R. Comproportionation and Disproportionation in Nickel and Copper Complexes. *Chem. Soc. Rev.* **2023**, *52* (19), 6601–6616. https://doi.org/10.1039/d2cs00494a.

(129) Friesen, R. W.; Allouche, E. M. D. Tetrakis(Triphenylphosphine)Palladium(0). In *Encyclopedia of Reagents for Organic Synthesis*; John Wiley & Sons, Ltd, 2017; pp 1–7. https://doi.org/10.1002/047084289x.rt049.pub2.

(130) Wender, P. A.; Smith, T. E.; Duong, H. A.; Louie, J.; Standley, E. A.; Tasker, S. Z. Bis(1,5-Cyclooctadiene)Nickel(0). In *Encyclopedia of Reagents for Organic Synthesis*; John Wiley & Sons, Ltd, 2015; pp 1–15. https://doi.org/10.1002/047084289x.rb118.pub3.

(131) Stille, J. R.; Pigge, F. C.; Regens, C. S.; Chen, K.; Ortiz, A.; Eastgate, M. D. Bis(Dibenzylideneacetone)Palladium(0). In *Encyclopedia of Reagents for Organic Synthesis*; John Wiley & Sons, Ltd, 2013. https://doi.org/10.1002/047084289x.rb138.pub3.

(132) Grushin, V. V; Alper, H. The Existence and Stability of Mononuclear and Binuclear Organopalladium Hydroxo Complexes, [(R 3 P) 2 Pd(R′)(OH)] and [(R 3 P) 2 Pd 2 (R′) 2 (μ-OH) 2]. *Organometallics* **1996**, *15* (24), 5242–5245.

(133) Kepp, K. P. A Quantitative Scale of Oxophilicity and Thiophilicity. *Inorg. Chem.* **2016**, *55* (18), 9461–9470. https://doi.org/10.1021/acs.inorgchem.6b01702.

(134) Tamaru, Y. *Modern Organonickel Chemistry*; Wiley-VCH, 2005.

(135) Fang, X.; Yu, P.; Morandi, B. Catalytic Reversible Alkene-Nitrile Interconversion through Controllable Transfer Hydrocyanation. *Science* **2016**, *351* (6275), 832–836.

(136) Whittaker, A. M.; Dong, V. M. Nickel-Catalyzed Dehydrogenative Cross-Coupling: Direct Transformation of Aldehydes into Esters and Amides. *Angew. Chem. Int. Ed.* **2015**, *54* (4), 1312–1315. https://doi.org/10.1002/anie.201410322.

(137) Tobisu, M.; Shimasaki, T.; Chatani, N. Nickel-Catalyzed Cross-Coupling of Aryl Methyl Ethers with Aryl Boronic Esters. *Angew. Chem. Int. Ed.* **2008**, *47* (26), 4866–4869. https://doi.org/10.1002/anie.200801447.

(138) Guan, B. T.; Wang, Y.; Li, B. J.; Yu, D. G.; Shi, Z. J. Biaryl Construction via Ni-Catalyzed C-O Activation of Phenolic Carboxylates. *J. Am. Chem. Soc.* **2008**, *130* (44), 14468–14470. https://doi.org/10.1021/ja8056503.

(139) Quasdorf, K. W.; Tian, X.; Garg, N. K. Cross-Coupling Reactions of Aryl Pivalates with Boronic Acids. *J. Am. Chem. Soc.* **2008**, *130* (44), 14422–14423. https://doi.org/10.1021/ja806244b.

(140) Dankwardt, J. W. Nickel-Catalyzed Cross-Coupling of Aryl Grignard Reagents with Aromatic Alkyl Ethers: An Efficient Synthesis of Unsymmetrical Biaryls. *Angew. Chem. Int. Ed.* **2004**, *43* (18), 2428–2432. https://doi.org/10.1002/anie.200453765.

(141) Takise, R.; Muto, K.; Yamaguchi, J. Cross-Coupling of Aromatic Esters and Amides. *Chem. Soc. Rev.* **2017**, *46* (19), 5864–5888. https://doi.org/10.1039/c7cs00182g.

(142) Cornella, J.; Zarate, C.; Martin, R. Metal-Catalyzed Activation of Ethers via C-O Bond Cleavage: A New Strategy for Molecular Diversity. *Chem. Soc. Rev.* **2014**, *43* (23), 8081–8097. https://doi.org/10.1039/c4cs00206g.

(143) Tamaki, T.; Nagata, M.; Ohashi, M.; Ogoshi, S. Synthesis and Reactivity of Six-Membered Oxa-Nickelacycles: A Ring-Opening Reaction of Cyclopropyl Ketones. *Chem. Eur. J.* **2009**, *15* (39), 10083–10091. https://doi.org/10.1002/chem.200900929.

(144) Liu, L.; Montgomery, J. Dimerization of Cyclopropyl Ketones and Crossed Reactions of Cyclopropyl Ketones with Enones as an Entry to Five-Membered Rings. *J. Am. Chem. Soc.* **2006**, *128* (16), 5348–5349. https://doi.org/10.1021/ja0602187.

(145) Ogoshi, S.; Nagata, M.; Kurosawa, H. Formation of Nickeladihydropyran by Oxidative Addition of Cyclopropyl Ketone. Key Intermediate in Nickel-Catalyzed Cycloaddition. *J. Am. Chem. Soc.* **2006**, *128* (16), 5350–5351. https://doi.org/10.1021/ja060220y.

(146) Gilbert, M. M.; Trenerry, M. J.; Longley, V. R.; Castro, A. J.; Berry, J. F.; Weix, D. J. Ligand-Metal Cooperation Enables Net Ring-Opening C-C Activation/Difunctionalization of Cyclopropyl Ketones. *ACS Catal.* **2023**, *13* (17), 11277–11290. https://doi.org/10.1021/acscatal.3c02643.

(147) Molinaro, C.; Jamison, T. F. Nickel-Catalyzed Reductive Coupling of Alkynes and Epoxides. *J. Am. Chem. Soc.* **2003**, *125* (27), 8076–8077. https://doi.org/10.1021/ja0361401.

(148) Nielsen, D. K.; Doyle, A. G. Nickel-Catalyzed Cross-Coupling of Styrenyl Epoxides with Boronic Acids. *Angew. Chem. Int. Ed.* **2011**, *50* (27), 6056–6059. https://doi.org/10.1002/anie.201101191.

(149) Erica L. Lanni; Anne J. McNeil. Mechanistic Studies on Ni(Dppe)Cl2-Catalyzed Chain-Growth Polymerizations: Evidence for Rate-Determining Reductive Elimination. *J. Am. Chem. Soc.* **2009**, *131* (45), 16573–16579. https://doi.org/10.1021/cr900041c.

(150) Kashin, A. S.; Ananikov, V. P. Catalytic C-C and C-Heteroatom Bond Formation Reactions: In Situ Generated or Preformed Catalysts? Complicated Mechanistic Picture behind Well-Known Experimental Procedures. *J. Org. Chem.* **2013**, *78* (22), 11117–11125. https://doi.org/10.1021/jo402038p.

(151) Dawson, G. A.; Lin, Q.; Neary, M. C.; Diao, T. Ligand Redox Activity of Organonickel Radical Complexes Governed by the Geometry. *J. Am. Chem. Soc.* **2023**, *145* (37), 20551–20561. https://doi.org/10.1021/jacs.3c07031.

(152) Ju, L.; Lin, Q.; LiBretto, N. J.; Wagner, C. L.; Hu, C. T.; Miller, J. T.; Diao, T. Reactivity of (Bi-Oxazoline)Organonickel Complexes and Revision of a Catalytic Mechanism. *J. Am. Chem. Soc.* **2021**, *143* (36), 14458–14463. https://doi.org/10.1021/jacs.1c07139.

Chapter 2: Nickel-photoredox catalysis enables amide *N*-arylation under mild conditions

2.1 Transition metal-catalyzed strategies for C-N cross-coupling of amides

Amides and other N-containing functional groups are ubiquitous in drugs, natural products, polymers, and biologically important macromolecules[1]. Out of the top 100 best-selling small molecule drugs of 2022, 91 contained at least one nitrogen atom, and 71 of these contained an amide functional group[2]. Because of the importance of amides and their derivatives, synthetic methods that form C-N bonds are an essential part of the synthetic chemist's toolkit. Generally, the methods used to form $C(sp^3)$-N bonds are different from those that are used to form $C(sp^2)$-N bonds. The formation of $C(sp^3)$-N bonds is relatively simple and usually does not require carefully designed transition metal catalysts. $C(sp^3)$-N bond formation can be achieved via robust and simple protocols such as reductive amination, S_N2 alkylation, and the Mitsunobu reaction[3]. Enantioselective processes to yield enantioenriched amides have also been developed[4].

In contrast, the formation of $C(sp^2)$-N bonds poses a greater synthetic challenge since these bonds cannot be accessed via reductive amination or S_N2 reactions. Additionally, nucleophilic aromatic substitution to form $C(sp^2)$-N bonds has poor functional group tolerance and a narrow scope[5]. Instead, transition metal catalysts are required to forge $C(sp^2)$-N bonds from primary or secondary amides

with broad scope and high efficiency. Transition metal-catalyzed $C(sp^2)$-N cross-coupling to form secondary or tertiary amides is most often achieved via the Pd-catalyzed Buchwald-Hartwig amination reaction **(Scheme 1a)**[1,6]. Cu-catalyzed cross-coupling to access $C(sp^2)$-N bonds in functionalized amides has been known for much longer but is less robust than Pd catalysis, often requiring stoichiometric Cu for good yields or suffering from biaryl formation[5,7,8]. Thermally-driven Ni-catalyzed $C(sp^2)$-N cross-coupling to generate aryl amides has also been reported by the Stradiotto group **(Scheme 1b)**[9], although this is a rare example of Ni-catalyzed amide arylation. These transition metal-catalyzed strategies all activate an aryl halide coupling partner via oxidative addition. This is followed by ligand substitution of the halide ligand on the metal aryl halide complex by the weakly nucleophilic amide, thus producing a metal aryl amido complex which is able to form the $C(sp^2)$-N cross-coupled product upon reductive elimination.

One drawback of these thermally-driven Pd, Cu, and Ni-catalyzed methods is that they require elevated temperatures to trigger the difficult reductive elimination to render the desired $C(sp^2)$-N amide bond[6]. As mentioned in Chapter 1.2, C-N reductive elimination from Ni(II), isoelectronic Cu(III), and Pd(II) all require elevated temperatures to overcome a high kinetic barrier[10]. This can be problematic for substrates that are unstable at elevated temperatures in the presence of strong bases (e.g. substrates bearing epimerizable stereocenters or functional groups that can undergo hydrolysis). What separates Ni from Pd and Cu is that it has access to an alternative and facile pathway to C-N reductive

elimination via open-shell Ni(III), enabling the bond-forming step to occur at ambient temperature[11]. This alternative low-temperature pathway to C-N reductive elimination is enabled by Ni having access to 1-electron redox processes and is supported by stoichiometric[11–14] and computational[10] experimental results. In this manner, a Ni(II) aryl amido catalytic intermediate can be oxidized to Ni(III) by a competent oxidant, whether it be via stoichiometric oxidants[11,14], photoredox catalysts[13,15], or electrochemical oxidation[16]. In some cases, a Ni(I/III) catalytic cycle can be promoted such that single-electron oxidation in each catalytic turnover can be avoided[13,17].

Ni-photoredox catalysis presents a powerful strategy for enabling mild $C(sp^2)$-N cross-coupling via highly reactive Ni(III) catalytic intermediates. Ni-photoredox-catalyzed amine arylation was first reported by the MacMillan group in 2016 [15]. This methodology was reported to be effective for arylating strong *N*-nucleophiles like alkylamines and anilines at unprecedented low temperatures. However, one notable weakness of this catalytic system was that it was less effective for arylating *N*-nucleophiles of low nucleophilicity such as amides, carbamates, and imides. A single example of sulfonamide arylation was provided in the report but required elevated temperature, a strong base, and DMSO in order to produce the aryl sulfonamide product. The lack of reported protocols for Ni-photoredox-catalyzed amide arylation under mild conditions intrigued our group, and so we sought to enable such a transformation **(Scheme 1c)**. Such a catalytic system would circumvent the need for high temperatures and strong bases that

are used in the well-precedented and thermally-driven Pd-, Cu-, and Ni-catalyzed amide arylation protocols **(Scheme 1a-b)**. Additionally, our envisioned reaction would complement the currently existing synthetic methodologies that can be used to access aryl amides since it would involve a retrosynthetic disconnection at the *N*-aryl bond instead of the *N*-carbonyl bond of the amide substrate. Most of the commonly employed methods to synthesize amides involve a retrosynthetic disconnection at the *N*-carbonyl bond, such as in the coupling of amines and carboxylic acids[18], nucleophilic acyl substitutions[19], rearrangements (e.g. Beckmann[20] and Favorskii[21]), and transamidations[22].

Scheme 1: Transition metal-catalyzed amide arylation

a) Cu- and Pd-catalyzed amide arylation

X = Br, I, OTf

b) Rare Ni-catalyzed amide arylation: Stradiotto (2016)

X = Cl, Br, I, OTf, OTs, etc.

up to 87% yield

c) This work: photocatalysis enables mild amide arylation conditions

up to 89% yield

dtbbpy
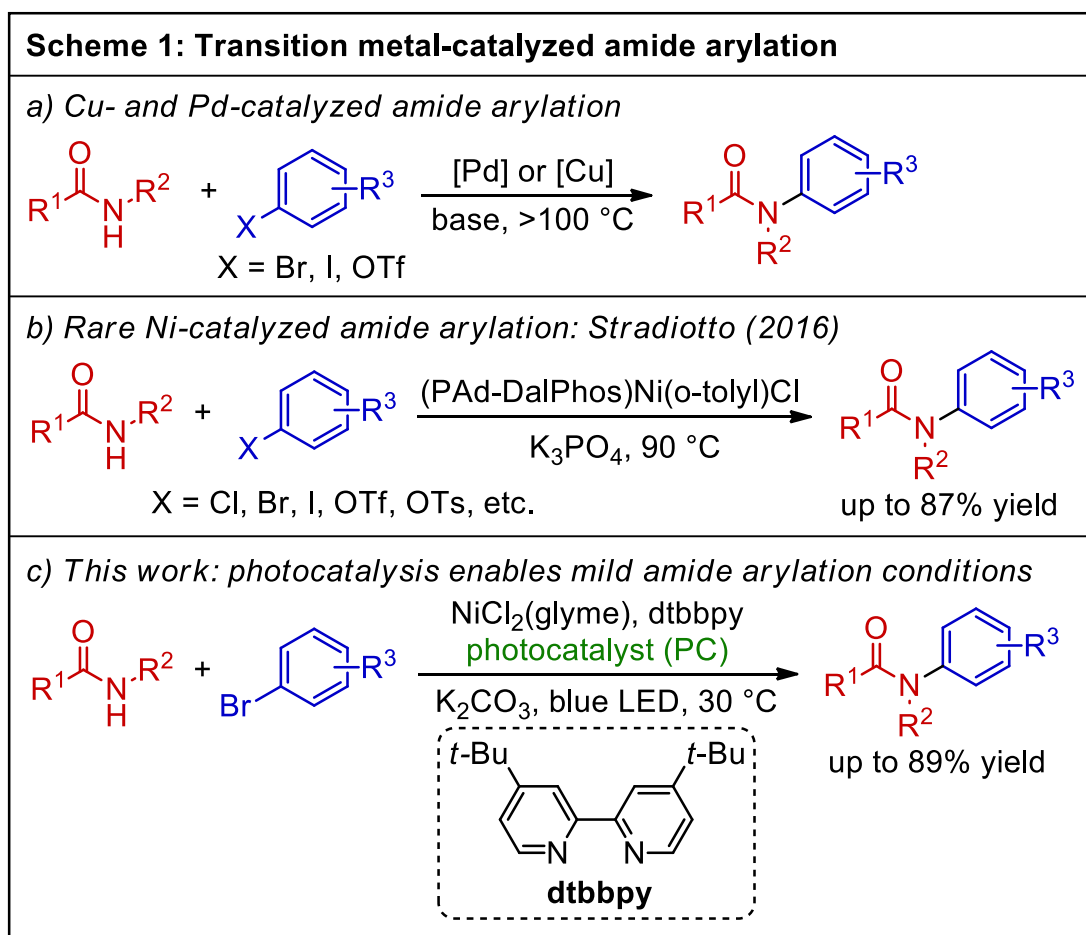
The difficulty of enabling amide arylation under mild conditions stems from the unique properties of the amide functional group. Amides can coordinate to transition metals via both their N and O atoms and readily form stable κ^2-amidate complexes that have been shown to inhibit reductive elimination[23]. Changes in oxidation state of ligated Ni complexes have also been shown to affect the coordination mode of amidate ligands[24]. The rate of reductive elimination from Pd complexes to form aryl amides was found to be accelerated when a bulkier ligand that promoted a κ^1-amidate coordination mode was employed[25]. Donation of the N atom's lone pair of electrons into the carbonyl leads to amides being much weaker nucleophiles than alkyl- and arylamines. This reduced nucleophilicity of amides can be responsible for very slow rates of reaction when they are chosen as nucleophilic substrates[26]. Another consequence of the dampened nucleophilicity of amides is that there can be competition with other weak nucleophiles that may be present in the reaction media such as trace water. In this manner, diminished yields of aryl amide products can sometimes be attributed to undesired phenol production via the cross-coupling of water with the aryl halide substrate[27,28]. This problem is compounded by the fact that many amides are hygroscopic and only soluble in polar aprotic or protic solvents[23], and these solvents are often hygroscopic and water-miscible. The formation of phenol is not a concern for cross-coupling alkyl- and arylamines because they are much more nucleophilic than water, leading to negligible competition.

The limited solubility of many amides in nonpolar solvents also complicates the development of cross-coupling reactions that involve amides, since the reaction solvent must be compatible with the catalyst system and also accommodate the limited solubility of the amide substrate. Polar aprotic solvents are often required to dissolve amides at ambient temperature, limiting the number of solvents that can be screened in a mild cross-coupling reaction involving these poorly soluble nucleophiles. Polar aprotic solvents often coordinate to transition metals, which may disrupt catalysis. Additionally, the transition metal catalyst(s), aryl halide coupling partners, and other reaction components may have very different solubility profiles than the highly polar amides, making it a challenge to find a suitable solvent or solvent combination to enable the desired cross-coupling reaction.

Another challenge in enabling a mild Ni-photoredox amide arylation protocol is that all previously reported Ni-photoredox C-N coupling strategies are limited by the need for a strong organic base like DABCO or TMG to act as an electron shuttle between the photocatalyst (PC) and reaction intermediates[13]. These conditions are incompatible with base-sensitive substrates and can lead to undesired side reactivity occurring due to the propensity of these bases to facilitate hydrogen atom transfer when oxidized[29–31]. Herein, a Ni-photoredox catalyst system is used to promote amide arylation with a broad scope of coupling partners under mild temperatures and without a strong, redox-active base.

2.2 Initial results of Ni-photoredox-catalyzed amide arylation and optimization

The successful Ni-photoredox cross-coupling of amides and aryl bromides was first observed in the reaction between 2-pyrrolidone (**1r**) and methyl 4-bromobenzoate (**2a**), which was chosen as a model system to study this reactivity. Upon receiving a gratifying initial result of low conversion to the desired aryl amide **(Table 1, entry 1)**, control reactions were run to determine if all of the reaction components were necessary. When the photocatalyst was omitted but irradiation was maintained, the reaction did not proceed **(Table 1, entry 2)**. When the Ni catalyst and ligand were omitted, the reaction did not proceed **(Table 1, entry 3)**. When the reaction was thoroughly protected from light but contained all of the reaction components, the reaction did not proceed **(Table 1, entry 4)**. Replacing the aryl bromide with the analogous aryl chloride led to greatly diminished yields **(Table 1, entry 5)**.

Table 1: Initial hit and reaction controls

Entry	Altered conditions	X =	Yield (%)
1	none	Br	22
2	no **PC2**	Br	0
3	no NiCl$_2$(glyme) or dtbbpy	Br	0
4	fully protected from light	Br	0
5	none	Cl	5

Solvent selection proved to be particularly crucial in order for cross-coupling to be observed. Trace or low conversion to product was observed in most of the solvents tested. The best yields were initially obtained in dimethylformamide (DMF) **(Table 2, entry 4)**. Despite this encouraging result, it was soon identified that these reactions also led to substantial formation of the debrominated phenol side product, methyl 4-hydroxybenzoate, with ~25% conversion. Attempts to limit the cross-coupling of water by using molecular sieves as an additive or by using rigorously dried glassware did not succeed and the phenol was still observed.

Table 2: Optimization of solvent and reaction temperature

Entry	Solvent	Temp. (°C)	Yield (%)
1	MeOH	rt	11
2	MeCN	rt	39
3	$PhCF_3$	rt	< 5
4	DMF	rt	45
5	3:1 $PhCF_3$:DMF	rt	62
6	3:1 $PhCF_3$:DMF	10	26
7	3:1 $PhCF_3$:DMF	20	57
8	3:1 $PhCF_3$:DMF	30	79

A solution to the problem was found by using a combination of DMF and $PhCF_3$ as the solvent **(Table 2, entry 5)**. The solvent combination led to substantially higher yields of aryl amide than with either solvent alone, and it lowered conversion to undesired phenol to only ~10%. Notably, only trace aryl amide product was observed when $PhCF_3$ was used by itself **(Table 2, entry 3)**, owing to the poor solubility of benzamide in this solvent. We hypothesized that the beneficial effect of the presence of $PhCF_3$ in the solvent combination with DMF could be explained by a known phenomenon in which coordination of Ni to a π-acidic, electron-poor arene increases the rate of reductive elimination[32]. Interestingly, optimal ratios of $PhCF_3$ to DMF varied by substrate. For instance, the

reaction between 4-cyanobenzamide and methyl 4-bromobenzoate proceeded with highest yield with a 1:1 ratio of PhCF$_3$ to DMF, whereas the analogous reaction with benzamide gave the highest yield when the solvent ratio was 3:1 PhCF$_3$ to DMF **(Table 3)**. This difference is likely due to the increased polarity of 4-cyanobenzamide and its reduced solubility in nonpolar solvents.

Table 3: Optimal solvent ratio varies with substrate polarity

Entry	Solvent	R=	Yield (%)
1	3:1 PhCF$_3$:DMF	H	79
2	2:1 PhCF$_3$:DMF	H	49
3	3:1 PhCF$_3$:DMF	CN	43
4	2:1 PhCF$_3$:DMF	CN	61
5	1:1 PhCF$_3$:DMF	CN	65

Reaction temperature also had a significant effect on yield, with lower yields obtained at temperatures lower than ambient temperature **(Table 2, entries 5-8)**. The greatest yields were achieved when the reaction was maintained at 30 °C under gentle heating **(Table 2, entry 8)**. Temperatures higher than 30 °C produced equivalent or inferior yields. A temperature-controlled water bath was necessary to ensure that yields were reproducible, since the reaction is sensitive to subtle changes in temperature and different reaction vessels may be heated to different degrees by the incident blue light. Additionally, the fans commonly used in

photoredox setups were found to be unsuitable for reproducibly maintaining a constant reaction temperature.

Table 4: Optimization of base

Entry	Solvent	Base	Yield (%)
1	3:1 $PhCF_3$:DMF	Na_2CO_3	30
2	3:1 $PhCF_3$:DMF	$KHCO_3$	52
3	3:1 $PhCF_3$:DMF	dry K_3PO_4	64
4	3:1 $PhCF_3$:DMF	K_3PO_4 (not dried)	70
5	3:1 $PhCF_3$:DMF	K_2CO_3	79
6	3:1 $PhCF_3$:DMF	TMG	61
7	3:1 $PhCF_3$:DMF	$Na_3PO_4 \cdot 12H_2O$	<5
8[a]	$PhCF_3$	$Na_3PO_4 \cdot 12H_2O$	69[b]

[a] 2-pyrrolidone **(1p)** used instead of benzamide **(1a)**
[b] yield of aryl amide **3p**

Identification of a suitably mild base was necessary in order to identify a Ni-photoredox system that could cross-couple base-sensitive substrates. To the best of our knowledge, all Ni-photoredox methods yet reported that form C-N bonds via reductive elimination from Ni(III) call for a strong, redox-noninnocent base. This difference will be discussed further in Chapter 3. Fortunately, K_2CO_3 **(Table 4, entry 5)** was identified as a suitable base for the Ni-photoredox amide arylation

reaction, outperforming a variety of other weak inorganic bases **(Table 4, entries 1-4, 7)**. Strong organic bases that are able to facilitate electron transfer processes, such as TMG, were also suitable for this transformation, although they were inferior to K_2CO_3 in terms of yield **(Table 4, entry 6)**.
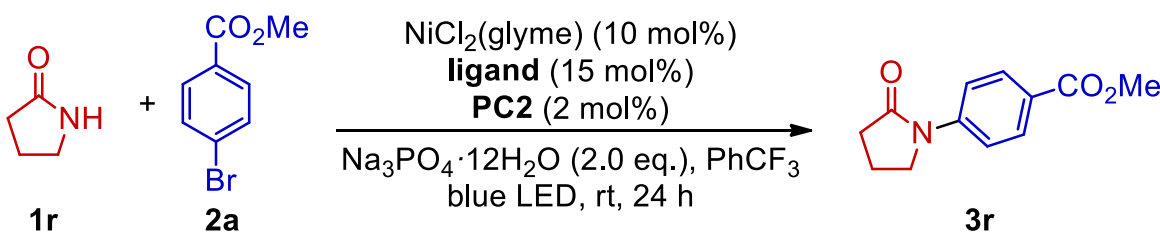
K_3PO_4 was another inorganic base that was effective at enabling the reaction. Interestingly, K_3PO_4 that was thoroughly dried overnight at 150 °C was effective for the amide coupling reaction and avoided the formation of phenol side product **(Table 4, entry 3)**. When K_3PO_4 was used from the bottle without being dried, the yield of the aryl amide increased to 70% despite an additional ~15% conversion to phenol **(Table 4, entry 4)**. K_2CO_3 still produced higher yields of aryl amide despite consistently forming the phenol in ~10% conversion. Notably, even if K_2CO_3 is dried, it still produces water upon reacting with an acidic proton. The phenol becomes the dominant product when $Na_3PO_4 \cdot 12H_2O$ is employed, with only trace conversion to the aryl amide observed **(Table 4, entry 7)**. However, when DMF is removed from the system and an amide substrate that is soluble in $PhCF_3$ is chosen, the desired amide arylation reaction is restored and phenol formation is no longer observed. Aryl amide **(3r)** was obtained in 69% yield when employing 2-pyrrolidone **(1r)**, $Na_3PO_4 \cdot 12H_2O$, and $PhCF_3$ as the only solvent **(Table 4, entry 8)** with only trace conversion to phenol. These results suggest that a small amount of water may be beneficial to the reaction despite the occurrence of phenol side products. However, this comes at the cost of the formation of the

pesky phenol side product, although it can easily be removed by basic extraction or flash chromatography.

Table 5: Optimization of photocatalyst

Entry	Photocatalyst	Yield (%)
1	4CzIPN	13
2	Ir(ppy)$_3$	<5
3	Ir(ppy)$_2$(bpy)PF$_6$	<5
4	Ir(dF(CF$_3$)ppy)$_2$(bpy)PF$_6$	0
5	Ru(bpy)$_3$(PF$_6$)$_2$	0
6	Ir(ppy)$_2$(dtbbpy)PF$_6$ **(PC1)**	79
7	Ir(dF(CF$_3$)ppy)$_2$(dtbbpy)PF$_6$ **(PC2)**	33

Optimization of the photocatalyst revealed that a variety of commonly used Ir, Ru, and organic photocatalysts led to no product formation or no more than 1 catalytic turnover **(Table 5, entries 1-5)**. However, two Ir photocatalysts: **PC1 (Table 5, entry 6)** and **PC2 (Table 5, entry 7)**, were found to enable catalytic turnover and forge the aryl amide product in greater yields. We observed that **PC2** produced diminished yields of the aryl amide product due to a competitive side reaction in which the DMF solvent was undergoing C(sp$_3$)-H activation and subsequent arylation (presumably via HAT by Cl radicals generated from Ni-Cl

photolysis, a well-studied process[33,34]). **PC1** did not suffer from the same side reaction, presumably because it is less oxidizing ($E_{1/2}(M^*/M^-)$ = +0.66 V vs. SCE in MeCN) than **PC2** ($E_{1/2}(M^*/M^-)$ = +1.21 V vs. SCE in MeCN)[35] and thus unable to promote the side reaction with the solvent. These results provided us with the important insight that using a more strongly oxidizing photocatalyst is not always preferable, since a more weakly oxidizing photocatalyst may be able to enable the desired reaction while avoiding unwanted side reactions that occur at higher potentials.
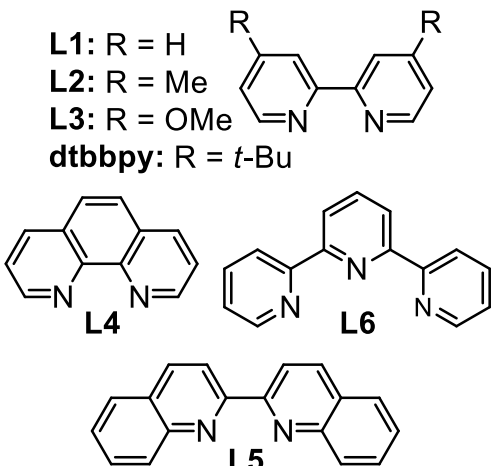
Table 6: Ligand optimization

Entry	Ligand	Yield (%)
1	bpy (**L1**)	10
2	4,4'-dimethyl-bpy (**L2**)	8
3	4,4'-dimethoxy-bpy (**L3**)	8
4	phenanthroline (**L4**)	12
5	biQuin (**L5**)	<5
6	terpyridine (**L6**)	<5
7	**dtbbpy**	69
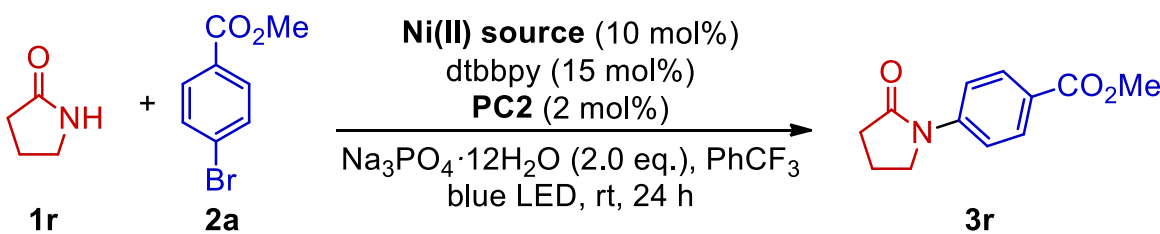
L1: R = H
L2: R = Me
L3: R = OMe
dtbbpy: R = *t*-Bu

A selection of bipyridine derivatives were screened as ligands for the amide arylation reaction, although all but one of these ligands produced yields that were no greater than 1 catalytic turnover **(Table 6, entries 1-6)**. 4,4'-di-*tert*-butylbipyridine (dtbbpy) greatly exceeded the performance of the other ligands, forming the desired product in 69% yield **(Table 6, entry 7)**. The observation that even a subtle change in the ligand structure leads to a near complete loss in reactivity is an example of how Ni catalysis is sensitive to subtle changes in ligand identity.

Table 7: Optimization of Ni(II) source

Entry	Ligand	Yield (%)
1	NiBr$_2$(glyme)	5
2	NiCl$_2$(glyme)	69
3	NiCl$_2$·6H$_2$O	7
4	Ni(OAc)$_2$·4H$_2$O	13
5	NiSO$_4$·6H$_2$O	0
6	Ni(NO$_3$)$_2$·6H$_2$O	8
7	Ni(II) cyclohexanebutyrate	61

The reaction was also highly particular regarding the identity of the Ni(II) precatalyst. Intriguingly, employment of NiBr$_2$(glyme) **(Table 7, entry 1)** in place of NiCl$_2$(glyme) **(Table 7, entry 2)** led to a near complete loss of reactivity despite the

subtle change in halide identity. Most other Ni salts screened led to very poor product yields with one catalytic turnover or less **(Table 7, entries 3-6)**, likely complicated by their reduced solubility and presence of hydrates. Apart from NiCl$_2$(glyme), Ni(II) cyclohexanebutyrate was the only Ni(II) source that formed the aryl amide product with moderate yield **(Table 7, entry 5)**, possibly due to it being anhydrous and highly soluble in PhCF$_3$.

2.3 Substrate scope

With the optimized reaction conditions in hand, the arylation of a diverse array of amides was tested **(Figure 1)**. Since amide solubility varies greatly between substrates, the ratio of PhCF$_3$ to DMF affected the conversion of each substrate differently. Use of either solvent alone almost always led to a significant decrease in yield, except for *tert*-butylcarbamate **(3t)**. Moderate to high yields were obtained for electron-poor benzamides **(3a-c)**. The reaction forming aryl amide product **3a** was subjected to a 10x scale-up experiment (scalability is often a concern with photochemistry). Fortunately, 74% of the aryl amide product was obtained, a loss of only 5% yield compared to the smaller scale reaction. Low to moderate yields were obtained for the more electron-rich benzamides **(3d-f)**. The higher yields obtained with electron-poor amides may be explained by their enhanced acidity, facilitating ligand exchange to form the nickel-amido catalytic intermediate that is prerequisite to produce C-N cross-coupling. In addition to aromatic amides, the reaction tolerates aliphatic primary amides, yielding the

44

corresponding *N*-aryl amides with good yields **(3g-I)**. Amides with steric bulk adjacent to the carbonyl were able to undergo *N*-arylation **(3j-I)**. A *Z*-olefin tethered to a primary amide could have its configuration preserved while arylating the amide under the mild conditions **(3h)**. Unprotected phenols can be preserved with selective arylation of primary amides **(3e)**. Gratifyingly, a variety of *N*-, *O*-, and *S*-heterocycles **(3l-o)** were tolerated, furnishing the desired aryl amides in good yields.

To further investigate the tolerance of base-sensitive functional groups (which remain a challenge for other amide functionalization strategies), enantioenriched *N*-Boc-protected glutamine *tert*-butyl ester, which contains an epimerizable stereocenter, was tested as a substrate. We were delighted to isolate the expected aryl amide **(3p)** in moderate yield, and it was determined through chiral supercritical fluid chromatography that there was no quantifiable erosion of enantiomeric excess when compared to the starting material. This result highlights the mildness of this procedure and its potential application for derivatizing bioactive molecules.

Moving beyond primary amides, cyclic secondary amides were also suitable substrates for the reaction and were arylated in good yields **(3q-r)**. The tolerance of this protocol to cyclic secondary amides that bear $C(sp^3)$-H bonds adjacent to the amide N atom is especially interesting because C-H arylation at this position occurs under very similar Ni-photoredox conditions[36]. Luckily, the reaction conditions did not lead to the competitive formation of C-H arylated products on

these secondary amide substrates. The cross-coupling reaction was unsuccessful for most of the acyclic secondary amides tested **(3x-z)**. Acetanilide was the only acyclic secondary amide that formed the arylated product with low yield **(3w)**.

Figure 1: Amide scope

Reaction scheme: **1** + **2a** (4-bromomethyl benzoate with CO$_2$Me) → **3**

Conditions: NiCl$_2$(glyme) (10 mol%), dtbbpy (15 mol%), **PC1** (2 mol%), K$_2$CO$_3$ (2.0 eq.), 3:1 PhCF$_3$:DMF, blue LED, 30 °C, 24 h

Primary amides

3a, 79%

R = CN; **3b**, 65%[a]
R = CF$_3$; **3c**, 63%[a]

3d, 53%[a]

R = H; **3e**, 64%
R = Me; **3f**, 42%[a]

3g, 64%

3h, 60%

3i, 66%

3j, 68%

X = CH$_2$; **3k**, 53%[a]
X = NBoc; **3l**, 58%

3m, 78%

X = O; **3n**, 77%
X = S; **3o**, 72%

tolerance of epimerizable centers

3p, 58%, > 99% es[b,c]

Secondary amides and other nitrogenated groups

n = 1; **3q**, 63%
n = 2; **3r**, 72%

3s, 72%

R = Boc; **3t**, 58%[c,d,e]
R = Ts; **3u**, 74%

3v, 89%

Secondary acyclic amides

R^1 = Me; **R^2** = Ph; **3w**, 20%
R^1 = Ph; **R^2** = Ph; **3x**, 0%
R^1 = Me; **R^2** = Me; **3y**, 0%
R^1 = Ph; **R^2** = Me; **3z**, 0%

Substrates with undesired regioselectivity

3aa, 0%[f]

3ab, 0%[f]

3ac, 0%[g]

[a] 1:1 PhCF$_3$:DMF as solvent.
[b] 10:1 PhCF3:DMF as solvent.
[c] Stirred for 48 h.
[d] PhCF$_3$ as solvent.
[e] At 40 °C.
[f] Formed the *O*-arylation product.
[g] Formed the aniline arylation product.
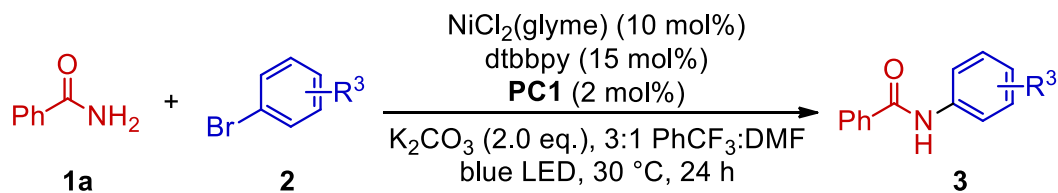
A variety of weak *N*-nucleophiles related to amides such as phthalimide **(3s)**, Boc carbamate **(3t)**, *p*-toluenesulfonamide **(3u)**, and trifluoroacetamide **(3v)** were also able to undergo *N*-arylation with the Ni-photoredox reaction conditions. This methodology provides a route to protected anilines from aryl halides **(3s-u)**. Despite tolerating a broad range of weak *N*-nucleophiles, the reaction occasionally led to O-arylation instead of *N*-arylation when a nucleophilic N and O atom were both present, as was observed with 2-pyridone **(3aa)** and (+/-)-mandelamide **(3ab)**. If both a nucleophilic aniline and primary amide are present in the substrate, the aniline N atom selectively undergoes arylation **(3ac)**.

The reaction also tolerated a variety of substituted (hetero)aryl bromides as electrophilic coupling partners **(Figure 2)**. Electron-poor aryl bromides performed best under the reaction conditions, rendering the aryl amide products in high yields **(3a, 3ad-ah)**. Electron-neutral and electron-rich aryl bromides were also tolerated but were found to require slightly elevated temperatures and longer reaction times to form the aryl amide products in low to good yields **(3ai-ap)**. This behavior is consistent with other literature reports that demonstrate slower rates of oxidative addition for electron-rich aryl halides[37]. A sterically demanding *ortho*-substituted aryl bromide was also cross-coupled with good yield **(3an)**, although longer reaction times were required (likely due to a slower rate of oxidative addition, as has been observed previously[37]). Heteroaryl bromides were also cross-coupled in low to moderate yields **(3aq-as)**, although the cross-coupling was complicated by the presence of coordinating heteroatoms which can bind to the Ni center.

Figure 2: Aryl bromide scope

Ph(C=O)NH₂ (**1a**) + Br–aryl–R³ (**2**)

NiCl₂(glyme) (10 mol%)
dtbbpy (15 mol%)
PC1 (2 mol%)

K₂CO₃ (2.0 eq.), 3:1 PhCF₃:DMF
blue LED, 30 °C, 24 h

→ Ph(C=O)NH–aryl–R³ (**3**)

Successful substrates

3a, 79% — CO₂Me

3ad, 89%[a,b] — COPh

3ae, 69% — CF₃

3af, 81%[a,b] — CF₃

3ag, 69% — CN

3ah, 61%[b,c] — Cl

3ai, 40%[d,e] — F

3aj, 65%[a,b] — H

3ak, 66%[c,d] — Me

3al, 66%[c,d] — n-Pn

3am, 78%[c,d] — Me, Me

3an, 76%[d,f] — Me

3ao, 44%[d,f] — OMe

3ap, 38%[d,f] — OMe, OMe

3aq, 33%[d,e] — pyridin-2-yl

3ar, 66%[a,b] — pyridin-3-yl

3as, 17%[a,b] — pyrimidin-5-yl

3at, 29%[a,b] — vinyl

3au, 50%[a,b] (30:70 E/Z) — CH=CH–Ph

3av, 0%[a,b] — furan-3-yl

Failed substrates

3aw, 0%[a,b,g] — B(OH)₂

3ax, 0% — C₆F₅ (pentafluorophenyl)

3ay, 0%[a,b] — OCH₂CH₂-pyrrolidine

[a] Stirred for 48 h.   [c] Stirred for 4 d.   [e] Stirred for 5 d.   [g] Formed the protodeborylated product, **3aj**.
[b] At 40 °C.   [d] At 50 °C.   [f] Stirred for 7 d.

49

Another interesting observation was that when 4-chlorobromobenzene was used as the aryl halide coupling partner, the bromide was selectively functionalized and the chloride was retained, forming **3ah**. This is also despite a 2:1 stoichiometry of amide to aryl halide used in the reaction. Such selectivity could be synthetically useful if the aryl chloride were to be functionalized in a subsequent cross-coupling step. Electron-rich styrenes could also be formed with the cross-coupling methodology, although these products were very unstable **(3at)**. The reaction also tolerates vinyl bromides, forming the product **3au** in 50% yield with a 30:70 ratio of *E*/*Z* diastereomers despite the starting β-bromostyrene having an 87:13 ratio of *E*/*Z* diastereomers. This indicates that the reaction system preferentially isomerizes *E*-olefins to *Z*-olefins, which agrees with the complete stereoretention of the *Z*-isomer observed in product **3h**. When attempting to cross-coupling an arene with both bromide and boronic acid functional groups, the aryl amide product was formed, however the boronic acid group underwent protodeborylation, forming **3aj** instead of the desired **3aw**. Extremely electron-rich **(3av)** or extremely electron-poor **(3ax)** aryl bromides were not tolerated, in addition to unprotected tertiary alkylamines **(3ay)**.

2.4   Initial mechanistic hypothesis

At this point in our investigation of this mild Ni-photoredox amide arylation chemistry, we had few results to base our mechanistic hypotheses on, although literature precedent suggested the necessity of access to Ni(III) for mild C-N bond

formation, as discussed in Chapter 2.1. Our initial mechanistic hypothesis was that in situ-generated Ni(0) **I** would undergo oxidative

Figure 3: Mechanistic proposal before in-depth study
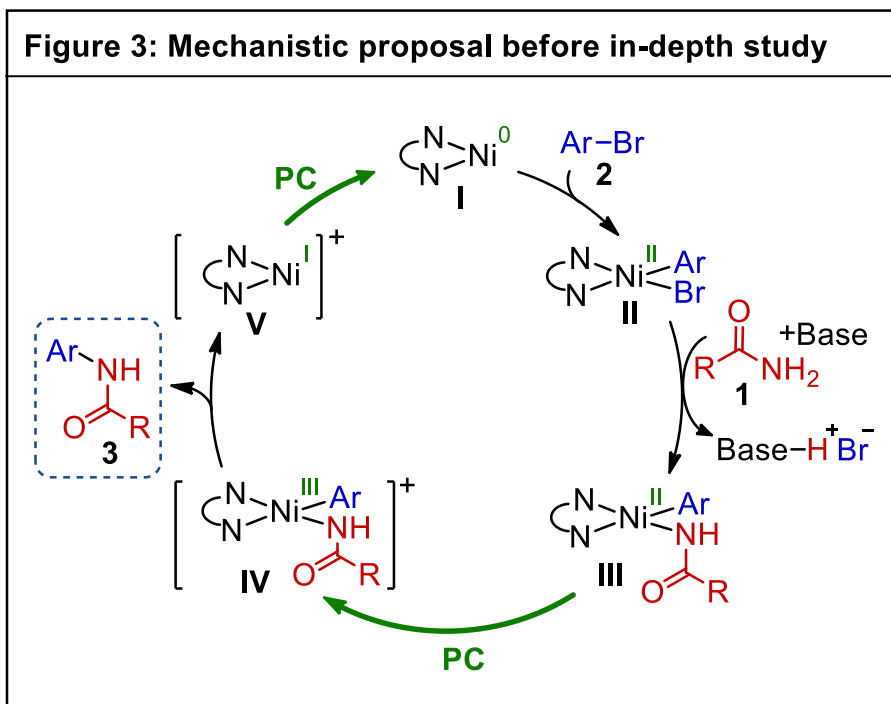
addition with aryl halide **(2)** to form Ni(II) oxidative adduct **II**. Because K_2CO_3 is not sufficiently basic to directly deprotonate amides, amide **(1)** coordination to the Ni center likely occurs before deprotonation to produce catalytic intermediate **III**. This Ni(II) aryl amido complex can then be oxidized to Ni(III) intermediate **IV** via photoinduced electron transfer to an excited photocatalyst. This unstable Ni(III) intermediate would undergo rapid reductive elimination to generate the $C(sp^2)$-N cross-coupling product **(3)**. Lastly, both the Ni catalyst and photocatalyst are regenerated upon electron transfer from the reduced photocatalyst to Ni(I) intermediate **V**, regenerating **I**.

In an initial attempt to challenge this hypothesis, we considered that reductive elimination could instead occur from a putative ground-state Ni(II) aryl amido complex. Testing this hypothesis was simple since the necessary control

experiments were performed when the transformation was first observed by our group. Because no reactivity was observed in the absence of either light or photocatalyst, oxidative addition from ground-state Ni(II) was unlikely. Additionally, the reaction did not proceed in the absence of Ni catalyst, or in the absence of both Ni and photocatalyst. It is worth noting that reductive elimination from an excited-state Ni(II) aryl amido complex in an energy transfer-mediated process could not be ruled out at this point, although the fact that the reaction did not proceed in the absence of photocatalyst under both 390 and 427 nm irradiation is weak evidence against an energy transfer (EnT) mechanism. The necessity of both photocatalyst and light suggested that a photoinduced electron transfer event was occurring in the catalytic cycle[38].

Because of the drastic differences in properties between strong and weak *N*-nucleophiles, we considered the possibility of alternative mechanisms for the Ni-photoredox-catalyzed arylation of weak *N*-nucleophiles. Chapter 3 of this thesis will describe a much more in-depth investigation of the mechanism of this reaction in which we interrogate our mechanistic hypothesis against alternative pathways.

2.5   Conclusion

In summary, we have developed a methodology for amide arylation which is effective at ambient temperature and avoids the use of redox-active or strong bases. A wide scope is enabled by these mild reaction conditions, which allows for the tolerance of a variety of base-sensitive functional groups like phenols and

epimerizable stereocenters. Notable weaknesses of this methodology include the long reaction times required with electron-rich aryl bromides and the lack of reactivity observed with most acyclic secondary amides, although these could potentially be overcome by future efforts to identify more reactive forms of nickel or specialized ligands that enable these transformations. The use of Ir, one of the least abundant elements in the Earth's crust, as a photocatalyst is another weakness since it negates the benefits of using an Earth-abundant metal like Ni. Identification of a suitable organic photocatalyst could greatly reduce the overall cost and environmental impact of this chemistry.

Despite these weaknesses, our publication of this work represents the first example of Ni-catalyzed amide arylation at ambient temperature and with a weak base. This study shows how Ni-photoredox catalysis can be used to overcome the low nucleophilicity of the amide functional group by accelerating the elusive C–N reductive elimination step.

2.6   Experimental section

2.6.1 Synthesis of (*S*)- and (*R*)-Boc-Gln-O*t*-Bu (1p):
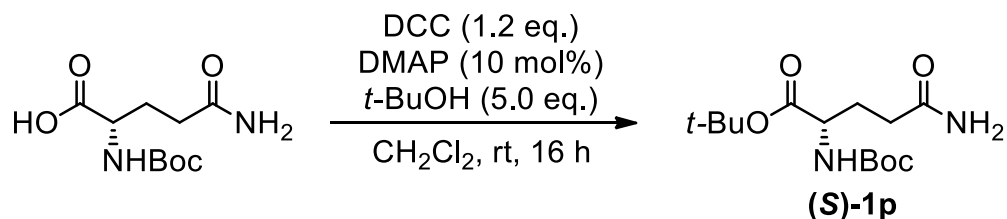
A modified procedure to achieve a Steglich esterification was followed.[39] A 50 mL round-bottom flask was charged with a stir bar and oven dried. The round-

bottom flask was taken out of the oven, evacuated, and backfilled with nitrogen gas. Once the reaction vessel was cooled to room temperature, Boc-Gln-OH (739 mg, 3.0 mmol) of the desired enantiomer was added under constant nitrogen efflux. 1.42 mL (15 mmol) of dry *t*-butanol was injected, followed by 12 mL of dichloromethane. Once the Boc-Gln-OH was fully dissolved, 4-dimethylaminopyridine (37 mg, 0.30 mmol) and *N,N'*-dicyclohexylcarbodiimide (743 mg, 3.6 mmol) were added under constant nitrogen efflux. The reaction was stirred for 16 hours at room temperature under nitrogen pressure. After the reaction was complete, the crude mixture was filtered through a Büchner funnel. The solid *N,N'*-dicyclohexylurea that collected on top of the filter paper was rinsed with an additional 20 mL of dichloromethane, and the filtrate was collected and evaporated onto silica in order to dry load a flash column. The product **((S)-1p)** was isolated by flash column chromatography (silica, 25% acetone in dichloromethane) as a white solid (461 mg, 51% yield); **R**$_f$ = 0.21 (25% acetone in dichloromethane). **^{1}H NMR** (400 MHz, CDCl$_3$) δ 6.38 (bs, 1H), 5.47 (bs, 1H), 5.27 (bd, *J* = 7.8 Hz, 1H), 4.24 – 4.14 (bm, 1H), 2.40 – 2.24 (m, 2H), 2.21 – 2.14 (m, 1H), 1.92 – 1.81 (m, 1H), 1.46 (s, 9H), 1.44 (s, 9H). **^{13}C NMR** (101 MHz, CDCl$_3$) δ 174.8, 171.5, 156.2, 82.6, 80.2, 53.5, 32.2, 29.8, 28.4, 28.1. **HRMS** (ESI-TOF) *m/z* calculated for C$_{14}$H$_{26}$N$_2$O$_5$ (M)$^+$: 302.1842, found 302.1838. **Melting point:** 109-111 °C. For **(S)-1p** 82:19 er determined by analytical SFC, Trefoil™ CEL1 column, 40 °C, MeOH:CO$_2$ = 3:97, 1.5 mL/min, t$_R$ (major): 14.19 min, t$_R$ (minor): 12.77 min; **[α]$_D^{20}$**

= + 21 ± 2 (c = 0.02155 g/mL, MeCN). Refer to the characterization entry for aryl amide product **3p** for chiral separation chromatograms (Chapter 2.6.3).

2.6.2 Amide arylation general procedure:

N-*Arylation of amides (general procedure A):*

A 10 mL Schlenk tube was charged with a magnetic stir bar and capped with a 14/20 ground glass stopper. The reaction vessel was evacuated and dried with a heat gun for 5 minutes, then the vessel was refilled with nitrogen gas. Solid reagents were then added to the Schlenk tube through a weighing paper cone while constant efflux of nitrogen gas maintained inert conditions in the reaction vessel. The Schlenk tube was charged with 4,4'-di-*tert*-butyl-2,2'-dipyridyl (8.1 mg, 0.03 mmol), Ir(dtbbpy)(ppy)$_2$PF$_6$ (3.7 mg, 0.004 mmol), NiCl$_2$(glyme) (4.4 mg, 0.02 mmol), K$_2$CO$_3$ (55 mg, 0.4 mmol), aryl bromide **2** (0.2 mmol), and amide **1** (0.4 mmol). After the addition of the solids, the reaction vessel was evacuated and refilled with nitrogen gas 3 times. 1.0 mL of solvent was added to the reaction vessel under constant efflux of nitrogen gas. The ground glass stopper was coated in vacuum grease before sealing the reaction vessel, and the stopper was subsequently wrapped in parafilm. The reaction vessel was placed 1 inch in front of a 427 nm Kessil LED lamp while being submerged in a temperature-controlled water bath in a crystallizing dish held at a constant 30 °C (unless specified otherwise). The reaction was stirred at 450 rpm.

After 24 hours (unless specified otherwise), the lamp was shut off and the reaction vessel was removed from the water bath. The crude reaction mixture was filtered through a short celite plug using acetone (unless specified otherwise). The crude filtrate was evaporated and subsequently redissolved in methylene chloride. 2-3 mL of silica were added to this methylene chloride solution, and the suspension was slowly evaporated at <100 rpm until dryness to adsorb the crude material onto the silica. The crude material adsorbed onto silica was used to dry load a flash chromatography column in order to isolate the aryl amide product Pure hexanes were used both for making the silica slurry and as the initial mobile phase to prevent the product from diffusing into the eluent during dry loading. An eluent specific to each substrate was used to elute the product.

N-*Arylation of amides (general procedure B, for oily or sticky amide substrates):*

A 10 mL Schlenk tube was tared on a scale, then charged with amide **1** (0.4 mmol). The reaction vessel was charged with a stir bar and capped with a 14/20 ground glass stopper. The reaction vessel was not dried with a heat gun. Next, the reaction vessel was evacuated and refilled with nitrogen gas. The solvent was added to the reaction vessel under constant efflux of nitrogen gas. Solid reagents were then added to the Schlenk tube through a weighing paper cone while constant efflux of nitrogen gas maintained inert conditions in the reaction vessel. The Schlenk tube was charged with 4,4'-di-*tert*-butyl-2,2'-dipyridyl (8.1 mg, 0.03 mmol), Ir(dtbbpy)(ppy)$_2$PF$_6$ (3.7 mg, 0.004 mmol), NiCl$_2$(glyme) (4.4 mg, 0.02

mmol), K$_2$CO$_3$ (55 mg, 0.4 mmol), and aryl bromide **2** (0.2 mmol). The ground glass stopper was coated in vacuum grease before sealing the reaction vessel, and the stopper was subsequently wrapped in parafilm. The reaction vessel was placed 1 inch in front of a 427 nm Kessil LED lamp while being submerged in a temperature-controlled water bath in a crystallizing dish held at a constant 30 °C (unless specified otherwise). The reaction was stirred at 450 rpm. The workup and column chromatography were performed in the same manner as in general procedure A.

General extraction procedure:

The purified amide containing phenol side product was extracted with 20 mL of EtOAc and 20 mL of 5% sat. NaOH. The organic layer was washed with 20 mL of sat. NH$_4$Cl and dried over Na$_2$SO$_4$. The dried organic layer was evaporated to afford the aryl amide product free of phenol impurity.

2.6.3 Characterization:

Amide scope:

methyl 4-benzamidobenzoate (3a)
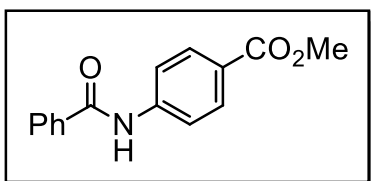
Following general procedure A, benzamide (**1a**, 48.5 mg, 0.4 mmol) and methyl 4-bromobenzoate (**2a**, 43.0 mg, 0.2 mmol) were employed using 3:1 PhCF$_3$:DMF as solvent. Purification of the residue by flash chromatography (silica, 30% EtOAc in hexanes) afforded a mixture of **3a** and methyl 4-hydroxybenzoate;

R_f = 0.40 (30% EtOAc in hexanes). The general extraction procedure was followed to afford **3a** (40.4 mg, 79% yield) as a white solid.

This reaction was also conducted at a 2 mmol scale. The same procedure was followed to afford **3a** (40.4 mg, 74% yield) as a white solid.

¹H NMR (400 MHz, CDCl₃): δ 8.20 (bs, 1H), 8.03 (d, *J* = 8.8 Hz, 2H), 7.86 (d, *J* = 7.5 Hz, 2H), 7.75 (d, *J* = 8.8 Hz, 2H), 7.55 (t, *J* = 7.5 Hz, 1H), 7.46 (t, *J* = 7.5 Hz, 2H), 3.90 (s, 3H). **¹³C NMR** (101 MHz, CDCl₃) δ 166.8, 166.1, 142.3, 134.6, 132.3, 131.0, 129.0, 127.2, 125.9, 119.4, 52.2. **HRMS** (ESI-TOF) *m/z* calculated for $C_{15}H_{14}NO_3$ (M+H)⁺: 256.0968, found 256.0963. **Melting point:** 169-172 °C. The characterization data matches previous reports.[40]

methyl 4-(4-cyanobenzamido)benzoate (3b)
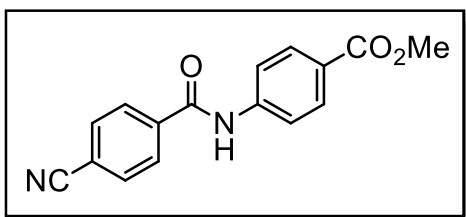
Following general procedure A, 4-cyanobenzamide (**1b**, 58.5 mg, 0.4 mmol) and methyl 4-bromobenzoate (**2a**, 43.0 mg, 0.2 mmol) were employed using 1:1 PhCF₃:DMF as solvent. Purification of the residue by flash chromatography (silica, 20% EtOAc in hexanes until methyl 4-hydroxybenzoate side product elutes, then 40% EtOAc in hexanes) afforded **3b** (36.5 mg, 65% yield) as a white solid; R_f = 0.10 (20% EtOAc in hexanes), 0.43 (40% EtOAc in hexanes). **¹H NMR** (400 MHz, DMSO-*d₆*)

δ 10.78 (bs, 1H), 8.11 (d, J = 8.7 Hz, 2H), 8.04 (d, J = 8.7 Hz, 2H), 7.98 (d, J = 9.0

Hz, 2H), 7.94 (d, J = 9.0 Hz, 2H), 3.84 (s, 3H). **^{13}C NMR** (101 MHz, DMSO-d_6) δ

165.8, 164.7, 143.2, 138.6, 132.5, 130.2, 128.7, 124.7, 119.7, 118.3, 114.1, 52.0.

HRMS (ESI-TOF) *m/z* calculated for $C_{16}H_{11}N_2O_3$ (M-H)$^-$: 279.0776, found

279.0780. **Melting point:** 240-244 °C. The characterization data matches previous
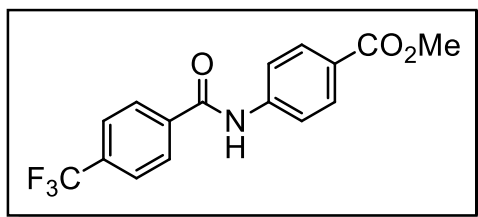
reports.[41]

methyl 4-(4-(trifluoromethyl)benzamido)benzoate (3c)

Following general procedure A, 4-trifluoromethylbenzamide (**1c**, 75.7 mg, 0.4 mmol) and methyl 4-bromobenzoate (**2a**, 43.0 mg, 0.2 mmol) were employed using 1:1

PhCF$_3$:DMF as solvent. Purification of the residue by flash chromatography (silica,

20% EtOAc in hexanes) afforded a mixture of **3c** and methyl 4-hydroxybenzoate;

R$_f$ = 0.24 (20% EtOAc in hexanes). The general extraction procedure was followed

to afford **3c** (40.7 mg, 63% yield) as a white solid. **^{1}H NMR** (400 MHz, DMSO-d_6)

δ 10.77 (bs, 1H), 8.16 (d, J = 8.5 Hz, 2H), 8.00 – 7.94 (m, 4H), 7.92 (d, J = 8.5 Hz,

2H), 3.84 (s, 3H). **^{13}C NMR** (101 MHz, DMSO-d_6) δ 165.8, 164.9, 143.3, 138.4,

131.6 (q, J = 31.8 Hz), 130.2, 128.8, 125.4 (q, J = 3.8 Hz), 124.7, 123.9 (q, J =

273.2 Hz), 119.7, 52.0. **^{19}F NMR** (376 MHz, CDCl$_3$) δ -64.3. **HRMS** (ESI-TOF) *m/z*

calculated for $C_{16}H_{13}F_3NO_3$ (M+H)$^+$: 324.0842, found 324.0827. **Melting point:**

225-226 °C.

methyl 4-(2-naphthamido)benzoate (3d)
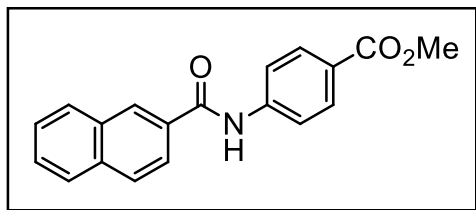
Following general procedure A, 2-naphthamide (**1d**, 68.5 mg, 0.4 mmol) and methyl 4-bromobenzoate (**2a**, 43.0 mg, 0.2 mmol) were employed using 1:1 PhCF$_3$:DMF as solvent. Purification of the residue by flash chromatography (silica, 30% EtOAc in hexanes) afforded a mixture of **3d** and methyl 4-hydroxybenzoate; R_f = 0.38 (30% EtOAc in hexanes). The general extraction procedure was followed to afford **3d** (32.2 mg, 53% yield) as a white solid. **^{1}H NMR** (400 MHz, CDCl$_3$): δ 8.37 (s, 1H), 8.22 (bs, 1H), 8.07 (d, J = 8.6 Hz, 2H), 7.91 (m, 4H), 7.80 (d, J = 8.7 Hz, 2H), 7.64 – 7.53 (m, 2H), 3.92 (s, 3H). **^{13}C NMR** (101 MHz, CDCl$_3$) δ 166.8, 166.0, 142.4, 135.1, 132.7, 131.8, 131.1, 129.2, 129.1, 128.3, 128.0, 127.9, 127.3, 126.0, 123.6, 119.4, 52.2. **HRMS** (ESI-TOF) *m/z* calculated for C$_{19}$H$_{16}$NO$_3$ (M+H)$^+$: 306.1125, found 306.1120. **Melting point:** 197-198 °C. The characterization data matches previous reports.[42]

methyl 4-(4-hydroxybenzamido)benzoate (3e)
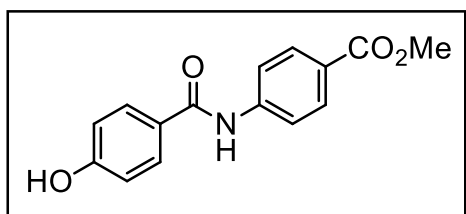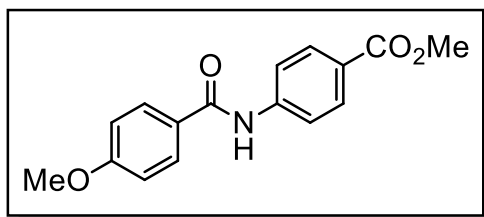

Following general procedure A, 4-hydroxybenzamide (**1e**, 59.9 mg, 0.4 mmol) and methyl 4-bromobenzoate (**2a**, 43.0 mg, 0.2 mmol) were employed using 3:1 PhCF$_3$:DMF as solvent. Purification of the residue by flash chromatography (silica,

50% EtOAc in hexanes) afforded **3e** (34.5 mg, 64% yield) as a white solid; **R**$_f$ = 0.29 (50% EtOAc in hexanes). **^{1}H NMR** (400 MHz, DMSO-d$_6$) δ 10.30 (s, 1H), 10.18 (s, 1H), 7.94 (s, 4H), 7.88 (d, J = 8.7 Hz, 2H), 6.89 (d, J = 8.7 Hz, 1H), 3.83 (s, 3H). **^{13}C NMR** (101 MHz, DMSO-d$_6$) δ 165.9, 165.5, 160.9, 144.1, 130.1, 130.0, 125.0, 123.9, 119.4, 115.0, 51.9. **HRMS** (ESI-TOF) *m/z* calculated for C$_{15}$H$_{14}$NO$_4$ (M+H)$^+$: 272.0918, found 272.0918. **Melting point:** 244-245 °C.

Methyl 4-(4-methoxybenzamido)benzoate (3f)

Following general procedure A, 4-methoxybenzamide (**1f**, 60.5 mg, 0.4 mmol) and methyl 4-bromobenzoate (**2a**, 43.0 mg, 0.2 mmol) were employed using 1:1 PhCF$_3$:DMF as solvent. Purification of the residue by flash chromatography (silica, 20% EtOAc in hexanes until methyl 4-hydroxybenzoate side product elutes, then 40% EtOAc in hexanes) afforded **3f** (24.1 mg, 42% yield) as a white solid; **R**$_f$ = 0.13 (20% EtOAc in hexanes), 0.43 (40% EtOAc in hexanes). **^{1}H NMR** (400 MHz, CDCl$_3$): δ 8.05 (d, J = 8.8 Hz, 2H), 7.91 (bs, 1H), 7.85 (d, J = 8.8 Hz, 2H), 7.73 (d, J = 8.8 Hz, 2H), 6.98 (d, J = 8.8 Hz, 2H), 3.91 (s, 3H), 3.88 (s, 3H). **^{13}C NMR** (101 MHz, CDCl$_3$) δ 166.8, 165.4, 162.9, 142.5, 131.1, 129.2, 126.8, 125.8, 119.2, 114.3, 55.7, 52.2. **HRMS** (ESI-TOF) *m/z* calculated for C$_{16}$H$_{16}$NO$_4$ (M+H)$^+$: 286.1074, found 286.1069. **Melting point:** 209-210 °C. The characterization data matches previous reports.[43]

methyl 4-butyramidobenzoate (3g)

Following general procedure A, butyramide (**1g**, 34.8 mg, 0.4 mmol) and methyl 4-bromobenzoate (**2a**, 43.0 mg, 0.2 mmol) were employed using 3:1 PhCF$_3$:DMF as solvent. Purification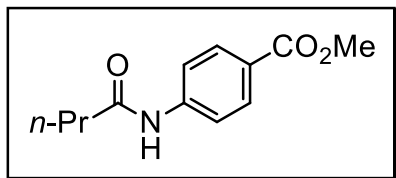 of the residue by flash chromatography (silica, 20% EtOAc in hexanes until methyl 4-hydroxybenzoate side product elutes, then 30% EtOAc in hexanes) afforded **3g** (28.3 mg, 64% yield) as a white solid; **R$_f$** = 0.16 (20% EtOAc in hexanes), 0.29 (30% EtOAc in hexanes). **^{1}H NMR** (400 MHz, CDCl$_3$): δ 7.99 – 7.85 (bs, 3H), 7.62 (d, J = 8.8 Hz, 2H), 3.88 (s, 3H), 2.36 (t, J = 7.4 Hz, 2H), 1.74 (sext, J = 7.4 Hz, 2H), 0.97 (t, J = 7.4 Hz, 3H). **^{13}C NMR** (101 MHz, CDCl$_3$) δ 172.0, 166.9, 142.5, 130.9, 125.4, 119.0, 52.1, 39.8, 19.1, 13.8. **HRMS** (ESI-TOF) *m/z* calculated for C$_{12}$H$_{16}$NO$_3$ (M+H)$^+$: 222.1125, found 222.1125. **Melting point:** 130-131 °C. The characterization data matches previous reports.[44]

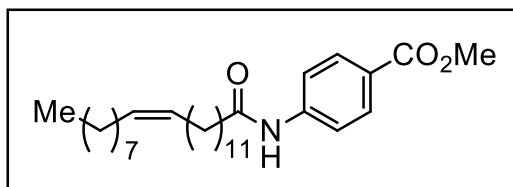## (*Z*)-methyl 4-(tricos-13-enamido)benzoate (3h)
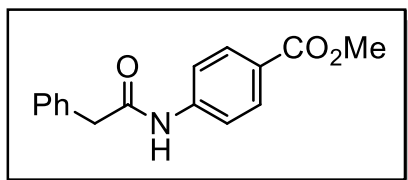
Following general procedure A, *cis*-13-docosenoamide (**1h**, 135.0 mg, 0.4 mmol) and methyl 4-bromobenzoate (**2a**, 43.0 mg, 0.2 mmol) were employed using 3:1 PhCF$_3$:DMF as solvent. Purification of the residue by flash chromatography (silica, 20% EtOAc in hexanes) afforded **3h** (56.2 mg, 60% yield) as a white solid; **R$_f$** = 0.28 (20% EtOAc in hexanes). **^{1}H NMR** (400

MHz, CDCl$_3$): δ 7.97 (d, J = 8.7 Hz, 2H), 7.84 – 7.77 (bs, 1H), 7.62 (d, J = 8.7 Hz, 2H), 5.33 (m, 2H), 3.88 (s, 3H), 2.37 (t, J = 7.6 Hz, 2H), 2.00 (q, J = 6.6 Hz, 4H), 1.70 (p, J = 7.5 Hz, 2H), 1.51 – 1.11 (m, 28H). 1.02 – 0.75 (m, 3H). **^{13}C NMR** (101 MHz, CDCl$_3$) δ 172.1, 166.8, 142.5, 130.9, 130.0, 130.0, 125.4, 118.9, 52.1, 38.0, 32.0, 29.9, 29.8, 29.8, 29.7, 29.7, 29.6, 29.6, 29.5, 29.4, 29.4, 27.3, 25.6, 22.8, 14.2. **HRMS** (ESI-TOF) *m/z* calculated for C$_{30}$H$_{50}$NO$_3$ (M+H)$^+$: 472.3785, found 472.3799. **Melting point:** 78-81 °C.

methyl 4-(2-phenylacetamido)benzoate (3i)

Following general procedure A, 2-phenylacetamide (**1i**, 54.1 mg, 0.4 mmol) and methyl 4- bromobenzoate (**2a**, 43.0 mg, 0.2 mmol) were employed using 3:1 PhCF$_3$:DMF as solvent. Purification of the residue by flash chromatography (silica (20% EtOAc in hexanes until methyl 4-bromobenzoate side product elutes, then 30% EtOAc in hexanes) afforded **3i** (35.5 mg, 66% yield) as a white solid; **R$_f$** = 0.12 (20% EtOAc in hexanes), 0.28 (30% EtOAc in hexanes). **^{1}H NMR** (400 MHz, CDCl$_3$) δ 7.94 (d, J = 8.8 Hz, 2H), 7.66 (bs, 1H), 7.52 (d, J = 8.8 Hz, 2H), 7.41 – 7.35 (m, 2H), 7.35 – 7.29 (m, 3H), 3.87 (s, 3H), 3.73 (s, 2H). **^{13}C NMR** (101 MHz, CDCl$_3$) δ 169.6, 166.7, 142.0, 134.1, 130.8, 129.6, 129.4, 127.9, 125.8, 119.0, 52.2, 44.9. **HRMS** (ESI-TOF) *m/z* calculated for C$_{16}$H$_{16}$NO$_3$ (M+H)$^+$: 270.1125, found 270.1123. **Melting point:** 156-157 °C. The characterization data matches previous reports.[45]

methyl 4-(2,2-diphenylacetamido)benzoate (3j)
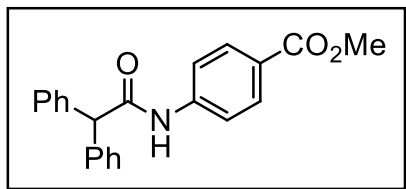
Following general procedure A, 2,2-diphenylacetamide (**1j**, 84.5 mg, 0.4 mmol) and methyl 4- bromobenzoate (**2a**, 43.0 mg, 0.2 mmol) were employed using 3:1 PhCF$_3$:DMF as solvent. Purification of the residue by flash chromatography (silica, 20% EtOAc in hexanes) afforded a mixture of **3j** and methyl 4-hydroxybenzoate; **R**$_f$ = 0.16 (20% EtOAc in hexanes). The general extraction procedure was followed to afford **3j** (47.1 mg, 68% yield) as a white solid. **^{1}H NMR** (400 MHz, CDCl$_3$): δ 7.95 (d, J = 8.8 Hz, 2H), 7.83 (bs, 1H), 7.53 (d, J = 8.8 Hz, 2H), 7.38 – 7.27 (m, 10H), 5.08 (s, 1H), 3.88 (s, 3H). **^{13}C NMR** (101 MHz, CDCl$_3$) δ 170.7, 166.7, 142.0, 138.8, 130.9, 129.1, 129.0, 127.7, 125.9, 119.1, 60.1, 52.2. **HRMS** (ESI-TOF) *m/z* calculated for C$_{22}$H$_{20}$NO$_3$ (M+H)$^+$: 346.1440, found 346.1441. **Melting point:** 185-186 °C.

methyl 4-(cyclohexanecarboxamido)benzoate (3k)

Following general procedure A, cyclohexanecarboxamide (**1k**, 50.9 mg, 0.4 mmol) and methyl 4- bromobenzoate (**2a**, 43.0 mg, 0.2 mmol) were employed using 1:1 PhCF$_3$:DMF as solvent. Purification of the residue by flash chromatography (silica, 30% EtOAc in hexanes) afforded a mixture of **3k** and methyl 4-hydroxybenzoate; **R**$_f$ = 0.36 (30% EtOAc in hexanes). The general extraction procedure was followed to afford **3k** (27.7 mg, 53% yield) as a white

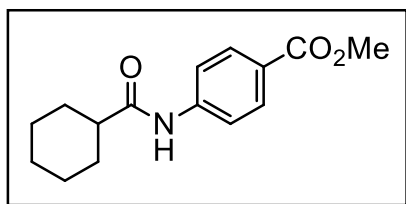solid. **¹H NMR** (400 MHz, CDCl₃) δ 7.99 (d, *J* = 8.8 Hz, 2H), 7.61 (d, *J* = 8.8 Hz,

2H), 7.41 (bs, 1H), 3.89 (s, 3H), 2.25 (tt, *J* = 11.7, 3.5 Hz, 1H), 2.00 – 1.91 (m, 2H),

1.89 – 1.79 (m, 2H), 1.74 – 1.67 (m, 1H), 1.61 – 1.48 (m, 2H), 1.37 – 1.18 (m, 3H).

¹³C NMR (101 MHz, CDCl₃) δ 174.8, 166.8, 142.5, 131.0, 125.5, 118.9, 52.2, 46.8,

29.7, 25.7. **HRMS** (ESI-TOF) *m/z* calculated for $C_{15}H_{20}NO_3$ (M+H)⁺: 262.1438,

found 262.1436. **Melting point:** 160-161 °C. The characterization data matches

previous reports.[46]

tert-butyl   **4-((4-(methoxycarbonyl)phenyl)carbamoyl)piperidine-1-**

carboxylate (3l)
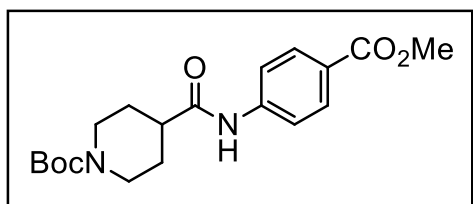
Following general procedure A, tert-butyl 4-carbamoylpiperidine-1-carboxylate (**1l**, 91.3 mg, 0.4 mmol) and methyl 4-bromobenzoate

(**2a**, 43.0 mg, 0.2 mmol) were employed using 3:1 PhCF₃:DMF as solvent. The

crude reaction mixture was flushed through the celite plug with hot acetone due to

the poor solubility of the product at room temperature. Purification of the residue

by flash chromatography (silica, 50% EtOAc in hexanes) afforded **3l** (41.9 mg, 58%

yield) as a white solid; R_f = 0.33 (50% EtOAc in hexanes). **¹H NMR** (400 MHz,

CDCl₃) δ 8.15 (bs, 1H), 7.96 (d, *J* = 8.8 Hz, 2H), 7.62 (d, *J* = 8.8 Hz, 2H), 4.21 –

4.07 (m, 2H), 3.87 (s, 3H), 2.73 (t, *J* = 13.5 Hz, 2H), 2.42 (tt, *J* = 11.6, 3.8 Hz, 1H),

1.89 – 1.80 (m, 2H), 1.72 (dtd, *J* = 13.5, 11.6, 4.3 Hz, 2H), 1.44 (s, 9H). **¹³C NMR**

(101 MHz, CDCl₃) δ 173.3, 166.8, 154.8, 142.5, 130.9, 125.5, 119.0, 80.0, 52.2,

44.3, 43.2 (bs), 28.6, 28.5. **HRMS** (ESI-TOF) *m/z* calculated for $C_{19}H_{25}N_2O_5$ (M-H)⁻: 361.1770, found 361.1780. **Melting point:** 194-197 °C.

methyl 4-(nicotinamido)benzoate (3m)
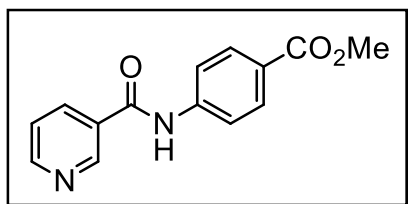
Following general procedure A, nicotinamide (**1m**, 48.9 mg, 0.4 mmol) and methyl 4- bromobenzoate (**2a**, 43.0 mg, 0.2 mmol) were employed using 3:1 PhCF₃:DMF as solvent. Purification of the residue by flash chromatography (silica, 100% EtOAc) afforded **3m** (39.8 mg, 78% yield) as a white solid; **R***f* = 0.41 (100% EtOAc). **¹H NMR** (400 MHz, DMSO-d₆) δ 10.75 (bs, 1H), 9.12 (dd, *J* = 2.3, 0.9 Hz, 1H), 8.78 (dd, *J* = 4.8, 1.7 Hz, 1H), 8.31 (ddd, *J* = 7.9, 2.3, 1.7 Hz, 1H), 7.98 (d, *J* = 9.1 Hz, 2H), 7.94 (d, *J* = 9.1 Hz, 2H), 7.59 (ddd, *J* = 7.9, 4.8, 0.9 Hz, 1H), 3.84 (s, 3H). **¹³C NMR** (101 MHz, DMSO-d₆) δ 165.8, 164.6, 152.4, 148.8, 143.3, 135.6, 130.3, 130.2, 124.6, 123.5, 119.6, 52.0. **HRMS** (ESI-TOF) *m/z* calculated for $C_{14}H_{13}N_2O_3$ (M+H)+: 257.0921, found 257.0917. **Melting point:** 197-198 °C.

methyl 4-(furan-2-carboxamido)benzoate (3n)
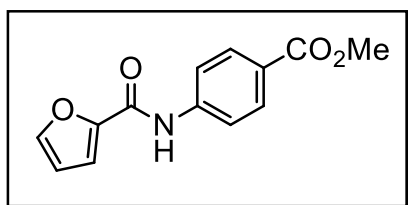
Following general procedure A, furan-2-carboxamide (**1n**, 44.4 mg, 0.4 mmol) and methyl 4-bromobenzoate (**2a**, 43.0 mg, 0.2 mmol) were employed using 3:1 PhCF₃:DMF as solvent. Purification of the residue by flash chromatography (silica, 20% EtOAc in hexanes until methyl 4-hydroxybenzoate

side product elutes, then 40% EtOAc in hexanes) afforded **3n** (37.8 mg, 77% yield) as a white solid; $\mathbf{R}_f$ = 0.12 (20% EtOAc in hexanes), 0.37 (40% EtOAc in hexanes).

¹H NMR (400 MHz, CDCl₃) δ 8.35 (bs, 1H), 8.02 (d, *J* = 8.8 Hz, 2H), 7.74 (d, *J* = 8.8 Hz, 2H), 7.48 (dd, *J* = 1.8, 0.8 Hz, 1H), 7.24 (dd, *J* = 3.5, 0.8 Hz, 1H), 6.54 (dd, *J* = 3.5, 1.8 Hz, 1H), 3.88 (s, 3H). **¹³C NMR** (101 MHz, CDCl₃) δ 166.7, 156.2, 147.5, 144.7, 141.8, 131.0, 125.9, 119.1, 116.0, 112.9, 52.1. **HRMS** (ESI-TOF) *m/z* calculated for $C_{13}H_{12}NO_4$ (M+H)⁺: 246.0761, found 246.0759. **Melting point:** 141-142 °C. The characterization data matches previous reports.[41]

methyl 4-(thiophene-2-carboxamido)benzoate (3o)
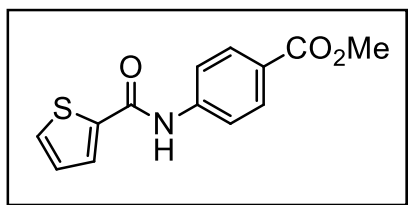
Following general procedure A, furan-2-carboxamide (**1o**, 50.9 mg, 0.4 mmol) and methyl 4- bromobenzoate (**2a**, 43.0 mg, 0.2 mmol) were employed using 3:1 PhCF₃:DMF as solvent. Purification of the residue by flash chromatography (silica, 20% EtOAc in hexanes until methyl 4-hydroxybenzoate side product elutes, then 25% EtOAc in hexanes) afforded **3o** (37.5 mg, 72% yield) as a white solid; $\mathbf{R}_f$ = 0.11 (20% EtOAc in hexanes), 0.22 (25% EtOAc in hexanes).

¹H NMR (400 MHz, CDCl₃) δ 8.12 (bs, 1H), 8.01 (d, *J* = 8.8 Hz, 2H), 7.71 (d, *J* = 8.8 Hz, 2H), 7.68 (dd, *J* = 3.8, 1.1 Hz, 1H), 7.56 (dd, *J* = 5.0, 1.1 Hz, 1H), 7.10 (dd, *J* = 5.0, 3.8 Hz, 1H), 3.90 (s, 3H). **¹³C NMR** (101 MHz, CDCl₃) δ 166.8, 160.2, 142.0, 139.0, 131.6, 131.0, 129.0, 128.1, 125.9, 119.4, 52.2. **HRMS** (ESI-TOF) *m/z*

calculated for $C_{13}H_{12}NO_3S$ (M+H)$^+$: 262.0533, found 262.0529. **Melting point:** 161-164 °C. The characterization data matches previous reports.[47]

(*S*)-methyl 4-(5-(*tert*-butoxy)-4-((*tert*-butoxycarbonyl)amino)-5-oxopentanamido)benzoate (3p)
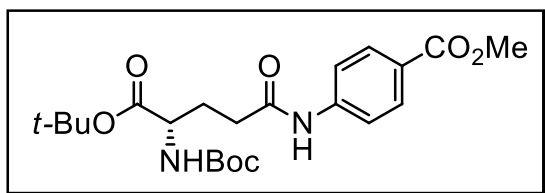
Following general procedure B, (*S*)-Boc-Gln-O*t*-Bu (**1p**, 120.9 mg, 0.4 mmol) and methyl 4-bromobenzoate (**2a**, 43.0 mg, 0.2 mmol) were employed using 1.1 mL of 10:1 PhCF$_3$:DMF as solvent and reacted for 48 h. Purification of the residue by flash chromatography (silica, 3:1 DCM:acetone) afforded **3p** (50.2 mg, 58% yield) as a clear, highly viscous oil; R_f = 0.21 (3:1 DCM:acetone). **¹H NMR** (400 MHz, CDCl$_3$) δ 9.31 (bs, 1H), 7.98 (d, *J* = 8.6 Hz, 2H), 7.69 (d, *J* = 8.6 Hz, 2H), 5.41 (d, *J* = 8.0 Hz, 1H), 4.25 – 4.14 (m, 1H), 3.88 (s, 3H), 2.49 – 2.43 (m, 2H), 2.30 – 2.21 (m, 1H), 1.93 – 1.82 (m, 1H), 1.45 (s, 9H), 1.44 (s, 9H). **¹³C NMR** (101 MHz, CDCl$_3$) δ 171.3, 171.2, 166.9, 156.8, 142.9, 130.9, 125.3, 118.9, 83.0, 80.8, 53.3, 52.1, 34.4, 30.7, 28.4, 28.1. **HRMS** (ESI-TOF) *m/z* calculated for $C_{22}H_{33}N_2O_7$ (M+H)$^+$: 437.2283, found 437.2281. 81.5:18.5 er (identical to the er of the starting amide **1n**) determined by analytical SFC, Trefoil™ AMY1 column, 40 °C, MeOH:CO$_2$ = 8:92, 1 mL/min, t$_R$ (major): 5.08 min, t$_R$ (minor): 6.13 min; **[α]$_D^{20}$** = – 102 ± 13 (c = 0.0225 g/mL, MeCN).

Separation of enantiomers by SFC:

Arylated products **3p**: Trefoil™ AMY1 column, 40 °C, MeOH:CO_2 = 8:92, 1 mL/min, t_R (major): 5.08 min, t_R (minor): 6.13 min for **(S)-3p** and t_R (major): 6.09 min, t_R (minor): 5.11 min for **(R)-1p**.

Starting amides **1p**: Trefoil™ CEL1 column, 40 °C, MeOH:CO_2 = 3:97, 1.5 mL/min, t_R (major): 14.19 min, t_R (minor): 12.77 min for **(S)-1p** and t_R (major): 12.45 min, t_R (minor): 14.38 min for **(R)-1p**.

	Peak Results		
	RT	Area	% Area
1	5.083	2366722	81.57
2	6.132	534825	18.43

	Peak Results		
	RT	Area	% Area
1	12.767	435508	18.68
2	14.187	1895514	81.32

(R)-3p

(R)-1p
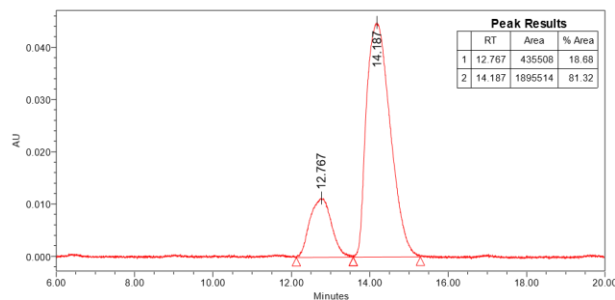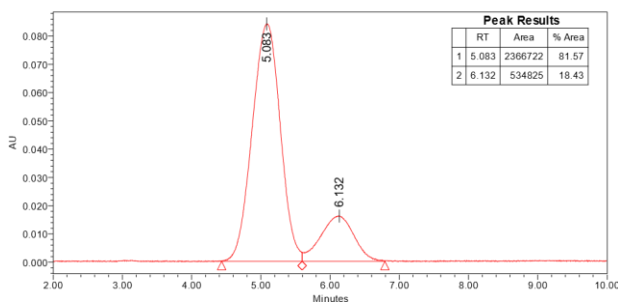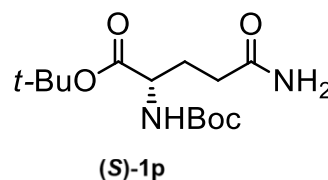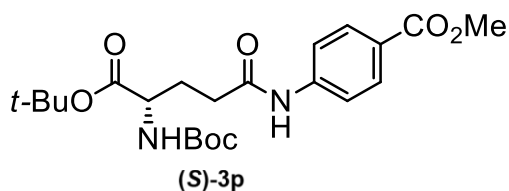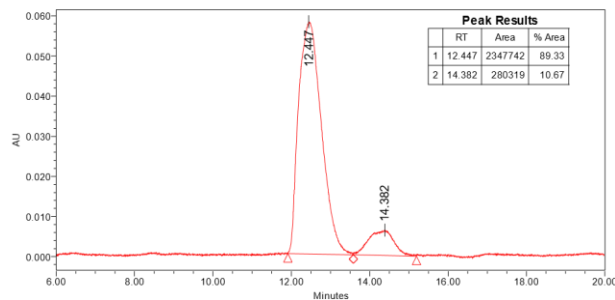
Secondary amide and other weakly nucleophilic N-*nucleophile scope:*

methyl 4-(2-oxoazetidin-1-yl)benzoate (3q)
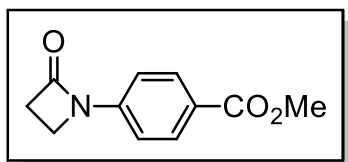
Following general procedure A, 2-azetidinone (**1q**, 28.4 mg, 0.4 mmol) and methyl 4- bromobenzoate (**2a**, 43.0 mg, 0.2 mmol) were employed using 3:1 PhCF$_3$:DMF as solvent. Purification of the residue by flash chromatography (silica, 20% EtOAc in hexanes until methyl 4-hydroxybenzoate side product elutes, then 40% EtOAc in hexanes) afforded **3q** (25.8 mg, 63% yield) as a white solid; **R$_f$** = 0.13 (20% EtOAc in hexanes), 0.34 (40% EtOAc in hexanes). **^{1}H NMR** (400 MHz, CDCl$_3$): δ 8.00 (d, *J* = 8.9 Hz, 2H), 7.37 (d, *J* = 8.9 Hz, 2H), 3.88 (s, 3H), 3.66 (t, *J* = 4.6 Hz, 2H), 3.15 (t, *J* = 4.6 Hz, 2H). **^{13}C NMR** (101 MHz, CDCl$_3$) δ 166.6, 164.9, 142.1, 131.1, 125.3, 115.7, 52.1, 38.4, 36.6. **HRMS** (ESI-TOF) *m/z* calculated for C$_{11}$H$_{12}$NO$_3$ (M+H)$^+$: 206.0811, found 206.0808. **Melting point:** 128-129 °C.

methyl 4-(2-oxopyrrolidin-1-yl)benzoate (3r)
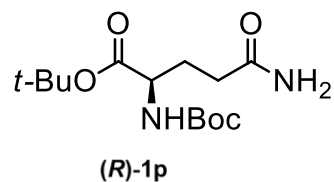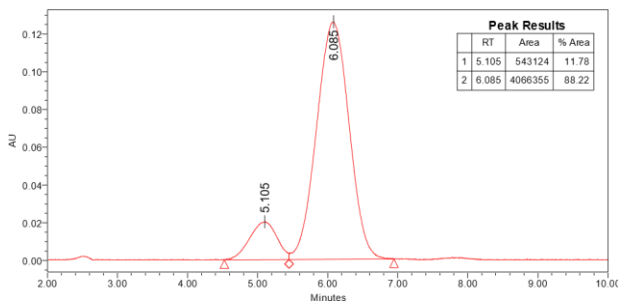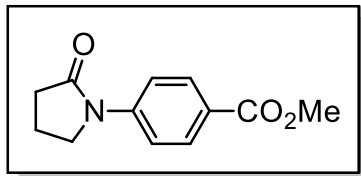
Following general procedure A, 2-pyrrolidone (**1r**, 34.0 mg, 0.4 mmol) and methyl 4- bromobenzoate (**2a**, 43.0 mg, 0.2 mmol) were employed using 3:1 PhCF$_3$:DMF as solvent. Purification of the residue by flash chromatography (silica, 30% EtOAc in hexanes until methyl 4-hydroxybenzoate side product elutes, then 50% EtOAc in hexanes) afforded **3r** (31.6 mg, 72% yield) as a white solid; **R**$_f$ = 0.11 (30% EtOAc in hexanes), 0.26 (50% EtOAc in hexanes). **^{1}H NMR** (400 MHz, CDCl$_3$) δ 8.01 (d, J = 8.9 Hz, 2H), 7.71 (d, J = 8.9 Hz, 2H), 3.88 (s, 3H), 3.87 (t, J = 7.7 Hz, 2H), 2.61 (t, J = 7.7 Hz, 2H), 2.16 (quint, J = 7.7 Hz, 2H). **^{13}C NMR** (101 MHz, CDCl3) δ 174.7, 166.7, 143.5, 130.5, 125.5, 118.7, 52.1, 48.6, 33.0, 17.9. **HRMS** (ESI-TOF) *m/z* calculated for C$_{12}$H$_{14}$NO$_3$ (M+H)$^+$: 220.0968, found 220.0969. **Melting point:** 123-124 °C. The characterization data matches previous reports.[48]
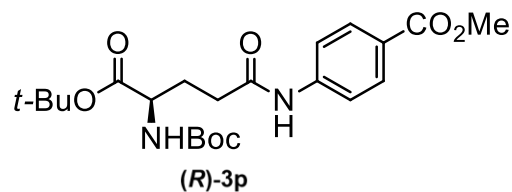
methyl 4-(1,3-dioxoisoindolin-2-yl)benzoate (3s)

Following general procedure A, phthalimide (**1s**, 58.9 mg, 0.4 mmol) and methyl 4-bromobenzoate (**2a**, 43.0 mg, 0.2 mmol) were employed using 3:1 PhCF$_3$:DMF as solvent. The crude reaction mixture was flushed through the celite plug with hot methanol instead of acetone due to the poor solubility of the product. Purification of the residue by flash chromatography (silica, 10% EtOAc in hexanes) afforded a mixture of **3s**, methyl 4-hydroxybenzoate, and residual phthalimide; **R**$_f$

= 0.09 (10% EtOAc in hexanes). Although this R_f is quite low, it was necessary in order to elute the diaryl ether side product before the desired product since the diaryl ether cannot be removed by extraction. The general extraction procedure was followed to afford **3s** (40.4 mg, 72% yield) as a white solid. **¹H NMR** (400 MHz, CDCl$_3$) δ 8.18 (d, J = 8.9 Hz, 2H), 7.97 (dd, J = 5.5, 3.0 Hz, 2H), 7.82 (dd, J = 5.5, 3.0 Hz, 2H), 7.60 (d, J = 8.9 Hz, 2H), 3.95 (s, 3H). **¹³C NMR** (101 MHz, CDCl$_3$) δ 166.9, 166.5, 136.0, 134.8, 131.7, 130.6, 129.4, 126.1, 124.1, 52.5. **HRMS** (ESI-TOF) *m/z* calculated for C$_{16}$H$_{10}$NO$_4$ (M-H)⁻: 280.0615, found 280.0621. **Melting point:** 193-198 °C. The characterization data matches previous reports.[49]

methyl 4-((*tert*-butoxycarbonyl)amino)benzoate (3t)

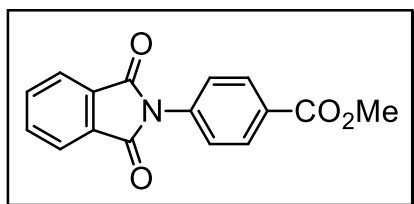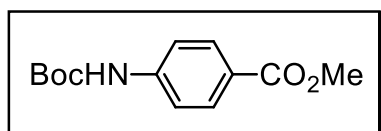Following general procedure A, tert-butyl carbamate (**3t**, 46.9 mg, 0.4 mmol) and methyl 4-bromobenzoate (**2a**, 43.0 mg, 0.2 mmol) were employed using PhCF$_3$ as solvent and reacted for 48 h at 40 °C. Purification of the residue by flash chromatography (silica, 10% EtOAc in hexanes) afforded **3t** (29.2 mg, 58% yield) as a white solid; R_f = 0.06 (10% EtOAc in hexanes). Although this R_f is quite low, it was necessary in order to elute the impurities before the desired product. **¹H NMR** (400 MHz, CDCl$_3$) δ 7.96 (d, J = 8.8 Hz, 2H), 7.43 (d, J = 8.8 Hz, 2H), 6.82 (bs, 1H), 3.88 (s, 3H), 1.51 (s, 9H). **¹³C NMR** (101 MHz, CDCl$_3$) δ 166.9, 152.4, 142.9, 131.0, 124.4, 117.5, 81.3, 52.1, 28.4. **HRMS** (ESI-TOF) *m/z* calculated for C$_{13}$H$_{16}$NO$_4$ (M-H)⁻:

250.1085, found 250.1088. **Melting point:** 169-172 °C. The characterization data

matches previous reports.[50]

methyl 4-(4-methylphenylsulfonamido)benzoate (3u)

TsHN—⟨benzene ring⟩—CO$_2$Me
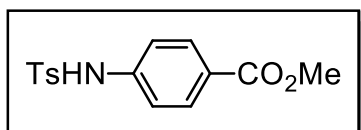
Following general procedure A, *p*-toluenesulfonamide

(**1u**, 68.5 mg, 0.4 mmol) and methyl 4- bromobenzoate

(**2a**, 43.0 mg, 0.2 mmol) were employed using 3:1 PhCF$_3$:DMF as solvent. The

crude reaction mixture was flushed through the celite plug with hot methanol

instead of acetone due to the poor solubility of the product. Purification of the

residue by flash chromatography (silica, 20% EtOAc in hexanes until methyl 4-

hydroxybenzoate side product elutes, then 25% EtOAc in hexanes) afforded **3u**

(45.4 mg, 74% yield) as a white solid; **R$_f$** = 0.11 (20% EtOAc in hexanes), 0.22

(25% EtOAc in hexanes). **^{1}H NMR** (400 MHz, DMSO-d$_6$) δ 10.80 (bs, 1H), 7.81 (d,

J = 8.8 Hz, 2H), 7.70 (d, *J* = 8.0 Hz, 2H), 7.36 (d, *J* = 8.0 Hz, 2H), 7.20 (d, *J* = 8.8

Hz, 2H), 3.77 (s, 3H), 2.32 (s, 3H). **^{13}C NMR** (101 MHz, DMSO-d$_6$) δ 165.7, 143.7,

142.6, 136.4, 130.6, 129.8, 126.7, 124.2, 118.1, 51.9, 21.0. **HRMS** (ESI-TOF) *m/z*

calculated for C$_{15}$H$_{14}$NO$_4$S (M-H)$^-$: 304.0651, found 304.0646. **Melting point:** 199-

201 °C. The characterization data matches previous reports.[51]

methyl 4-(2,2,2-trifluoroacetamido)benzoate (3v)
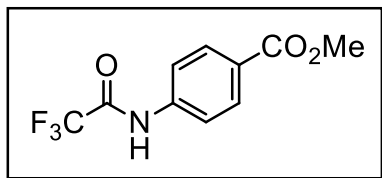
Following general procedure A, 2,2,2-trifluoroacetamide (**1v**, 45.2 mg, 0.4 mmol) and methyl 4- bromobenzoate (**2a**, 43.0 mg, 0.2 mmol) were employed using 3:1 PhCF$_3$:DMF as solvent. Purification of the residue by flash chromatography (silica, 20% EtOAc in hexanes) afforded **3v** (43.9 mg, 89% yield) as a white solid; **R$_f$** = 0.30 (20% EtOAc in hexanes). **^{1}H NMR** (400 MHz, CDCl$_3$) δ 8.22 (bs, 1H), 8.07 (d, *J* = 8.9 Hz, 2H), 7.68 (d, *J* = 8.9 Hz, 2H), 3.92 (s, 3H). **^{13}C NMR** (101 MHz, CDCl$_3$) δ 166.4, 155.1 (q, *J* = 38.4 Hz), 139.3, 131.2, 127.9, 120.0, 115.7 (q, *J* = 289.9 Hz), 52.4. **^{19}F NMR** (376 MHz, CDCl$_3$) δ -76.9. **HRMS** (ESI-TOF) *m/z* calculated for C$_{10}$H$_7$F$_3$NO$_3$ (M-H)$^-$: 246.0384, found 246.0392. **Melting point:** 123-126 °C. The characterization data matches previous reports.[44]

methyl 4-(*N*-phenylacetamido)benzoate (3w)
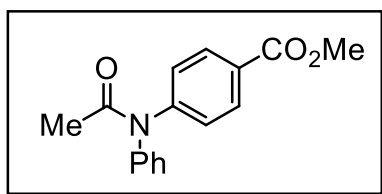
Following general procedure A, acetanilide (**1w**, 54.1 mg, 0.4 mmol) and methyl 4- bromobenzoate (**2a**, 43.0 mg, 0.2 mmol) were employed using 3:1 PhCF$_3$:DMF as solvent. Purification of the residue by flash chromatography (silica, 25% EtOAc in hexanes) afforded **3w** (10.8 mg, 20% yield) as a colorless oil; **R$_f$** = 0.22 (25% EtOAc in hexanes). **^{1}H NMR** (400 MHz, CDCl$_3$) δ 8.00 (d, *J* = 8.6 Hz, 2H), 7.42 (t, *J* = 7.5 Hz, 2H), 7.37 – 7.30 (m, 3H), 7.28 – 7.23 (m, 2H), 3.89 (s, 3H),

2.07 (s, 3H). **¹³C NMR** (101 MHz, CDCl₃) δ 170.6, 166.5, 147.0, 142.7, 130.6, 129.9, 128.4, 128.0, 126.3, 126.1, 52.3, 24.3. **HRMS** (ESI-TOF) *m/z* calculated for $C_{16}H_{16}NO_3$ (M+H)⁺: 270.1126, found 270.1126. The characterization data matches previous reports.[52]

Aryl bromide scope:

N-(4-benzoylphenyl)benzamide (3ad)

Following general procedure A, benzamide (**1a**, 48.5 mg, 0.4 mmol) and 4-bromobenzophenone (**2ad**, 52.2 mg, 0.2 mmol) were employed using 3:1 PhCF₃:DMF as solvent and reacted at 40 °C for 48 h. Purification of the residue by flash chromatography (silica, 30% EtOAc in hexanes) afforded a mixture of **3ad** and phenol side product; **R$_f$** = 0.32 (30% EtOAc in hexanes). The general extraction procedure was followed to afford **3ad** (53.4 mg, 89% yield) as a white solid. **¹H NMR** (400 MHz, CDCl₃) δ 8.78 (bs, 1H), 7.90 – 7.85 (m, 2H), 7.82 (d, *J* = 9.0 Hz, 2H), 7.78 (d, *J* = 9.0 Hz, 2H), 7.75 – 7.71 (m, 2H), 7.59 – 7.54 (m, 1H), 7.52 – 7.43 (m, 3H), 7.42 – 7.36 (m, 2H). **¹³C NMR** (101 MHz, CDCl₃) δ 196.1, 166.4, 142.4, 137.8, 134.5, 133.1, 132.4, 132.2, 131.7, 130.0, 128.8, 128.4, 127.4, 119.5. **HRMS** (ESI-TOF) *m/z* calculated for $C_{20}H_{16}NO_2$ (M+H)⁺: 302.1176, found 302.1170. **Melting point:** 153-155 °C. The characterization data matches previous reports.[53]

N-(4-(trifluoromethyl)phenyl)benzamide (3ae)

Following general procedure A, benzamide (**1a**, 48.5 mg, 0.4 mmol) and 4-bromobenzotrifluoride (**2ae**, 28.0 μL, 0.2 mmol) were employed using 3:1 PhCF$_3$:DMF as solvent. Purification of the residue by flash chromatography (silica, 20% EtOAc in hexanes) afforded **3ae** (36.7 mg, 69% yield) as a white solid; **R**$_f$ = 0.29 (20% EtOAc in hexanes). ^{1}**H NMR** (400 MHz, DMSO-d$_6$) δ 10.59 (bs, 1H), 8.03 (d, *J* = 8.4 Hz, 2H), 7.98 (d, *J* = 7.3 Hz, 2H), 7.72 (d, *J* = 8.4 Hz, 2H), 7.62 (t, *J* = 7.3 Hz, 1H), 7.55 (t, *J* = 7.3 Hz, 2H). ^{13}**C NMR** (101 MHz, DMSO-d$_6$) δ 166.1, 142.9, 134.5, 131.9, 128.5, 127.8, 125.9 (q, *J* = 3.6 Hz), 124.4 (q, *J* = 272.7 Hz), 123.6 (q, *J* = 32.3 Hz), 120.1. ^{19}**F NMR** (376 MHz, CDCl3) δ -63.4. **HRMS** (ESI-TOF) *m/z* calculated for C$_{14}$H$_{11}$F$_3$NO (M+H)$^+$: 266.0788, found 266.0783. **Melting point:** 205-208 °C. The characterization data matches previous reports.[54]

N-(3-(trifluoromethyl)phenyl)benzamide (3af)

Following general procedure A, benzamide (**1a**, 48.5 mg, 0.4 mmol) and 3-bromobenzotrifluoride (**2af**, 27.9 μL, 0.2 mmol) were employed using 3:1 PhCF$_3$:DMF as solvent and reacted at 40 °C for 48 h. Purification of the residue by flash chromatography (silica, 20% EtOAc in hexanes) afforded **3af** (42.8 mg, 81% yield) as a white solid; **R**$_f$ = 0.34 (20% EtOAc in hexanes). ^{1}**H NMR** (400 MHz, CDCl$_3$) δ 8.34 (bs, 1H), 7.93 (s, 1H), 7.88 – 7.81 (m, 3H), 7.56 – 7.50 (m, 1H), 7.46 – 7.34 (m, 4H). ^{13}**C**

NMR (101 MHz, CDCl$_3$) δ 166.4, 138.6, 134.4, 132.3, 131.5 (q, J = 32.6 Hz), 129.7, 128.9, 127.2, 124.0 (q, J = 273.4 Hz), 123.6, 121.2 (q, J = 4.0 Hz), 117.2 (q, J = 4.1 Hz). **^{19}F NMR** (376 MHz, CDCl$_3$) δ -64.0. **HRMS** (ESI-TOF) *m/z* calculated for C$_{14}$H$_{11}$F$_3$NO (M+H)+: 266.0787, found 266.0784. Melting point: 108-110 °C. The characterization data matches previous reports.[55]

N-(4-cyanophenyl)benzamide (3ag)
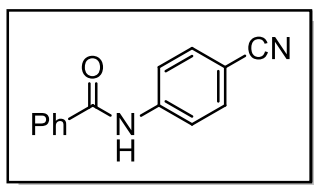
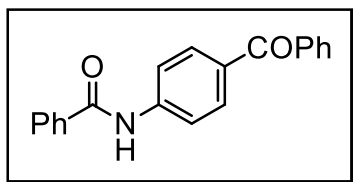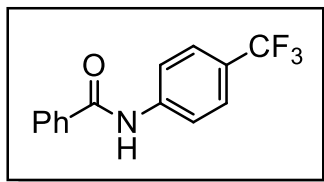

Following general procedure A, benzamide (**1a**, 48.5 mg, 0.4 mmol) and 4-bromobenzonitrile (**2ag**, 36.4 mg, 0.2 mmol) were employed using 3:1 PhCF$_3$:DMF as solvent. Purification of the residue by flash chromatography (silica, 20% EtOAc in hexanes until phenol side product elutes, then 30% EtOAc in hexanes) afforded **3ag** (30.7 mg, 69% yield) as a white solid; **R$_f$** = 0.15 (20% EtOAc in hexanes), 0.30 (30% EtOAc in hexanes). **^{1}H NMR** (400 MHz, DMSO-d$_6$) δ 10.66 (bs, 1H), 8.01 (d, J = 8.9 Hz, 2H), 7.97 (d, J = 7.2 Hz, 2H), 7.82 (d, J = 8.9 Hz, 2H), 7.62 (t, J = 7.2 Hz, 1H), 7.55 (t, J = 7.2 Hz, 2H). **^{13}C NMR** (101 MHz, DMSO-d$_6$) δ 166.2, 143.5, 134.4, 133.1, 132.1, 128.5, 127.9, 120.2, 119.1, 105.4. **HRMS** (ESI-TOF) *m/z* calculated for C$_{14}$H$_{11}$N$_2$O (M+H)$^+$: 223.0866, found 223.0862. **Melting point:** 169-171 °C. The characterization data matches previous reports.[6]
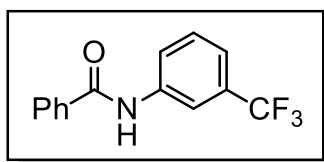
N-(4-chlorophenyl)benzamide (3ah)

Following general procedure A, benzamide (**1a**, 48.5 mg, 0.4 mmol) and 1-bromo-4- chlorobenzene (**2ah**, 38.3 mg, 0.2 mmol) were employed using 3:1 PhCF$_3$:DMF as solvent and reacted at 40 °C for 96 h. Purification of the residue by flash chromatography (silica, 20% EtOAc in hexanes) afforded **3ah** (28.2 mg, 61% yield) as a white solid; **R**$_f$ = 0.32 (20% EtOAc in hexanes). **¹H NMR** (400 MHz, DMSO-d$_6$) δ 10.38 (bs, 1H), 7.95 (d, *J* = 7.2 Hz, 2H), 7.83 (d, *J* = 8.9 Hz, 2H), 7.60 (t, *J* = 7.2 Hz, 1H), 7.53 (t, *J* = 7.2 Hz, 2H), 7.41 (d, *J* = 8.9 Hz, 2H). 13C NMR (101 MHz, DMSO-d$_6$) δ 165.7, 138.2, 134.7, 131.7, 128.5, 128.4, 127.7, 127.3, 121.8. **HRMS** (ESITOF) *m/z* calculated for C$_{13}$H$_{11}$ClNO (M+H)$^+$: 232.0525, found 232.0516. **Melting point:** 192-194 °C. The characterization data matches previous reports.[56]

N-(4-fluorophenyl)benzamide (3ai)

Following general procedure A, benzamide (**1a**, 48.5 mg, 0.4 mmol) and 1-bromo-4-fluorobenzene (**2ai**, 21.8 µL, 0.2 mmol) were employed using 3:1 PhCF$_3$:DMF as solvent and reacted at 50 °C for 5 days. Purification of the residue by flash chromatography (silica, 20% EtOAc in hexanes) afforded **3ai** (17.0 mg, 40% yield) as a white solid; **R**$_f$ = 0.30 (20% EtOAc in hexanes). **¹H NMR** (500 MHz, DMSO-d$_6$) δ 10.32 (s, 1H), 7.95 (d, *J* = 7.4 Hz, 2H), 7.80 (dd, *J* = 8.9, 5.0 Hz, 2H), 7.59 (t, *J* = 7.4 Hz, 1H), 7.53 (t, *J* = 7.4 Hz, 2H), 7.20 (t, *J* = 8.9 Hz, 2H). **¹³C NMR** (151 MHz, DMSO-d$_6$) δ

165.5, 158.3 (d, J = 240.3 Hz), 135.6 (bs), 134.8, 131.6, 128.4, 127.7, 122.2 (d, J = 8.0 Hz), 115.2 (d, J = 22.2 Hz). **^{19}F NMR** (376 MHz, DMSO-d6) δ -120.2 (tt, J = 8.9, 4.5 Hz). The characterization data matches previous reports.[57]

N-phenylbenzamide (3aj)

Following general procedure A, benzamide (**1a**, 48.5 mg, 0.4 mmol) and bromobenzene (**2aj**, 21.0 μL, 0.2 mmol) were employed using 3:1 PhCF$_3$:DMF as solvent and reacted at 40 °C for 48 h. Purification of the residue by flash chromatography (silica, 20% EtOAc in hexanes) afforded **3aj** (25.7 mg, 65% yield) as a white solid; **R$_f$** = 0.35 (20% EtOAc in hexanes). **^{1}H NMR** (400 MHz, CDCl$_3$) δ 7.98 (bs, 1H), 7.89 – 7.81 (m, 2H), 7.65 (d, J = 7.4 Hz, 2H), 7.54 (t, J = 7.4 Hz, 1H), 7.46 (t, J = 7.4 Hz, 2H), 7.41 – 7.31 (m, 2H), 7.15 (t, J = 7.4 Hz, 1H). **^{13}C NMR** (101 MHz, CDCl$_3$) δ 166.0, 138.1, 135.1, 131.9, 129.2, 128.9, 127.2, 124.7, 120.4. **HRMS** (ESI-TOF) *m/z* calculated for C$_{13}$H$_{12}$NO (M+H)$^+$: 198.0914, found 198.0909. **Melting point:** 163-165 °C. The characterization data matches previous reports.[7]

N-(*p*-tolyl)benzamide (3ak)
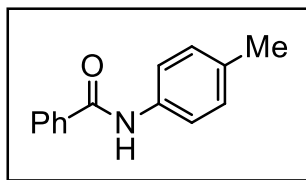
Following general procedure A, benzamide (**1a**, 48.5 mg, 0.4 mmol) and 4-bromotoluene (**2ak**, 34.2 mg, 0.2 mmol) were employed using 3:1 PhCF$_3$:DMF as solvent and reacted at 50 °C for 96 h. Purification of the residue by flash chromatography

(silica, 20% EtOAc in hexanes) afforded **3ak** (28.0 mg, 66% yield) as a white solid; **R**$_f$ = 0.24 (20% EtOAc in hexanes). **¹H NMR** (400 MHz, CDCl$_3$) δ 8.00 (bs, 1H), 7.84 (d, *J* = 7.2 Hz, 2H), 7.56 – 7.48 (m, 3H), 7.43 (t, *J* = 7.2 Hz, 2H), 7.15 (d, *J* = 8.2 Hz, 2H), 2.33 (s, 3H). **¹³C NMR** (101 MHz, CDCl$_3$) δ 165.9, 135.5, 135.2, 134.3, 131.8, 129.6, 128.8, 127.2, 120.5, 21.0. **HRMS** (ESI-TOF) *m/z* calculated for C$_{14}$H$_{14}$NO (M+H)$^+$: 212.1070, found 212.1069. **Melting point:** 159-161 °C. The characterization data matches previous reports.[57]
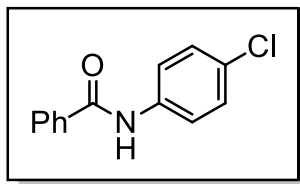
N-(4-pentylphenyl)benzamide (3al)

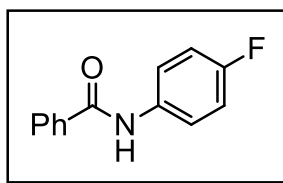Following general procedure A, benzamide (**1a**, 48.5 mg, 0.4 mmol) and 4-pentylbromobenzene (**2al**, 35.7 μL, 0.2 mmol) were employed using 3:1 PhCF$_3$:DMF as solvent and reacted at 50 °C for 96 h. Purification of the residue by flash chromatography (silica, 10% EtOAc in hexanes) afforded **3al** (35.4 mg, 66% yield) as a white solid; **R**$_f$ = 0.22 (10% EtOAc in hexanes). **¹H NMR** (400 MHz, CDCl$_3$) δ 7.89 – 7.82 (m, 3H), 7.57 – 7.50 (m, 3H), 7.47 (t, *J* = 7.3 Hz, 2H), 7.17 (d, *J* = 8.4 Hz, 2H), 2.59 (t, *J* = 7.8 Hz, 2H), 1.62 (p, *J* = 7.8 Hz, 2H), 1.40 – 1.27 (m, 4H), 0.89 (t, *J* = 7.2 Hz, 3H). **¹³C NMR** (101 MHz, CDCl$_3$) δ 165.8, 139.5, 135.6, 135.2, 131.9, 129.1, 128.9, 127.1, 120.4, 35.5, 31.6, 31.3, 22.7, 14.2. **HRMS** (ESI-TOF) *m/z* calculated for C$_{18}$H$_{22}$NO (M+H)$^+$: 268.1697, found 268.1697. **Melting point:** 118-120 °C.

N-(3,5-dimethylphenyl)benzamide (3am)

Following general procedure A, benzamide (**1a**, 48.5 mg, 0.4 mmol) and 5-bromo-m-xylene (**2am**, 27.2 µL, 0.2 mmol) were employed using 3:1 PhCF$_3$:DMF as solvent and reacted at 50 °C for 96 h. Purification of the residue by flash chromatography (silica, 20% EtOAc in hexanes) afforded **3am** (35.1 mg, 78% yield) as a white solid; **R**$_f$ = 0.35 (20% EtOAc in hexanes). **^{1}H NMR** (400 MHz, CDCl$_3$) δ 7.99 (bs, 1H), 7.88 – 7.83 (m, 2H), 7.55 – 7.48 (m, 1H), 7.47 – 7.40 (m, 2H), 7.29 (s, 2H), 6.79 (s, 1H), 2.30 (s, 6H). **^{13}C NMR** (101 MHz, CDCl$_3$) δ 165.9, 138.8, 137.9, 135.2, 131.8, 128.8, 127.1, 126.4, 118.2, 21.5. **HRMS** (ESI-TOF) *m/z* calculated for C$_{15}$H$_{16}$NO (M+H)$^+$: 226.1227, found 226.1222. **Melting point:** 144-145 °C. The characterization data matches previous reports.[58]
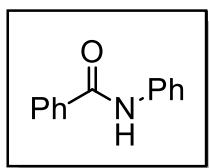
N-(*o*-tolyl)benzamide (3an)
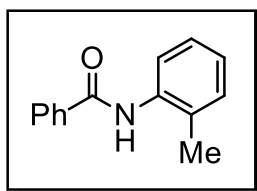
Following general procedure A, benzamide (**1a**, 48.5 mg, 0.4 mmol) and 2-bromotoluene (**2an**, 24.1 µL, 0.2 mmol) were employed using 3:1 PhCF$_3$:DMF as solvent and reacted at 50 °C for 7 days. Purification of the residue by flash chromatography (silica, 20% EtOAc in hexanes) afforded **3an** (31.9 mg, 76% yield) as a white solid; **R**$_f$ = 0.31 (20% EtOAc in hexanes). **^{1}H NMR** (400 MHz, CDCl$_3$) δ 7.91 – 7.85 (m, 3H), 7.81 (bs, 1H), 7.58 – 7.52 (m, 1H), 7.51 – 7.44 (m, 2H), 7.27 – 7.20 (m, 2H), 7.12 (td, *J* = 7.4, 1.3 Hz, 1H), 2.32 (s, 3H). **^{13}C NMR** (101 MHz, CDCl$_3$) δ 165.9, 135.8, 135.0,

131.9, 130.7, 129.8, 128.9, 127.2, 126.9, 125.6, 123.5, 17.9. **HRMS** (ESI-TOF) *m/z* calculated for $C_{14}H_{14}NO$ (M+H)$^+$: 212.1070, found 212.1068. **Melting point:** 138-139 °C. The characterization data matches previous reports.[59]

N-(4-methoxyphenyl)benzamide (3ao)
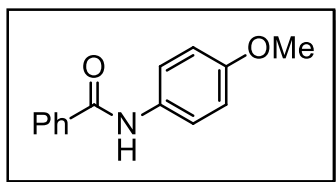
Following general procedure A, benzamide (**1a**, 48.5 mg, 0.4 mmol) and 4-bromoanisole (**2ao**, 25.0 μL, 0.2 mmol) were employed using 3:1 PhCF$_3$:DMF as solvent and reacted at 50 °C for 7 days. Purification of the residue by flash chromatography (silica, 20% EtOAc in hexanes) afforded **3ao** (20.0 mg, 44% yield) as a white solid; R$_f$ = 0.24 (20% EtOAc in hexanes). **¹H NMR** (400 MHz, CDCl$_3$) δ 7.91 – 7.79 (m, 3H), 7.57 – 7.49 (m, 3H), 7.46 (t, *J* = 7.3 Hz, 2H), 6.89 (d, *J* = 9.0 Hz, 2H), 3.81 (s, 3H). **¹³C NMR** (101 MHz, CDCl$_3$) δ 165.8, 156.8, 135.2, 131.8, 131.1, 128.9, 127.1, 122.3, 114.4, 55.6. **HRMS** (ESI-TOF) *m/z* calculated for $C_{14}H_{14}NO_2$ (M+H)$^+$: 228.1019, found 228.1013. **Melting point:** 159-162 °C. The characterization data matches previous reports.[60]
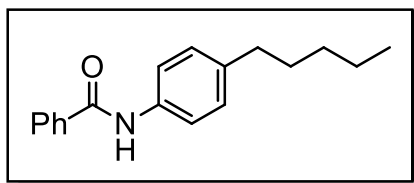
N-(3,4-dimethoxyphenyl)benzamide (3ap)
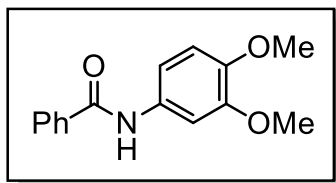
Following general procedure A, benzamide (**1a**, 48.5 mg, 0.4 mmol) and 4-bromoveratrole (**2ap**, 28.8 μL, 0.2 mmol) were employed using 3:1 PhCF$_3$:DMF as solvent and reacted at 50 °C for 7 days. Purification of the residue by flash chromatography

(silica, 20% EtOAc in hexanes) afforded **3ap** (19.4 mg, 38% yield) as a white solid;

R_f = 0.30 (20% EtOAc in hexanes). **¹H NMR** (500 MHz, DMSO-d₆) δ 10.12 (s, 1H),

7.95 (d, J = 7.3 Hz, 2H), 7.58 (t, J = 7.3 Hz, 1H), 7.52 (t, J = 7.3 Hz, 2H), 7.49 (s,

1H), 7.35 (d, J = 8.7 Hz, 1H), 6.93 (d, J = 8.7 Hz, 1H), 3.76 (s, 3H), 3.74 (s, 3H).

¹³C NMR (101 MHz, DMSO-d₆) δ 165.1, 148.4, 145.2, 135.1, 132.7, 131.4, 128.4,

127.5, 112.3, 111.9, 105.5, 55.7, 55.4. The characterization data matches previous

reports.[61]

N-(pyridine-2-yl)benzamide (3aq)
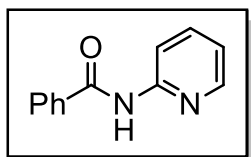
Following general procedure A, benzamide (**1a**, 48.5 mg, 0.4

mmol) and 2-bromopyridine (**2aq**, 19.1 µL, 0.2 mmol) were

employed using 3:1 PhCF₃:DMF as solvent and reacted at 50

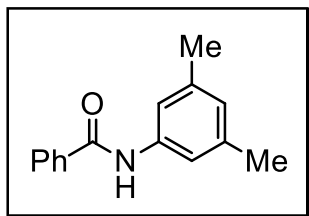°C for 5 days. Purification of the residue by flash chromatography (silica, 25%

EtOAc in dichloromethane) afforded **3aq** (13.2 mg, 33% yield) as a colorless oil;

R_f = 0.28 (25% EtOAc in dichloromethane). **¹H NMR** (400 MHz, CDCl₃) δ 8.71 (bs,

1H), 8.40 (d, J = 8.4 Hz, 1H), 8.28 (ddd, J = 4.9, 1.9, 0.9 Hz, 1H), 7.97 – 7.89 (m,

2H), 7.77 (ddd, J = 8.4, 7.4, 1.9 Hz, 1H), 7.61 – 7.54 (m, 1H), 7.54 – 7.46 (m, 2H),

7.08 (ddd, J = 7.4, 4.9, 1.0 Hz, 1H). **¹³C NMR** (101 MHz, CDCl₃) δ 166.0, 151.7,

147.8, 138.8, 134.4, 132.4, 129.0, 127.4, 120.0, 114.4. The characterization data

matches previous reports.[62]

N-(pyridine-3-yl)benzamide (3ar)
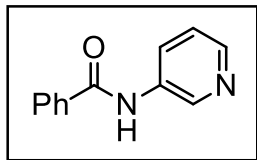
Following general procedure A, benzamide (**1a**, 48.5 mg, 0.4 mmol) and 3-bromopyridine (**2ar**, 19.3 μL, 0.2 mmol) were employed using 3:1 PhCF$_3$:DMF as solvent and reacted at 40 °C for 48 h. Purification of the residue by flash chromatography (silica, 3:1 DCM:EtOAc) afforded **3ar** (26.0 mg, 66% yield) as a light-yellow solid; **R$_f$** = 0.11 (3:1 DCM:EtOAc). The low R$_f$ is necessary in order to elute the residual benzamide before the product. **^{1}H NMR** (400 MHz, CDCl$_3$) δ 8.69 (d, *J* = 2.6 Hz, 1H), 8.52 (bs, 1H), 8.36 – 8.27 (m, 2H), 7.89 (d, *J* = 7.4 Hz, 2H), 7.55 (t, *J* = 7.4 Hz, 1H), 7.46 (t, *J* = 7.4 Hz, 2H), 7.30 (dd, *J* = 8.3, 4.8 Hz, 1H). **^{13}C NMR** (101 MHz, CDCl$_3$) δ 166.5, 145.3, 141.6, 135.3, 134.3, 132.4, 129.0, 128.1, 127.4, 124.0. **HRMS** (ESI-TOF) *m/z* calculated for C$_{12}$H$_{11}$N$_2$O (M+H)$^+$: 199.0865, found 199.0864. **Melting point:** 116-118 °C. The characterization data matches previous reports.[63]

N-(pyrimidin-5-yl)benzamide (3as)
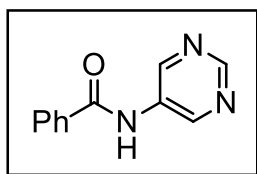
Following general procedure A, benzamide (**1a**, 48.5 mg, 0.4 mmol) and 5-bromopyrimidine (**2as**, 31.8 mg, 0.2 mmol) were employed using 3:1 PhCF$_3$:DMF as solvent and reacted at 40 °C for 48 h. Purification of the residue by flash chromatography (silica, 3:1 DCM:EtOAc) afforded **3as** (6.7 mg, 17% yield) as a white solid; **R$_f$** = 0.11 (3:1 DCM:EtOAc). The low R$_f$ is necessary in order to elute the residual benzamide before the product. **^{1}H NMR** (500 MHz, CDCl$_3$) δ 9.21 (s, 2H), 8.98 (s, 1H), 8.75

(bs, 1H), 7.94 (d, J = 7.5 Hz, 2H), 7.57 (t, J = 7.5 Hz, 1H), 7.47 (t, J = 7.5 Hz, 2H).

**¹³C NMR** (151 MHz, CDCl₃) δ 166.5, 153.9, 148.4, 133.3, 133.3, 132.7, 129.0, 127.6.

N-(4-vinylphenyl)benzamide (3at)
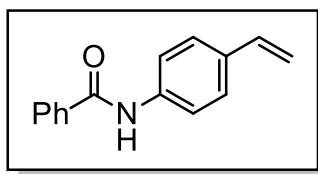
Following general procedure A, benzamide (**1a**, 48.5 mg, 0.4 mmol) and 4-bromostyrene (**2at**, 26.2 µL, 0.2 mmol) were employed using 3:1 PhCF₃:DMF as solvent and reacted at 40 °C for 48 h. The 4-bromostyrene was added in 2 portions (13.1 µL, 0.1 mmol each). The first addition of 4-bromostyrene was at the beginning of the reaction and the second addition was after 24 h. Purification of the residue by flash chromatography (silica, 20% EtOAc in hexanes) afforded **3at** (12.9 mg, 29% yield) as a light-yellow solid; **R**$_f$ = 0.30 (20% EtOAc in hexanes). **¹H NMR** (500 MHz, DMSO-d₆) δ 10.32 (s, 1H), 7.96 (d, J = 7.6 Hz, 2H), 7.79 (d, J = 8.6 Hz, 2H), 7.69 (t, J = 7.6 Hz, 1H), 7.53 (t, J = 7.6 Hz, 2H), 7.47 (d, J = 8.6 Hz, 2H), 6.70 (dd, J = 17.6, 10.9 Hz, 1H), 5.77 (d, J = 17.6 Hz, 1H), 5.20 (d, J = 10.9 Hz, 1H). **¹³C NMR** (101 MHz, DMSO-d₆) δ 165.4, 139.4, 137.3, 135.0, 131.5, 128.4, 127.9, 127.6, 126.7, 120.4, 119.7. The product decomposes before melting. The characterization data matches previous reports.[64]

(*E/Z*)-*N*-styrylbenzamide (3au)
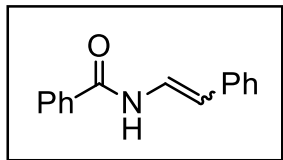
Following general procedure A, benzamide (**1a**, 48.5 mg, 0.4 mmol) and β-bromostyrene (**2au**, 25.7 µL, 0.2 mmol, 87:13 *E/Z*) were employed using 3:1 PhCF$_3$:DMF as solvent and reacted at 40 °C for 48 h. Purification of the residue by flash chromatography (silica, 10% EtOAc in hexanes) afforded **3au** (22.2 mg, 50% yield, 30:70 *E/Z*) as a yellow oil; **R$_f$** (*Z*-isomer) = 0.24 (10% EtOAc in hexanes); **R$_f$** (*E*-isomer) = 0.10. **^{1}H NMR** (*Z*-isomer, 400 MHz, CDCl$_3$) δ 8.38 (bd, *J* = 11.1 Hz, 1H), 7.81 – 7.72 (m, 2H), 7.57 – 7.51 (m, 1H), 7.49 – 7.41 (m, 4H), 7.38 – 7.33 (m, 2H), 7.31 – 7.26 (m, 1H), 7.21 (dd, *J* = 11.2, 9.5 Hz, 1H), 5.90 (d, *J* = 9.5 Hz, 1H). **^{1}H NMR** (*E*-isomer, 400 MHz, CDCl$_3$) δ 7.90 (bs, 1H), 7.88 – 7.83 (m, 2H), 7.74 (dd, *J* = 14.7, 10.8 Hz, 1H), 7.59 – 7.54 (m, 1H), 7.52 – 7.47 (m, 2H), 7.40 – 7.29 (m, 4H), 7.23 – 7.18 (m, 1H), 6.26 (d, *J* = 14.5 Hz, 1H). The characterization data matches previous reports.[65,66]

2.7 References

(1) Ruiz-Castillo, P.; Buchwald, S. L. Applications of Palladium-Catalyzed C−N Cross-Coupling Reactions. *Chem. Rev.* **2016**, *116* (19), 12564–12649. https://doi.org/10.1021/acs.chemrev.6b00512.

(2) Mcgrath, N. A.; Brichacek, M.; Njardarson, J. T. A Graphical Journey of Innovative Organic Architectures That Have Improved Our Lives. *J. Chem. Educ.* **2010**, *87* (12), 1348. https://doi.org/10.1021/ed1003806.

(3) Carey, F. A.; Sundberg, R. J. *Advanced Organic Chemistry Part B: Reactions and Synthesis*, 5th ed.; Springer, 2007.

(4) Chen, C.; Peters, J. C.; Fu, G. C. Photoinduced Copper-Catalysed Asymmetric Amidation via Ligand Cooperativity. *Nature* **2021**, *596* (7871), 250–256. https://doi.org/10.1038/s41586-021-03730-w.

(5) Forero-Cortés, P. A.; Haydl, A. M. The 25th Anniversary of the Buchwald-Hartwig Amination: Development, Applications, and Outlook. *Org. Process Res. Dev.* **2019**, *23* (8), 1478–1483. https://doi.org/10.1021/acs.oprd.9b00161.

(6) Yin, J.; Buchwald, S. L. Palladium-Catalyzed Intermolecular Coupling of Aryl Halides and Amides. *Org. Lett.* **2000**, *2* (8), 1101–1104. https://doi.org/10.1021/ol005654r.

(7) Goldberg, I. Ueber Phenylirungen Bei Gegenwart von Kupfer Als Katalysator. *Ber. Dtsch. Chem. Ges.* **1906**, *39*, 1691–1692.

(8) Deng, W.; Wang, Y. F.; Zou, Y.; Liu, L.; Guo, Q. X. Amino Acid-Mediated Goldberg Reactions between Amides and Aryl Iodides. *Tetrahedron Lett.* **2004**, *45* (11), 2311–2315. https://doi.org/10.1016/j.tetlet.2004.01.119.

(9) Lavoie, C. M.; MacQueen, P. M.; Stradiotto, M. Nickel-Catalyzed N-Arylation of Primary Amides and Lactams with Activated (Hetero)Aryl Electrophiles. *Chem. Eur. J.* **2016**, *22* (52), 18752–18755. https://doi.org/10.1002/CHEM.201605095.

(10) Zhu, C.; Uifeng Yue, H.; Jia, J.; Rueping, M. Cross-Coupling Nickel-Catalyzed C-Heteroatom Cross-Coupling Reactions under Mild Conditions via Facilitated Reductive Elimination. *Angew. Chem. Int. Ed.* **2021**, *60*, 17810–17831. https://doi.org/10.1002/anie.202013852.

(11)   Koo, K.; Hillhouse, G. L. Carbon-Nitrogen Bond Formation by Reductive
       Elimination from Nickel(II) Amido Alkyl Complexes. *Organometallics* **1995**,
       14, 4421–4423.

(12)   Cloutier, J. P.; Zargarian, D. Functionalization of the Aryl Moiety in the
       Pincer Complex (NCN)NiIIIBr2: Insights on NiIII-Promoted Carbon-
       Heteroatom Coupling. *Organometallics* **2018**, *37* (9), 1446–1455.
       https://doi.org/10.1021/acs.organomet.8b00103.

(13)   Till, N. A.; Tian, L.; Dong, Z.; Scholes, G. D.; MacMillan, D. W. C.
       Mechanistic Analysis of Metallaphotoredox C-N Coupling: Photocatalysis
       Initiates and Perpetuates Ni(I)/Ni(III) Coupling Activity. *J. Am. Chem. Soc.*
       2020, *142* (37), 15830–15841. https://doi.org/10.1021/jacs.0c05901.

(14)   Bradley, R. D.; McManus, B. D.; Yam, J. G.; Carta, V.; Bahamonde, A.
       Mechanistic Evidence of a Ni(0/II/III) Cycle for Nickel Photoredox Amide
       Arylation. *Angew. Chem. Int. Ed.* **2023**, *62* (43), e202310753.
       https://doi.org/10.1002/anie.202310753.

(15)   Corcoran, E. B.; Pirnot, M. T.; Lin, S.; Dreher, S. D.; Dirocco, D. A.; Davies,
       I. W.; Buchwald, S. L.; Macmillan, D. W. C. Aryl Amination Using Ligand-
       Free Ni(II) Salts and Photoredox Catalysis. *Science* **2016**, *353* (6296),
       279–283.

(16)   Kawamata, Y.; Vantourout, J. C.; Hickey, D. P.; Bai, P.; Chen, L.; Hou, Q.;
       Qiao, W.; Barman, K.; Edwards, M. A.; Garrido-Castro, A. F.; Degruyter, J.
       N.; Nakamura, H.; Knouse, K.; Qin, C.; Clay, K. J.; Bao, D.; Li, C.; Starr, J.
       T.; Garcia-Irizarry, C.; Sach, N.; White, H. S.; Neurock, M.; Minteer, S. D.;
       Baran, P. S. Electrochemically Driven, Ni-Catalyzed Aryl Amination: Scope,
       Mechanism, and Applications. *J. Am. Chem. Soc.* **2019**, *141* (15), 6392–
       6402. https://doi.org/10.1021/jacs.9b01886.

(17)   Sun, R.; Qin, Y.; Nocera, D. G. General Paradigm in Photoredox Nickel-
       Catalyzed Cross-Coupling Allows for Light-Free Access to Reactivity.
       Angew. Chem. Int. Ed. **2020**, *59* (24), 9527–9533.
       https://doi.org/10.1002/anie.201916398.

(18)   Valeur, E.; Bradley, M. Amide Bond Formation: Beyond the Myth of
       Coupling Reagents. *Chem. Soc. Rev.* **2009**, *38*, 606–631.
       https://doi.org/10.1039/b701677h.

(19)   Massolo, E.; Pirola, M.; Benaglia, M. Amide Synthesis Amide Bond
       Formation Strategies: Latest Advances on a Dateless Transformation. *Eur.*

J. Org. Chem. **2020**, No. 30, 4641–4651.
https://doi.org/10.1002/ejoc.202000080.

(20) Kaur, K.; Srivastava, S. Beckmann Rearrangement Catalysis: A Review of Recent Advances. *New J. Chem.* **2020**, *44*, 18530–18572. https://doi.org/10.1039/d0nj02034f.

(21) Satoh, T.; Oguro, K.; Shishikura, J.-I.; Kanetaka, N.; Okada, K.; Yamakawa, K. Favorskii Rearrangement of α-Chloro β-Keto Sulfones with Amines: A New Synthesis of Amides and α,β-Unsaturated Amides from Aldehydes and Ketones. *Tetrahedron Lett.* **1992**, *33* (11), 1455–1458.

(22) Li, G.; Szostak, M. Highly Selective Transition-Metal-Free Transamidation of Amides and Amidation of Esters at Room Temperature. *Nat. Commun.* **2018**, *9*, 4165. https://doi.org/10.1038/s41467-018-06623-1.

(23) Ikawa, T.; Barder, T. E.; Biscoe, M. R.; Buchwald, S. L. Pd-Catalyzed Amidations of Aryl Chlorides Using Monodentate Biaryl Phosphine Ligands: A Kinetic, Computational, and Synthetic Investigation. *J. Am. Chem. Soc.* **2007**, *129* (43), 13001–13007. https://doi.org/10.1021/ja0717414.

(24) Beattie, D. D.; Bowes, E. G.; Drover, M. W.; Love, J. A.; Schafer, L. L. Oxidation State Dependent Coordination Modes: Accessing an Amidate-Supported Nickel(I) Δ-bis(C−H) Agostic Complex. *Angew. Chem. Int. Ed.* **2016**, *128* (42), 13484–13489. https://doi.org/10.1002/ange.201607243.

(25) Fujita, K. I.; Yamashita, M.; Puschmann, F.; Alvarez-Falcon, M. M.; Incarvito, C. D.; Hartwig, J. F. Organometallic Chemistry of Amidate Complexes. Accelerating Effect of Bidentate Ligands on the Reductive Elimination of N-Aryl Amidates from Palladium(II). *J. Am. Chem. Soc.* **2006**, *128* (28), 9044–9045. https://doi.org/10.1021/ja062333n.

(26) Monti, A.; López-Serrano, J.; Prieto, A.; Nicasio, M. C. Broad-Scope Amination of Aryl Sulfamates Catalyzed by a Palladium Phosphine Complex. *ACS Catal.* **2023**, *13* (16), 10945–10952. https://doi.org/10.1021/acscatal.3c03166.

(27) Liu, L.; Nevado, C. Diaryl Ether Formation Merging Photoredox and Nickel Catalysis. *Organometallics* **2021**, *40* (14), 2188–2193. https://doi.org/10.1021/acs.organomet.1c00018.

(28) Terrett, J. A.; Cuthbertson, J. D.; Shurtleff, V. W.; MacMillan, D. W. C. Switching on Elusive Organometallic Mechanisms with Photoredox Catalysis. *Nature* **2015**, *524* (7565), 330–334. https://doi.org/10.1038/nature14875.

(29) Rosemann, N. W.; Eußner, J. P.; Beyer, A.; Koch, S. W.; Volz, K.; Dehnen, S.; Chatterjee, S. A Highly Efficient Directional Molecular White-Light Emitter Driven by a Continuous-Wave Laser Diode. *Science (1979)* **2016**, *352* (6291), 1301–1304. https://doi.org/10.1126/science.aaf6138.

(30) Lin, K.; Chen, Q.; Gerhardt, M. R.; Tong, L.; Kim, S. B.; Eisenach, L.; Valle, A. W.; Hardee, D.; Gordon, R. G.; Aziz, M. J.; Marshak, M. P. Alkaline Quinone Flow Battery. *Science (1979)* **2015**, *349* (6255), 1529–1532. https://doi.org/10.1126/science.aab3033.

(31) Le, C.; Liang, Y.; Evans, R. W.; Li, X.; MacMillan, D. W. C. Selective Sp 3 C-H Alkylation via Polarity-Match-Based Cross-Coupling. *Nature* **2017**, *547* (7661), 79–83. https://doi.org/10.1038/nature22813.

(32) Yamamoto, T.; Abla, M. Reductive Elimination of Et-Et from NiEt2(Bpy) Promoted by Electron-Accepting Aromatic Compounds. *J. Organomet. Chem.* **1997**, *535*, 209–211.

(33) Hwang, S. J.; Anderson, B. L.; Powers, D. C.; Maher, A. G.; Hadt, R. G.; Nocera, D. G. Halogen Photoelimination from Monomeric Nickel(III) Complexes Enabled by the Secondary Coordination Sphere. *Organometallics* **2015**, *34* (19), 4766–4774. https://doi.org/10.1021/acs.organomet.5b00568.

(34) Shields, B. J.; Doyle, A. G. Direct C(Sp3)-H Cross Coupling Enabled by Catalytic Generation of Chlorine Radicals. *J. Am. Chem. Soc.* **2016**, *138* (39), 12719–12722. https://doi.org/10.1021/jacs.6b08397.

(35) Prier, C. K.; Rankic, D. A.; Macmillan, D. W. C. Visible Light Photoredox Catalysis with Transition Metal Complexes: Applications in Organic Synthesis. *Chem. Rev.* **2013**, *113*, 5322. https://doi.org/10.1021/cr300503r.

(36) Heitz, D. R.; Tellis, J. C.; Molander, G. A. Photochemical Nickel-Catalyzed C-H Arylation: Synthetic Scope and Mechanistic Investigations. *J. Am. Chem. Soc.* **2016**, *138* (39), 12715–12718. https://doi.org/10.1021/jacs.6b04789.

(37) Ting, S. I.; Williams, W. L.; Doyle, A. G. Oxidative Addition of Aryl Halides to a Ni(I)-Bipyridine Complex. *J. Am. Chem. Soc.* **2022**, *144* (12), 5575–5582. https://doi.org/10.1021/jacs.2c00462.

(38) Zuo, Z.; Ahneman, D. T.; Chu, L.; Terrett, J. A.; Doyle, A. G.; Macmillan, D. W. C. Merging Photoredox with Nickel Catalysis: Coupling of α-Carboxyl Sp 3-Carbons with Aryl Halides. *Science* **2014**, *345* (6195), 437–440.

(39) Neises, B.; Steglich, W. Simple Method for the Esterification of Carboxylic Acids. *Angew. Chem. Int. Ed.* **1978**, *17* (7), 522–524. https://doi.org/10.1002/anie.197805221.

(40) Ren, W.; Yamane, M. Mo(CO)6-Mediated Carbamoylation of Aryl Halides. *J. Org. Chem* **2010**, *75* (24), 8410–8415. https://doi.org/10.1021/jo101611g.

(41) Hwang, S.; Choi, S. Y.; Lee, J. H.; Kim, S.; In, J.; Ha, S. K.; Lee, E.; Kim, T. Y.; Kim, S. Y.; Choi, S.; Kim, S. Identification of a Potent and Noncytotoxic Inhibitor of Melanin Production. *Bioorg. Med. Chem.* **2010**, *18* (15), 5602–5609. https://doi.org/10.1016/j.bmc.2010.06.034.

(42) Nijampatnam, B.; Ahirwar, P.; Pukkanasut, P.; Womack, H.; Casals, L.; Zhang, H.; Cai, X.; Michalek, S. M.; Wu, H.; Velu, S. E. Discovery of Potent Inhibitors of Streptococcus Mutans Biofilm with Antivirulence Activity. *ACS Med. Chem. Lett.* **2021**, *12* (1), 48–55. https://doi.org/10.1021/acsmedchemlett.0c00373.

(43) Dong, Q. L.; Liu, G. S.; Zhou, H. Bin; Chen, L.; Yao, Z. J. Metal-Free Synthesis of Alkynyl Imines Using an Oxophosphonium-Mediated Approach at Ambient Temperatures. *Tetrahedron Lett.* **2008**, *49* (10), 1636–1640. https://doi.org/10.1016/j.tetlet.2008.01.024.

(44) Karaki, F.; Ohgane, K.; Fukuda, H.; Nakamura, M.; Dodo, K.; Hashimoto, Y. Structure-Activity Relationship Study of Non-Steroidal NPC1L1 Ligands Identified through Cell-Based Assay Using Pharmacological Chaperone Effect as a Readout. *Bioorg. Med. Chem.* **2014**, *22* (14), 3587–3609. https://doi.org/10.1016/j.bmc.2014.05.022.

(45) Alexandratos, S. D.; Trochimczuk, A. W.; Crick, D. W.; Philip Horwitz, E.; Gatrone, R. C.; Chiarizia, R. Synthesis and Ion-Complexing Properties of a Novel Polymer-Supported Reagent with Diphosphonate Ligands. *Macromolecules* **1996**, *29*, 1021–1026.

(46) Xie, S.; Zhang, Y.; Ramström, O.; Yan, M. Base-Catalyzed Synthesis of Aryl Amides from Aryl Azides and Aldehydes. *Chem. Sci.* **2016**, *7* (1), 713–718. https://doi.org/10.1039/c5sc03510d.

(47) Lundrigan, T.; Tassone, J. P.; Stradiotto, M. Nickel-Catalyzed N -Arylation of Amides with (Hetero)Aryl Electrophiles by Using a DBU/NaTFA Dual-Base System. *Synlett* **2021**, *32* (16), 1665–1669. https://doi.org/10.1055/a-1337-6459.

(48) Atigadda, V. R.; Brouillette, W. J.; Duarte, F.; Ali, S. M.; Babu, Y. S.; Bantia, S.; Chand, P.; Chu, N.; Montgomery, J. A.; Walsh, D. A.; Sudbeck, E. A.; Finley, J.; Luo, M.; Air, G. M.; Laver, G. W. Potent Inhibition of Influenza Sialidase by a Benzoic Acid Containing a 2-Pyrrolidinone Substituent. *J. Med. Chem.* **1999**, *42* (13), 2332–2343. https://doi.org/10.1021/jm980707k.

(49) Kim, H.; Kim, T.; Gil Lee, D.; Weon Roh, S.; Lee, C. Nitrogen-Centered Radical-Mediated C–H Imidation of Arenes and Heteroarenes via Visible Light Induced Photocatalysis. *Chem. Comm.* **2014**, *50* (66), 9273–9276. https://doi.org/10.1039/c4cc03905j.

(50) Chandrasekhar, S.; Reddy, C. R.; Rao, R. J. Unprecedented Direct Conversion of N-N and N=N Bonds to N-(Tert-Butyloxy)-Carbamates 1. *Synlett* **2001**, *10*, 1561–1562.

(51) Raju, B.; Kogan, T. P. Solid Phase Synthesis of Sulfonamides Using a Carbamate Linker. *Tetrahedron Lett.* **1997**, *38* (19), 3373–3376.

(52) Chan, A. Y.; Ghosh, A.; Yarranton, J. T.; Twilton, J.; Jin, J.; Arias-Rotondo, D. M.; Sakai, H. A.; McCusker, J. K.; C MacMillan, D. W. Exploiting the Marcus Inverted Region for First-Row Transition Metal-Based Photoredox Catalysis. *Science (1979)* **2023**, *382*, 191–197.

(53) Dannhardt, G.; Fiebich, B. L.; Schweppenhäuser, J. COX-1/COX-2 Inhibitors Based on the Methanone Moiety. *Eur. J. Med. Chem.* **2002**, *37*, 147–161.

(54) Raghuvanshi, D. S.; Gupta, A. K.; Singh, K. N. Nickel-Mediated N-Arylation with Arylboronic Acids: An Avenue to Chan-Lam Coupling. *Org. Lett.* **2012**, *14* (17), 4326–4329. https://doi.org/10.1021/ol3021836.

(55) Tundel, R. E.; Anderson, K. W.; Buchwald, S. L. Expedited Palladium-Catalyzed Amination of Aryl Nonaflates through the Use of Microwave-Irradiation and Soluble Organic Amine Bases. *J. Org. Chem.* **2006**, *71* (1), 430–433. https://doi.org/10.1021/jo052131u.

(56) Li, H.; Neumann, H.; Beller, M.; Wu, X. F. Aryl Formate as Bifunctional Reagent: Applications in Palladium-Catalyzed Carbonylative Coupling Reactions Using in Situ Generated CO. *Angew. Chem. Int. Ed.* **2014**, *53* (12), 3183–3186. https://doi.org/10.1002/anie.201311198.

(57) Zhang, D. X.; Xiang, S. K.; Hu, H.; Tan, W.; Feng, C.; Wang, B. Q.; Zhao, K. Q.; Hu, P.; Yang, H. An Improved Protocol for Synthesis of N-Arylamides and Benzoxazoles by the Copper-Catalyzed Reaction of Aryl Halides with

Nitriles. *Tetrahedron* **2013**, *69* (47), 10022–10029. https://doi.org/10.1016/j.tet.2013.09.059.

(58) Klapars, A.; Antilla, J. C.; Huang, X.; Buchwald, S. L. A General and Efficient Copper Catalyst for the Amidation of Aryl Halides and the N-Arylation of Nitrogen Heterocycles [2]. *J. Am. Chem. Soc.* **2001**, *123* (31), 7727–7729. https://doi.org/10.1021/ja016226z.

(59) Ling, L.; Chen, C.; Luo, M.; Zeng, X. Chromium-Catalyzed Activation of Acyl C-O Bonds with Magnesium for Amidation of Esters with Nitroarenes. *Org. Lett.* **2019**, *21* (6), 1912–1916. https://doi.org/10.1021/acs.orglett.9b00554.

(60) Teo, Y. C.; Yong, F. F.; Ithnin, I. K.; Yio, S. H. T.; Lin, Z. Efficient Manganese/Copper Bimetallic Catalyst for N-Arylation of Amides and Sulfonamides under Mild Conditions in Water. *Eur. J. Org. Chem.* **2013**, No. 3, 515–524. https://doi.org/10.1002/ejoc.201201218.

(61) Bering, L.; Vogt, M.; Paulussen, F. M.; Antonchick, A. P. Selective, Catalytic, and Metal-Free Coupling of Electron-Rich Phenols and Anilides Using Molecular Oxygen as Terminal Oxidant. *Org. Lett.* **2018**, *20* (13), 4077–4080. https://doi.org/10.1021/acs.orglett.8b01631.

(62) Sakhare, P. R.; Subramanian, P.; Kaliappan, K. P. Copper Catalyzed Oxidative C-C Bond Cleavage of 1,2-Diketones: A Divergent Approach to 1,8-Naphthalimides, Biphenyl-2,2′-Dicarboxamides, and N-Heterocyclic Amides. *J. Org. Chem.* **2019**, *84* (4), 2112–2125. https://doi.org/10.1021/acs.joc.8b03114.

(63) Jóźwiak, A.; Brzeziński, J. Z.; Płotka, M. W.; Szcześniak, A. K.; Malinowski, Z.; Epsztajn, J. Behaviour of N-Pyridylbenzamides versus Benzanilides in the Ortho-Directed Lithiation of Masked Aromatic Carboxylic Acids. *Eur. J. Org. Chem.* **2004**, No. 15, 3254–3261. https://doi.org/10.1002/ejoc.200400156.

(64) Chatterjee, T.; Dey, R.; Ranu, B. C. An Easy Access to Styrenes: Trans Aryl 1,3-, 1,4- and 1,5-Dienes, and 1,3,5-Trienes by Hiyama Cross-Coupling Catalyzed by Palladium Nanoparticles. *New J. Chem.* **2011**, *35* (5), 1103–1110. https://doi.org/10.1039/c0nj01019g.

(65) Bolshan, Y.; Batey, R. A. Enamide Synthesis by Copper-Catalyzed Cross-Coupling of Amides and Potassium Alkenyltrifluoroborate Salts. *Angew. Chem. Int. Ed.* **2008**, *47* (11), 2109–2112. https://doi.org/10.1002/anie.200704711.

(66) Gooßen, L. J.; Salih, K. S. M.; Blanchot, M. Synthesis of Secondary Enamides by Ruthenium-Catalyzed Selective Addition of Amides to Terminal Alkynes. *Angew. Chem. Int. Ed.* **2008**, *47* (44), 8492–8495. https://doi.org/10.1002/anie.200803068.

Chapter 3: Mechanistic investigation of the catalytic mechanism of Ni-photoredox amide *N*-arylation

3.1 Introduction

In recent years, Ni-photoredox dual catalysis has emerged as a robust platform for a variety of C-heteroatom cross-coupling reactions[1–5]. Although the suite of Ni-photoredox C-heteroatom coupling methods reported thus far accommodate a broad scope, reports describing in-depth mechanistic studies of such reactions remain uncommon[6–11]. Previous reports proposed that the low temperature reductive elimination in these dual Ni photocatalyst (PC) systems is enabled by access to either excited Ni(II) species[2,5,6,12–18] (via energy transfer, or EnT) or oxidized Ni(III) species[3,4,6,18–24] (via photoinduced electron transfer, or PET). This is in contrast to thermally-driven Ni-catalyzed C-heteroatom coupling, which requires elevated temperatures to promote the endothermic reductive elimination from Ni(II)[2,25].

Most studies of Ni-photoredox C-N coupling systems published thus far have proposed the intermediacy of Ni(III) to enable facile reductive elimination[4,7,10]. In fact, C-N reductive elimination triggered by 1-electron oxidation of Ni(II) alkyl amido complexes had been known for decades before the advent of Ni-photoredox catalysis, with seminal work from Hillhouse & Koo demonstrating that such complexes could undergo oxidatively-induced reductive elimination when treated with a variety of stoichiometric chemical oxidants[21]. DFT calculations further

support facile C-N reductive elimination from Ni(III) with a drastic reduction in the kinetic barrier to reductive elimination for both alkylamines and amides[2]. Alternatively, EnT mechanisms involving excited Ni(II) species to enable the difficult C-N reductive elimination have been proposed[26,27]. It is also possible that reductive elimination in these EnT systems is occurring from Ni(III) rather than Ni(II) since Förster-type EnT has been shown to provide access to highly reactive Ni(III) intermediates in similar C-O coupling platforms via metal-to-ligand charge transfer (MLCT)[17].

Within the field of mild Ni-photoredox C-N cross-coupling, our group published a report describing a Ni-photoredox-catalyzed amide arylation reaction, which was the subject of Chapter 2 of this thesis[28]. The main advantage of this methodology is that it circumvents the high temperatures required in other transition metal-mediated amide arylation strategies[29–38]. Additionally, it was the first report of a general Ni-photoredox $C(sp^2)$-N coupling reaction utilizing amides as nucleophiles. To further leverage the mildness of this transformation and accommodate both temperature- and base-sensitive substrates, we identified conditions that employ weak inorganic bases instead of the strong alkoxide bases that are commonly used in amide functionalization reactions. This facilitated access to a broad substrate scope which included amides with epimerizable stereocenters that underwent N-arylation with excellent stereoretention. A major consequence of choosing weak, inorganic bases for Ni-photoredox catalysis is that they are not known to act as electron shuttles. This is unlike many soluble organic

tertiary amine bases (e.g., DABCO, quinuclidine, TMG) which have been shown to facilitate electron transfers between photocatalyst and Ni catalyst [4,6,10,39]. These organic bases are often selected for Ni-photoredox C-heteroatom cross-coupling reactions due to their unique redox properties.

We posited that the operative mechanism of this Ni-photoredox amide arylation reaction may be divergent from those previously reported for C-N cross-coupling due to the relatively low nucleophilicity of the amide functional group (compared to other *N*-nucleophiles) and the absence of a redox-active base. All prior published Ni-photoredox C-X cross-coupling methods require a redox-active base, unlike the redox-inactive and insoluble phosphates and carbonates that were most effective for our amide arylation

Figure 1: Four mechanistic hypotheses for Ni-catalyzed amide arylation
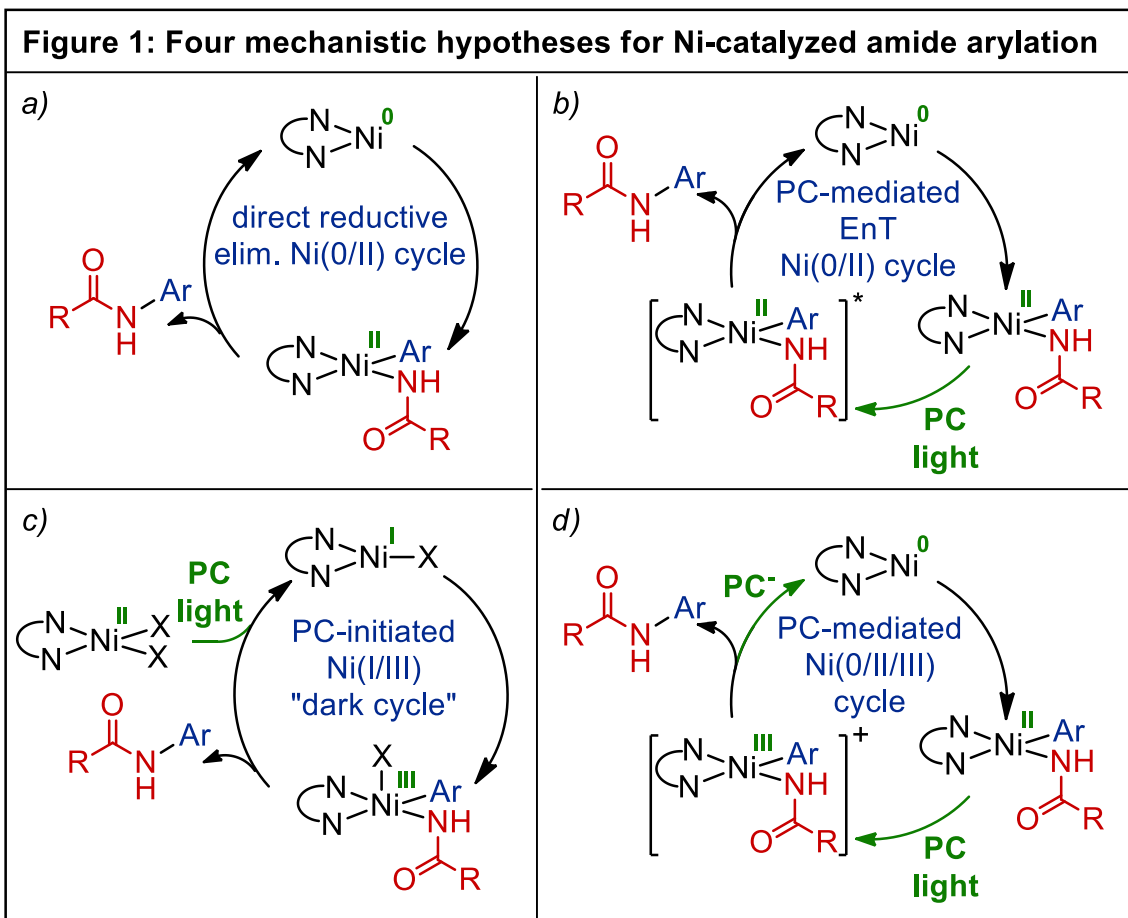
reaction. As shown in Chapter 2, redox-active bases like TMG produced lower yields than the optimal inorganic, redox-innocent bases. Heterogeneous photoredox systems, although uncommon in C-heteroatom cross-coupling, are still often encountered in other types of Ni-photoredox reactions[3,40–42]. The study of these heterogeneous photochemical systems is complicated by light scattering from the insoluble base, altering the effective photon flux. Thus, heterogeneity prevents the accurate determination of quantum yield for these reactions. This issue could be circumvented by instead choosing a soluble base, although most soluble bases are redox-active amines that could exert a great influence on the

mechanism being studied. Instead, we decided to study the original heterogeneous conditions to better understand the optimized amide arylation reaction.

Based on the preceding mechanistic studies, we envisioned that the dominant mechanism of the amine arylation reaction would fall into one of four mechanistic manifolds **(Figure 1)**. The simplest mechanistic hypothesis involves oxidative addition to Ni(0) and a thermally-driven reductive elimination from Ni(II) **(Figure 1a)**. This mechanism can be discarded since the reaction only proceeds at ambient temperature under blue light irradiation and in the presence of a photocatalyst, implicating the involvement of the photocatalyst in either an EnT or PET process that is necessary for productive coupling. Thus, three mechanistic hypotheses could not yet be ruled out: an EnT-driven Ni(0/II) cycle **(Figure 1b)**, a PET-driven Ni(I/III) cycle **(Figure 1c)**, or a PET-driven Ni(0/II/III) cycle **(Figure 1d)**. For Ni-photoredox C-heteroatom coupling reactions that involve Ni(III) intermediates, mechanistic studies have consistently revealed a Ni(I/III) cycle rather than the commonly proposed Ni(0/II/III) cycle. In the context of both amine and alcohol arylation reactions enabled by Ni-photoredox systems, quantum yield measurements have revealed self-sustained Ni(I/III) "dark cycles", in which the PET step serves only to initiate the catalytic cycle or to reintroduce off-cycle Ni species back into the Ni(I/III) manifold[7,8]. In contrast, a Ni(0/II/III) cycle would necessitate at least 1 PET event per catalytic turnover, which would produce a quantum yield of less than 1. Insights gleaned from these studies were later leveraged to design other Ni(I/III) cycles for C-heteroatom cross-couplings that

operate in the absence of PC or light by utilizing electrochemical or stoichiometric chemical reductants to promote the Ni(I/III) "dark cycle" [9,10].

Our approach to probing the mechanism of the amide arylation reaction was multifaceted. To interrogate the catalytic cycle, we aimed to synthesize Ni complexes that were analogs of catalytic intermediates. The reactivity of these complexes under light irradiation, heating, chemical oxidation, and electrochemical oxidation could reveal the necessary trigger for C-N reductive elimination. We also wanted to test whether isolable reaction intermediates could be used as competent catalysts in the Ni-photoredox reaction at catalytic loadings. Additionally, the spectroscopic and electrochemical properties of these intermediate complexes could be studied to provide clues about the reaction mechanism.

Since stoichiometric experiments of Ni complexes do not directly probe the original catalytic system, they are not conclusive on their own. To more directly observe the behavior of the Ni catalyst in the Ni-photoredox system, we measured the kinetic profiles of product formation for the catalytic amide arylation reaction under the normal catalytic conditions. This involved the measurement of kinetic profiles for parallel reactions varying stoichiometries of reaction components and other reaction parameters. This was a challenge since reproducibility in Ni-photoredox systems can be impacted by small changes in parameters such as the distance from the source of irradiation, the intensity of irradiation, and the dimensions and UV-Vis absorption profile of the reaction glassware (see Chapter 3.3). The goal of this study was to provide insights into the initial rate and to see if

there were any interesting features present in the early time points that may provide clues to elucidate the dominant mechanism.

Since the reaction being studied uses a Ni(II) source, 1- or 2-electron reduction must be invoked to access the low-valent Ni(I) or Ni(0) intermediates that are necessary to perform oxidative addition with the electrophilic coupling partner and kick off the catalytic cycle, and we wanted to study the nature of this process. We sought to conduct kinetic trials with various Ni(II), Ni(I), and Ni(0) precatalysts (and combinations thereof) to determine if there are any identifiable off-cycle oxidation states and to learn about the nature of redox events occurring between the various Ni species in solution. Conveniently, commercially available Ni(0) and Ni(II) sources exist, and Ni(I) precatalysts can easily be synthesized following simple protocols[43]. To further test hypotheses regarding the oxidation state of the catalyst resting state, in situ EPR spectroscopy was employed.

3.2   Stoichiometric experiments involving nickel(aryl)(amido) complexes

In order to differentiate between mechanisms 1b, 1c, and 1d (i.e. EnT vs. PET mechanisms for reductive elimination), we proceeded to probe the plausible steps in the catalytic cycle stoichiometrically. Specifically, we aimed to synthesize isolable Ni(II) aryl amido complexes, which we hypothesized would be relatively stable based on literature precedents that synthesized related Ni(II) aryl amido complexes[7,21]. In the amide arylation reaction being studied, these Ni(II) aryl amido

species are likely present in solution as either on-cycle species in a Ni(0/II/III) cycle or off-cycle species in a Ni(I/III) cycle.

Scheme 1: Synthesis of Ni(II) complexes relevant to Ni-photoredox-catalyzed amide arylation

4a: $R^1 = CH_3$, $R^2 = F$
4b: $R^1 = CF_3$, $R^2 = H$

5a: $R^1 = CH_3$, $R^2 = F$
5b: $R^1 = CF_3$, $R^2 = H$
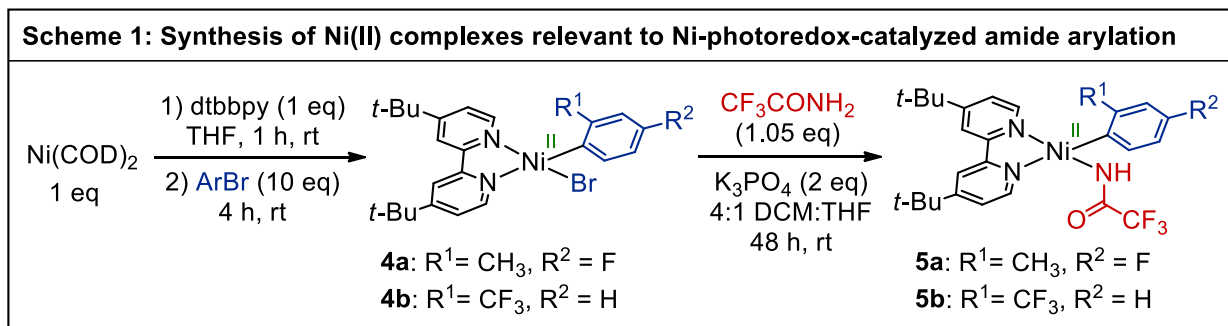
Since the ^{1}H NMR spectra of Ni(II) complexes can be complex, we wanted to synthesize Ni(II) aryl amido complexes with fluorinated handles on both aryl and amido groups, allowing for complex formation to be monitored by ^{19}F NMR spectroscopy. To synthesize the desired Ni(II) aryl amido complexes, the corresponding Ni(II) aryl bromide complexes were first made by stirring Ni(COD)$_2$ with a large excess of *ortho*-substituted aryl bromide, rendering the complexes **4a** and **4b (Scheme 1)**. These Ni complexes were synthesized in the glovebox. When *para*-substituted 4-bromobenzotrifluoride was stirred with Ni(COD)$_2$, the resulting Ni(II) aryl bromide complex quickly decomposed and only homocoupled biaryl and Ni

Figure 2: X-ray crystal structure of 5b
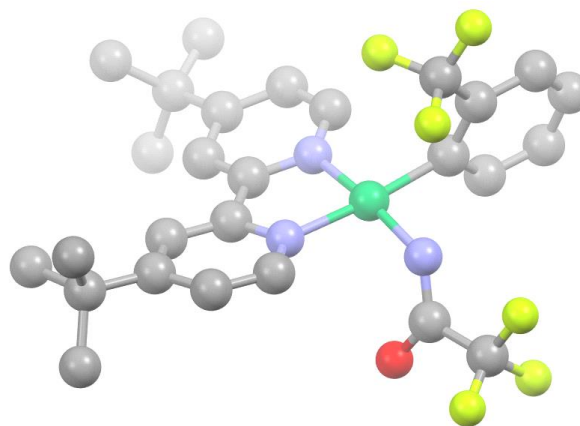
H atoms omitted for clarity.

aggregates were obtained. This demonstrates the need for an *ortho*-substituent to prevent undesired transmetalation between Ni(II) species in order to form a stable Ni(II) aryl bromide complex. The Ni(II) aryl amido complexes **5a** and **5b** could be accessed by stirring **4a** or **4b** with trifluoroacetamide and K₃PO₄ **(Scheme 1)**. All of these complexes were prone to speciation when they were dissolved, necessitating minimal workup (simple

Figure 3: Spectroscopic and redox properties of 5a and 5b

a) UV-Vis spectra

(L = dtbbpy)
5a: $R^1 = CH_3$, $R^2 = F$
5b: $R^1 = CF_3$, $R^2 = H$

b) Cyclic voltammetry

filtration and evaporation) in order to avoid partial decomposition of the desired complexes. This decomposition could be quantified by observing the ^{1}H NMR signal of the free ligand, dtbbpy.

These four complexes were characterized by ^{1}H and ^{19}F NMR spectroscopy and their mass ions were detected with HRMS. Additionally, a single crystal of **5b** was grown. The X-ray structural analysis of this crystal was conducted by Veronica
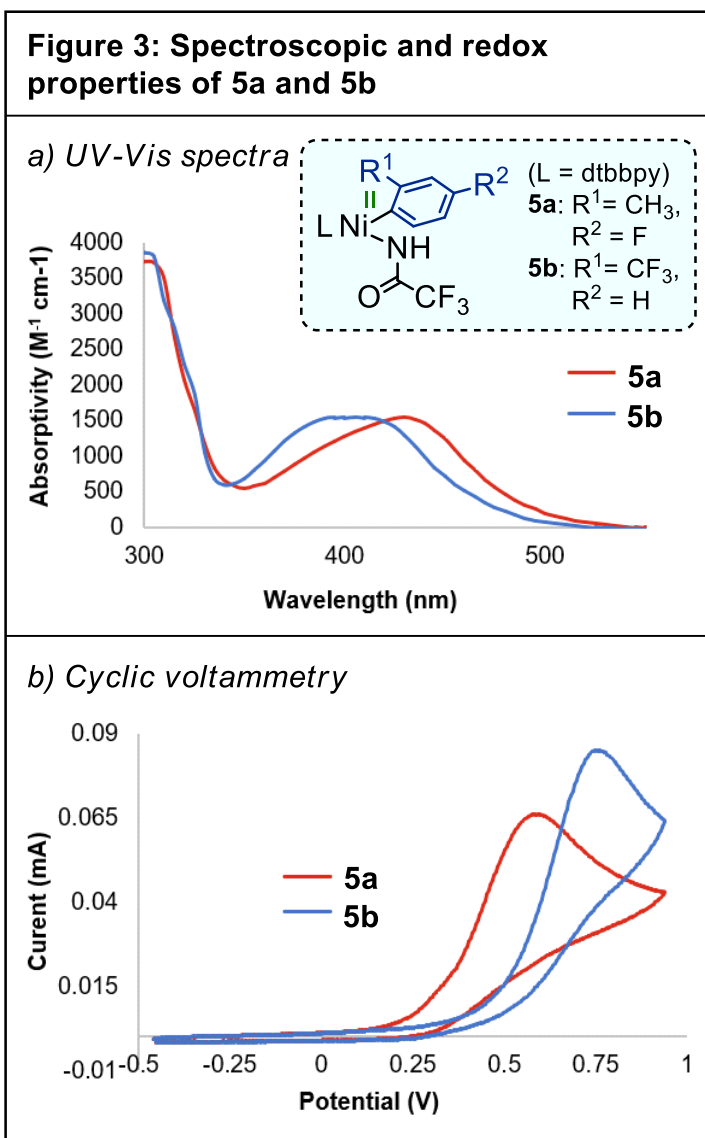
Carta, and revealed a distorted square planar geometry around the Ni center[44] **(Figure 2)**. Both **5a** and **5b** appear orange in color in the solid state and have similar UV-Vis absorption profiles in acetonitrile solutions **(Figure 3a)**. The Ni(II) aryl amido complexes were studied by cyclic voltammetry **(Figure 3b)** and irreversible oxidations were observed for both complexes ($E_{1/2}$ = +0.19 V and +0.50 V for **5a** and **5b**, respectively). The irreversible traces demonstrate that a reaction is occurring upon oxidation to Ni(III) (presumably, C-N reductive elimination).

Next, the complexes **5a** and **5b** were subjected to chemical oxidants, blue LED irradiation, or 50 °C and no light to determine what conditions may be triggering the reductive elimination and form the aryl amide **(Scheme 2)**. For both complexes, neither blue LED irradiation nor heating to 50 °C led to the formation of reductive elimination products. Complex **5a** was relatively unstable and decomposed under these conditions, losing its red color after decomposition. Complex **5b** retained its color and NMR spectra showed that it remained intact after heating and light irradiation. When the two amido complexes were treated stoichiometrically with the chemical oxidant acetylferrocenium tetrafluoroborate ($E_{1/2}$ = +0.32 V vs. Ag/AgNO$_3$ in CH$_3$CN, **Figure 21)**, different results were obtained for each complex. While complex **5b** ($E_{1/2}$ = 0.50 V vs. Ag/AgNO$_3$) did not undergo any reaction when stirred with the oxidant, complex **5a** ($E_{1/2}$ = 0.19 V vs. Ag/AgNO$_3$) underwent reductive elimination to form aryl amide **3b**, isolated in 67% yield **(Scheme 2)**. The redox potentials are in line with acetylferrocenium not being a sufficiently strong oxidant for Ni(II) complex **5b**. This experiment demonstrates

that oxidation to Ni(III) is necessary to trigger reductive elimination at ambient temperature (i.e., oxidatively-induced reductive elimination). Exposure of complex **5a** to air also led to trace amounts of aryl amide being formed. The analogous catalytic Ni-photoredox cross-coupling reaction between 2-bromo-5-fluorotoluene **(2b)** and trifluoroacetamide **(1b)** also produced aryl amide **3b**, but in lower yield (46% instead of 67%). When 2-bromobenzotrifluoride **(2c)** was chosen as the electrophilic coupling partner, no product formation was observed. This agrees with the lack of reactivity observed when the analogous Ni(II) aryl amido complex **(5b)** was exposed to the stoichiometric oxidant.

Scheme 2: Stoichiometric reactions of Ni(II) aryl amido complexes 5a and 5b
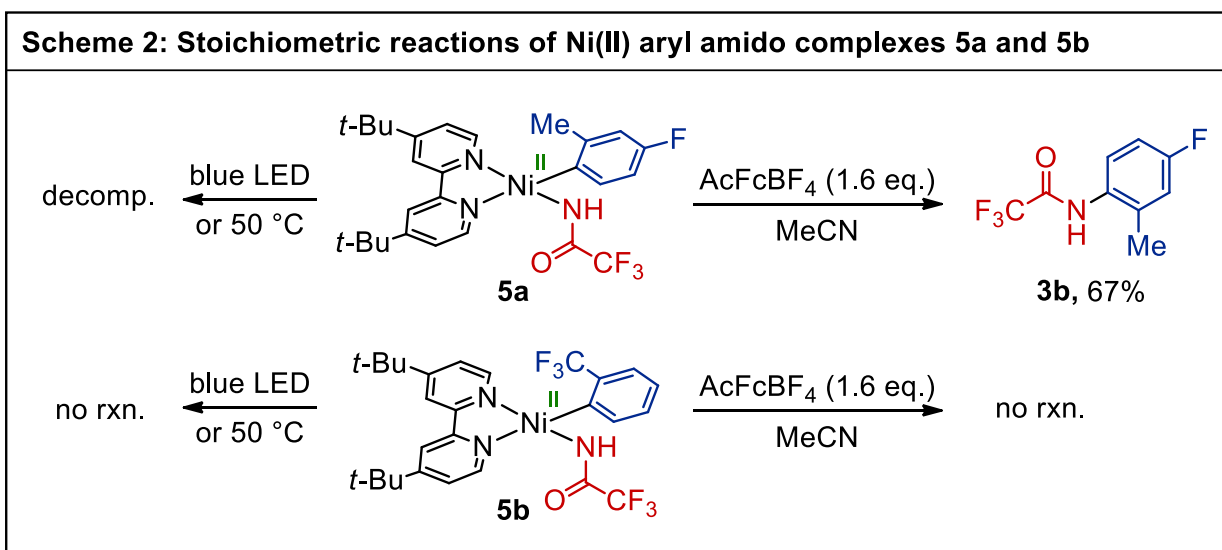
The divergent reactivity of these two complexes can be understood in terms of their relative redox potentials, with **5b** displaying a more positive oxidation potential than **5a**, possibly due to **5b** having a more electron-poor aryl ligand. As a result, oxidatively-induced reductive elimination will be more facile for **5a** than for

5b. Additionally, both complexes display similar absorption at 427 nm (the wavelength of the narrow emission blue LEDs used in the catalytic reaction) despite having dramatically different reactivity. The observation of facile oxidatively-induced reductive elimination along with the lack of correlation between spectroscopic properties and complex reactivity both support the intermediacy of Ni(III) in the dominant catalytic cycle and provide evidence against a Ni(0/II) EnT-mediated process. This is in line with our prior studies that also showed no catalytic reaction occurring when a higher energy 390 nm light source was used in the absence of the Ir photocatalyst[28].

Scheme 3: Complex 5a is a competent precatalyst for the amide arylation reaction
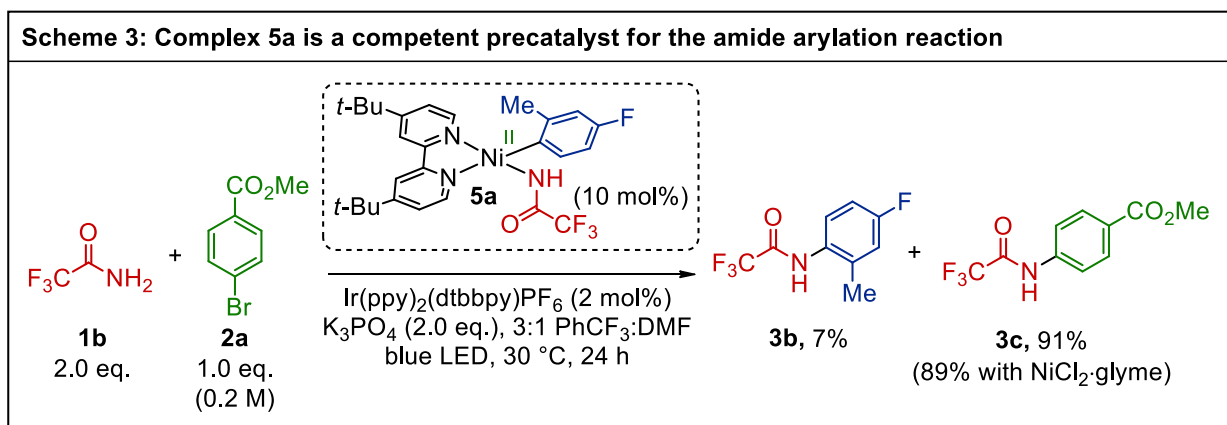
Aiming to further probe the intermediacy of Ni(II) aryl amido complexes in the catalytic reaction, the suitability of **5a** as a precatalyst for the coupling of **1b** and **2a** was tested **(Scheme 3)**. Amide **1b** was chosen as the nucleophilic coupling partner to reduce the complexity of the product mixture due to the reversible nature of amide binding. After 24 hours of irradiation with blue light, two products were isolated. Product **3b** was isolated in 7% yield (70% with respect to Ni precatalyst

loading), showing that an initial reductive elimination was required for conversion of the Ni(II) precatalyst **5a** to the Ni(0) active catalyst. Product **3c** was also obtained in 91% yield, demonstrating that the catalytic efficiency of **5a** is comparable to that of $NiCl_2$(glyme) (89% yield[28]). Complex **5a** was also compared to Ni(0) and Ni(II) precatalysts in kinetic trials, which will be discussed in Chapter 3.3.

3.3   Kinetic experiments probing nickel-photoredox amide arylation

To further investigate the reaction mechanism and differentiate between mechanisms 1c and 1d, we set out to conduct a variety of kinetics experiments in which product formation over time was compared to the initial concentration of various reaction components. The reaction between 2-pyrrolidone **(1a)** and methyl 4-bromobenzoate **(2a)** with K_3PO_4 as base was chosen as a model system **(Figure 4)**. Identification of a highly reproducible reaction setup was key to the generation of reliable kinetic measurements to compare multiple parallel reactions. To do so, all of the experiments were performed in identical Schlenk flasks that were positioned in pairs 1.5 cm away from the same two 427 nm Kessil lamps. In all of the experiments, one of the two reactions was varied to study the effect of different conditions on the reaction rate, while the other flask was kept constant with the generic reaction conditions to ensure that the different reaction sets could be compared. This assurance of reproducibility also confirmed that the two lamps provided similar intensities of blue light irradiation. Additionally, the experiments to study each reaction parameter were all performed simultaneously and utilized the

same stock solutions. The stock solutions containing the Ni precatalysts and 4,4'-di-*tert*-butyl-2,2'-bipyridine (dtbbpy) as the ligand were stirred for at least 10 minutes to enable ligand exchange and dtbbpy complexation. This procedure was conducted in duplicate on different days to ensure that the results could be reproduced.

Figure 4: Reaction profiles varying NiCl$_2$(glyme) precatalyst loading
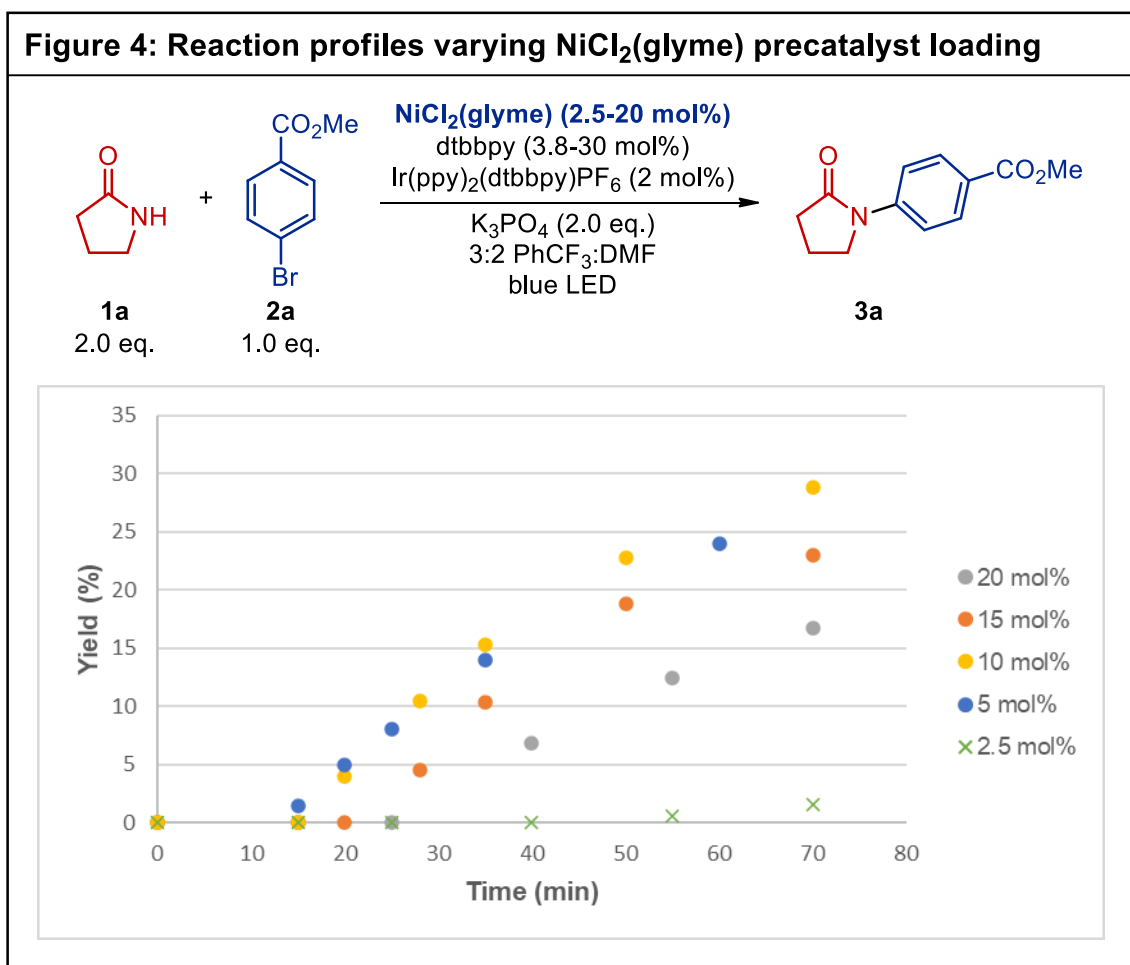
It quickly became apparent that all reactions performed with a Ni(II) precatalyst (NiCl$_2$(glyme)) displayed an induction period in which no product formation was detected in the first 10 to 15 minutes of the catalytic amide arylation

reaction. The presence of an induction period could be in line with either a Ni(0/II/III) cycle or a Ni(I/III) cycle, in which the Ni(II) precatalyst is initially reduced to either Ni(I) or Ni(0) prior to on-cycle aryl bromide oxidative addition.

Figure 5: Possible explanations for the observed induction period
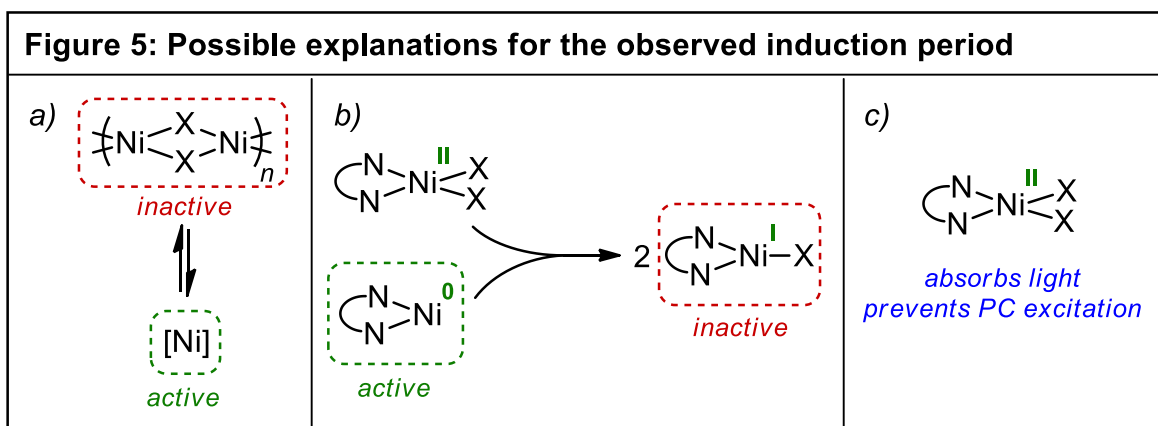
Varying the initial Ni(II) precatalyst loading between 2.5 and 20 mol% **(Figure 4)** revealed that the length of the induction period was dependent on the initial Ni(II) loading. A consistent trend was observed in which higher initial Ni(II) loadings produced longer induction periods. Upon completion of the induction period, initial rates of reaction were similar for all conditions tested between 5 and 20 mol% Ni(II) loading, with the exception of 2.5 mol% Ni(II), which presented distinct behavior from higher Ni loadings with sluggish reactivity. It is important to note that the Ni to dtbbpy ligand ratio was kept constant at 1:1.5 to reduce the complexity stemming from catalyst speciation[9,45]. The observed elongation in induction period with higher initial loadings of Ni(II) precatalyst could be explained by one of the following hypotheses: aggregation of Ni that sequesters the supposedly active mononuclear complex **(Figure 5a)**, the presence of

comproportionation or other bimolecular Ni processes that quench the active species **(Figure 5b)**, or the presence of an inner filter effect in which strongly absorbing Ni intermediates formed during the induction period compete with the PC for light absorption **(Figure 5c)**.

Figure 6: Reaction profiles using isolable Ni(I) precatalyst
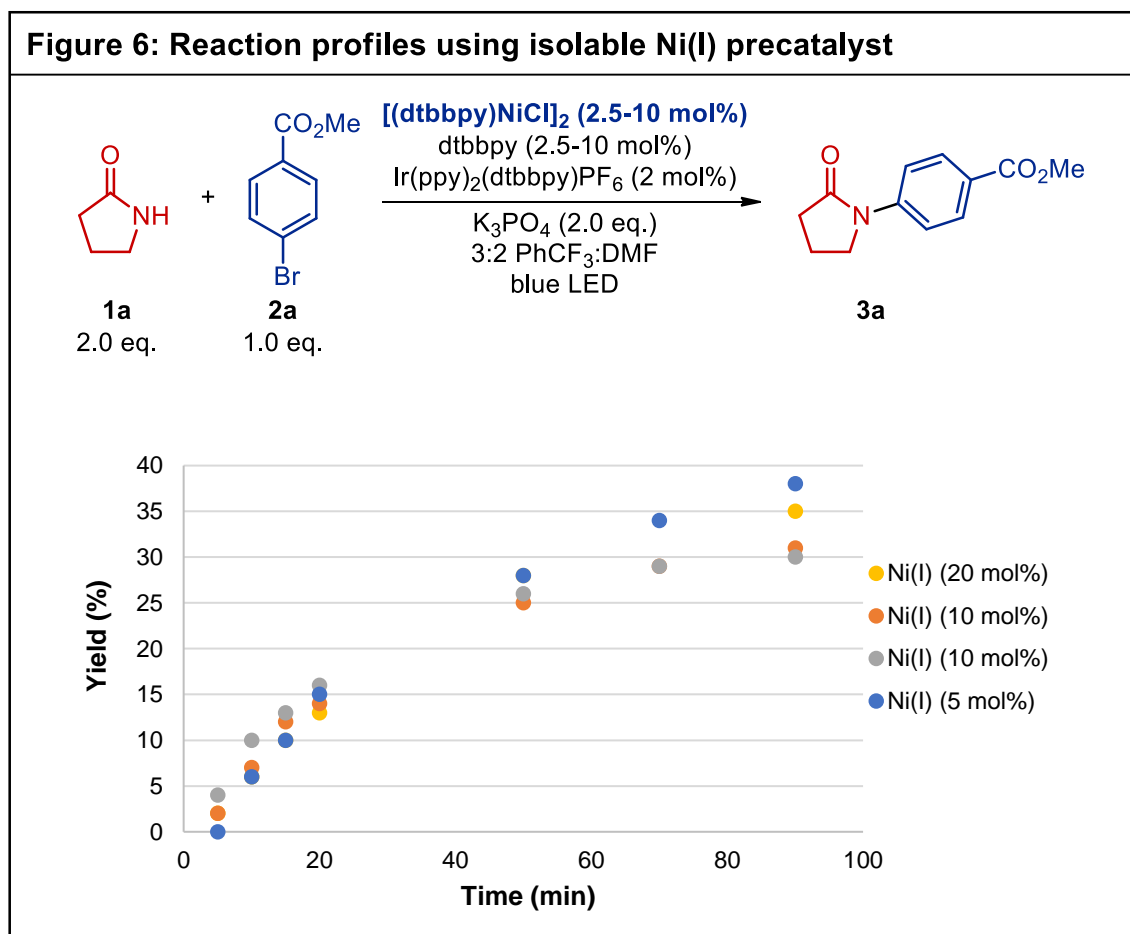
If the induction period is being caused by the formation of inactive dimers or other aggregate species, it is expected that these species would become more prevalent at higher Ni loadings. If such species are indeed being formed, then they are certainly not the active species, since faster rates of reaction would be observed, in contrast to the results shown in **Figure 4**. Halogen-bridged Ni(I)

dimers have previously been postulated in analogous Ni-photoredox C-O coupling reactions[8]. In order to determine if these inactive dimers were being formed in the reaction, the dtbbpy Ni(I) chloride dimer was synthesized following the procedure reported by Hazari & coworkers[43]. This dimer was found to be a suitable precatalyst, affording the aryl amide product **3a** in 71% yield after 24 hours. The catalytic efficiency of this Ni(I) dimer was comparable to that of $NiCl_2$(glyme) (72% yield after 24 hours[28]). We then measured the reaction profiles with varied the Ni(I) loading between 5 and 20 mol% (which corresponds to between 2.5 and 10 mol% loading of the dimer). To mimic the reaction conditions used with $NiCl_2$(glyme), additional dtbbpy ligand was added to reactions that used the Ni(I) dimer in order to maintain a 1:1.5 Ni to ligand ratio. No induction period was observed using this Ni(I) precatalyst. Additionally, the reaction rate was unaffected by the initial loading of Ni(I) dimer, suggesting that zero-order kinetics were being observed with respect to Ni **(Figure 6)**. The lack of induction period observed with the dimeric Ni(I) precatalyst contrasts the prolonged induction periods observed with equal loadings of Ni(II) precatalyst, suggesting that the formation of Ni(I) aggregates is not the cause of the induction period. Furthermore, the fast kinetics and absence of induction period observed when using the dimeric Ni(I) precatalyst indicate that this dimer can readily convert to an on-cycle active species under the conditions specified. Still, the formation of Ni(II) aggregates cannot be discarded as a contributor to the induction period observed with the Ni(II) precatalyst.

Figure 7: Reaction profiles varying Ni(0) or Ni(II) precatalyst loading
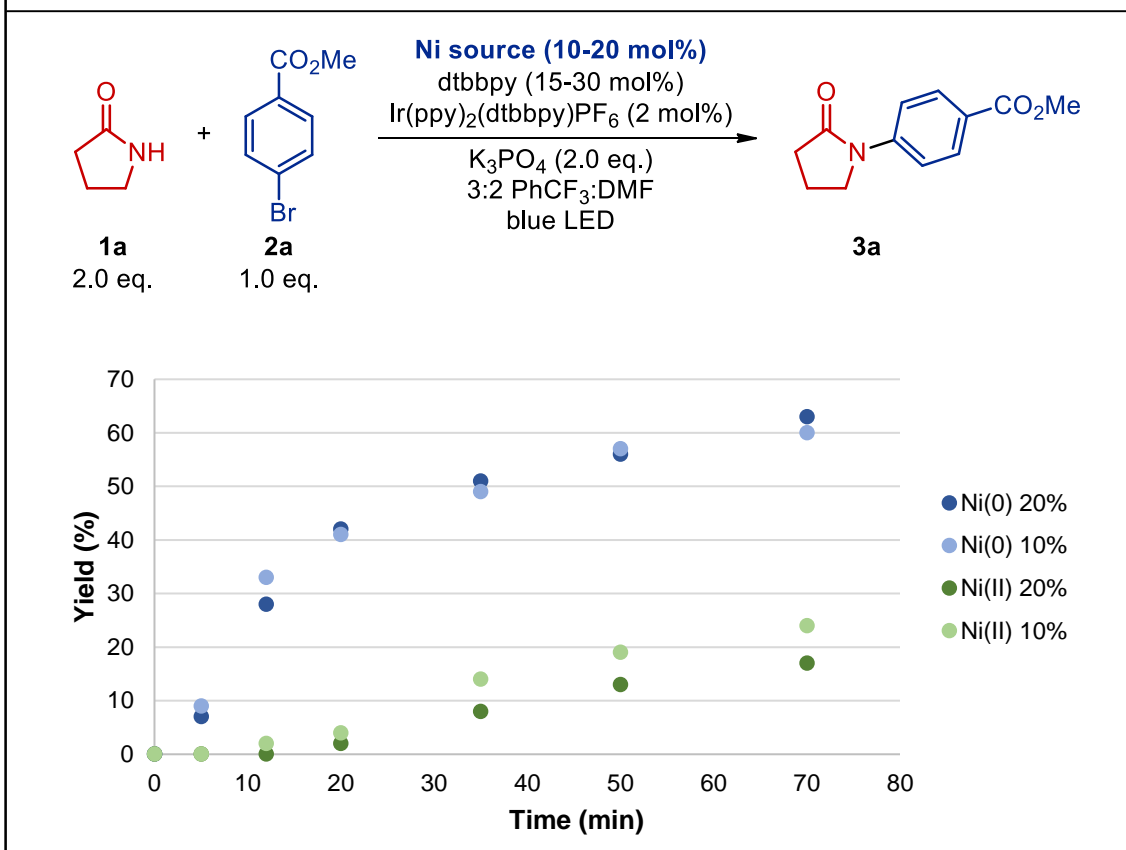
Next, we probed the possible involvement of Ni(0) species in catalysis. The induction periods and kinetic profiles of reactions initiated with the common Ni(0) precatalyst Ni(COD)$_2$ were compared to the induction periods and kinetic profiles of reactions initiated with the common Ni(II) precatalyst NiCl$_2$(glyme). It is important to note that catalytic reactions utilizing 10 mol% Ni(COD)$_2$ and those utilizing 10 mol% NiCl$_2$(glyme) both produce similar yields of aryl amide after 24 hours of irradiation, allowing for comparison of these two nickel sources (and combinations thereof). We were surprised to observe a lack of induction period with the Ni(0) precatalyst **(Figure 7)**, much like how there was no induction period observed with

the Ni(I) precatalyst. Reactions using the Ni(0) precatalyst also displayed faster kinetics than the reactions that was simultaneously studied using the Ni(II) precatalyst. This observation led us to hypothesize that if the reaction was being mediated by Ni(0) instead of Ni(I), the influence of initial Ni(II) loading on the induction period could be due to unproductive Ni(0)/Ni(II) comproportionation events that generate off-cycle Ni(I) species[9]. If these comproportionation events are indeed occurring, they should occur with faster rates at higher initial Ni(II) loadings, since the effective concentration of Ni(II) in solution would be higher if the solvent volume is held constant. Thus, comproportionation would reduce the concentration of purportedly active Ni(0) catalyst in the reaction media, stalling the initiation of the productive catalytic cycle. Although this evidence supports the hypothesis in **Figure 5b**, we still could not rule out the hypothesis in **Figure 5c** involving potential inner filter effects as an explanation for the observed induction period with Ni(II).

Rapid Ni(0)/Ni(II) comproportionation has previously been demonstrated in stoichiometric experiments[43]. Still, we wanted to be sure that comproportionation between Ni(0) and Ni(II) species in solution was a feasible process, so we sought to confirm to viability of this pathway by using EPR spectroscopy. A 1:1 mixture of Ni(COD)$_2$ and NiCl$_2$(glyme) in PhCF$_3$ produced a characteristic Ni(I) EPR signal within 2 minutes of stirring **(Figure 24)**. EPR spectroscopy was also used to determine if Ni(I) intermediates are present in the catalytic reaction. To test for the presence of Ni(I) species in the reaction mixture during and after the induction

113

period, reactions with 20 mol% Ni loading were sampled at the 5- and 45-minute time points and immediately submersed in a dewar of liquid N_2. No EPR signal was detected for either of the aliquots, suggesting that if Ni(I) species are present, they would not be the catalyst resting state and would exist in low concentration. Alternatively, EPR-silent Ni(I) dimers[43] could explain the absence of an EPR signal in these experiments.

Figure 8: Reaction profiles comparing Ni(0) to Ni(0)/Ni(II) combinations
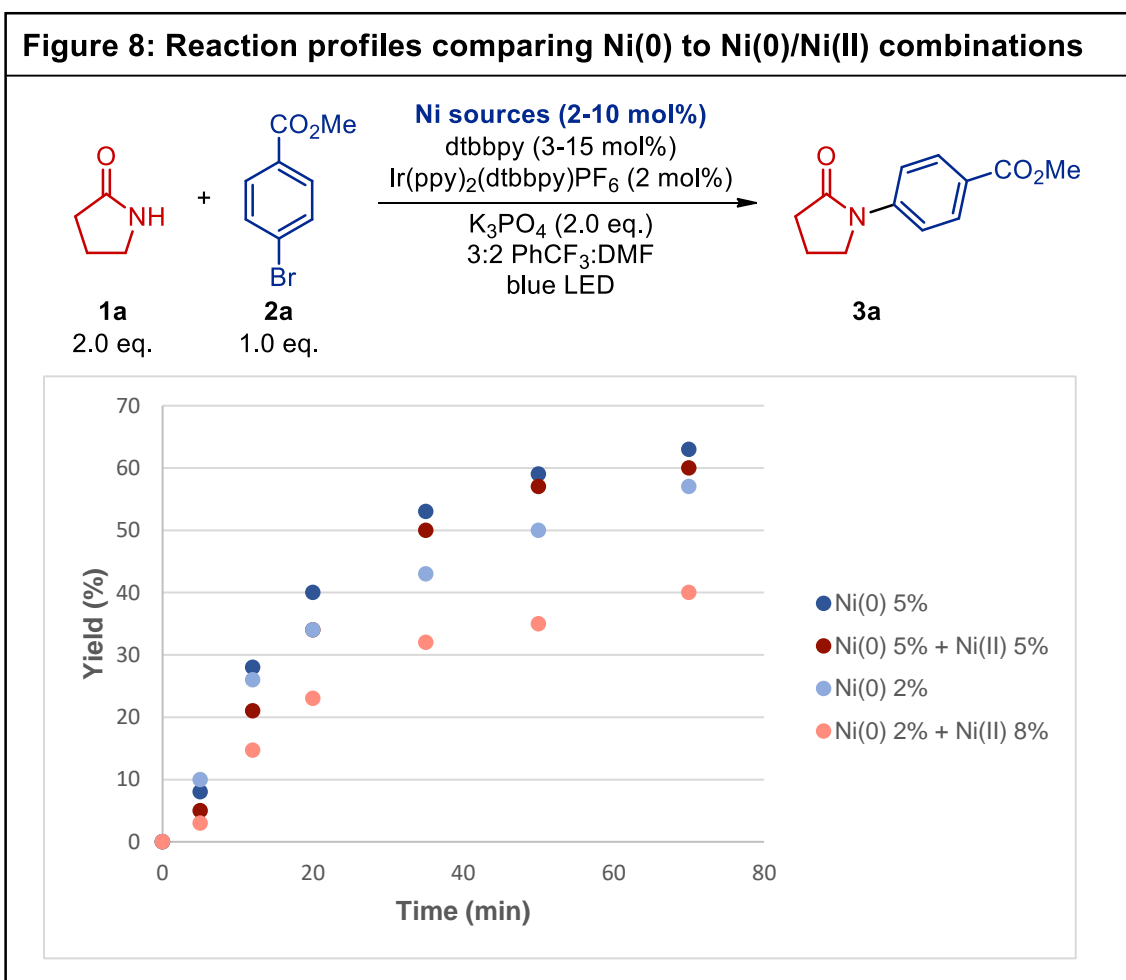
Next, reaction profiles for mixtures of Ni(COD)$_2$ and NiCl$_2$(glyme) precatalysts were compared to those only containing Ni(COD)$_2$. The fast kinetic profiles observed with the Ni(0) precatalyst allowed us to evaluate whether bimolecular quenching via comproportionation **(Figure 5b)** or inner filter effects at high Ni(II) loadings **(Figure 5c)** was responsible for the observed induction period. First, we compared the reactivity of 2 mol% Ni(0) to a mixture of 2 mol% Ni(0) and 8 mol% Ni(II) (**Figure 8**, light blue and light red points, respectively). The reaction containing 2 mol% Ni(0) (**Figure 8**, light blue points) exhibited a profile similar to those measured for higher Ni(0) loadings (5 to 20 mol%, **Figures 7-8**). The reaction containing a mixture of 2 mol% Ni(0) and 8 mol% Ni(II) displayed slower reactivity than when 2 mol% Ni(0) was used alone. When the reaction containing 5 mol% Ni(0) (**Figure 8**, dark blue points) was compared to the reaction containing a mixture of 5 mol% Ni(0) and 5 mol% Ni(II) (**Figure 8**, dark red points), initial rates were similar with the Ni(0)+Ni(II) mixture being slightly slower.

Figure 9: Ni(0) vs. Ni(0)/Ni(II) combinations at 1.8 cm distance to lamp
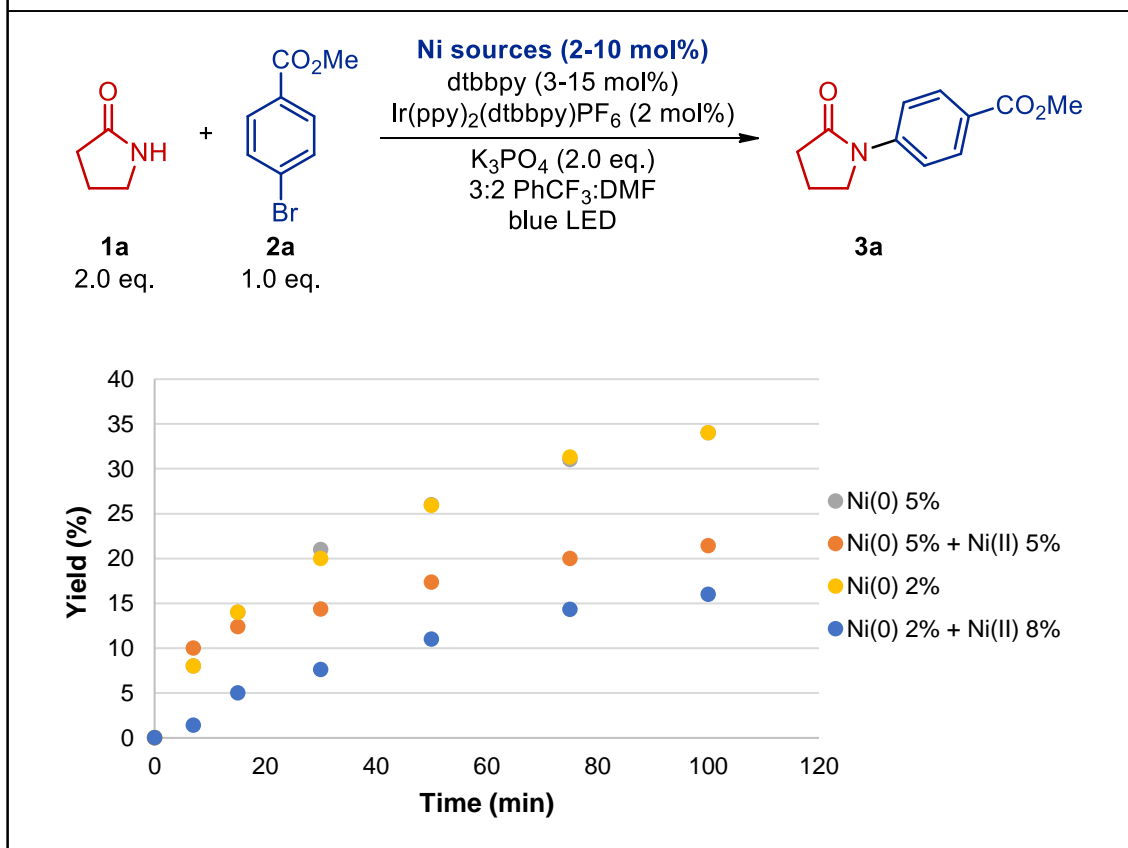
To corroborate this trend, these experiments were repeated with a slight increase in the distance between the lamp and the reaction flasks from 1.5 to 1.8 cm, aiming to slow the overall kinetics of the reaction and magnify the differences between the reaction profiles at the early time points. The same trends were observed, with a notably longer induction period for the mixture of 2 mol% Ni(0) and 8 mol% Ni(II) (**Figure 9**, blue points). Curiously, the mixture of 5 mol% Ni(0) and 5 mol% Ni(II) (**Figure 9**, orange points) did not display an induction period, although one could have been present before the reaction was analyzed at the first time point. The shortening of the induction period at higher Ni(0)/Ni(II) ratios with

total Ni loading held constant could be consistent with Ni(0) being the active catalytic species since it would be less prone to unproductive comproportionation. At this point, additional kinetics experiments involving combinations of Ni(I) and Ni(II) precatalysts were required to interrogate the roles of Ni(0) and Ni(I) as on-cycle or off-cycle species.

Figure 10: Reaction profiles comparing Ni(I) to Ni(I)/Ni(II) combinations
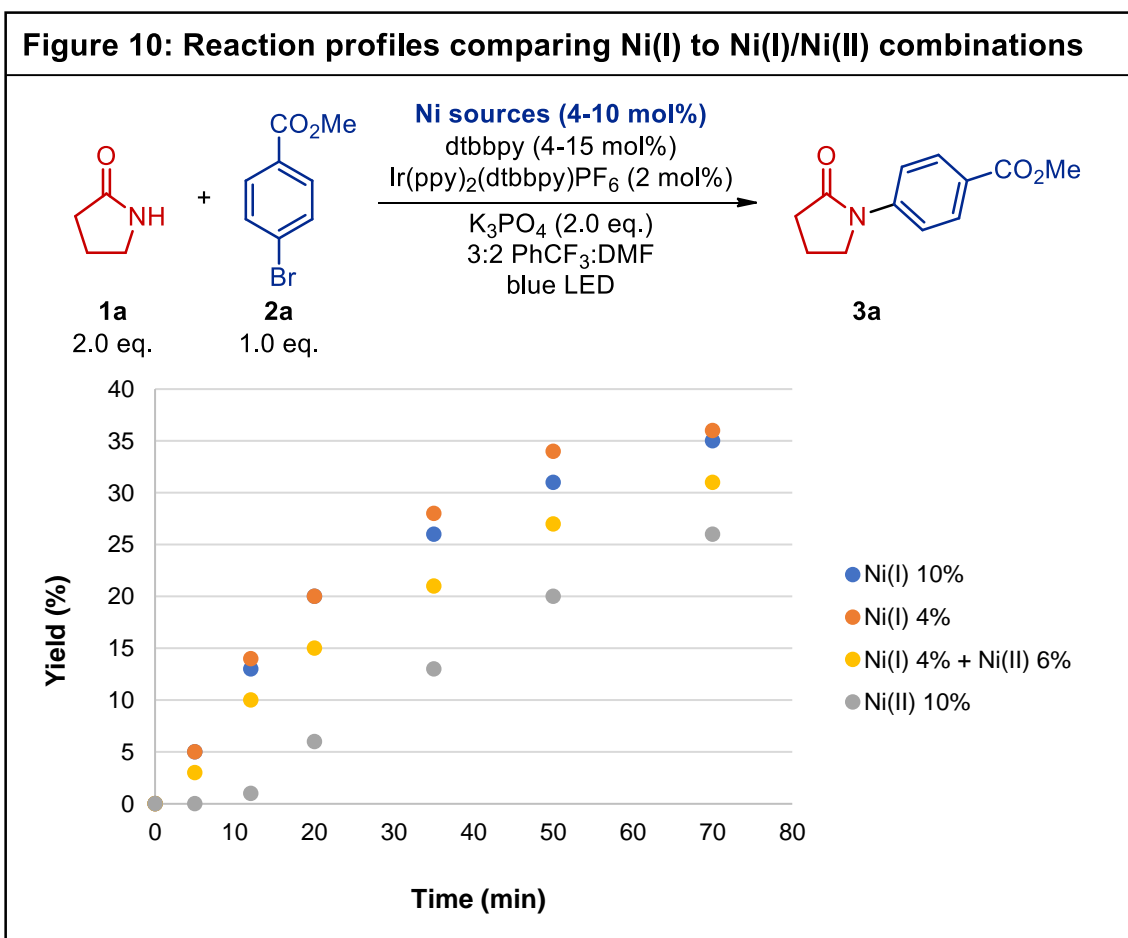
Various loadings of Ni(I) precatalyst were also compared to Ni(II) precatalyst and a combination of Ni(I) and Ni(II) precatalysts. 10 mol% Ni(I) (**Figure 10**, dark blue points) and 4 mol% Ni(I) (**Figure 10**, light blue points) displayed roughly identical kinetic profiles. This indicates that under both of these conditions, the

reaction is under zero-order kinetics with respect to the active low-valent form of Ni, whether that be Ni(I) itself or Ni(0) generated via disproportionation between Ni(I) species. An important piece of information was obtained when comparing 4 mol% Ni(I) to a mixture of 4 mol% Ni(I) and 6 mol% Ni(II) (**Figure 10**, dark red points). Despite the latter reaction containing a higher total Ni loading, reaction kinetics were slightly slower than the reaction containing only the 4 mol% Ni(I). This supports the hypothesis that Ni(0) is the prerequisite low-valent oxidation state necessary to initiate the productive catalytic cycle because additional Ni(II) would reduce the concentration of active Ni(0) species in solution, producing slower reaction kinetics that could easily be observed. However, if any induction period was occurring in the Ni(I) + Ni(II) mixture, then it ended too quickly to be observed by the 5 minute time point. As expected, 10 mol% loading of Ni(II) precatalyst without added Ni(I) again displayed a prolonged induction period (**Figure 10**, green trace) compared to the reactions that were administered Ni(I) precatalyst.

Figure 11: Saturation kinetics observed at high Ni(0)/Ni(II) loadings
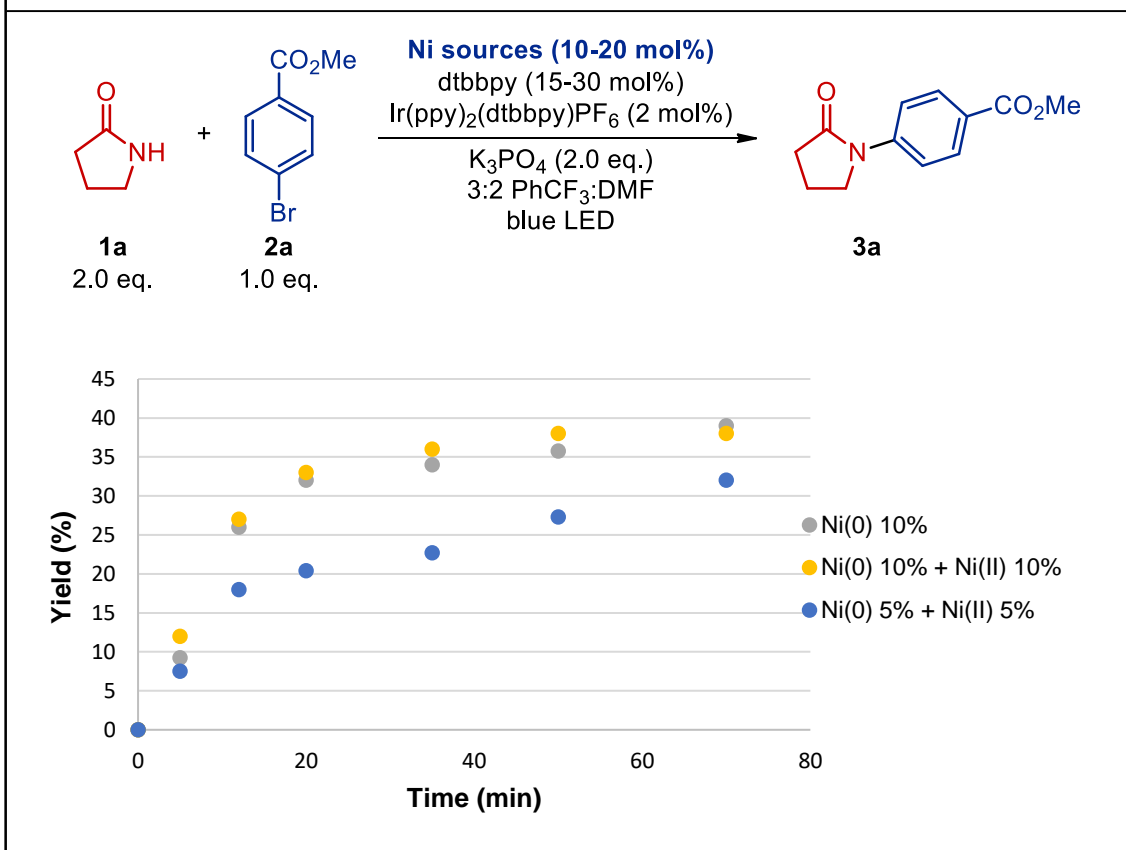
Another set of reactions was carried out to compare the reactivity of 10 mol% Ni(0) to a mixture of 10 mol% Ni(0) and 10 mol% Ni(II) precatalysts **(Figure 11)**. Unlike previous experiments that compared Ni(0) loadings to the same Ni(0) loading with additional Ni(II), this experiment produced no difference in reaction profiles between the two conditions. This suggests that at high initial Ni(0) loadings in reactions that combine equal amounts of Ni(0) and Ni(II) precatalysts, there is enough surviving Ni(0) present despite the comproportionation events for the reaction to still be under saturation kinetics with respect to Ni(0). This is corroborated by the observation that even at initial Ni(0) loadings as low as 2 mol%,

there is still a high enough concentration of Ni(0) present in solution to be under saturation kinetics, displaying nearly identical reaction profiles for initial Ni(0) loadings up to 20 mol%.

Figure 12: Rate dependence with respect to light intensity
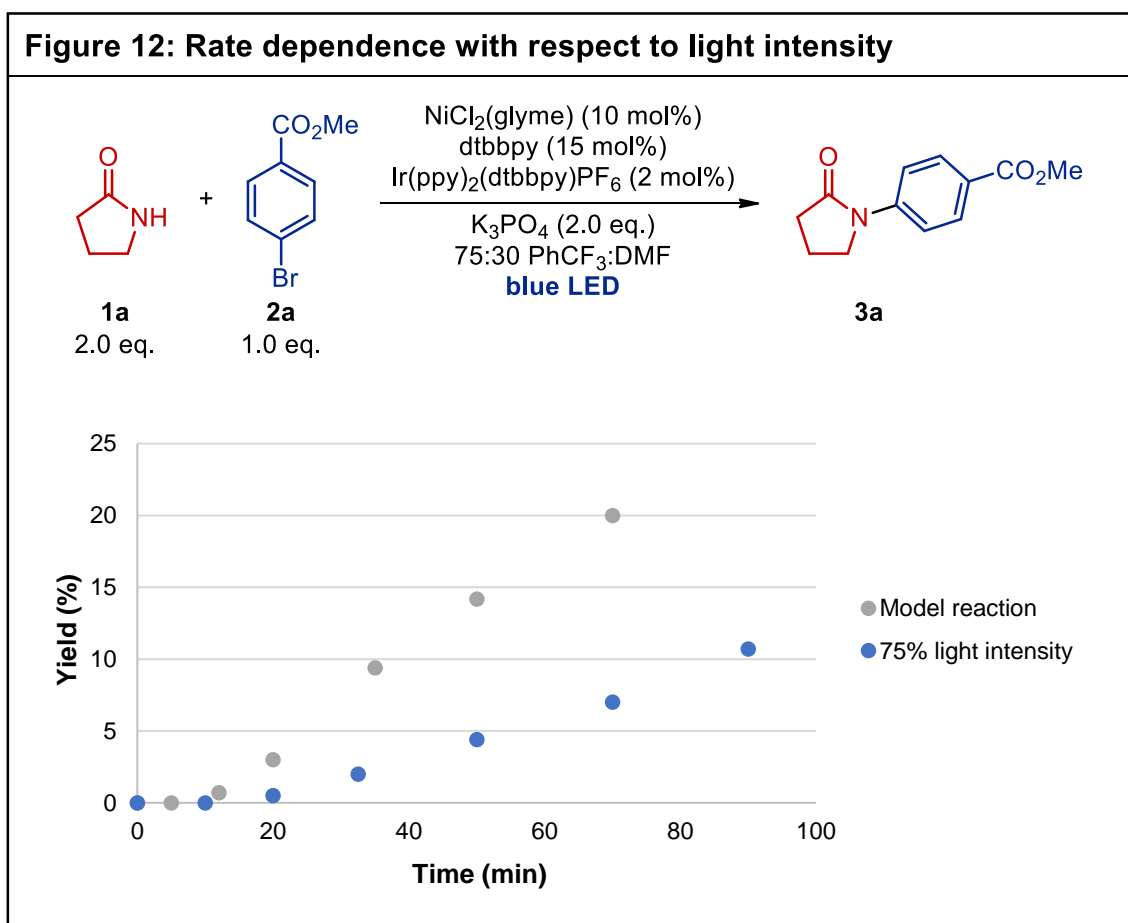
In contrast to the zero-order kinetics observed for Ni, a marked effect of the light intensity on the reaction rate was observed **(Figure 12)**. The induction period was also significantly longer at reduced blue light intensity. As a result, it would be expected that the addition of species that slow the reaction due to competitive light absorption would have an increasingly negative effect with increasing concentration of the chromophore competing with the PC for blue light absorption.

Although Ni(II) species are strongly absorbing at visible wavelengths, increasing the initial concentration of Ni(II) in Ni(0)/Ni(II) precatalyst mixtures from 5 mol% (**Figure 11**, blue points) to 10 mol% (**Figure 11**, yellow points) did not lead to a prolonged induction period. Thus, these results are not consistent with the hypothesis that the induction period is caused by inner filter effects.

Altogether, the results of the Ni precatalyst experiments support the hypothesis that unproductive comproportionation events between Ni(0) and Ni(II) are responsible for the induction periods observed under the standard reaction conditions that use $NiCl_2$(glyme). At the beginning of the reaction, the Ni(II) precatalyst must be reduced to Ni(0) to enter the proposed Ni(0/II/III) productive cross-coupling cycle. Ni(0)-initiated catalytic cycles are often invoked in mechanistic proposals of Ni-photoredox-catalyzed reactions that use Ni(II) precatalysts[3,4,40,46,47], but this process is poorly understood. There are a number of plausible hypotheses that could explain how this prerequisite reduction is achieved, but this was not the focus of our study. The induction periods observed at high Ni(II) loadings support the notion that the active Ni(0) that is being generated is quenched via comproportionation by the abundant Ni(II) before engaging the electrophilic

Figure 13: Sacrificial reductant shortens induction period
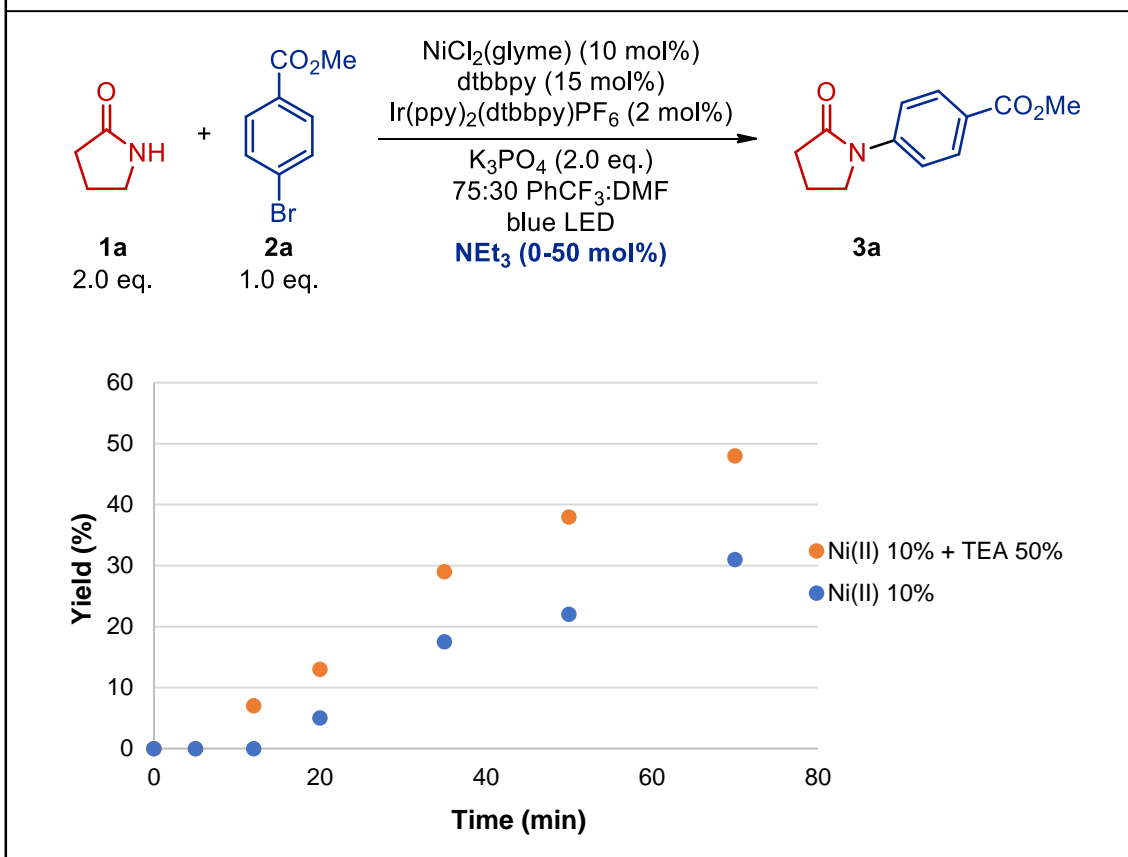
coupling partner in oxidative addition. In other words, the buildup of Ni(0) species must be slow relative to the rate of comproportionation. At high Ni(0) loadings, little to no difference in kinetic profile was observed by adding Ni(II), which could mean that there are competitive kinetics between oxidative addition and comproportionation, and that there is a point where the concentration of Ni(0) is high enough to start displaying the zero-order kinetics observed in the absence of Ni(II) additives. Considering that Ni(0) loadings as low as 2 mol% display the same kinetic profile as that of 10 mol%, if at least one fifth of the Ni(0) undergoes oxidative addition instead of comproportionation, this would be consistent with the

aforementioned identical reaction rates for 10 mol% Ni(0) versus a mixture of 10 mol% Ni(0) and 10 mol% Ni(II).

Figure 14: Protection from light extends induction period
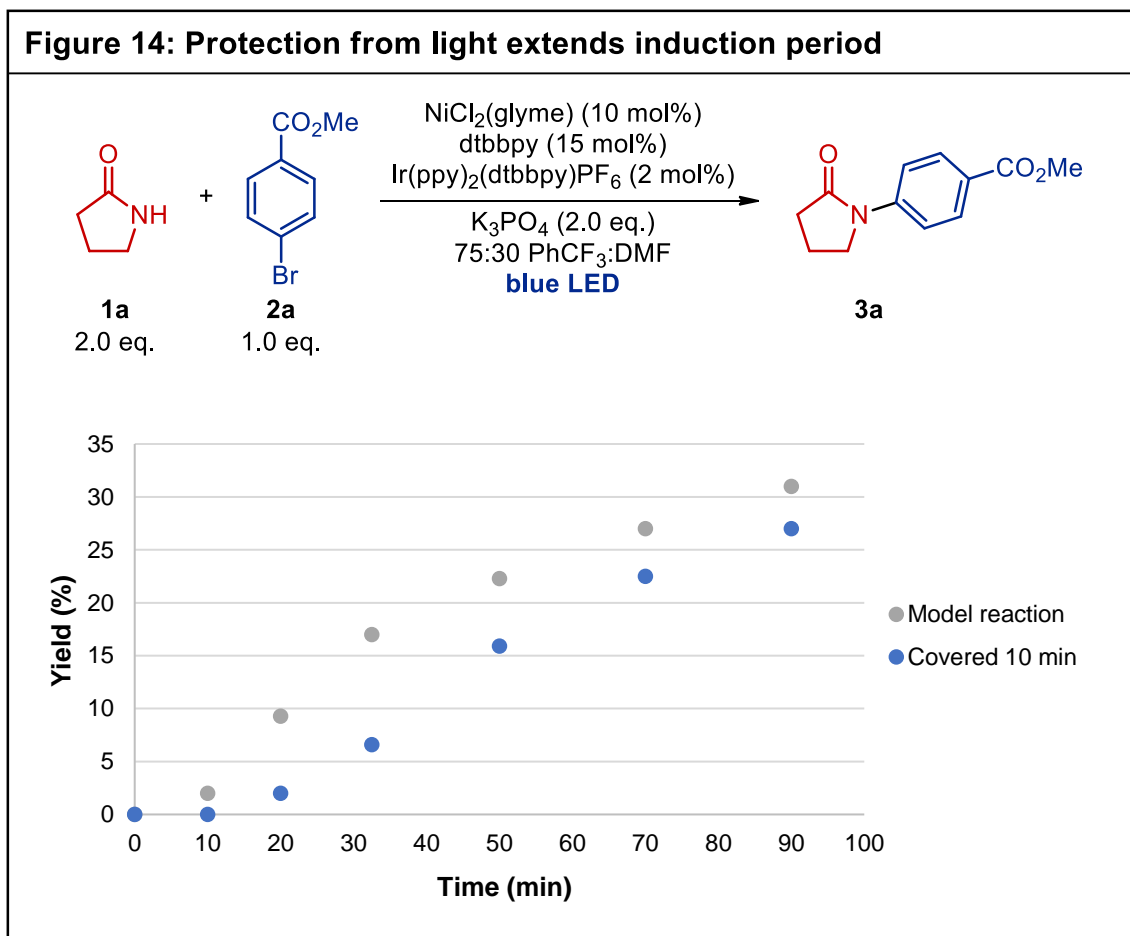
Based on these results, it was hypothesized that the addition of a weak reductant should reduce the induction period. This was tested by comparing the kinetic profile of the standard reaction conditions using 10 mol% NiCl$_2$(glyme) to another identical reaction that included 50 mol% triethylamine as an additive. The expected reduction of the induction period by adding a sacrificial reductant was observed, and after the induction periods, both reactions proceeded with similar rates **(Figure 13)**.

The effect of light irradiation on the length of the induction period was also tested. Together with the model reaction, an identical reaction was monitored in which it was thoroughly protected from light for the first 10 minutes of irradiation **(Figure 14)**. The dark reaction was still irradiated to ensure that the temperature was still similar to the reaction being irradiated. When the progress of both reactions was compared, the induction period persisted for an additional 10 minutes for the reaction not exposed to light. The induction period for this reaction still ended approximately 10 minutes after the reaction was exposed to light. This suggests that photochemical processes are necessary to reduce Ni(II) to active Ni(0), and that this process is delayed in the absence of light. This is an important observation because it indicates that if non-photochemical processes are responsible for the reduction of the precatalyst, then these processes are much slower than the photochemical one. After the induction periods of both reactions were complete, the initial rates of product formation were nearly identical.

Figure 15: Rate dependence with respect to Ir photocatalyst
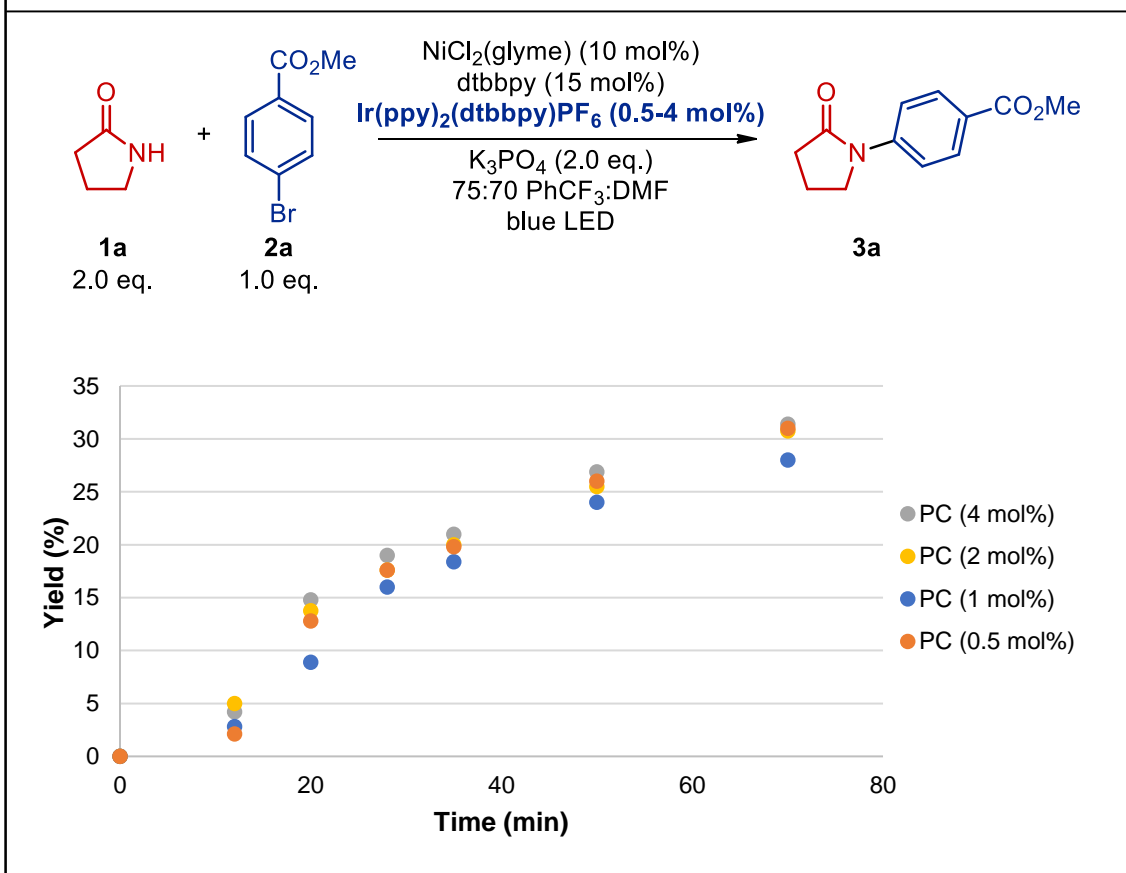
In order to probe the catalyst resting state and turnover-limiting step, further kinetic experiments were set up to determine the effect of the stoichiometry of the various reaction components on the initial rate of reaction. The photocatalyst concentration did not appear to influence the induction period or reaction rate when varied between 0.5 and 4 mol% **(Figure 15)**. With respect to the standard reaction conditions, increasing the concentration of amide **(Figure 16)** and aryl bromide **(Figure 17)** led to no appreciable change in either the induction period or the reaction rate.

Figure 16: Rate dependence with respect to amide 1a
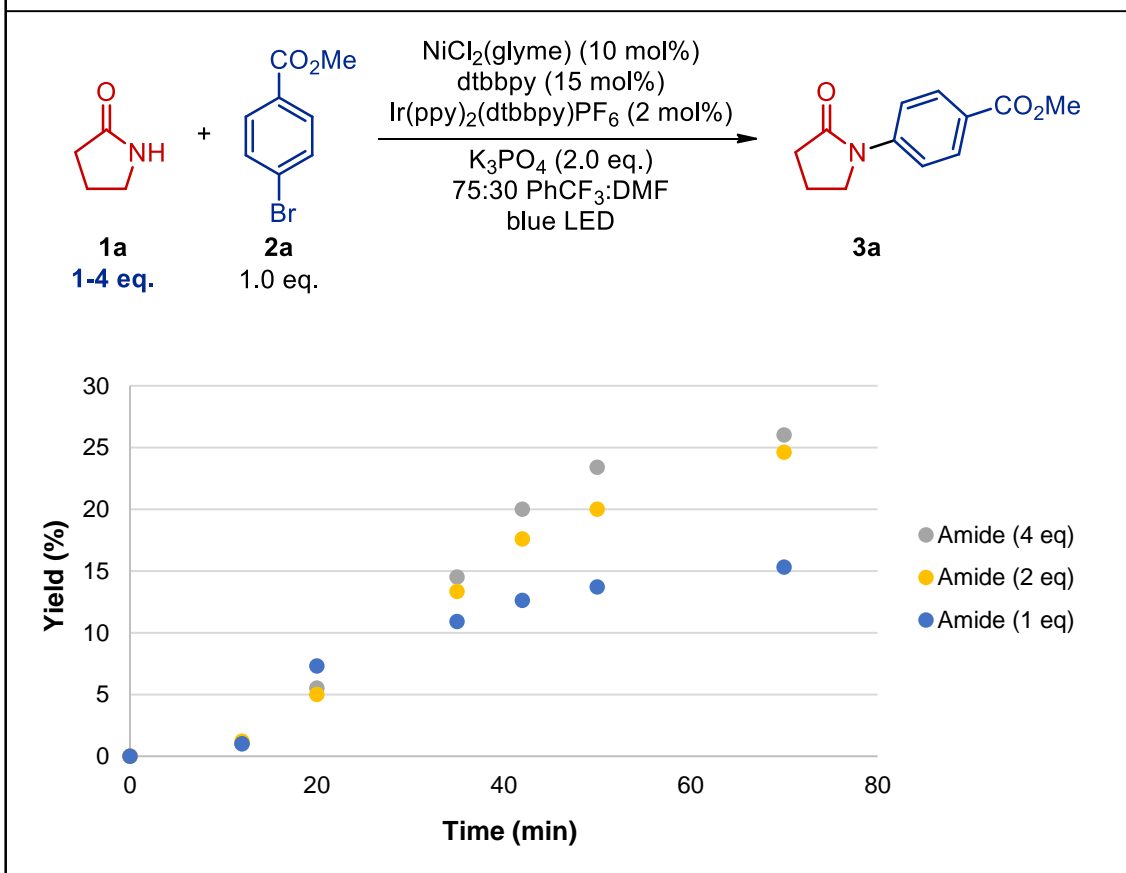
When reducing the concentration of either coupling partner by 50%, initial rates remained unchanged, although lower conversions to the aryl amide product were observed at longer reaction times. Interestingly, blue light irradiation was the only reaction component that did not display zero-order kinetics within the range of conditions tested, with faster rates measured at higher light intensity **(Figure 12)**. The observation of zero-order kinetics with respect to all other reaction components supports a mechanism in which the Ni(II) aryl amido intermediate **5** is the catalyst resting state and oxidatively-induced reductive elimination is the turnover-limiting step. To test this hypothesis, the progress of the catalytic reaction

between 2-bromo-5-fluorotoluene **(2b)** and trifluoroacetamide **(1b)** using 10 mol%

Ni(COD)$_2$ precatalyst was monitored by ^{19}F NMR. After 20 minutes of irradiation,

the Ni(II) aryl amido complex **5a** was observed and integrated to 30% of the total

Ni loading. Notably, the Ni(II) aryl bromide intermediate **4a** was not detected.

Figure 17: Rate dependence with respect to aryl bromide 2a
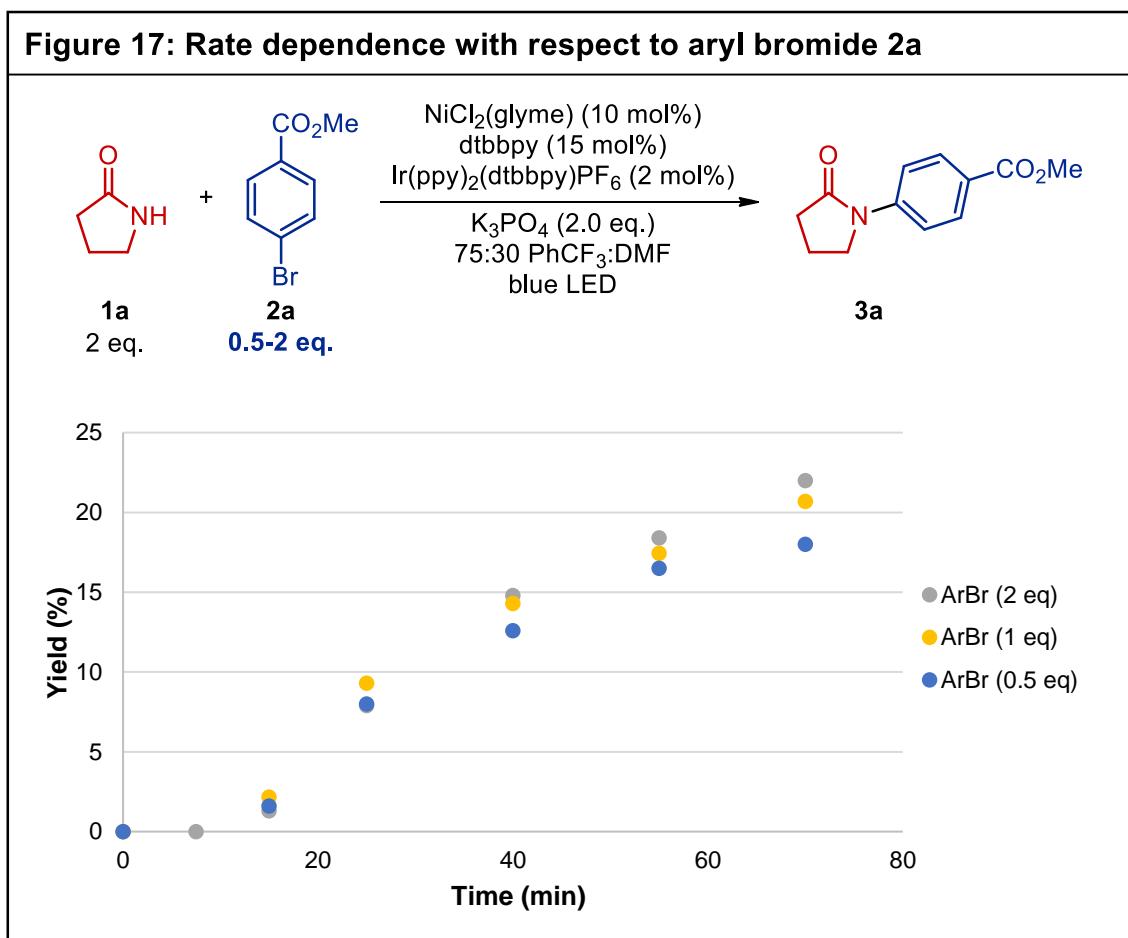
We also compared the kinetic profile using 10 mol% Ni(II) aryl amido

complex **5a** to reactions using the same mol% loadings of Ni(COD)$_2$ and

NiCl$_2$(glyme) **(Figure 18)**. The reaction containing **5a** showed a distinct profile

compared to the other two traces. Two different regimes of slow kinetics at the

beginning followed by fast kinetics were observed. During the first 12 minutes, the

formation of **3b** at a slower rate was observed. Subsequently, after 10 minutes the formation of both **3b** and **3a** was observed. At this stage, the formation of **3b** remained slower than the formation of **3a**. It is hypothesized that the lower reactivity displayed when yielding **3b** is due to the steric congestion around the Ni center in complex **5a**. The *ortho*-substituted aryl group of **5a** was introduced to slow bimolecular reactions like transmetalation (as mentioned in Chapter 3.2), allowing for tractable synthesis and isolation of these reactive complexes. It is believed that this design also slows other bimolecular processes, which in this case reduces the rate of oxidatively-induced reductive elimination. This lower reactivity of *ortho*-substituted aryl halides is also observed under catalytic conditions that use $NiCl_2$(glyme) as the precatalyst in which reaction times vary from 24 hours for **3c** to 5 days for **3b**.

Figure 18: Kinetic profiles of reactions using Ni(COD)$_2$, NiCl$_2$(glyme), and 5a
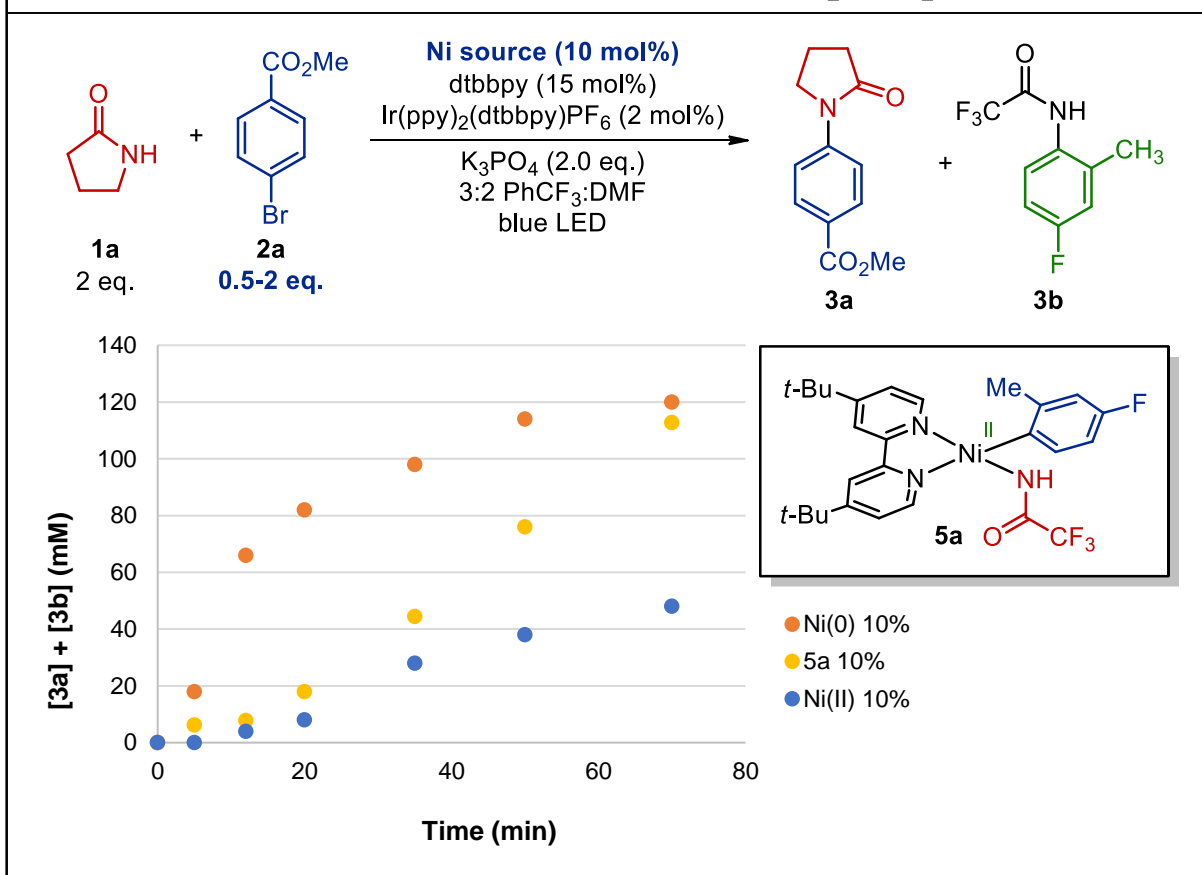
At this stage, we had gathered a compelling collection of evidence to support a Ni(0/II/III) cycle, but we could not yet definitively rule out a self-sustained Ni(I/III) cycle[6,8,9,11]. To further test which cycle was predominant, the reaction profiles obtained under Ni-photoredox conditions were compared to reaction profiles of reactions that utilize Zn as a chemical reductant under light-free conditions **(Figure 19)**. This approach has been shown by the Nocera group to facilitate access to Ni(I/III) cycles in the context of alcohol, amine, and carboxylic acid arylations[10]. We initially tested the reactivity of the Zn system by replacing the

light irradiation and photocatalyst with various Zn loadings. After 24 hours of stirring

at room temperature, reactions carried out with 10 mol% NiCl$_2$(glyme) and 5 mol%

Zn showed no reactivity, whereas the reaction carried out with the same Ni loading

and 50 mol% Zn produced a 39% yield of aryl amide **3a**. Thus, a 50 mol% Zn

loading was chosen to study the effect of initial Ni(II) loading on the kinetic profiles.

Figure 19: Reaction profiles of Ni(II) loading under light-free conditions
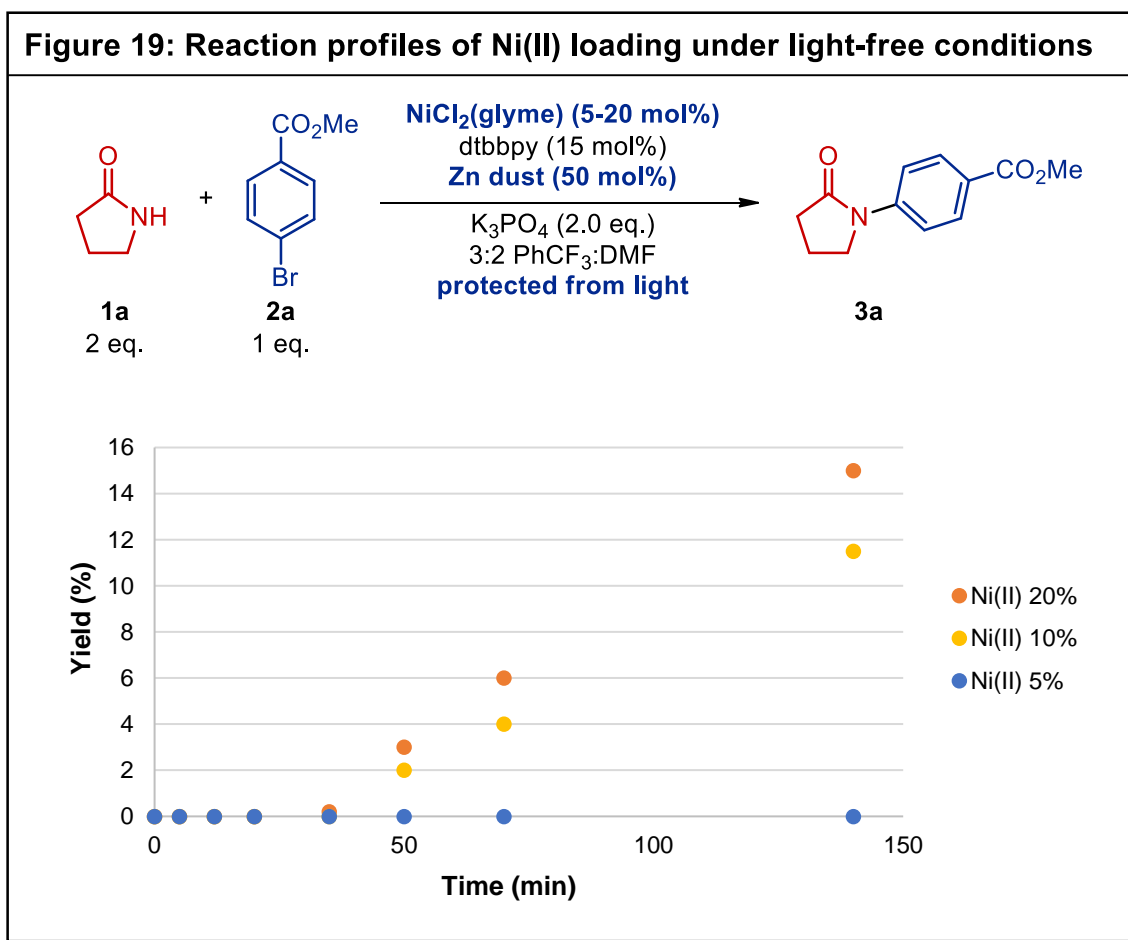
As depicted in **Figure 19**, these unoptimized conditions generally lead to

poor reactivity when compared to our optimized photochemical conditions. Using

50 mol% Zn, an induction period is also observed, likely due to slow initial reduction

of the Ni(II) precatalyst by the heterogeneous Zn reductant. It should be noted that

the original report of this Ni/Zn dual system includes redox-active bases, which are known to accelerate electron transfers[10]. When comparing the effect of Ni loading on the kinetic profiles, a slight reduction of the induction period and faster kinetics are observed for higher Ni loadings. Notably, this behavior is opposite to the trend observed for the photochemical reaction under study, which presents longer induction periods for higher Ni(II) loadings and zero-order kinetics in this range of Ni concentrations. The striking difference in the effect of Ni loading between these two catalytic systems strongly suggests that different reaction mechanisms are operative in each.

Therefore, it is proposed that, if operative, a Ni(I/III) manifold likely presents a minor contribution to the mechanistic landscape in our photochemical system. Critically, in a self-sustained Ni(I/III) cycle, one would expect that the use of Ni(0)/Ni(II) mixtures would outperform reactions carried out with a Ni(0) precursor. Here, the opposite effect was observed. The only way to reconcile this behavior with a Ni(I/III) cycle would be if catalytically inactive Ni(I) aggregates are formed at high concentrations of Ni(I)[8,43]. However, we have discarded this possibility by verifying that the Ni(I) chloride-bridged dimer is an excellent precatalyst for the Ni-photoredox amide arylation reaction. Moreover, no Ni(I) EPR signal was detected during the catalytic reaction, suggesting that the concentration of mononuclear Ni(I) species is low.

3.4   Revised mechanistic proposal and synthetic applications of this knowledge

Based on the results described in Chapters 3.2 and 3.3, we have produced a revised catalytic cycle for the amide arylation reaction developed by our group, shown in **Figure 20**. A Ni(0/II/III) cycle is proposed herein. An induction period dependent on light intensity and Ni loading was observed when a Ni(II) precatalyst was employed. This induction period was explained by a series of photochemically-mediated reduction events, depicted by the green arrows between intermediates **6**, **7**, and **8**, together with an unproductive comproportionation between **6** and **8** to generate off-cycle **7**, portrayed by the blue arrows. This comproportionation is competitive with oxidative addition to generate Ni(II) aryl bromide adduct **4**. Such adducts were stoichiometrically synthesized, demonstrating that they are easily accessed.

Next, base-assisted ligand exchange forms Ni(II) aryl amido intermediate **5**.

In situ ^{19}F NMR studies of catalytic reactions directly observed such amido

complexes, as mentioned previously, providing evidence for their status as the

catalyst resting state. These complexes were also synthesized from their corresponding Ni(II) aryl bromide adducts using the same K_3PO_4 base as the catalytic process, proving that these intermediates are stable enough to

Figure 20: Revised mechanistic proposal for Ni-photoredox amide arylation
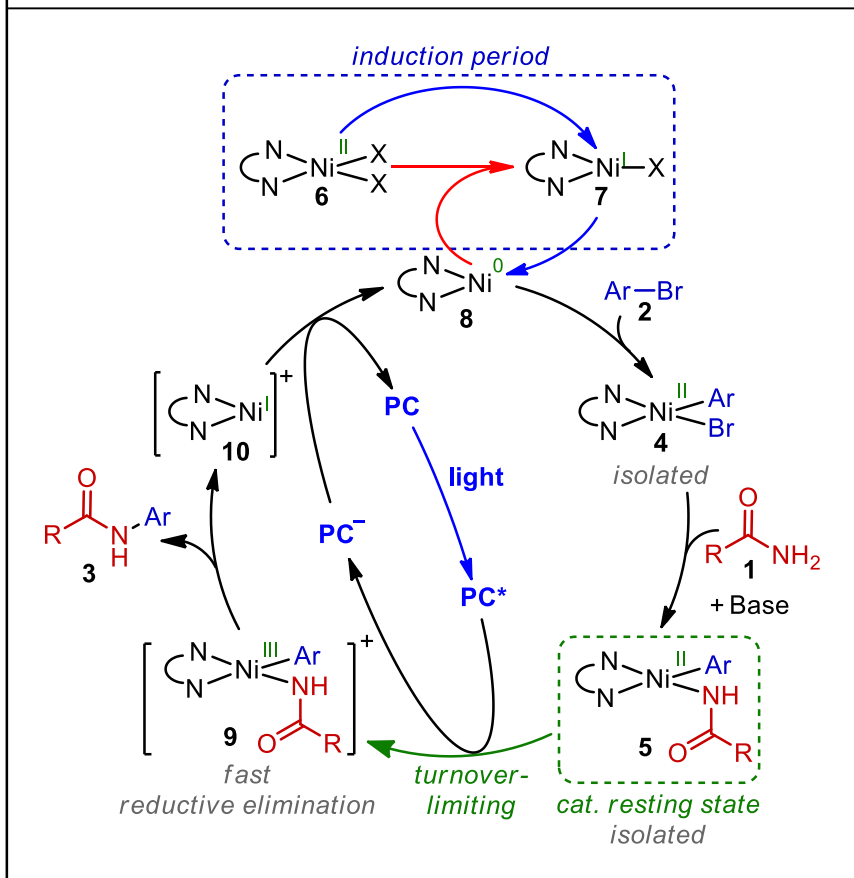
be isolated when designed to limit undesired bimolecular processes. A rate-limiting

photochemical oxidation is proposed to generate Ni(III) intermediate **9**, which can

readily undergo reductive elimination as suggested by the irreversible cyclic

voltammetry traces for **5** and the observed reactivity with acetylferrocenium

tetrafluoroborate. After product formation, Ni(I) intermediate **10** is formed. This

species, along with Ni(I) intermediate **7**, are likely in equilibrium with their halide-bridged dimeric forms[8,43]. These halide-bridged Ni(I) dimers were revealed to be suitable precatalysts by our experiments. Dimer equilibria are not shown in **Figure 20** for simplicity. Subsequent electron transfer from the reduced PC to **10** is proposed to regenerate active Ni(0) complex **8**, allowing both catalytic cycles to undergo catalytic turnover.

Table 1: Leveraging mechanistic insights for reaction reoptimization

Entry	Ni source	Ni loading	X =	Yield (%)
1	$NiCl_2(glyme)$	10 mol%	Br	72
2	$Ni(COD)_2$	0.5 mol%	Br	73
3	$NiCl_2(glyme)$	10 mol%	Cl	<5
4	$Ni(COD)_2$	10 mol%	Cl	58

Finally, we aimed to leverage our newly obtained mechanistic understanding to further optimize the Ni-photoredox amide arylation protocol. In our original reaction optimization campaign, no effect on the product yield was observed when the Ni source was substituted from $NiCl_2(glyme)$ to $Ni(COD)_2$ [28]. However, the kinetic studies detailed in this paper highlight that, unlike for Ni(II), similar kinetic profiles are observed when using Ni(0) loadings below 5 mol%. With

this in mind, we tested the effect of lowering the Ni loading on the reaction yield. Gratifyingly, a similar yield of aryl amide **3a** was obtained for both 0.5 mol% Ni(0) and 10 mol% Ni(II), corresponding to a 20-fold decrease in catalyst loading **(Table 1, entries 1 and 2)**.

Encouraged by these results, the possibility of utilizing aryl chlorides as reaction partners with Ni(0) as the precatalyst was studied. Again, a striking difference between the use of Ni(II) and Ni(0) precatalysts was observed, with a dramatic increase in product yield from a trace conversion to 58% isolated yield **(Table 1, entries 3 and 4)**.

3.5   Conclusion

In summary, we have leveraged complementary insights from studies of both stoichiometric reactivity and catalytic reaction kinetics. The stoichiometric studies of nickel aryl amide complexes demonstrated the necessity of access to Ni(III) for low-temperature C-N reductive elimination to form aryl amides. The divergent reactivity of **5a** and **5b** was corroborated by differences in reactivity to generate the same products in catalytic reactions, which demonstrated higher reactivity for the Ni(II) aryl amido complex with the lower oxidation potential. UV-Vis spectra and blue light irradiation of these Ni(II) aryl amido complexes provide evidence that is not consistent with an EnT mechanism due to major differences in reactivity despite similar absorption at 427 nm, the λ_{max} of the blue LEDs used in the catalytic amide arylation reaction.

Our studies of the reaction kinetics of the Ni-photoredox amide arylation provided evidence of a precatalyst-dependent induction period which was prolonged by excessive Ni(II) loadings. The precatalyst studies demonstrated that rapid Ni(0)/Ni(II) comproportionation generates off-cycle Ni(I) species. This enabled us to discount the dominance of a self-sustaining Ni(I/III) cycle, despite the fact that these heterogeneous reactions were not amenable to quantum yield measurements. The unusual observation of approximately zero-order kinetics with respect to all reaction components except light intensity led us to propose that oxidatively-induced reductive elimination is the turnover-limiting step and that Ni(II) aryl amido intermediate **5** is the catalyst resting state. This was corroborated by ^{19}F NMR which detected **5a** but not **4a** in catalytic reactions that generate aryl amide **3b**.

Overall, we have provided the first mechanistic study of C-N Ni-photoredox cross-coupling that supports a divergent Ni(0/II/III) catalytic cycle rather than the commonly observed self-sustaining Ni(I/III) cycle[7–9,11], showing how minor changes in reaction conditions can lead to the predominance of alternative mechanisms. It is hypothesized that the low nucleophilicity of the amide functional group and the absence of a redox-active base both play a role in the shift of mechanism. Our studies have provided a rare view into precatalyst-dependent induction periods in Ni-catalyzed reactions and the consequences of bimolecular reactions between Ni species of various oxidation states for the kinetics of Ni-photoredox reactions. The stoichiometric studies conducted further corroborate

the conclusions made from the kinetic trials regarding the intermediacy of Ni(III) in mild C-N cross-coupling processes. We applied these mechanistic insights to reoptimize the Ni-photoredox amide arylation reaction, allowing for lower catalyst loadings and extending the scope to include aryl chlorides, which were previously unreactive. It is anticipated that this study will aid further development of Ni-catalyzed C-heteroatom cross-coupling strategies by highlighting the influence of precatalyst and base identity, substrate nucleophilicity, and the redox potentials of intermediates and oxidizing species in order to enable difficult or slow reactions.

3.6   Experimental section

3.6.1 Synthesis and characterization of aryl amides (3):

General procedure A (using NiCl$_2$(glyme): An oven-dried 10 mL Schlenk tube was charged with a magnetic stir bar and capped with a 14/20 Suba-Seal® septum. The flask was evacuated and refilled with nitrogen gas three times, after which the septum was replaced with an oven-dried 14/20 ground glass stopper while under nitrogen gas pressure. Solid reagents were then added to the Schlenk tube through a weighing paper cone while constant efflux of nitrogen gas maintained inert conditions in the reaction vessel. The Schlenk tube was charged with 4,4'-di-*tert*-butyl-2,2'-dipyridyl (8.1 mg, 0.03 mmol), Ir(dtbbpy)(ppy)$_2$PF$_6$ (3.7 mg, 0.004 mmol), NiCl$_2$(glyme) (4.4 mg, 0.02 mmol), trifluoroacetamide (**1b**, 45.2 mg, 0.40 mmol), and K$_2$CO$_3$ (55 mg, 0.40 mmol). After these solids were added, benzotrifluoride (0.75 mL, distilled under nitrogen gas and over oven-dried 3 Å

137

molecular sieves), *N*,*N*-dimethylformamide (0.25 mL, dispensed from solvent purification system), and 2-bromo-5-fluorotoluene (**2b**, 25.3 μL, 0.20 mmol) were added under constant efflux of nitrogen gas. The ground glass stopper was coated in vacuum grease before sealing the reaction vessel, and the stopper was subsequently wrapped in parafilm. The reaction vessel was placed 1 cm in front of a 427 nm Kessil LED lamp while being submerged in a temperature-controlled water bath in a large crystallizing dish held at a constant temperature (50 °C for **3b** and other *ortho*-substituted aryl bromides; electron-poor aryl bromides without an *ortho*-substituent only require 24 hours at 30 °C). The reaction was stirred at 450 rpm.

For **3b**: After 120 hours at 50 °C, the lamp was shut off and the reaction vessel was removed from the water bath. The crude reaction mixture was filtered through a frit filter covered in Celite® using acetone. To this crude filtrate was added 2-3 mL silica and the suspension was slowly evaporated at <100 rpm until dryness to adsorb the crude material onto the silica. The crude material adsorbed onto silica was used to dry load a flash chromatography column in order to isolate the aryl amide product. Pure hexanes was used for making the silica slurry. The column was initially run in pure hexanes before gradually transitioning to 10% ethyl acetate in hexanes (**R***f* = 0.22); this was to prevent the product from diffusing into the eluent during dry loading. The product **3b** was obtained as a colorless oil (20.3 mg, 46% yield). **^{1}H NMR** (600 MHz, CDCl$_3$) δ 7.80 (bs, 1H), 7.57 (dd, *J* = 8.8, 5.2 Hz, 1H),

6.99 – 6.90 (m, 2H), 2.26 (s, 3H). **^{13}C NMR** (101 MHz, CDCl$_3$) δ 162.5, 160.0, 155.6

(q, *J* = 74.7 Hz), 133.9 (d, *J* = 8.6 Hz), 128.6 (d, *J* = 3.1 Hz), 126.0 (d, *J* = 9.1 Hz),

117.7 (d, *J* = 22.7 Hz), 116.0 (q, *J* = 289.9 Hz), 113.9 (d, *J* = 22.7 Hz), 17.7. **^{19}F**

NMR (564 MHz, CDCl$_3$) δ -75.60, -114.26 (q, *J* = 7.5 Hz). **HRMS** (ESI-TOF) *m/z*

calculated for C$_9$H$_6$F$_4$NO (M-H)$^-$: 220.0391, found 220.0400.

General procedure B (using Ni(COD)$_2$): An oven-dried 10 mL Schlenk tube,

magnetic stir bar, and 14/20 Suba-Seal® septum were brought into the glovebox.

A stock solution was made containing 4,4'-di-*tert*-butyl-2,2'-dipyridyl (dtbbpy, 16.1

mg, 0.060 mmol), Ni(COD)$_2$ (11.0 mg, 0.040 mmol), and 1.5 mL dry PhCF$_3$: the

dtbbpy was weighed into a 1-dram vial and dissolved in the solvent, which was

then transferred to a second 1-dram vial containing the Ni(COD)$_2$. The stock

solution was tightly capped and stirred to slowly dissolve the Ni(COD)$_2$, which

formed a dark purple solution. After 30 minutes of stirring, 0.75 mL of the stock

solution was added to the Schlenk tube, which was capped and brought out of the

glovebox and onto the Schlenk line. The rubber septum was replaced with an oven-

dried 14/20 ground glass stopper while under nitrogen gas pressure. Solid

reagents were then added to the Schlenk tube through a weighing paper cone

while constant efflux of nitrogen gas maintained inert conditions in the reaction

vessel. The Schlenk tube was charged with Ir(dtbbpy)(ppy)$_2$PF$_6$ (3.7 mg, 0.004

mmol), methyl 4- bromobenzoate (**2a**, 43.0 mg, 0.20 mmol), and K$_3$PO$_4$ (84.9 mg,

0.40 mmol). After these solids were added, *N,N*-dimethylformamide (0.25 mL,

dispensed from solvent purification system), and 2-pyrrolidone (**1a**, 30.4 µL, 0.40 mmol) were added under constant efflux of nitrogen gas. The ground glass stopper was coated in vacuum grease before sealing the reaction vessel, and the stopper was subsequently wrapped in parafilm. The reaction vessel was placed 1 cm in front of a 427 nm Kessil LED lamp while being submerged in a temperature-controlled water bath in a large crystallizing dish held at a constant 30 °C. The reaction was stirred at 450 rpm. After 24 hours, the reaction vessel was uncapped and ~ 3 mg dimethyl fumarate (internal standard) and 1 mL dichloromethane were added to the crude reaction mixture. An aliquot was taken for ^{1}H NMR analysis, which demonstrated a 78% internal standard yield of **3a**. Product spectra matched those previously reported for **3a**[28].

When 0.5 mol% Ni(COD)$_2$ and 0.75 mol% dtbbpy were employed, **3a** was formed with a 73% internal standard yield. The Ni(0) stock solution procedure was modified so that the total stock volume was 2.0 mL PhCF$_3$. 0.050 mL of this stock solution in addition to 0.7 mL dry PhCF$_3$ were added to the reaction flask in the glovebox.

When methyl 4-bromobenzoate **(2a)** was replaced with methyl 4-chlorobenzoate (using 10 mol% Ni(COD)$_2$ and 15 mol% dtbbpy), **3a** was formed with a 58% internal standard yield.

3.6.2 Kinetic experiments:

Experimental setup and standard reaction conditions for the kinetic trials:
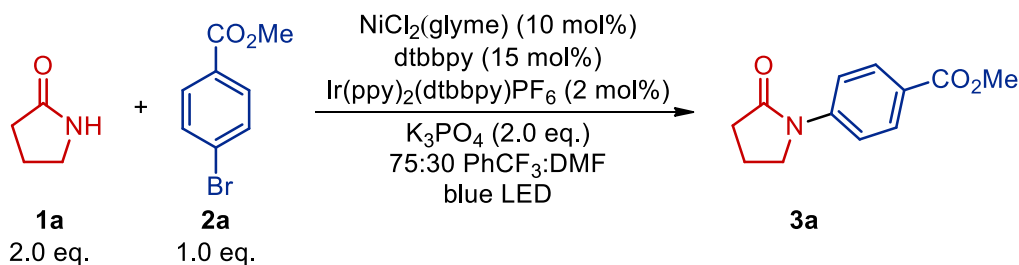
Kinetics experiments were conducted in identical Schlenk tubes with two Schlenk tubes in front of each 427 nm Kessil lamp and two lamps total so that there were four Schlenk tubes in total running experiments simultaneously. The same two lamps were used for all of the reported experiments. The Schlenk tubes containing the reaction mixtures were positioned side by side, 1.5 cm in front of the light source. The 427 nm Kessil lamps were used at 100% light intensity and the reactions were stirred at 350 rpm. Among each pair of Schlenk tubes, one Schlenk tube contained the prototypical control reaction, and one Schlenk tube contained a new reaction condition to be tested. If the control reaction is labeled "A" and the new conditions to be tested are labeled "B" and "C", then one pair of experiments in front of the first lamp would be "A" and "B" and the other pair of experiments in front of the second lamp would be "A" and "C". If the control reactions "A" among each pair display consistent reaction profiles, then the kinetic profiles of experiments testing new conditions ("B" and "C") would be considered

valid data. Small aliquots were taken at the indicated times by opening the flasks under positive N_2 pressure to ensure that the inert atmosphere inside the Schlenk tubes were maintained. For every plot depicted, all reactions were carried out on the same day using the same stock solutions. This procedure was later repeated on a different day to ensure reproducibility and accuracy of the results.

Two stock solutions were used to set up the reactions:

- Stock solution A containing: 22.0 mg $NiCl_2$(glyme) (0.1 mmol) and 40.3 mg 4,4'-di-*tert*-butyl-2,2'-dipyridyl (0.15 mmol) dissolved in 1 mL dry DMF. The solution was stirred for 10 minutes to ensure full complexation of the Ni precatalyst.

- Stock solution B containing: 18.4 mg Ir(dtbbpy)(ppy)$_2$PF$_6$ (0.02 mmol), 215.3 mg aryl bromide **2a** (1 mmol), 0.152 mL amide **1a** (2 mmol), 0.5 mL dry DMF, and 3.75 mL dry PhCF$_3$. The solution was stirred to ensure all reaction components were fully dissolved.

Oven-dried Schlenk tubes were kept under N_2 and charged with 84.9 mg K_3PO_4 (0.4 mmol), 0.85 mL stock solution B, and 0.2 mL stock solution A. After irradiating for the indicated time, the amide **1a** conversion was determined by ^1H NMR analysis. These conditions account for the following amounts: $NiCl_2$(glyme) (0.02 mmol), 4,4'-di-*tert*-butyl-2,2'-dipyridyl (dtbbpy, 0.03 mmol), Ir(dtbbpy)(ppy)$_2$PF$_6$

(0.004 mmol), K$_3$PO$_4$ (0.4 mmol), aryl bromide **2a** (0.2 mmol), amide **1a** (0.4 mmol), 0.30 mL dry DMF, and 0.75 mL dry PhCF$_3$.

As detailed below, for some measurements the solvent ratio was adapted from the standard conditions to ensure solubility and stability of all reactants in the prepared stock solutions. For those experiments, all reactions measured had the same solvent ratio and total volume.

*Rate dependence with respect to Ir photocatalyst stoichiometry **(Figure 15)***:

Reaction conditions: NiCl$_2$(glyme) (0.02 mmol), 4,4'-di-*tert*-butyl-2,2'-dipyridyl (dtbbpy, 0.03 mmol), Ir(dtbbpy)(ppy)$_2$PF$_6$ (0.001 to 0.008 mmol), K$_3$PO$_4$ (0.4 mmol), aryl bromide **2a** (0.2 mmol), amide **1a** (0.4 mmol), 0.70 mL dry DMF, and 0.75 mL dry PhCF$_3$. The solvent ratio was adapted from the standard conditions to ensure solubility of the photocatalyst in stock solution C.

Prepared according to the general procedure, but the Ir photocatalyst was removed from stock solution B. A third solution (stock solution C) containing Ir(dtbbpy)(ppy)$_2$PF$_6$ (18.4 mg, 0.02 mmol) and 1 mL dry DMF was prepared. Different volumes of stock solution C, and dry DMF were added to the reactions to maintain a constant volume: 4 mol% Ir (0.4 mL stock solution C), 2 mol% Ir (0.2 mL stock solution C and 0.2 mL dry DMF), 1 mol% Ir (0.1 mL stock solution C and 0.3 mL dry DMF), 0.5 mol% Ir (0.05 mL stock solution C and 0.35 mL dry DMF).

*Rate dependence with respect to amide **1a** stoichiometry (**Figure 16**):*

Reaction conditions: NiCl$_2$(glyme) (0.02 mmol), 4,4'-di-*tert*-butyl-2,2'-dipyridyl (dtbbpy, 0.03 mmol), Ir(dtbbpy)(ppy)$_2$PF$_6$ (0.004 mmol), K$_3$PO$_4$ (0.4 mmol), aryl bromide **2a** (0.2 mmol), amide **1a** (0.2 to 0.8 mmol), 0.30 mL dry DMF, and 0.75 mL dry PhCF$_3$.

Prepared according to the general procedure, but the amide **1a** was added individually: 1 eq of 2-pyrrolidone (**1a**, 0.0152 mL, 0.2 mmol), 2 eq of 2-pyrrolidone (**1a**, 0.0304 mL, 0.4 mmol), and 4 eq of 2-pyrrolidone (**1a**, 0.0608 mL, 0.4 mmol).

*Rate dependence with respect to aryl bromide **2a** stoichiometry (**Figure 17**):*

Reaction conditions: NiCl$_2$(glyme) (0.02 mmol), 4,4'-di-*tert*-butyl-2,2'-dipyridyl (dtbbpy, 0.03 mmol), Ir(dtbbpy)(ppy)$_2$PF$_6$ (0.004 mmol), K$_3$PO$_4$ (0.4 mmol), aryl bromide **2a** (0.1 to 0.4 mmol), amide **1a** (0.4 mmol), 0.30 mL dry DMF, and 0.75 mL dry PhCF$_3$.

Prepared according to the general procedure, but the aryl bromide **2a** was added individually: 0.5 eq of methyl 4-bromobenzoate (**2a**, 21.5 mg, 0.1 mmol), 1 eq of methyl 4-bromobenzoate (**2a**, 43.0 mg, 0.2 mmol), and 2 eq of methyl 4-bromobenzoate (**2a**, 86.0 mg, 0.4 mmol).

144

Rate dependence with respect to light intensity **(Figure 12)**:

Reaction conditions: NiCl$_2$(glyme) (0.02 mmol), 4,4'-di-_tert_-butyl-2,2'-dipyridyl (dtbbpy, 0.03 mmol), Ir(dtbbpy)(ppy)$_2$PF$_6$ (0.004 mmol), K$_3$PO$_4$ (0.4 mmol), aryl bromide **2a** (0.2 mmol), amide **1a** (0.4 mmol), 0.3 mL dry DMF, and 0.75 mL dry PhCF$_3$.

Prepared according to the general procedure. The reaction depicted in grey was irradiated with 100% light intensity, whereas the blue reaction was irradiated with 75% light intensity.

Rate dependence with respect to NiCl$_2$(glyme) loading **(Figure 4)**:

Reaction conditions: NiCl$_2$(glyme) (0.005 mmol to 0.04 mmol), 4,4'-di-_tert_-butyl-2,2'-dipyridyl (dtbbpy, 0.0075 to 0.06 mmol), Ir(dtbbpy)(ppy)$_2$PF$_6$ (0.004 mmol), K$_3$PO$_4$ (0.4 mmol), aryl bromide **2a** (0.2 mmol), amide **1a** (0.4 mmol), 0.5 mL dry DMF, and 0.75 mL dry PhCF$_3$. The solvent ratio was adapted from the standard conditions to ensure solubility of the Ni complex in stock solution A.

Prepared according to the general procedure, the reactions contained varying amounts of stock solution A and added dry DMF to maintain a constant volume: 20 mol% Ni (0.4 mL stock solution A), 15 mol% Ni (0.3 mL stock solution A and 0.1 mL dry DMF), 10 mol% Ni (0.2 mL stock solution A and 0.2 mL dry DMF), 5 mol% Ni (0.1 mL stock solution A and 0.3 mL dry DMF), 2.5 mol% Ni (0.05 mL stock solution A and 0.35 mL dry DMF).

*Rate dependence with respect to [(dtbbpy)NiCl]₂ **(Figure 6)**:*

Reaction conditions: [(dtbbpy)NiCl]$_2$ (0.005 mmol to 0.02 mmol), 4,4'-di-*tert*-butyl-2,2'-dipyridyl (dtbbpy, 0.005 mmol to 0.02 mmol), Ir(dtbbpy)(ppy)$_2$PF$_6$ (0.004 mmol), K$_3$PO$_4$ (0.4 mmol), aryl bromide **2a** (0.2 mmol), amide **1a** (0.4 mmol), 0.3 mL dry DMF, and 0.75 mL dry PhCF$_3$. Additional dtbbpy was added to the mixture to maintain a consistent ratio of Ni to ligand (1:1.5) throughout all experiments. Two stock solutions were used to set up the reactions:

- Stock solution A containing: 58.0 mg [(dtbbpyNiCl]$_2$ (0.08 mmol) and 21.5 mg 4,4'-di-*tert*-butyl-2,2'-dipyridyl (0.08 mmol) dissolved in 1 mL dry DMF.

- Stock solution B containing: 21.9 mg Ir(dtbbpy)(ppy)$_2$PF$_6$ (0.024 mmol), 258.0 mg aryl bromide **2a** (1.2 mmol), 0.182 mL amide **1a** (2.4 mmol), 0.3 mL dry DMF, and 4.5 mL dry PhCF$_3$.

Oven-dried Schlenk tubes were kept under N$_2$ and charged with 84.9 mg K$_3$PO$_4$ (0.4 mmol) and 0.80 mL stock solution B. Varying amounts of dry DMF (0 mL to 0.188 mL) and stock solution A (0.063 mL to 0.25 mL) were then added before turning on the lamps and stir plates. After irradiating for the indicated time, the amide **1a** conversion was determined by ^{1}H NMR analysis.

*Rate dependence with respect to Ni(0) or Ni(II) source **(Figure 7)**:*

Ni(II) reaction conditions: NiCl$_2$(glyme) (0.02 mmol to 0.04 mmol), 4,4'-di-*tert*-butyl-2,2'- dipyridyl (dtbbpy, 0.03 to 0.06 mmol), Ir(dtbbpy)(ppy)$_2$PF$_6$ (0.004 mmol),

K$_3$PO$_4$ (0.4 mmol), aryl bromide **2a** (0.2 mmol), amide **1a** (0.4 mmol), 0.5 mL dry DMF, and 0.75 mL dry PhCF$_3$.

Ni(0) reaction conditions: Ni(COD)$_2$ (0.02 mmol to 0.04 mmol), 4,4'-di-*tert*-butyl-2,2'-dipyridyl (dtbbpy, 0.03 to 0.06 mmol), Ir(dtbbpy)(ppy)$_2$PF$_6$ (0.004 mmol), K$_3$PO$_4$ (0.4 mmol), aryl bromide **2a** (0.2 mmol), amide **1a** (0.4 mmol), 0.5 mL dry DMF, and 0.75 mL dry PhCF$_3$.

The stock solution solvents and overall solvent ratio were slightly modified to increase the solubility of Ni complexes. Three stock solutions were used to set up the reactions:

- Stock solution A containing: 35.2 mg NiCl$_2$(glyme) (0.16 mmol) and 64.4 mg 4,4'-di-*tert*-butyl-2,2'-dipyridyl (0.24 mmol) dissolved in 1 mL dry DMF.

- Stock solution A' containing: 44.0 mg Ni(COD)$_2$ (0.16 mmol) and 64.4 mg 4,4'-di-*tert*-butyl-2,2'-dipyridyl (0.24 mmol) dissolved in 2 mL dry PhCF$_3$, which was prepared in the glovebox.

- Stock solution B containing: 21.9 mg Ir(dtbbpy)(ppy)$_2$PF$_6$ (0.024 mmol), 258.0 mg aryl bromide **2a** (1.2 mmol), 0.182 mL amide **1a** (2.4 mmol), 1.5 mL dry DMF, and 1.5 mL dry PhCF$_3$.

The reactions were carried out according to the general procedure except 0.5 mL of stock B was added to each reaction. Reactions contained varying amounts of Ni stock solutions, and dry PhCF$_3$ and DMF were added to maintain a constant

volume: Ni(0) 20 % (0.5 mL stock solution A' and 0.25 mL dry DMF), Ni(0) 10 % (0.25 mL stock solution A', 0.25 mL dry PhCF$_3$, and 0.25 mL dry DMF), Ni(II) 20 % (0.25 mL stock solution A and 0.5 mL dry PhCF$_3$), and Ni(II) 10 % (0.125 mL stock solution A and 0.5 mL dry PhCF$_3$).

*Rate dependence with respect to different Ni(0)/Ni(II) mixtures (**Figure 11**)*:

Ni(II) reaction conditions: NiCl$_2$(glyme) (0.01 mmol to 0.02 mmol), 4,4'-di-*tert*-butyl-2,2'- dipyridyl (dtbbpy, 0.015 to 0.03 mmol), Ir(dtbbpy)(ppy)$_2$PF$_6$ (0.004 mmol), K$_3$PO$_4$ (0.4 mmol), aryl bromide **2a** (0.2 mmol), amide **1a** (0.4 mmol), 0.3 mL dry DMF, and 1.35 mL dry PhCF$_3$.

Ni(0) reaction conditions: Ni(COD)$_2$ (0.01 mmol to 0.02 mmol), 4,4'-di-*tert*-butyl-2,2'-dipyridyl (dtbbpy, 0.015 to 0.03 mmol), Ir(dtbbpy)(ppy)$_2$PF$_6$ (0.004 mmol), K$_3$PO$_4$ (0.4 mmol), aryl bromide **2a** (0.2 mmol), amide **1a** (0.4 mmol), 0.3 mL dry DMF, and 1.35 mL dry PhCF$_3$.

The reactions were carried out according to the general procedure, contained varying amounts of Ni stock solutions, and added dry PhCF$_3$ to maintain a constant volume: Ni(0) 10 % (0.4 mL stock solution A' and 0.4 mL dry PhCF$_3$), Ni(0) 10% + Ni(II) 10% (0.4 mL stock solution A', 0.4 mL stock solution A), and Ni(0) 5% + Ni(II) 5% (0.2 mL stock solution A', 0.2 mL stock solution A, and 0.4 mL dry PhCF3).

*Rate dependence with respect to different Ni(0)/Ni(II) mixtures (**Figure 8**):*

Reaction conditions: combinations of $Ni(COD)_2$ and $NiCl_2(glyme)$ (0.004 mmol to 0.04 mmol total Ni), 4,4'-di-*tert*-butyl-2,2'-dipyridyl (dtbbpy, 0.006 to 0.06 mmol), $Ir(dtbbpy)(ppy)_2PF_6$ (0.004 mmol), K_3PO_4 (0.4 mmol), aryl bromide **2a** (0.2 mmol), amide **1a** (0.4 mmol), 0.5 mL dry DMF, and 0.75 mL dry $PhCF_3$. The stock solution solvents and overall solvent ratio were slightly modified to increase the solubility of Ni complexes.

Three stock solutions were used to set up the reactions:

- Stock solution A containing: 35.2 mg $NiCl_2(glyme)$ (0.16 mmol) and 64.4 mg 4,4'-di-*tert*-butyl-2,2'-dipyridyl (0.24 mmol) dissolved in 2.5 mL dry DMF.

- Stock solution A' containing: 27.5 mg $Ni(COD)_2$ (0.1 mmol) and 40.3 mg 4,4'-di-*tert*-butyl-2,2'-dipyridyl (0.15 mmol) dissolved in 2.5 mL dry $PhCF_3$, which was prepared in the glovebox.

- Stock solution B containing: 21.9 mg $Ir(dtbbpy)(ppy)_2PF_6$ (0.024 mmol), 258.0 mg aryl bromide **2a** (1.2 mmol), 0.182 mL amide **1a** (2.4 mmol), 3.0 mL dry DMF, and 1.5 mL dry $PhCF_3$.

The reactions were carried out according to the general procedure except 0.75 mL of stock B was added to each reaction. Reactions contained varying amounts of Ni stock solutions, and dry $PhCF_3$ and DMF were added to maintain a constant volume: 2% Ni(0) (0.1 mL stock solution A', 0.15 mL dry $PhCF_3$, and 0.25 mL dry

DMF), 2% Ni(0) + 8% Ni(II) (0.25 mL stock solution A, 0.1 mL stock solution A', and

0.15 mL dry $PhCF_3$), 5% Ni(0) (0.25 mL stock solution A' and 0.25 mL dry DMF),

and 5% Ni(0) + 5% Ni(II) (0.156 mL stock solution A, 0.25 mL stock solution A', and

0.094 mL dry DMF).

*Repetition of plot in **Figure 8** with 1.8 cm lamp distance (0.3 cm farther) **(Figure 9)**:*

Ni(II) reaction conditions: $NiCl_2$(glyme) (0.01 mmol to 0.016 mmol), 4,4'-di-*tert*-butyl-2,2'- dipyridyl (dtbbpy, 0.015 to 0.024 mmol), Ir(dtbbpy)(ppy)$_2$PF$_6$ (0.004 mmol), K_3PO_4 (0.4 mmol), aryl bromide **2a** (0.2 mmol), amide **1a** (0.4 mmol), 0.3 mL dry DMF, and 0.95 mL dry $PhCF_3$.

Ni(0) reaction conditions: Ni(COD)$_2$ (0.004 mmol to 0.01 mmol), 4,4'-di-*tert*-butyl-2,2'-dipyridyl (dtbbpy, 0.006 to 0.015 mmol), Ir(dtbbpy)(ppy)$_2$PF$_6$ (0.004 mmol), K_3PO_4 (0.4 mmol), aryl bromide **2a** (0.2 mmol), amide **1a** (0.4 mmol), 0.3 mL dry DMF, and 0.75 mL dry $PhCF_3$.

The reactions were carried out according to the general procedure, contained varying amounts of Ni stock solutions, and added dry $PhCF_3$ to maintain a constant volume: Ni(0) 5 % (0.2 mL stock solution A' and 0.2 mL dry $PhCF_3$), Ni (0) 5% + Ni (II) 5% (0.2 mL stock solution A', 0.2 mL stock solution A), Ni(0) 2 % (0.08 mL stock

solution A' and 0.32 mL dry PhCF$_3$), and Ni(0) 2% + Ni(II) 8% (0.08 mL stock solution A', 0.32 mL stock solution A).

While the solvent mixtures of the reaction profiles depicted in Figures S9 and S10 are slightly different, it is hypothesized that the slower behavior displayed in by the reactions depicted in S10 is only due to the farther distance to the lamp.

*Rate dependence with respect to aryl bromide **2a** (**Figure 10**)*:

Reaction conditions: combinations of [(dtbbpy)NiCl]$_2$ and NiCl$_2$(glyme) (0.008 to 0.02 mmol total Ni treating 1 mmol of Ni(I) dimer as 2 mmol of Ni), 4,4'-di-*tert*-butyl-2,2'-dipyridyl (dtbbpy, 0.012 to 0.03 mmol total dtbbpy accounting for the dtbbpy already coordinated to the Ni(I) dimer), Ir(dtbbpy)(ppy)$_2$PF$_6$ (0.004 mmol), K$_3$PO$_4$ (0.4 mmol), aryl bromide **2a** (0.2 mmol), amide **1a** (0.4 mmol), 0.5 mL dry DMF, and 0.75 mL dry PhCF$_3$.

The stock solution solvents and overall solvent ratio were slightly modified to increase the solubility of Ni complexes. Three stock solutions were used to set up the reactions:

- Stock solution A containing: 43.9 mg NiCl$_2$(glyme) (0.2 mmol) and 80.9 mg 4,4'-di-*tert*-butyl-2,2'-dipyridyl (0.3 mmol) dissolved in 2.5 mL dry DMF.

- Stock solution A' containing: 43.5 mg [(dtbbpy)NiCl]$_2$ (0.06 mmol) and 16.1 mg 4,4'-di-*tert*-butyl-2,2'-dipyridyl (0.06 mmol) dissolved in 3.0 mL dry PhCF$_3$, which was prepared in the glovebox.

- Stock solution B containing: 21.9 mg Ir(dtbbpy)(ppy)$_2$PF$_6$ (0.024 mmol), 258.0 mg aryl bromide **2a** (1.2 mmol), 0.182 mL amide **1a** (2.4 mmol), 1.5 mL dry DMF, and 1.5 mL dry PhCF$_3$.

The reactions were carried out according to the general procedure except 0.50 mL of stock B was added to each reaction. Reactions contained varying amounts of Ni stock solutions, and dry PhCF$_3$ and DMF were added to maintain a constant volume: 10% Ni(II) (0.25 mL stock solution A, 0.5 mL dry PhCF$_3$), 4% Ni(I) (0.2 mL stock solution A', 0.25 mL dry DMF, and 0.3 mL dry PhCF$_3$), 4% Ni(I) + 6% Ni(II) (0.15 mL stock solution A, 0.2 mL stock solution A', 0.3 mL dry PhCF$_3$, and 0.1 mL dry DMF), and 10% Ni(I) (0.5 mL stock solution A', 0.25 mL dry DMF).

Effect of triethylamine additive on induction period **(Figure 13)**:

Reaction conditions: NiCl$_2$(glyme) (0.02 mmol), 4,4'-di-*tert*-butyl-2,2'-dipyridyl (dtbbpy, 0.03 mmol), Ir(dtbbpy)(ppy)$_2$PF$_6$ (0.004 mmol), K$_3$PO$_4$ (0.4 mmol), aryl bromide **2a** (0.2 mmol), amide **1a** (0.4 mmol), 0.3 mL dry DMF, and 0.75 mL dry PhCF$_3$. The reaction with the triethylamine additive also contained 0.1 mmol of triethylamine, which was added individually after starting the irradiation.

These experiments were prepared according to the general procedure. The reaction depicted in orange included 50 mol % triethylamine.

Effect of dark period on induction period **(Figure 14)**:

Reaction conditions: $NiCl_2$(glyme) (0.02 mmol), 4,4'-di-_tert_-butyl-2,2'-dipyridyl (dtbbpy, 0.03 mmol), Ir(dtbbpy)(ppy)$_2$PF$_6$ (0.004 mmol), K$_3$PO$_4$ (0.4 mmol), aryl bromide **2a** (0.2 mmol), amide **1a** (0.4 mmol), 0.3 mL dry DMF, and 0.75 mL dry PhCF$_3$.

Prepared according to the general procedure, the reaction depicted in grey was irradiated from time = 0 minutes, whereas the reaction depicted in blue was set up alongside the model reaction but thoroughly covered with aluminum foil for the first 10 minutes.

3.6.3 Cyclic voltammetry:

All experiments were performed in the glovebox on the same day utilizing the same [0.1 M] $TBAPF_6$ solution in acetonitrile. $E_{1/2}$ calculations were performed by Ana Bahamonde.

Figure 21: Cyclic voltammetry trace of acetylferrocene
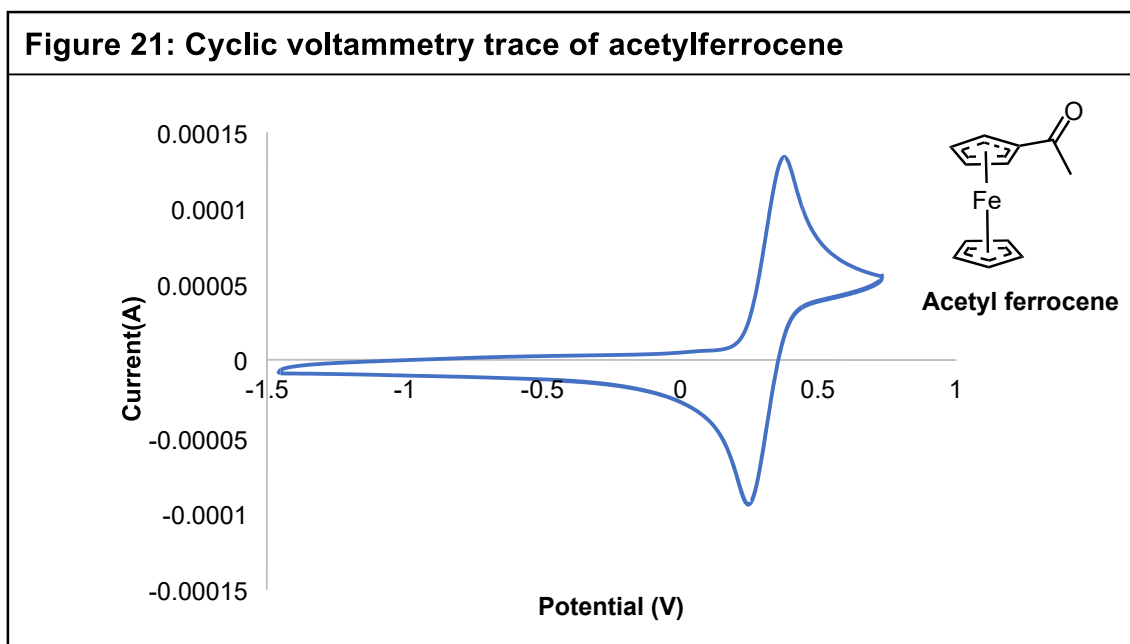
Figure 21: CV trace of 5 mM solution in [0.1 M] $TBAPF_6$ in acetonitrile. Sweep rate: 100 mV/s, glassy carbon working electrode, $Ag/AgNO_3$ reference electrode, Pt wire auxiliary electrode. $E_{1/2}$ = 0.32 V.

154

Figure 22: Cyclic voltammetry trace of Ni(II) aryl amido complex 5a
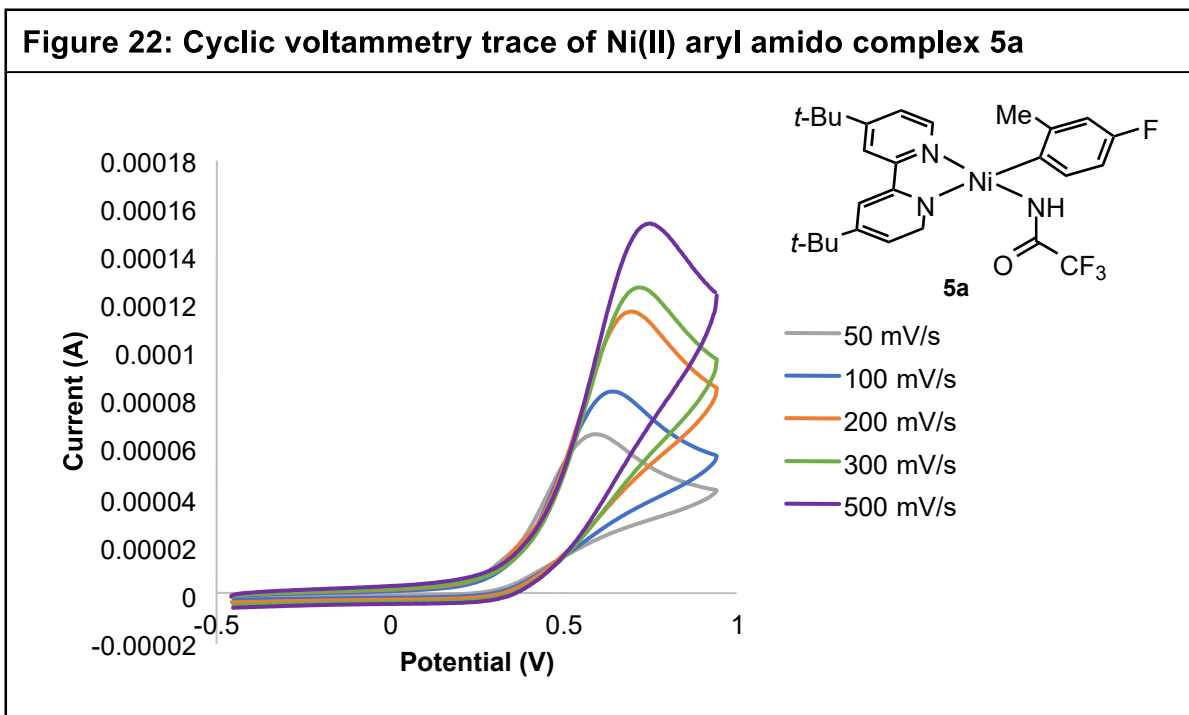
Figure 22: CV trace of 5 mM solution in [0.1 M] TBAPF$_6$ in acetonitrile. Sweep rates varied from 50 mV/s to 500 mV/s, glassy carbon working electrode, Ag/AgNO$_3$ reference electrode, Pt wire auxiliary electrode. $E_{p,a}$ = 0.59 V (measured at 50 mV/s). $E_{1/2}$ = 0.19 V (estimated using scan rate dependence measurements following the reported procedure[48].

Figure 23: Cyclic voltammetry trace of Ni(II) aryl amido complex 5b
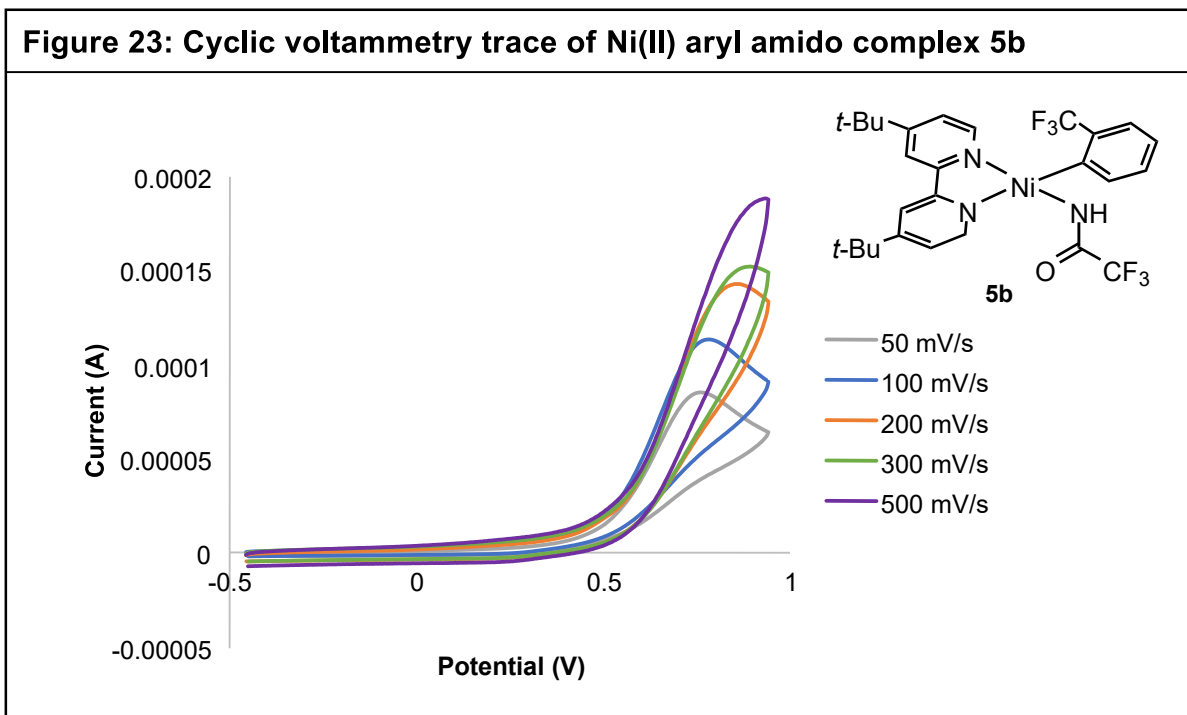
Figure 23: CV trace of 5 mM solution in [0.1 M] TBAPF$_6$ in acetonitrile. Sweep rates varied from 50 mV/s to 500 mV/s, glassy carbon working electrode, Ag/AgNO$_3$ reference electrode, Pt wire auxiliary electrode. E$_{p,a}$ = 0.75 V (measured at 50 mV/s). E$_{1/2}$ = 0.50 V (estimated using scan rate dependence measurements following the reported procedure[48].

3.6.4 EPR experiments:

Two stock solutions containing Ni(II) and Ni(0) complexes were prepared:

- Stock solution A containing: 22.0 mg $NiCl_2$(glyme) (0.1 mmol) and 40.3 mg 4,4'-di-*tert*-butyl-2,2'-dipyridyl (0.15 mmol) dissolved in 2 mL dry $PhCF_3$ and kept under nitrogen.

- Stock solution A' containing: 27.5 mg $Ni(COD)_2$ (0.1 mmol) and 40.3 mg 4,4'-di-*tert*-butyl-2,2'-dipyridyl (0.15 mmol) dissolved in 2 mL dry $PhCF_3$ was prepared in the glovebox, taken out, and kept under nitrogen.

0.5 mL of each of these solutions were added to a dried Schlenk flask and stirred under nitrogen. After 2 minutes, an aliquot of the solution was taken and added into an EPR tube kept under nitrogen. The tube was quickly cooled with liquid nitrogen and the frozen mixture was analyzed by EPR at 77 K **(Figure 24)**. Both starting solutions containing Ni(0) and Ni(II) are EPR-silent. The EPR spectrum obtained highly resembles the (dtbbpy)Ni(I) spectra reported in the literature[49].

Figure 24: EPR spectrum of a 1:1 mixture of NiCl$_2$(glyme)/Ni(COD)$_2$
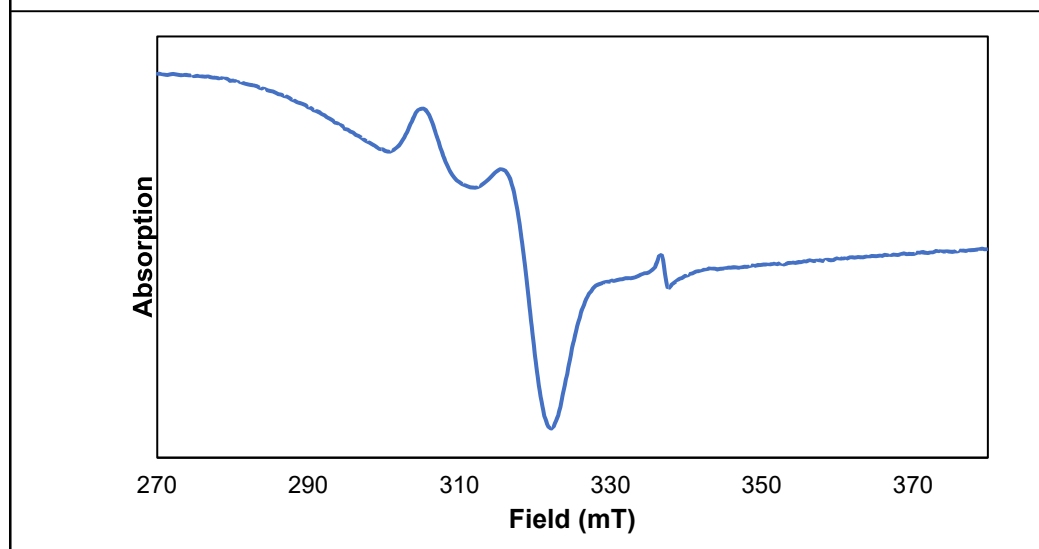
A coupling reaction between 1 eq of methyl 4-bromobenzoate (**2a**, 43.0 mg, 0.2 mmol) and 2 eq of 2-pyrrolidone (**1a**, 0.0304 mL, 0.4 mmol), was set up following the general procedure A (using NiCl$_2$(glyme)): with 4,4'-di-*tert*-butyl-2,2'-dipyridyl (16.2 mg, 0.06 mmol, 30 mol%), NiCl$_2$(glyme) (8.8 mg, 0.02 mmol, 20 mol%). Aliquots were collected after 5 and 45 minutes and analyzed by ^{1}H NMR and EPR. The NMR analysis revealed no reaction after 5 minutes and 5% yield after 45 minutes indicating that these samples were taking during and after the induction period, respectively. The EPR spectrum showed no signal in either case **(Figure 25**, orange and yellow spectra).

A coupling reaction between 1 eq of methyl 4-bromobenzoate (**2a**, 43.0 mg, 0.2 mmol) and 2 eq of 2-pyrrolidone (**1a**, 0.0304 mL, 0.4 mmol), was set up following the general procedure B (using Ni(COD)$_2$): with 4,4'-di-*tert*-butyl-2,2'-dipyridyl

(16.2 mg, 0.06 mmol, 30 mol%), Ni(COD)$_2$ (11.0 mg, 0.040 mmol, 20 mol%). An aliquot was collected after 5 minutes and analyzed by NMR and EPR. The NMR analysis revealed 35% yield. The EPR spectrum showed no signal **(Figure 25**, grey spectrum).

Figure 25: EPR comparison of reaction aliquot traces to Ni(I)
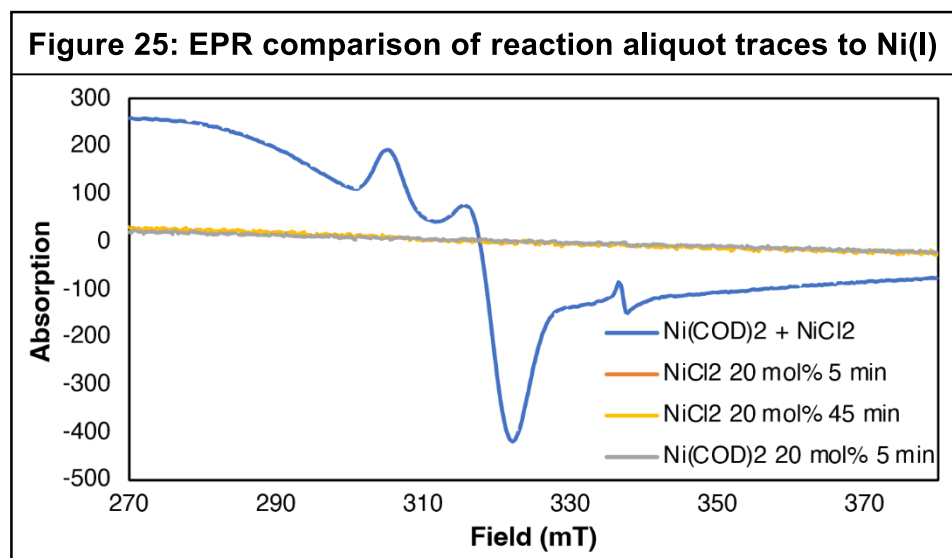
3.6.5 Synthesis and characterization of (dtbbpy)Ni(aryl)Br complexes 4a and 4b:

In the glovebox, a 20 mL scintillation vial was charged with a magnetic stir bar and Ni(COD)$_2$ (110 mg, 0.40 mmol). A second 20 mL scintillation vial was charged with 4,4'-di-*tert*-butyl-2,2'- dipyridyl (107 mg, 0.40 mmol) and 2 mL THF. Once the solid fully dissolved, the solution was transferred via pipet into the reaction vial which was then stirred at room temperature for 1 hour, during which the solution turned purple. Next, an excess quantity of *ortho*-substituted aryl bromide **2** (4.0 mmol) was added to the reaction mixture dropwise then stirred for 4 hours, resulting in a

red solution. Approximately half of the reaction volume was removed by evaporation before the product was precipitated by slow addition of *n*-pentane. The product **4** was collected on a fine frit, washed with additional *n*-pentane, and thoroughly dried.

(dtbbpy)Ni(aryl)Br complex **(4a)**
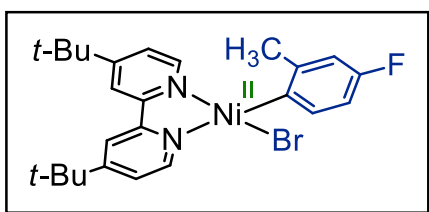
The general procedure was followed using 2-bromo-5-fluorotoluene **(2b)** as aryl bromide. The resulting Ni(II) aryl bromide complex **4a** was collected as an orange solid (202 mg, 98% yield). **^{1}H NMR** (400 MHz, C$_6$D$_6$) δ 9.69 (d, *J* = 5.8 Hz, 1H), 8.03 (td, *J* = 6.7, 1.7 Hz, 1H), 7.22 (d, *J* = 6.2 Hz, 1H), 7.19-7.17 (m, 2H), 7.02 – 6.96 (m, 2H), 6.60 (d, *J* = 5.6 Hz, 1H), 6.08 (dd, *J* = 6.2, 2.2 Hz, 1H), 3.42 (s, 3H), 0.92 (s, 9H), 0.82 (s, 9H). **^{19}F NMR** (376 MHz, C$_6$D$_6$) δ -126.7 (q, *J* = 9.1 Hz). **HRMS** (ESI-TOF) *m/z* calculated for C$_{26}$H$_{31}$BrFN$_2$NiO$_2$ (M+HCOO)$^-$: 559.0913, found 559.0909.

(dtbbpy)Ni(aryl)Br complex **(4b)**
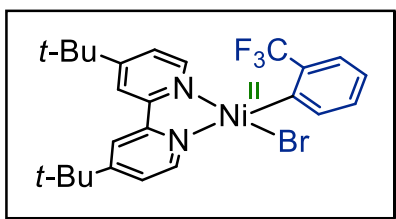
The general procedure was followed using 2-bromobenzotrifluoride **(2c)** as aryl bromide. The resulting Ni(II) aryl bromide complex **4b** was collected as an orange solid (186 mg, 84% yield). **^{1}H NMR** (400 MHz, C$_6$D$_6$) δ 9.65 (bs, 1H), 8.64 (d, *J* = 7.6 Hz, 1H), 7.62 (d, *J* = 7.7

Hz, 1H), 7.20 – 7.10 (m, 4H), 6.92 (t, J = 7.5 Hz, 1H), 6.51 (bs, 1H), 6.01 (bs, 1H), 0.89 (s, 9H), 0.80 (s, 9H). **^{19}F NMR** (376 MHz, C_6D_6) δ -58.2. **HRMS** (ESI-TOF) *m/z* calculated for $C_{26}H_{29}BrF_3N_2NiO_2$ (M+HCOO)$^-$: 595.0725, found 595.0718.

3.6.6 Synthesis and characterization of (dtbbpy)Ni(aryl)(amido) complexes 5a and 5b:

Potassium phosphate tribasic was thoroughly dried at 160 °C for 16 hours before being brought into the glovebox. In the glovebox, a 1-dram vial was charged with a magnetic stir bar, nickel(II) aryl bromide adduct **4** (0.080 mmol) and potassium phosphate tribasic (34.0 mg, 0.160 mmol). A second 1-dram vial was charged with trifluoroacetamide (**1b**, 9.5 mg, 0.084 mmol), 0.8 mL dichloromethane, and 0.2 mL THF. Once the amide was fully dissolved, this solution was transferred to the reaction vial via pipet. The reaction vial was capped and sealed with electrical tape, then stirred at room temperature in the glovebox for 32 hours. Once the reaction was complete, the crude reaction mixture was filtered through a fine frit and rinsed with dichloromethane (2 mL). The filtrate was evaporated to dryness to yield the product **5** as an orange solid.

(dtbbpy)Ni(aryl)(amido) complex **(5a)**
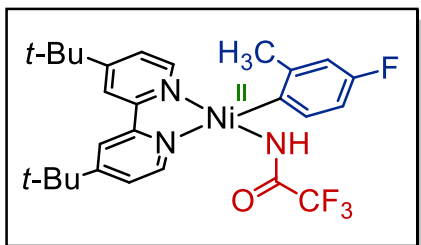
The general procedure was followed using Ni(II) aryl bromide complex **4a**. The resulting Ni(II) aryl amido complex **5a** was collected as an orange solid (40.1 mg, 91% yield). **^{1}H NMR** (400 MHz, C$_6$D$_6$) δ 8.39 (d, J = 5.8 Hz, 1H), 7.90 (dd, J = 9.0, 6.7 Hz, 1H), 7.23 – 7.14 (m, 2H), 7.06 (d, J = 2.1 Hz, 1H), 6.95 – 6.91 (m, 2H), 6.56 (dd, J = 5.9, 2.0 Hz, 1H), 5.99 (dd, J = 6.2, 2.1 Hz, 1H), 4.09 (bs, 1H), 3.26 (s, 3H), 0.92 (s, 9H), 0.82 (s, 9H). **^{19}F NMR** (564 MHz, C$_6$D$_6$) δ -74.0, - 123.5 (q, J = 9.9 Hz). **IR** 1660 cm^{-1}. **HRMS** (ESI-TOF) *m/z* calculated for C$_{28}$H$_{32}$F$_4$N$_3$NiO$_3$ (M+HCOO)$^-$: 592.1740, found 592.1737. The purity of this complex was calculated to be 63% using 4-(trifluoromethyl)benzonitrile as a ^{19}F NMR internal standard.

(dtbbpy)Ni(aryl)(amido) complex **(5b)**
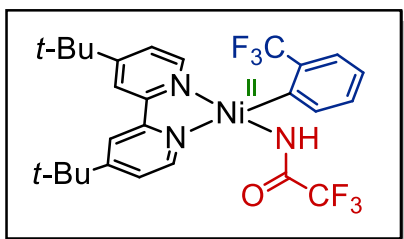
The general procedure was followed using Ni(II) aryl bromide complex **4b**. The resulting Ni(II) aryl amido complex **5b** was collected as an orange solid (44.6 mg, 96% yield). **^{1}H NMR** (400 MHz, C$_6$D$_6$) δ 8.77 (d, J = 7.6 Hz, 1H), 8.23 (d, J = 5.9 Hz, 1H), 7.59 (dd, J = 7.8, 1.4 Hz, 1H), 7.12 (d, J = 7.4 Hz, 1H), 7.06 (d, J = 1.9 Hz, 1H), 7.03 (d, J = 6.1 Hz, 1H), 6.99 (d, J = 2.1 Hz, 1H), 6.93 (t, J = 7.5 Hz, 1H), 6.50 (dd, J = 5.9, 1.8 Hz, 1H), 5.92 (dd, J = 6.1, 2.0 Hz, 1H), 4.19 (bs, 1H), 0.90 (s, 9H), 0.79 (s, 9H). **^{19}F NMR** (376 MHz,

C_6D_6) δ -59.9, -75.6. **IR** 1662 cm^{-1}. **HRMS** (ESI-TOF) *m/z* calculated for $C_{28}H_{30}F_6N_3NiO_3$ (M+HCOO)$^-$: 628.1550, found 628.1522.

3.6.7 Stoichiometric oxidation of (dtbbpy)Ni(aryl)(amido) complex 5a:

The oxidant acetylferrocenium tetrafluoroborate was prepared according to a literature procedure[50]. In the glovebox, two 1-dram vials were charged with magnetic stir bars. To vial A was added (dtbbpy)Ni(aryl)(amido) complex **5a** (21.9 mg, 0.025 mmol) and 0.8 mL MeCN. To vial B was added acetylferrocenium tetrafluoroborate ("AcFcBF$_4$", 12.6 mg, 0.040 mmol) and 0.8 mL MeCN. Both vials were capped and stirred at room temperature until the contents were dissolved. The cold well in the glovebox was chilled to -84 °C using an ethyl acetate/liquid nitrogen slurry. Vials A and B were moved onto a metal block to stir for five minutes in the cold well, allowing enough time for the contents to equilibrate to the cold temperature. Vials A and B were then uncapped, and the contents of vial B were added to vial A in portions, dropwise. The dark blue color of the AcFcBF$_4$ solution rapidly changes to orange as it is added to the Ni(II) complex solution. Once the transfer was complete, the metal block was moved to stir at room temperature for 16 hours, after which the solution was brought outside the glovebox for workup and product isolation. The crude material was evaporated to near-dryness and loaded on a short silica column. The product 3b was eluted with 10% ethyl acetate in hexanes (**R**$_f$ = 0.22), and isolated as a colorless oil (3.7 mg, 67% yield). The product spectra were identical to those previously reported herein.

3.6.8 Catalytic cross-coupling reaction using 5a as precatalyst:

An oven-dried 10 mL Schlenk tube equipped with a magnetic stir bar and 14/20 Suba-Seal® septum was brought into the glovebox. To this flask was added (dtbbpy)Ni(aryl)(amido) complex **5a** (16.4 mg, 0.02 mmol) and 0.75 mL dry PhCF$_3$. The Schlenk tube was brought out of the glovebox and onto the Schlenk line. The rubber septum was replaced with an oven-dried glass cap under nitrogen efflux. The Schlenk tube was charged with Ir(dtbbpy)(ppy)$_2$PF$_6$ (3.7 mg, 0.004 mmol), methyl 4- bromobenzoate (**2a**, 43.0 mg, 0.20 mmol), trifluoroacetamide (**1b**, 45.2 mg, 0.40 mmol), and K$_2$CO$_3$ (55 mg, 0.40 mmol). After these solids were added, *N,N*-dimethylformamide (0.25 mL, dispensed from solvent purification system) was added under constant efflux of nitrogen gas. The ground glass stopper was coated in vacuum grease before sealing the reaction vessel, and the stopper was subsequently wrapped in parafilm. The reaction vessel was placed 1 cm in front of a 427 nm Kessil LED lamp while being submerged in a temperature-controlled water bath in a large crystallizing dish held at a constant 30 °C. The reaction was stirred at 450 rpm.

After 24 hours, the lamp was shut off and the reaction vessel was removed from the water bath. The crude reaction mixture was filtered through a frit filter covered in Celite® using acetone. To this crude filtrate was added 2-3 mL of silica and the suspension was slowly evaporated at <100 rpm until dryness to adsorb the crude material onto the silica. The crude material adsorbed onto silica was used to dry

164

load a flash chromatography column in order to isolate the aryl amide product. Pure hexanes were used for making the silica slurry. The column was initially run in pure hexanes before gradually transitioning to 10% ethyl acetate in hexanes (R_f $_{(3b)}$ = 0.22, R_f $_{(3c)}$ = 0.10); this was to prevent the product from diffusing into the eluent during dry loading. The product **3b** was obtained as a colorless oil (3.0 mg, 7% yield). The product **3c** was obtained as a colorless crystalline solid (45.1 mg, 91% yield). Both products matched previously reported spectra[28].

3.6.9 Kinetic profiles comparing 5a as precatalyst to Ni(COD)$_2$ and NiCl$_2$(glyme) (Figure 18):

Ni(0) reaction conditions: Ni(COD)$_2$ (0.02 mmol), 4,4'-di-*tert*-butyl-2,2'-dipyridyl (dtbbpy, 0.03 mmol), Ir(dtbbpy)(ppy)$_2$PF$_6$ (0.004 mmol), K$_3$PO$_4$ (0.4 mmol), aryl bromide **2a** (0.2 mmol), amide **1a** (0.4 mmol), 0.5 mL dry DMF, and 0.75 mL dry PhCF$_3$.

Ni(II) reaction conditions: NiCl$_2$(glyme) (0.02 mmol), 4,4'-di-*tert*-butyl-2,2'-dipyridyl (dtbbpy, 0.03 mmol), Ir(dtbbpy)(ppy)$_2$PF$_6$ (0.004 mmol), K$_3$PO$_4$ (0.4 mmol), aryl bromide **2a** (0.2 mmol), amide **1a** (0.4 mmol), 0.5 mL dry DMF, and 0.75 mL dry PhCF$_3$.

5a reaction conditions: **5a** (0.02 mmol), Ir(dtbbpy)(ppy)$_2$PF$_6$ (0.004 mmol), K$_3$PO$_4$ (0.4 mmol), aryl bromide **2a** (0.2 mmol), amide **1a** (0.4 mmol), 0.5 mL dry DMF, and 0.75 mL dry PhCF$_3$.

The stock solution solvents and overall solvent ratio were slightly modified to increase the solubility of Ni complexes.

Three stock solutions were used to set up the reactions:

- Stock solution A containing: 22.0 mg NiCl$_2$(glyme) (0.1 mmol) and 40.3 mg 4,4'-di-*tert*-butyl-2,2'-dipyridyl (0.15 mmol) dissolved in 3.75 mL dry PhCF$_3$.

- Stock solution A' containing: 27.5 mg Ni(COD)$_2$ (0.1 mmol) and 40.3 mg 4,4'-di-*tert*-butyl-2,2'-dipyridyl (0.15 mmol) dissolved in 3.75 mL dry PhCF$_3$, which was prepared in the glovebox.

- Stock solution A'' containing: 41.2 mg **5a** (0.05 mmol) dissolved in 1.88 mL dry PhCF$_3$, which was prepared in the glovebox.

- Stock solution B containing: 18.4 mg Ir(dtbbpy)(ppy)$_2$PF$_6$ (0.02 mmol), 215.3 mg aryl bromide **2a** (1 mmol), 0.152 mL amide **1a** (2 mmol), 2.5 mL dry DMF.

The reactions were carried out according to the general procedure. Additionally, 0.5 mL of stock B was added to each reaction and 0.75 mL of the appropriate Ni stock solution (A, A' and A'') was added to each reaction.

3.6.10 Light-free experiments with Zn reductant:

Light- and photocatalyst-free conditions with added Zn as described by Nocera[10] were probed to compare the reaction profiles of the light-free Ni(I/III) cycle to the Ni-photoredox Ni(0/II/III) cycle proposed herein.

1a 2 eq. + **2a** 0.5-2 eq. →
NiCl$_2$(glyme) (10 mol%)
dtbbpy (15 mol%)
Zn dust (5-50 mol%)
K$_3$PO$_4$ (2.0 eq.)
3:1 PhCF$_3$:DMF
protected from light
→ **3a**
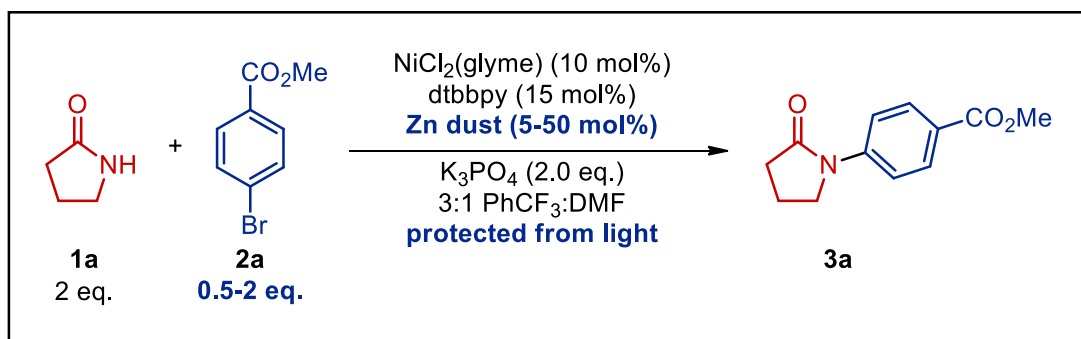
General procedure: An oven-dried 10 mL Schlenk tube was charged with a magnetic stir bar and capped with a 14/20 Suba-Seal® septum. The flask was evacuated and refilled with nitrogen gas three times, after which the septum was replaced with an oven-dried 14/20 ground glass stopper while under nitrogen gas pressure. The flask was fully wrapped in aluminum foil to prevent ambient light from entering. Solid reagents were then added to the Schlenk tube through a weighing paper cone while constant efflux of nitrogen gas maintained inert conditions in the reaction vessel. The Schlenk tube was charged with 4,4'-di-*tert*-butyl-2,2'-dipyridyl (8.1 mg, 0.03 mmol), NiCl$_2$(glyme) (4.4 mg, 0.02 mmol), methyl 4-bromobenzoate (43.0 mg, 0.2 mmol), 325 mesh Zn dust (0.7 to 6.5 mg, 0.01 to 0.1 mmol), and K$_3$PO$_4$ (84.9 mg, 0.4 mmol). After these solids were added, benzotrifluoride (0.75 mL, distilled under nitrogen gas and over oven-dried 3 Å molecular sieves), *N,N*-dimethylformamide (0.25 mL, dispensed from solvent

purification system), and 2-pyrrolidone (30.4 mL, 0.4 mmol) were added under constant efflux of nitrogen gas. The ground glass stopper was coated in vacuum grease before sealing the reaction vessel, and the stopper was subsequently wrapped in parafilm. The reaction was stirred at room temperature at 450 rpm. After 24 hours, the reaction vessel was uncapped and ~3 mg of dimethyl fumarate (internal standard) and 1 mL dichloromethane were added to the crude reaction mixture. An aliquot was taken for ^{1}H NMR analysis, which demonstrated a 39% internal standard yield of **3a** when 50 mol% Zn was used. No product was observed when only 5 mol% Zn was used. Product spectra matched those previously reported for **3a** [28].

*Kinetics experimental information **(Figure 19)**:*

Reaction conditions: NiCl$_2$(glyme) (0.01 to 0.04 mmol), 4,4'-di-*tert*-butyl-2,2'-dipyridyl (dtbbpy, 0.015 to 0.06), 325 mesh Zn dust (0.1 mmol), K$_3$PO$_4$ (0.4 mmol), aryl bromide **2a** (0.2 mmol), amide **1a** (0.4 mmol), 0.5 mL dry DMF, and 0.75 mL dry PhCF$_3$.

The stock solution solvents and overall solvent ratio were slightly modified to increase the solubility of Ni complexes. Two stock solutions were used to set up the reactions:

- Stock solution A containing: 52.7 mg NiCl$_2$(glyme) (0.24 mmol) and 96.6 mg 4,4'-di-*tert*-butyl-2,2'-dipyridyl (0.36 mmol) dissolved in 1.6 mL dry DMF.

- Stock solution B containing: 172.0 mg aryl bromide **2a** (0.8 mmol), 0.122 mL amide **1a** (1.6 mmol), 0.4 mL dry DMF, and 3.0 mL dry PhCF$_3$.

The light-protected reaction flasks were set up according to the general procedure for the light-free experiments. 325 mesh Zn dust (0.1 mmol) and K$_3$PO$_4$ (0.4 mmol) were added as solids to each reaction flask individually under N2 efflux before addition of the solvent and stock solutions. 0.85 mL of stock B was added to each reaction. Reactions contained varying amounts of Ni stock solution and dry DMF, which were added to maintain a constant volume: 5% Ni(II) (0.1 mL stock solution A and 0.3 mL dry DMF), 10% Ni(II) (0.2 mL stock solution A and 0.2 mL dry DMF), and 20% Ni(II) (0.4 mL stock solution A and no additional dry DMF). Aliquots taken for each timepoint were quickly diluted with approximately 0.6 mL CDCl$_3$ and stored in a dark ice bath until ^{1}H NMR spectra were ready to be acquired.

3.6.11 X-ray crystallographic data of 5b:

Data collection:

Single crystals suitable for X-ray diffraction were grown by vapor diffusion of *n*-pentane into dichloromethane. A yellow crystal (plate, approximate dimensions 0.12 × 0.05 × 0.04 mm^3) was placed onto the tip of a MiTeGen pin and mounted on a Bruker Venture D8 diffractometer equipped with a PhotonIII detector at 100.00 K. The data collection was carried out using Mo Kα radiation (λ = 0.71073 Å, IμS micro-source) with a frame time of 12 seconds and a detector distance of 40 mm.

A collection strategy was calculated and complete data to a resolution of 0.82 Å were collected. The frames were integrated with the Bruker SAINT[51] software package using a narrow-frame algorithm to 0.82 Å resolution. Data were corrected for absorption effects using the multi-scan method (SADABS)[52]. Please refer to Table S1 for additional crystal and refinement information.

Structure solution and refinement:

The space group P 2_1/n was determined based on intensity statistics and systematic absences. The structure was solved using the SHELX suite of programs[53,54] and refined using full-matrix leastsquares on F^2 within the OLEX2 suite[55]. An intrinsic phasing solution was calculated, which provided most non-hydrogen atoms from the E-map. Full-matrix least squares / difference Fourier cycles were performed, which located the remaining non-hydrogen atoms. All non-hydrogen atoms were refined with anisotropic displacement parameters. The hydrogen atoms were placed in ideal positions and refined as riding atoms with relative isotropic displacement parameters, except the hydrogen on N1, which was refined freely. The final full matrix least squares refinement converged to R1 = 0.0463 and wR2 = 0.1304 (F^2, all data). The goodness-of-fit was 1.056. On the basis of the final model, the calculated density was 1.413 g/cm^3 and F(000), 1208 e-.

Crystal data and structure refinement for **5b**:

Empirical formula	C27 H29 F6 N3 Ni O
Formula weight	584.24
Crystal color, shape, size	yellow plate, 0.12 x 0.05 x 0.04 mm^3
Temperature	100.00 K
Wavelength	0.71073 Å
Crystal system, space group	monoclinic, P 2$_1$/n
Unit cell dimensions	a = 12.0239(9) Å α = 90°.
	b = 20.0145(18) Å β = 115.621(2)°.
	c = 12.6542(10) Å γ = 90°.
Volume	2745.8(4) Å^3
Z	4
Density (calculated)	1.413 g/cm^3
Absorption coefficient	0.772 mm^{-1}
F(000)	1208

Data collection:

Diffractometer	Bruker D8 Venture
Theta range for data collection	1.953 to 25.350°.

Index ranges	-14<=h<=14, -24<=k<=24, -15<=1<=15
Reflections collected	85757
Independent reflections	5028 [Rint = 0.1430]
Observed reflections	3644
Completeness to theta = 25.242°	100.0 %

Solution and refinement:

Absorption correction	Semi-empirical from equivalents
Max. and min. transmission	0.7453 and 0.6547
Extinction coefficient	0.0076(8)
Solution	Intrinsic methods
Refinement method	Full-matrix least-squares on F^2
Weighting scheme	$w = [s^2 F_o^2 + AP^2 + BP]^{-1}$, with $P = (F_o^2 + 2 F_c^2)/3$, A = 0.064, B = 1.49
Data / restraints / parameters	5028 / 0 / 354
Goodness-of-fit on F^2	1.056
Final R indices [I>2s(I)]	R1 = 0.0463, wR2 = 0.1116
R indices (all data)	R1 = 0.0735, wR2 = 0.1304
Largest diff. peak and hole	0.496 and -0.562 e.$Å^{-3}$

3.7   References

(1)   Diccianni, J. B.; Diao, T. Mechanisms of Nickel-Catalyzed Cross-Coupling Reactions. *Trends Chem.* **2019**, *1* (9), 830–844. https://doi.org/10.1016/j.trechm.2019.08.004.

(2)   Zhu, C.; Uifeng Yue, H.; Jia, J.; Rueping, M. Cross-Coupling Nickel-Catalyzed C-Heteroatom Cross-Coupling Reactions under Mild Conditions via Facilitated Reductive Elimination. *Angew. Chem. Int. Ed.* **2021**, *60*, 17810–17831. https://doi.org/10.1002/anie.202013852.

(3)   Terrett, J. A.; Cuthbertson, J. D.; Shurtleff, V. W.; MacMillan, D. W. C. Switching on Elusive Organometallic Mechanisms with Photoredox Catalysis. *Nature* **2015**, *524* (7565), 330–334. https://doi.org/10.1038/nature14875.

(4)   Corcoran, E. B.; Pirnot, M. T.; Lin, S.; Dreher, S. D.; Dirocco, D. A.; Davies, I. W.; Buchwald, S. L.; Macmillan, D. W. C. Aryl Amination Using Ligand-Free Ni(II) Salts and Photoredox Catalysis. *Science* **2016**, *353* (6296), 279–283.

(5)   Welin, E. R.; Le, C.; Arias-Rotondo, D. M.; Mccusker, J. K.; Macmillan, D. W. C. Photosensitized, Energy Transfer-Mediated Organometallic Catalysis through Electronically Excited Nickel(II). *Science* **2017**, *355* (6323), 380–385.

(6)   Tian, L.; Till, N. A.; Kudisch, B.; MacMillan, D. W. C.; Scholes, G. D. Transient Absorption Spectroscopy Offers Mechanistic Insights for an Iridium/Nickel-Catalyzed C-O Coupling. *J. Am. Chem. Soc.* **2020**, *142* (10), 4555–4559. https://doi.org/10.1021/jacs.9b12835.

(7)   Till, N. A.; Tian, L.; Dong, Z.; Scholes, G. D.; MacMillan, D. W. C. Mechanistic Analysis of Metallaphotoredox C-N Coupling: Photocatalysis Initiates and Perpetuates Ni(I)/Ni(III) Coupling Activity. *J. Am. Chem. Soc.* **2020**, *142* (37), 15830–15841. https://doi.org/10.1021/jacs.0c05901.

(8)   Sun, R.; Qin, Y.; Ruccolo, S.; Schnedermann, C.; Costentin, C.; Nocera, D. G. Elucidation of a Redox-Mediated Reaction Cycle for Nickel-Catalyzed Cross Coupling. *J. Am. Chem. Soc.* **2019**, *141* (1), 89–93. https://doi.org/10.1021/jacs.8b11262.

(9)   Kawamata, Y.; Vantourout, J. C.; Hickey, D. P.; Bai, P.; Chen, L.; Hou, Q.; Qiao, W.; Barman, K.; Edwards, M. A.; Garrido-Castro, A. F.; Degruyter, J. N.; Nakamura, H.; Knouse, K.; Qin, C.; Clay, K. J.; Bao, D.; Li, C.; Starr, J. T.; Garcia-Irizarry, C.; Sach, N.; White, H. S.; Neurock, M.; Minteer, S. D.;

Baran, P. S. Electrochemically Driven, Ni-Catalyzed Aryl Amination: Scope, Mechanism, and Applications. *J. Am. Chem. Soc.* **2019**, *141* (15), 6392–6402. https://doi.org/10.1021/jacs.9b01886.

(10) Sun, R.; Qin, Y.; Nocera, D. G. General Paradigm in Photoredox Nickel-Catalyzed Cross-Coupling Allows for Light-Free Access to Reactivity. *Angew. Chem. Int. Ed.* **2020**, *59* (24), 9527–9533. https://doi.org/10.1002/anie.201916398.

(11) Chrisman, C. H.; Kudisch, M.; Puffer, K. O.; Stewart, T. K.; Lamb, Y. M. L.; Lim, C. H.; Escobar, R.; Thordarson, P.; Johannes, J. W.; Miyake, G. M. Halide Noninnocence and Direct Photoreduction of Ni(II) Enables Coupling of Aryl Chlorides in Dual Catalytic, Carbon-Heteroatom Bond-Forming Reactions. *J. Am. Chem. Soc.* **2023**, *145* (22), 12293–12304. https://doi.org/10.1021/jacs.3c02784.

(12) Shields, B. J.; Kudisch, B.; Scholes, G. D.; Doyle, A. G. Long-Lived Charge-Transfer States of Nickel(II) Aryl Halide Complexes Facilitate Bimolecular Photoinduced Electron Transfer. *J. Am. Chem. Soc.* **2018**, *140* (8), 3035–3039. https://doi.org/10.1021/jacs.7b13281.

(13) Ting, S. I.; Garakyaraghi, S.; Taliaferro, C. M.; Shields, B. J.; Scholes, G. D.; Castellano, F. N.; Doyle, A. G. 3d-d Excited States of Ni(II) Complexes Relevant to Photoredox Catalysis: Spectroscopic Identification and Mechanistic Implications. *J. Am. Chem. Soc.* **2020**, *142* (12), 5800–5810. https://doi.org/10.1021/jacs.0c00781.

(14) Cagan, D. A.; Bim, D.; Silva, B.; Kazmierczak, N. P.; McNicholas, B. J.; Hadt, R. G. Elucidating the Mechanism of Excited-State Bond Homolysis in Nickel-Bipyridine Photoredox Catalysts. *J. Am. Chem. Soc.* **2022**, *144* (14), 6516–6531. https://doi.org/10.1021/jacs.2c01356.

(15) Yang, L.; Lu, H. H.; Lai, C. H.; Li, G.; Zhang, W.; Cao, R.; Liu, F.; Wang, C.; Xiao, J.; Xue, D. Light-Promoted Nickel Catalysis: Etherification of Aryl Electrophiles with Alcohols Catalyzed by a NiII-Aryl Complex. *Angew. Chem. Int. Ed.* **2020**, *59* (31), 12714–12719. https://doi.org/10.1002/anie.202003359.

(16) Malik, J. A.; Madani, A.; Pieber, B.; Seeberger, P. H. Evidence for Photocatalyst Involvement in Oxidative Additions of Nickel-Catalyzed Carboxylate O-Arylations. *J. Am. Chem. Soc.* **2020**, *142* (25), 11042–11049. https://doi.org/10.1021/jacs.0c02848.

(17)   Ma, P.; Wang, S.; Chen, H. Reactivity of Transition-Metal Complexes in Excited States: C-o Bond Coupling Reductive Elimination of a Ni(Ii) Complex Is Elicited by the Metal-to-Ligand Charge Transfer State. *ACS Catal.* **2020**, *10* (1), 1–6. https://doi.org/10.1021/acscatal.9b03827.

(18)   Zhu, C.; Yue, H.; Nikolaienko, P.; Rueping, M. Merging Electrolysis and Nickel Catalysis in Redox Neutral Cross-Coupling Reactions: Experiment and Computation for Electrochemically Induced c-p and c-Se Bonds Formation. *CCS Chem.* **2020**, *2* (2), 179–190. https://doi.org/10.31635/ccschem.020.201900112.

(19)   Han, R.; Hillhouse, G. L. Carbon-Oxygen Reductive-Elimination from Nickel(II) Oxametallacycles and Factors That Control Formation of Ether, Aldehyde, Alcohol, or Ester Products. *J. Am. Chem. Soc.* **1997**, *119*, 8135–8136.

(20)   Koo, K.; Hillhouse, G. L. Indoline Synthesis via Coupling of Phenethyl Grignard Reagents with Organoazides Mediated by (Alkylphosphine)Nickel(II) Complexes. *Organometallics* **1996**, *15* (12), 2669–2671.

(21)   Koo, K.; Hillhouse, G. L. Carbon-Nitrogen Bond Formation by Reductive Elimination from Nickel(II) Amido Alkyl Complexes. *Organometallics* **1995**, *14*, 4421–4423.

(22)   Lin, B. L.; Clough, C. R.; Hillhouse, G. L. Interactions of Aziridines with Nickel Complexes: Oxidative-Addition and Reductive-Elimination Reactions That Break and Make C-N Bonds. *J. Am. Chem. Soc.* **2002**, *124* (12), 2890–2891. https://doi.org/10.1021/ja017652n.

(23)   Tasker, S. Z.; Jamison, T. F. Highly Regioselective Indoline Synthesis under Nickel/Photoredox Dual Catalysis. *J. Am. Chem. Soc.* **2015**, *137* (30), 9531–9534. https://doi.org/10.1021/jacs.5b05597.

(24)   Le Vaillant, F.; Reijerse, E. J.; Leutzsch, M.; Cornella, J. Dialkyl Ether Formation at High-Valent Nickel. *J. Am. Chem. Soc.* **2020**, *142* (46), 19540–19550. https://doi.org/10.1021/jacs.0c07381.

(25)   Wolfe, J. P.; Buchwald, S. L. Nickel-Catalyzed Amination of Aryl Chlorides. *J. Am. Chem. Soc.* **1997**, *119* (26), 6054–6058.

(26)   Kim, T.; McCarver, S. J.; Lee, C.; MacMillan, D. W. C. Sulfonamidation of Aryl and Heteroaryl Halides through Photosensitized Nickel Catalysis. *Angew. Chem. Int. Ed.* **2018**, *57* (13), 3488–3492. https://doi.org/10.1002/anie.201800699.

(27) Kudisch, M.; Lim, C. H.; Thordarson, P.; Miyake, G. M. Energy Transfer to Ni-Amine Complexes in Dual Catalytic, Light-Driven C-N Cross-Coupling Reactions. *J. Am. Chem. Soc.* **2019**, *141* (49), 19479–19486. https://doi.org/10.1021/jacs.9b11049.

(28) Bradley, R. D.; Bahamonde, A. Mild Amide N-Arylation Enabled by Nickel-Photoredox Catalysis. *Org. Lett.* **2022**, *24* (39), 7134–7139. https://doi.org/10.1021/acs.orglett.2c02808.

(29) Goldberg, I. Ueber Phenylirungen Bei Gegenwart von Kupfer Als Katalysator. *Ber. Dtsch. Chem. Ges.* **1906**, *39*, 1691–1692.

(30) Klapars, A.; Antilla, J. C.; Huang, X.; Buchwald, S. L. A General and Efficient Copper Catalyst for the Amidation of Aryl Halides and the N-Arylation of Nitrogen Heterocycles [2]. *J. Am. Chem. Soc.* **2001**, *123* (31), 7727–7729. https://doi.org/10.1021/ja016226z.

(31) Lavoie, C. M.; MacQueen, P. M.; Stradiotto, M. Nickel-Catalyzed N-Arylation of Primary Amides and Lactams with Activated (Hetero)Aryl Electrophiles. *Chem. Eur. J.* **2016**, *22* (52), 18752–18755. https://doi.org/10.1002/CHEM.201605095.

(32) Mcguire, R. T.; Lundrigan, T.; Macmillan, J. W. M.; Robertson, K. N.; Yadav, A. A.; Stradiotto, M. Mapping Dual-Base-Enabled Nickel-Catalyzed Aryl Amidations: Application in the Synthesis of 4-Quinolones. *Angew. Chem. Int. Ed.* **2022**, *61* (13), e202200352. https://doi.org/10.1002/anie.202200352.

(33) Ruiz-Castillo, P.; Buchwald, S. L. Applications of Palladium-Catalyzed C−N Cross-Coupling Reactions. *Chem. Rev.* **2016**, *116* (19), 12564–12649. https://doi.org/10.1021/acs.chemrev.6b00512.

(34) Yin, J.; Buchwald, S. L. Palladium-Catalyzed Intermolecular Coupling of Aryl Halides and Amides. *Org. Lett.* **2000**, *2* (8), 1101–1104. https://doi.org/10.1021/ol005654r.

(35) Dorel, R.; Grugel, C. P.; Haydl, A. M. The Buchwald–Hartwig Amination After 25 Years. *Angew. Chem. Int. Ed.* **2019**, *131* (48), 17276–17287. https://doi.org/10.1002/ange.201904795.

(36) Racine, E.; Monnier, F.; Vors, J. P.; Taillefer, M. A Simple Copper-Catalyzed Synthesis of Tertiary Acyclic Amides. *Org. Lett.* **2011**, *13* (11), 2818–2821. https://doi.org/10.1021/ol200750p.

(37) Shakespeare, W. C. Palladium-Catalyzed Coupling of Lactams with Bromobenzenes. *Tetrahedron Lett.* **1999**, *40*, 2035–2038.

(38) Larsson, P. F.; Correa, A.; Carril, M.; Norrby, P. O.; Bolm, C. Copper-Catalyzed Cross-Couplings with Part-per-Million Catalyst Loadings. *Angew. Chem. Int. Ed.* **2009**, *48* (31), 5691–5693. https://doi.org/10.1002/anie.200902236.

(39) Twilton, J.; Christensen, M.; DiRocco, D. A.; Ruck, R. T.; Davies, I. W.; MacMillan, D. W. C. Selective Hydrogen Atom Abstraction through Induced Bond Polarization: Direct A-Arylation of Alcohols through Photoredox, HAT, and Nickel Catalysis. *Angew. Chem. Int. Ed.* **2018**, *130* (19), 5467–5471. https://doi.org/10.1002/ange.201800749.

(40) Zuo, Z.; Ahneman, D. T.; Chu, L.; Terrett, J. A.; Doyle, A. G.; Macmillan, D. W. C. Merging Photoredox with Nickel Catalysis: Coupling of α-Carboxyl Sp 3-Carbons with Aryl Halides. *Science* **2014**, *345* (6195), 437–440.

(41) Tellis, J. C.; Primer, D. N.; Molander, G. A. Single-Electron Transmetalation in Organoboron Cross-Coupling by Photoredox/Nickel Dual Catalysis. *Science* **2014**, *345* (6195), 430–433. https://doi.org/10.1126/science.1251422.

(42) Shields, B. J.; Doyle, A. G. Direct C(Sp3)-H Cross Coupling Enabled by Catalytic Generation of Chlorine Radicals. *J. Am. Chem. Soc.* **2016**, *138* (39), 12719–12722. https://doi.org/10.1021/jacs.6b08397.

(43) Mohadjer Beromi, M.; Brudvig, G. W.; Hazari, N.; Lant, H. M. C.; Mercado, B. Q. Synthesis and Reactivity of Paramagnetic Nickel Polypyridyl Complexes Relevant to C(Sp 2)–C(Sp 3)Coupling Reactions . *Angew. Chem. Int. Ed.* **2019**, *58*, 6094–6098. https://doi.org/10.1002/ange.201901866.

(44) *Cambridge Crystallographic Data Centre (CCDC) deposition number 2267998*. https://doi.org/10.1002/anie.202310753.

(45) Vander Griend, D. A.; Bediako, D. K.; DeVries, M. J.; DeJong, N. A.; Heeringa, L. P. Detailed Spectroscopic, Thermodynamic, and Kinetic Characterization of Nickel(II) Complexes with 2,2′-Bipyridine and 1,10-Phenanthroline Attained via Equilibrium-Restricted Factor Analysis. *Inorg. Chem.* **2008**, *47* (2), 656–662. https://doi.org/10.1021/ic700553d.

(46) Primer, D. N.; Karakaya, I.; Tellis, J. C.; Molander, G. A. Single-Electron Transmetalation: An Enabling Technology for Secondary Alkylboron Cross-

Coupling. *J. Am. Chem. Soc.* **2015**, *137* (6), 2195–2198. https://doi.org/10.1021/ja512946e.

(47) Le, C.; Liang, Y.; Evans, R. W.; Li, X.; MacMillan, D. W. C. Selective Sp 3 C-H Alkylation via Polarity-Match-Based Cross-Coupling. *Nature* **2017**, *547* (7661), 79–83. https://doi.org/10.1038/nature22813.

(48) McCormick, M. C.; Keijzer, K.; Polavarapu, A.; Schultz, F. A.; Baik, M. H. Understanding Intrinsically Irreversible, Non-Nernstian, Two-Electron Redox Processes: A Combined Experimental and Computational Study of the Electrochemical Activation of Platinum(IV) Antitumor Prodrugs. *J. Am. Chem. Soc.* **2014**, *136* (25), 8992–9000. https://doi.org/10.1021/ja5029765.

(49) Song, G.; Li, Q.; Nong, D. Z.; Song, J.; Li, G.; Wang, C.; Xiao, J.; Xue, D. Ni-Catalyzed Photochemical C−N Coupling of Amides with (Hetero)Aryl Chlorides. *Chem. Eur. J.* **2023**, *29* (37). https://doi.org/10.1002/chem.202300458.

(50) Deb, M.; Hazra, S.; Dolui, P.; Elias, A. J. Ferrocenium Promoted Oxidation of Benzyl Amines to Imines Using Water as the Solvent and Air as the Oxidant. *ACS Sustainable Chem. Eng.* **2019**, *7* (1), 479–486. https://doi.org/10.1021/acssuschemeng.8b03966.

(51) SAINT 8.30A. Bruker Analytical X-Ray Systems: Madison, WI 2012.

(52) SADABS 2.03. Bruker Analytical X-Ray Systems: Madison, WI 2016.

(53) Sheldrick, G. M. . *Acta Cryst.* **2015**, *A71*, 3.

(54) Sheldrick, G. M. . *Acta Cryst.* **2008**, *A64*, 112.

(55) Dolomanov, O. V.; Bourhis, L. J.; Gildea, R. J.; Howard, J. A. K.; Puschmann, H. OLEX2: A Complete Structure Solution, Refinement and Analysis Program. *J. Appl. Crystallogr.* **2009**, *42* (2), 339–341. https://doi.org/10.1107/S0021889808042726.

Chapter 4: Nickel-catalyzed activation of benzonitriles as low-toxicity cyanide surrogates for cyclopropyl ketone ring-opening cyanation

4.1 Introduction to Ni-catalyzed C-C bond activation and the discovery of a rare Ni-catalyzed cross-coupling of electrophilic C-C bonds

As discussed in Chapter 1.2, low-valent Ni(0) is particularly effective for difficult bond activations. Ni(0) is a relatively nucleophilic transition metal due to its electropositivity[1,2] and small atomic radius[3]. These properties facilitate the insertion of Ni into strong C-C and C-heteroatom bonds. Electron-rich ligands such as phosphines and NHCs are often paired with Ni to promote difficult oxidative additions[4]. A variety of σ-C-C bonds have been functionalized in Ni-catalyzed methodologies, including C(sp$^{2/3}$)-C(sp^2) bonds in

Figure 1: possible sites of σ-C-C bond cleavage in Ni catalysis
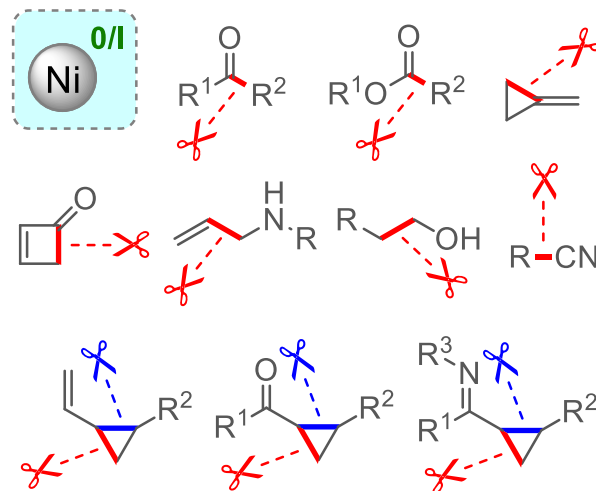
Red and blue bonds represent possible C-C bond cleavage sites enabled by low-valent Ni.

ketones[5–7] and esters[8], C(sp^2)-C(sp^3) bonds in alkylidenecyclopropanes[9–14], cyclobutenones[15,16], and allylamines[17], C(sp^3)-C(sp^3) bonds in vinyl cyclopropanes[18–20], cyclopropyl ketones (CPKs)[21–27], cyclopropyl imines[28], and alcohols[29], and C(sp$^{2/3}$)-C(sp) bonds in nitriles[30–32] **(Figure 1)**.

Within this diverse chemical space of Ni-catalyzed C-C bond activation, we were particularly interested in reactions involving $C(sp^3)$-$C(sp^3)$ bond cleavage in CPKs. These reactions have been shown by Ogoshi and coworkers to proceed via a 6-membered oxanickelacycle species[21,33]. These Ni intermediates have been used to couple CPKs to alkenes[21,23] and alkynes[27] forming cyclopentane derivatives and has also been leveraged for ring-opening alkylation[22,25,26], arylation[22], and borylation[24] cross-coupling reactions **(Figure 2)**. These Ni-catalyzed CPK ring-opening reactions are often (though not always) enabled by the cooperation of a Lewis acid (LA).
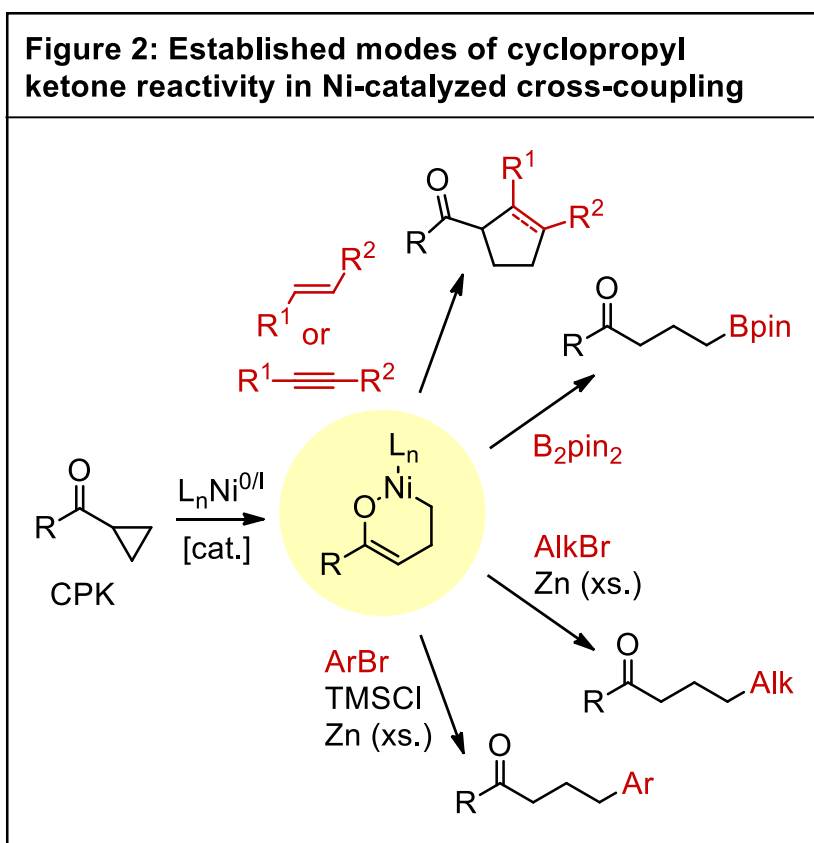
Figure 2: Established modes of cyclopropyl ketone reactivity in Ni-catalyzed cross-coupling

Due to the absence of reported Ni-catalyzed CPK ring-opening amination reactions, this transformation became the target of my studies. Attempts to generate the ring-opened secondary amine product with stoichiometric Ni(COD)$_2$ and aniline failed. Instead, a different ring-opened product was detected by ^{1}H NMR. This product matched previously

reported NMR and IR characterization data for **3a** and was isolated with a meager

1% yield **(Scheme 1)**. This nitrile product was hypothesized to be the result of

oxidative addition into acetonitrile by Ni(0) and subsequent cross-coupling of the

cyanide moiety with the ring-opened CPK, although the mechanism of this process

was poorly understood at this point. 1.0 eq. of trimethylsilyl chloride (TMSCl) was

Scheme 1: Serendipitous discovery of cyanide transfer reactivity with stoichiometric Ni
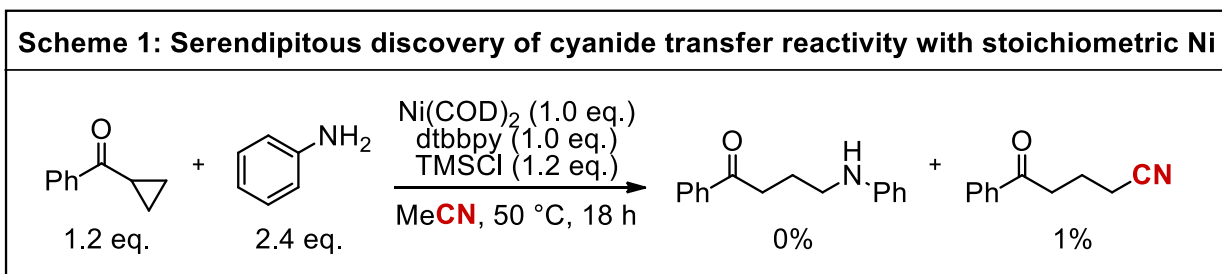
employed as a Lewis acid to enhance the electrophilicity of the ketone (and,

inadvertently, the nitrile also). We were excited by this serendipitous discovery of

a Ni(0)/LA system that was able to activate both CPKs and nitriles in a productive

cross-coupling reaction. Organic nitriles are relatively inert cyanide sources that

are much safer to handle than HCN, trimethylsilyl cyanide (TMSCN), or the variety

of cyanide salts and metal cyanide complexes that are commonly used as cyanide

sources and which all liberate deadly HCN upon exposure to acidic conditions or

workup[34].

Scheme 2: Cu/LA/photochemical radical CPK ring-opening cyanation
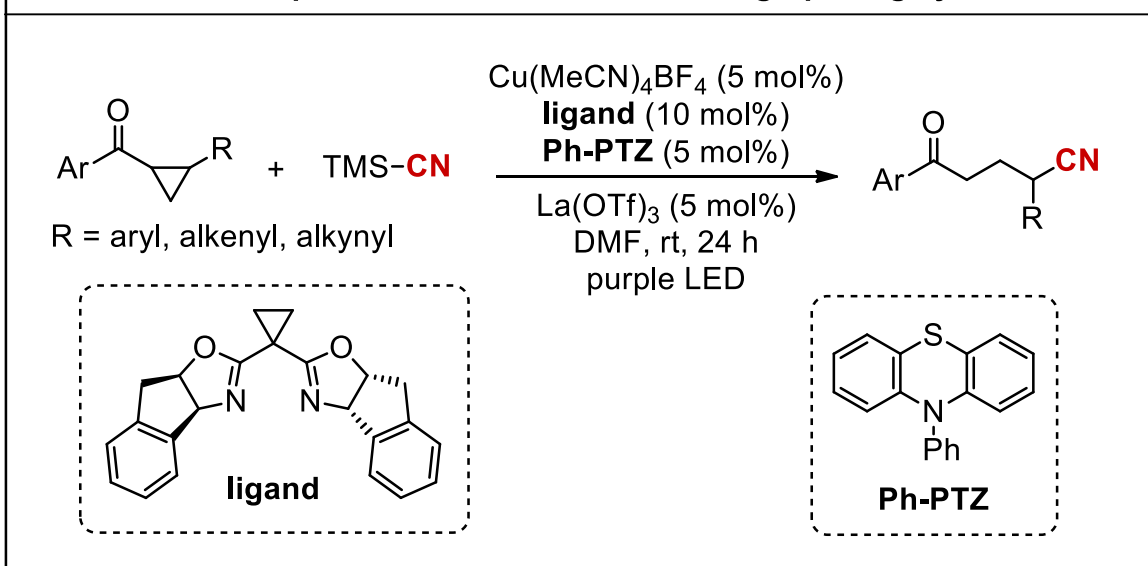
A thorough literature search revealed that a similar ring-opening cyanation of CPKs enabled by Cu, Lewis acid, photocatalyst, and visible light irradiation had already been reported[35] **(Scheme 2)**. However, this Cu-catalyzed reaction suffers from two major limitations: 1) a reduced scope due to the need for an additional radical-stabilizing aryl, alkenyl, or alkylnyl functional group on the cyclopropane ring and 2) a requirement for TMSCN as the cyanide source, which is highly toxic and much less challenging to activate than organic nitriles. Cyclopropyl phenyl ketone **1a** was not amenable to the Cu/photochemical cyanation conditions, contrasting the Ni/LA system that we were studying which was able to cyanate this substrate. This scope divergence, together with other regioselectivity data that will be discussed later, is not consistent with the generation of an alkyl radical from **1a** under the Ni/LA conditions of our reaction. Instead, a concerted oxidative addition

of low-valent Ni into the CPK species to form an oxanickelacycle intermediate is hypothesized to be more likely.

Figure 3: Catalytic nitrile transfer hydrocyanation (Morandi & coworkers)
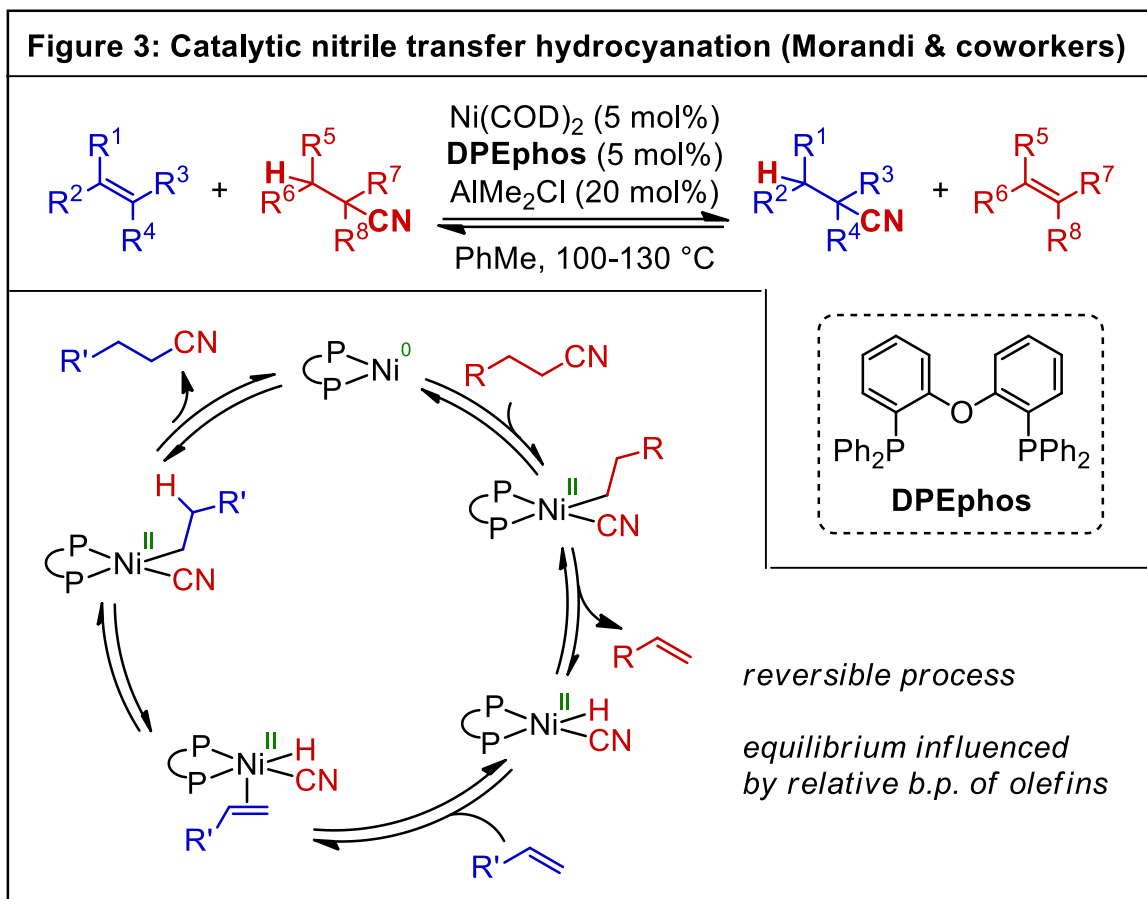
Although a variety of Ni-catalyzed and Ni/LA-catalyzed alkylnitrile and benzonitrile activation reactions are known, they most often transfer the alkyl/aryl group to a coupling partner, undergo protodecyanation, or engage in carbocyanation reactions with π-bond coupling partners[32]. Transfer of the cyanide functional group without transfer of the aryl or alkyl group from an organic nitrile to an organic substrate is less common, but has been reported in the context of aryl

(pseudo)halide cyanation[36–40] and for the hydrocyanation of alkenes[30] and alkynes[30,31].

An important literature precedent for Ni/LA-catalyzed cyanation chemistry comes from Morandi and coworkers, who first reported nitrile activation by a homogeneous Ni(0)/LA system in the context of olefin hydrocyanation[30] **(Figure 3)**. Because the starting alkylnitrile is converted to an olefin byproduct, the reaction is reversible. The equilibrium can be shifted towards the products if a low molecular weight nitrile is employed, generating volatile hydrocarbons that escape the reaction media and drive the catalytic process forward. This olefin hydrocyanation method contrasts the harsh conditions used by the much older and industrially critical DuPont adiponitrile process,

Scheme 3: The DuPont adiponitrile process
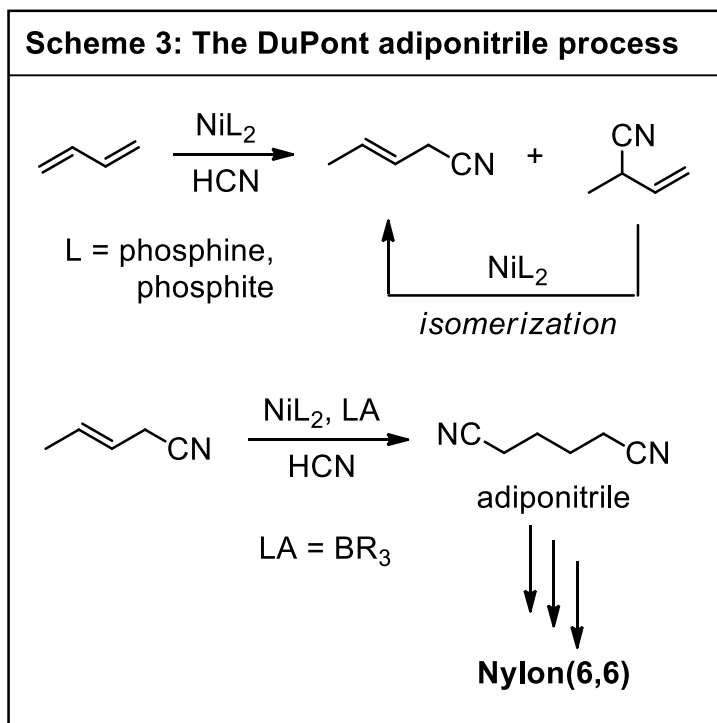
a Ni/LA-catalyzed process which uses highly toxic HCN to produce adiponitrile (a Nylon(6,6) precursor) from 1,3-butadiene[41,42] **(Scheme 3)**. The DuPont adiponitrile process is mechanistically similar to the Morandi catalytic transfer hydrocyanation reaction, except instead of an alkylnitrile, HCN is used. Ni(0) can undergo oxidative addition with HCN to directly access the Ni(II) hydrogen cyanide intermediate that

is required for olefin hydrocyanation. Although HCN is a powerful reagent for the hydrocyanation of olefins, it is incredibly toxic and volatile, unlike organic nitriles which are much less hazardous to work with.

4.2 Optimization of the Ni/LA-catalyzed CPK ring-opening cyanation reaction

After obtaining the initial fleeting result of 1% conversion to the cyanation product **3a** under 100 mol% Ni loading, our next goal was to render this process catalytic and produce high yields of cyanated product under low Ni loadings. This was not an easy task considering the extreme inefficiency of the ring-opening cyanation process at the onset of our investigation.

Table 1: Experiments probing the catalytic reactivity of the CPK ring-opening cyanation reaction

Ni(COD)$_2$ (20 mol%)
dtbbpy (20 mol%)
TMSCl (1.2 eq.)
solvent, 110 °C, 6 h

1a
(1.0 eq.)

3a

Entry	Solvent	Additive	Yield (%)
1	MeCN	none	0
2	PhMe	MeCN (2.0 eq.)	0
3	PhMe	**2a** (2.0 eq.)	9
4	PhMe	**2b** (2.0 eq.)	3

2a

2b

Attempts to produce the cyanation product in acetonitrile solvent at 20 mol% Ni(0)

precatalyst loading did not produce a detectable amount of product **(Table 1, entry 1)**. Likewise, using 2.0 eq. acetonitrile and toluene as the bulk solvent at 20 mol% Ni loading also did not produce any detectable product **(Table 1, entry 2)**. An encouraging result was obtained when the nitrile identity was switched to the aromatic nitrile, 4-trifluoromethylbenzonitrile **(2a)**, which produced 9% yield of the desired open-chain nitrile **(3a)** with only a 2:1 nitrile:CPK stoichiometry **(Table 1, entry 3)**. Benzonitrile activation by Ni(0)-phosphine complexes has previously been studied in stoichiometric experiments and is known to be accelerated by the addition of Lewis acids[32,43–46]. When conditions identical to **Table 1, entry 3** were used without the Lewis acid (TMSCl), no product was detected. This demonstrates the necessity of the Lewis acid for activation of at least one of the coupling partners. Replacing the electron-poor 4-trifluoromethylbenzonitrile with the electron-rich 4-methoxybenzonitrile led to a significantly lower yield of 3% **(Table 1, entry 4)**. This lower reactivity is in line with the Hammett studies from Jones and coworkers, which revealed slower rates of oxidative addition for electron-rich benzonitriles than for electron-poor benzonitriles with a Ni(0)-phosphine complex[47]. This observation mirrors the slower oxidative addition kinetics of electron-rich aryl halides for both Ni(0)-phosphine[48,49] and Ni(I)-bipyridine complexes[50]. A slower rate of oxidative addition with the electron-rich 4-methoxybenzonitrile could explain the reduced yield of **3a**, possibly due to competitive processes that lead to catalyst deactivation.

A variety of Lewis acids were then screened to try to increase the yield of the nitrile product. Our intial goal was to achieve >1 catalyst turnover to verify that catalysis was feasible. Replacing TMSCl with the analogous but slightly bulkier triethylsilyl chloride (TESCl) led to a similarly low yield **(Table 2, entry 2)** and the slightly more electrophilic trimethylsilyl bromide (TMSBr) **(Table 2, entry 3)** also produced similarly low yields of the nitrile product. Using trimethylsilyl iodide (TMSI) as the Lewis acid did not lead to any formation of the desired product, but instead led to a 41% yield of the open-chain alkyl iodide **(Table 2, entry 4)**. Similarly, when $AlCl_3$ was employed, no nitrile product was formed and instead a 90% yield of the open-chain alkyl chloride was formed **(Table 2, entry 5)**. It was later determined that these ring-opening halogenation reactions also proceeded in the absence of Ni catalyst, and that similar ring-opening halogenation reactions had previously been reported in the literature[51,52]. $ZnCl_2$, a much weaker Lewis acid, was also ineffective for the cyanation reaction **(Table 2, entry 6)**. A very encouraging yield of 21% was obtained when 1.2 eq. of trimethylsilyl trifluoromethanesulfonate (TMSOTf) was chosen as the Lewis acid, providing the first result in which the turnover number was at least 1. Additionally, this reaction produced butyrophenone **(4)** as an undesired side product in low yield (3%) **(Table 2, entry 7)**. Decreasing the stoichiometry of TMSOTf to only 0.2 eq. led to only trace formation of the desired nitrile product **(Table 2, entry 8)**, and increasing the stoichiometry of TMSOTf to 2.0 eq. led to a complete loss of reactivity **(Table 2, entry 9)**.

Table 2: Lewis acid optimization

Entry	Lewis acid	Yield (%)
1	TMSCl	9
2	TESCl	6
3	TMSBr	7
4	TMSI	0[a]
5	AlCl$_3$	0[b]
6	ZnCl$_2$	0
7	TMSOTf (1.2 eq.)	21[c]
8	TMSOTf (0.2 eq.)	trace
9	TMSOTf (2.0 eq.)	0

a: 41%

b: 90%

c: **4**, 3%

At this point in our optimization campaign, it was apparent that achieving catalytic turnover of the Ni catalyst was a formidable barrier to improving the efficiency of the cyanation reaction. Although the mechanism of the reaction was largely unknown at this point, it was hypothesized that catalytic turnover was being prevented by the lack of a suitable sacrificial reductant. Our hypothesis was that two oxidative additions were occurring: one with the CPK and one with the benzonitrile. Additionally, we hypothesized that only one reductive elimination was needed to form the product. Because of this redox imbalance, Ni intermediates of higher oxidation states could not be reduced back down to their active low-valent

oxidation states without a source of additional electrons (a reductant). We envisioned that this reduction could be achieved through the use of a formate salt or silane as a hydride surrogate. A variety of formate salts were found to be incompatible with the reaction, shutting down product formation completely. Most of the silanes screened were incompatible with the reaction and either shut down reactivity or did not improve the yields. A major advancement was made when adding 1.0 eq. of diphenylsilane to the reaction, which increased the yield to 43% of **3a** (corresponding to >2 turnovers) with an additional 15% yield of the undesired butyrophenone side product **(Table 3, entry 3)**. The reaction was found to be sensitive to the stoichiometry of the added silane, and inferior yields of the desired product were obtained when 0.5 eq. **(Table 3, entry 2)** or 2.0 eq. **(Table 3, entry 4)** of diphenylsilane were used. The yield of the undesired butyrophenone product appeared to increase with additional added silane, suggesting that the undesired product was not necessarily the result of protodemetalation and could also be due to an unproductive reaction between an oxanickelacycle intermediate and diphenylsilane. Attempts to increase the yield with the milder Lewis acid TMSCl by combining it with 1 to 4 eq. of diphenylsilane were unsuccessful, demonstrating the need for the stronger Lewis acid (TMSOTf) in order to achieve multiple catalytic turnovers. Temperatures lower than 110 °C did not result in improved yields under any of the conditions tested. Furthermore, reaction times longer than 6 h usually resulted in reduced yields of **3a** and greater side product **(4)** formation. The

reaction performs equally well in both toluene and xylenes, but no product

formation or very low yields were obtained in all other solvents screened.

Table 3: Diphenylsilane stoichiometry optimization

Entry	X =	Yield (*3a*, %)	Yield (*4*, %)
1	0	21	3
2	0.5	23	14
3	1.0	43	15
4	2.0	21	17

The necessity of an electron-poor benzonitrile was once again tested under

the improved reaction conditions employing diphenylsilane **(Table 4)**. Replacing

the *para*-trifluoromethyl group of **2a** with a slightly less electron-poor *para*-methyl

ester **(2c)** led to a modest decrease in the yield of **3a (Table 4, entry 2)**, and when

the relatively electron-rich 4-fluorobenzonitrile **(2d)** was employed, the yield of the

desired product declined sharply **(Table 4, entry 3)**. Once again, this is consistent

with the hypothesis that electron-poor benzonitriles are more labile cyanide

sources and thus more effective for the reaction being studied. Isovaleronitrile **(2e)**,

the optimal cyanide surrogate from the Morandi group's olefin hydrocyanation

protocol[30], was not suitable for the ring-opening cyanation reaction, yielding no

desired nitrile product and only producing 8% yield of undesired butyrophenone

(Table 4, entry 4). This suggests that different mechanisms of nitrile activation and subsequent cyanide transfer are operative when comparing the Morandi olefin hydrocyanation reaction to the CPK ring-opening cyanation reaction being developed by our group. Notably, the Morandi group did not report screening any benzonitriles as cyanide surrogates for hydrocyanation.
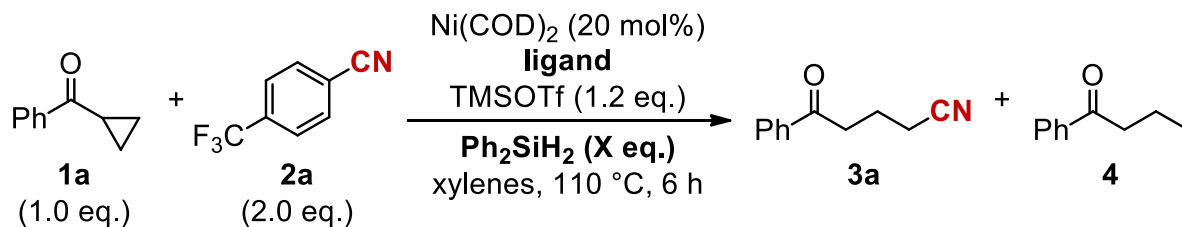
Table 4: Optimization of nitrile

Entry	R-CN	Yield (*3a*, %)	Yield (*4*, %)
1	**2a**	43	15
2	**2c**	33	17
3	**2d**	12	10
4	**2e**	0	8

2a: R' = CF$_3$
2c: R' = CO$_2$Me
2d: R' = F

2e

Next, a variety of ligands were screened at 20 mol% Ni(COD)$_2$ loading **(Table 5)**. Prior catalytic methods that involve oxidative addition of Ni(0) into benzonitriles usually require phosphine ligands[32], which are significantly more electron-donating than dtbbpy, the N,N bidentate ligand that we had been using up to this point. It was hypothesized that a more electron-donating ligand would help with the difficult C-C bond activation steps, possibly leading to improved catalytic efficiency. A variety of phosphine ligands of varying denticity and a P,N ligand were
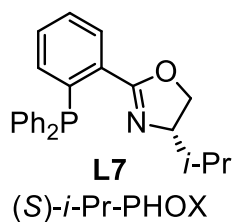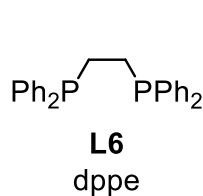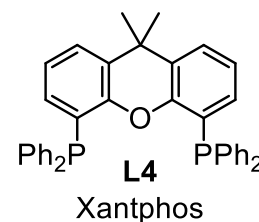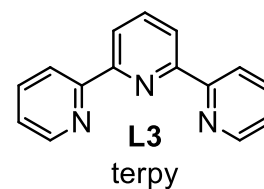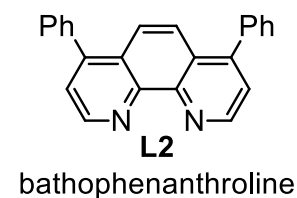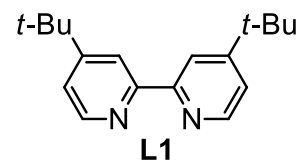
screened under the optimal reaction conditions, in addition to a selection of polypyridine ligands. When no additional ligand was added to Ni(COD)$_2$, very low yields of **3a** and **4** were obtained **(Table 5, entry 1)**. When dtbbpy **(L1)** was replaced with bathophenanthroline **(L2)**, a lower yield of **3a** was obtained with inferior product selectivity. Switching to the tridentate ligand terpy **(L3)** led to an even lower yield of **3a**, and significantly higher yields of **4** were obtained. Sterically bulky bisphosphines with large bite angles **(L4, L5)** produced very low yields of **3a** with a dramatic reversal in product selectivity towards **4**. It is possible that when these bulky bisphosphine ligands are used, the catalyst is too sterically encumbered to accommodate both coupling partners on one metal center. It is also possible that crucial bimolecular steps in the dominant catalytic mechanism (such as transmetalation) could have a high kinetic barrier due to the steric encumbrance of these ligands, with catalyst deactivation occurring instead of the productive bimolecular step(s). Dppe **(L6)**, a bidentate phosphine with a smaller bite angle and a less congested steric environment than **L4** and **L5**, produced markedly different results, forming **3a** in similar yield to **L1** but with nearly perfect product selectivity, as only trace **4** was detected. The P,N bidentate phosphinooxazoline ligand (*S*)-*i*-Pr-PHOX **(L7)** also formed **3a** with greater product selectivity than **L1** **(Table 5, entry 9)**, and when the stoichiometry of diphenylsilane was increased to 2.0 eq. **(Table 5, entry 10)**, both the yield of **3a** and the product ratio of **3a:4** were superior to that of the previously optimal ligand, dtbbpy **(L1)**. This contrasts the lower yield of **3a** and inferior product selectivity obtained when the stoichiometry

of diphenylsilane was increased from 1.0 to 2.0 eq. when using **L1 (Table 5, entries 2-3)**. A variety of monodentate phosphine ligands **(L8-L12, Table 5, entries 11-16)** produced inferior yields of **3a** when compared to **L1**, although many of these monodentate phosphines displayed good product selectivity. With these results in hand, (*S*)-*i*-Pr-PHOX **(L7)** was chosen as the ligand to continue the optimization campaign with since it gave the highest yield of **3a** and a low yield of the side product **4**. The excellent product selectivity obtained with dppe **(L6)** was also noted and we planned to screen both of these ligands again after further iterations of optimization.
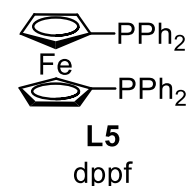
Table 5: Ligand optimization at 20 mol% Ni(0) loading

Ni(COD)$_2$ (20 mol%)
ligand
TMSOTf (1.2 eq.)
Ph$_2$SiH$_2$ (X eq.)
xylenes, 110 °C, 6 h

1a (1.0 eq.) + **2a** (2.0 eq.) → **3a** + **4**

Entry	Ligand	X =	Yield (*3a*, %)	Yield (*4*, %)
1	none	1.0	4	4
2	**L1** (20 mol%)	1.0	43	15
3	**L1** (20 mol%)	2.0	21	17
4	**L2** (20 mol%)	1.0	31	16
5	**L3** (20 mol%)	1.0	18	34
6	**L4** (20 mol%)	1.0	trace	26
7	**L5** (20 mol%)	1.0	2	30
8	**L6** (20 mol%)	2.0	40	trace
9	**L7** (20 mol%)	1.0	44	6
10	**L7** (20 mol%)	2.0	54	8
11	**L8** (40 mol%)	1.0	15	4
12	**L9** (40 mol%)	1.0	32	3
13	**L9** (40 mol%)	2.0	33	6
14	**L10** (40 mol%)	2.0	25	5
15	**L11** (40 mol%)	2.0	23	13
16	**L12** (40 mol%)	2.0	19	9

L1 dtbbpy

L2 bathophenanthroline

L3 terpy

L4 Xantphos

L6 dppe

L7 (*S*)-*i*-Pr-PHOX
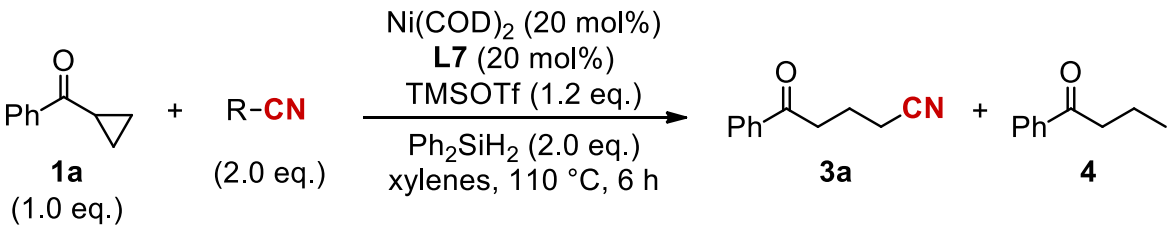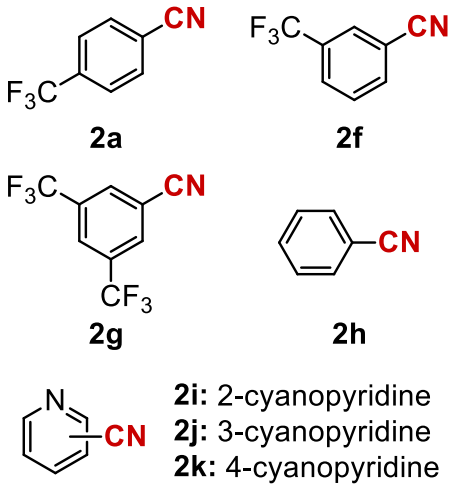
PR$_3$ **L8:** R = Cy
L9: R = Ph
L10: R = *p*-tol
L11: R = *p*-C$_6$H$_4$F
L12: PCyPh$_2$

L5 dppf

At this point in the optimization campaign, great strides had been made bringing a reaction with only 1% yield at 100 mol% Ni loading up to 54% yield at 20 mol% Ni loading, corresponding to a 270-fold increase in turnover number. Encouraged by this progress, we aimed to further increase catalytic efficiency for the desired nitrile product (**3a**), decrease butyrophenone **(4)** formation, and decrease the Ni loading. Based on the previous observation that the use of electron-poor benzonitriles led to greater yield and product selectivity, a selection of trifluoromethylated benzonitriles and cyanopyridines were screened in the ring-opening cyanation reaction of **1a (Table 6)**. 3-trifluoromethylbenzonitrile **(2f)** produced similar results to **2a** but with a slightly lower yield of **3a** and worse product selectivity of **3a:4 (Table 6, entry 2)**. Switching to an even more electron-poor benzonitrile, 3,5-bis(trifluoromethyl)benzonitrile **(2g)** gave the highest yield of **3a** obtained thus far at 62% with only 5% conversion to **4**. Unsubstituted benzonitrile **(2h)** was also screened to see if simpler cyanide surrogates could be used in the reaction, but the yield and product selectivity were very low, possibly due to benzonitrile being relatively electron-rich compared to the well-performing trifluoromethylated benzonitriles **(2a, 2f,** and **2g)**. It was hypothesized that the enhanced ability of cyanopyridines to coordinate to the Ni center could help promote oxidative addition and thus facilitate the cyanide transfer process. However, the use of cyanopyridines **2i**, **2j**, and **2k** gave very poor yields of **3a** **(Table 6, entries 5-7)**. Interestingly, formation of **4** could not be detected with these cyanopyridines.

Table 6: Optimization of nitrile with (S)-i-Pr-PHOX (L7)

Ph–C(=O)–cyclopropyl **1a** (1.0 eq.) + R–**CN** (2.0 eq.) → [Ni(COD)₂ (20 mol%), **L7** (20 mol%), TMSOTf (1.2 eq.), Ph₂SiH₂ (2.0 eq.), xylenes, 110 °C, 6 h] → Ph–C(=O)–CH₂CH₂CH₂–**CN** **3a** + Ph–C(=O)–CH₂CH₂CH₃ **4**

Entry	R-CN	Yield (3a, %)	Yield (4, %)
1	**2a**	54	8
2	**2f**	41	8
3	**2g**	62	5
4	**2h**	12	13
5	**2i**	3	0
6	**2j**	13	0
7	**2k**	7	0

2a (F₃C–C₆H₄–CN, para)   **2f** (F₃C–C₆H₄–CN, meta)

2g (3,5-bis-CF₃–C₆H₃–CN)   **2h** (C₆H₅–CN)

2i: 2-cyanopyridine
2j: 3-cyanopyridine
2k: 4-cyanopyridine

With the new optimal benzonitrile **2g** in hand, the CPK ring-opening cyanation reaction was screened at lower Ni(COD)₂ loadings **(Table 7)**. Decreasing the Ni loading to 10 mol% led to a modest increase in formation of **3a** **(Table 7, entry 2)**. Further decreasing the Ni loading to 5 mol% led to another increase in the yield of **3a**, now up to 75% with only 10% yield of **4 (Table 7, entry 3)**. 5 mol% Ni(0) precatalyst was determined to be the optimal precatalyst loading, since the yield of **3a** began to decrease again at 2.5 mol% Ni(0). The yield of **3a** could be pushed even higher to 81% by decreasing the loading of **2g** from 2.0 eq. to 1.5 eq. **(Table 8, entry 2)**. The reaction was found to be very sensitive to the

stoichiometry of **2g**, since only a 54% yield of **3a** was obtained when using 1.0 eq. of **2g (Table 8, entry 3)**.

Table 7: Optimization of Ni loading

Entry	X =	Yield (*3a*, %)	Yield (*4*, %)
1	20	62	5
2	10	68	10
3	5	75	10
4	2.5	65	11

Good yields were now being achieved with the carefully determined optimal set of conditions. In order to determine if (*S*)-*i*-Pr-PHOX **(L7)** was still the optimal ligand under the newly identified conditions, a selection of the previously best-performing ligands were compared, along with a few additional ligands from diverse ligand classes **(Table 9)**. At this point, Nathan Coddington joined this project and conducted the experiments shown in **Table 9, entries 3-7**. Under this new set of conditions, the yield of **3a** obtained with **L7** was no longer

Table 8: Optimization of benzonitrile (2g) stoichiometry

Entry	X =	Yield (**3a**, %)	Yield (**4**, %)
1	2.0	75	10
2	1.5	81	7
3	1.0	54	9

significantly higher than that of dppe **(L6)**. Additionally, formation of side product **4** was not detected with **L6**. Because of the excellent result obtained with **L6**, it was of interest to see what result would be obtained if the central ethane linker of **L6** was lengthened by one methylene unit. When dppp **(L13)** was employed under the reaction conditions, much lower yields of **3a** (46%) were obtained than with **L6**, and **4** was formed in 29% yield. This contrasts the exclusive formation of **3a** under the same set of conditions with **L6** despite the minor difference in structure between these two ligands. Dtbbpy **(L1)** still performed worse than **L6** and **L7** under the current reaction conditions, although product selectivity for **3a** was now better than the previous conditions that used a higher Ni loading and a suboptimal benzonitrile. A bisoxazoline (BOX) ligand was also screened under the reaction conditions **(L14, Table 9, entry 5)** and displayed excellent product selectivity despite a poor yield of **3a**. The Buchwald ligand *t*-Bu-XPHOS **(L15, Table 9, entry 6)** also provided excellent product selectivity despite a very low yield of **3a**. When

(*R*)-BINAP **(L16, Table 9, entry 7)** was used in the cyanation reaction, **3a** was not detected and **4** was formed in low yield, mirroring the unsuccessful results previously obtained with especially bulky bidentate phosphines **(Table 5, entries 6-7)**.

Table 9: Ligand reoptimization at 5 mol% Ni(0) loading

Entry	Ligand	Yield (**3a**, %)	Yield (**4**, %)
1	**L7**	81	7
2	**L6**	79	0
3	**L13**	46	29
4	**L1**	48	5
5	**L14**	29	trace
6	**L15**	24	trace
7	**L16**	0	9

L7
(*S*)-*i*-Pr-PHOX

L6
dppe

L13
dppp

L1
dtbbpy

L14
(*S*,*R*)-IndaBOX

L15
t-BuXPhos

L16
(*R*)-BINAP

4.3 Initial probing of the CPK substrate scope

After the extensive optimization campaign described in Chapter 4.2, we were pleased to have achieved yields for the Ni-catalyzed ring-opening cyanation reaction in excess of 80% (corresponding to turnover numbers of >16) when **1a** was used as the CPK substrate. In order to avoid overoptimizing for **1a**, we aimed to test our optimized reaction conditions against more challenging CPK substrates bearing 1,2-disubstitution patterns on the cyclopropane ring. These disubstituted cyclopropane substrates could be accessed in 2-3 synthetic steps (substrate synthesis is described in detail in Chapter 4.7). Two constitutional isomers of the cyanated product can form from the disubstituted cyclopropane substrates due to the fact that Ni can oxidatively insert into either one of two cleavable $C(sp^3)$-$C(sp^3)$ bonds (shown as the σ-bonds between the orange and green atoms and between the orange and pink atoms in substrates **1b-1d**, **Table 10**). Due to the modular nature of the phosphinooxazoline (PHOX) ligand scaffold, a sufficiently challenging CPK substrate could be screened against a variety of in-house designed PHOX ligands.

Dppe **(L6)** and (*S*)-*i*-Pr-PHOX **(L7)**, the two best-performing ligands identified in Chapter 4.2, were screened against the more challenging substrates **1b-1e (Table 10)**. The experiments described in **Table 10, entries 5-7** and the synthesis of substrate **1d** were conducted by Nathan Coddington. Two constitutional isomers of the cyanated product can form from the disubstituted cyclopropane substrates due to the fact that Ni can oxidatively insert itself into

200

either one of two cleavable $C(sp^3)$-$C(sp^3)$ bonds (shown as the σ-bonds between the orange and green atoms and between the orange and pink atoms in substrates **1b-1d**, **Table 10**). These consitituonal isomers are denoted as the branched **(3b-b, 3c-b, 3d-b)** and linear **(3b-l, 3c-l, 3d-l)** products. The branched product results from cleavage of the less sterically hindered $C(sp^3)$-$C(sp^3)$ bond in a 1,2-disubstituted cyclopropane substrate.

Table 10: Probing the reactivity of more challenging CPK substrates

Entry	CPK (**1**)	ligand	Yield (**3c**, %)	r.r. (b:l)
1	**1b**	**L6**	76	55:45
2	**1b**	**L7**	49	59:41
3	**1c**	**L6**	83	57:43
4	**1c**	**L7**	45	70:30
5	**1d**	**L6**	16	>95:5
6	**1d**	**L7**	16	>95:5
7	**1e**	**L6**	3	-

As expected, higher *b:l* regioselectivities are obtained with **1c** than with **1b** for both ligands because the ethyl group of **1c** is slightly larger than the methyl group of **1b**, creating a greater difference in the steric environment around each of

the two cleavable σ-bonds in these CPK substrates. Although **L6** and **L7** provided similar results when cyclopropyl phenyl ketone **(1a)** was employed as the substrate, differences in the performance between these two ligands became more apparent with the more challenging disubstituted cyclopropanes **1b** and **1c (Table 10, entries 1-4)**. For both **1b** and **1c**, **L6** led to much higher yields of **3b** and **3c** than were obtained using **L7**, although **L7** displayed greater regioselectivity for the branched products (**3b-b** and **3c-b**).

CPK **1d** was also screened against both **L6** and **L7 (Table 10, entries 5-6)**. Yields of **3d** were much lower than those of **3b** and **3c**, possibly due to the steric encumbrance of the phenyl group. Interestingly, the regioselectivity of both ligands studied when reacted with **3d** was biased towards the branched constitutional isomer as opposed to the linear constitutional isomer. This has mechanistic implications, since a linear product would be favored if alkyl radical intermediates were being formed due to the relative stability of benzylic radicals to secondary alkyl radicals[53]. Additionally, higher yields were obtained with substrates lacking radical-stabilizing functional groups. These data are again not consistent with the formation of alkyl radical intermediates in the dominant catalytic mechanism.

We were also interested in the potential for enantioselectivity in the ring-opening cyanation reaction with these chiral cyclopropane substrates since **L7** contains chiral information. Integration of UPC^2 traces acquired from products **3c** and **3d** (**Table 10, entry 4** and **Table 10, entry 6**) showed that the reaction was

racemic with respect to both constitutional isomers of **3c** and for **3d-b**, which was the only detected constitutional isomer of **3d**.

The necessity of the aryl ketone group in the substrate was probed by reacting methyl cyclopropyl ketone **(1e)** under the optimal conditions with **L6 (Table 10, entry 7)**. The reaction was incredibly inefficient with only 3% yield obtained for **3e**, and the lack of effective stains for visualization on TLC combined with the relative volatility of this product made isolation much more difficult than for the phenyl ketone products. The low yields obtained for **3e** were not unexpected, since Ogoshi and coworkers demonstrated in stoichiometric studies that Ni(0)-NHC complexes undergo oxidative addition with cyclopropyl phenyl ketone much more rapidly than with cyclopropyl methyl ketone or cyclopropanecarbaldehyde[33]. Additionally, previously reported catalytic ring-opening reactions involving Ni and alkyl CPKs were limited to strained bycyclic aliphatic ketones[22]. The low yield obtained with substrate **1e** could also be due to side reactions involving the readily enolizable methyl ketone, which could be converted to an undesired silyl enol ether by TMSOTf.

Based on this initial probing of the scope of substrates amenable to the Ni-catalyzed ring-opening cyanation reaction, it was determined that sterically bulky aryl CPKs are amenable to the reaction, and that alkyl CPKs show some reactivity but pose a greater challenge. We planned to revisit the substrate scope later after optimizing the PHOX ligand scaffold to convert **1c** to **3c** with superior yield and regioselectivity.

4.4 PHOX ligand optimization with the more challenging disubstituted cyclopropane substrate 1c
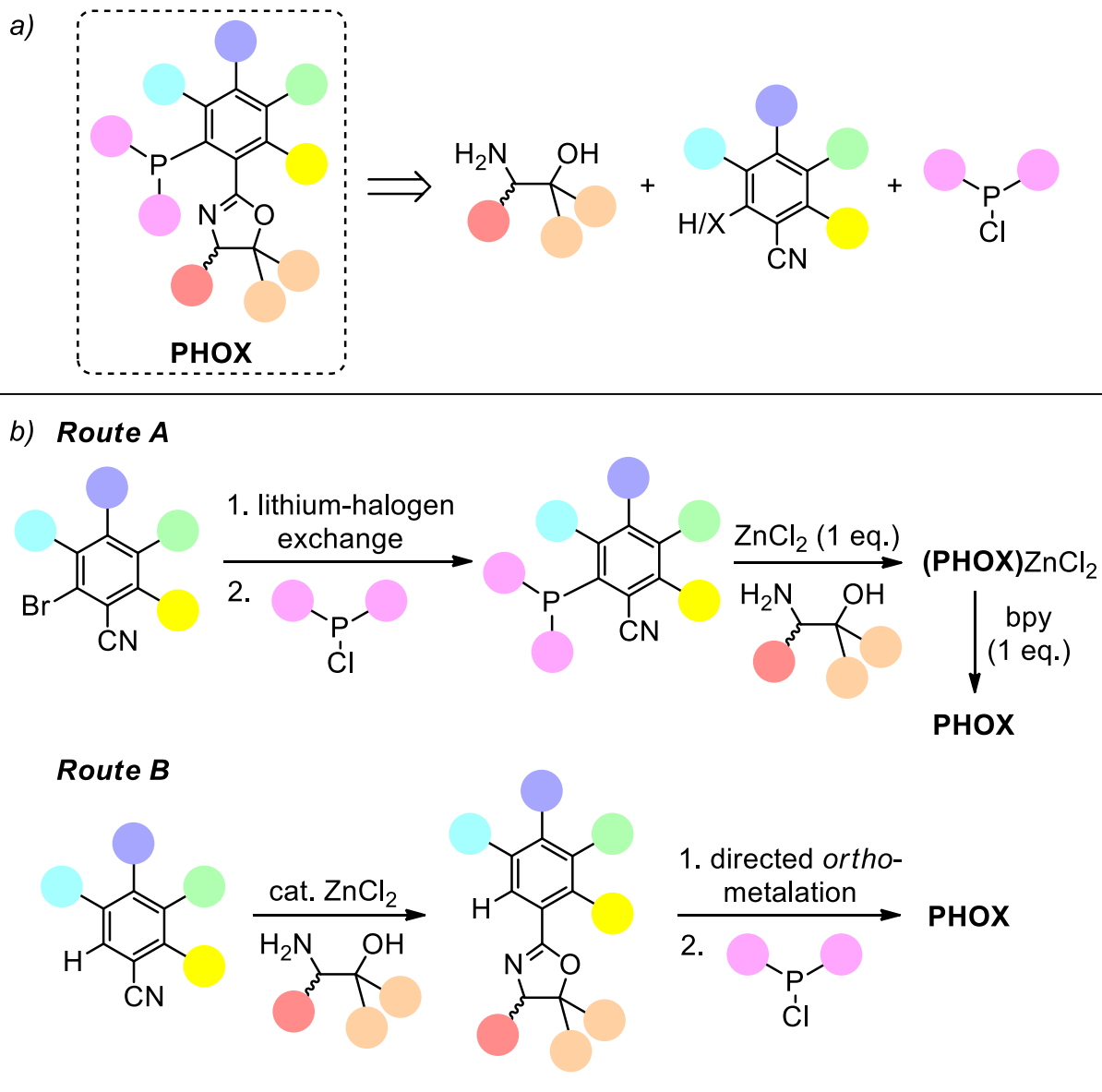
It was now apparent that there was still much room for improvement with respect to the yield and regioselectivity of the Ni-catalyzed, Lewis acid-assisted CPK ring-opening cyanation reaction. We elected to continue ligand optimization with the PHOX ligand scaffold using the substrate **1c** which bears an ethyl substituent since it provided a regioselectivity that was more tractable for optimization than **1b** (which displayed lower branched:linear selectivity with both **L6** and **L7** due to the small size of its methyl group) and **1d** (which was a more sterically biased substrate and thus already highly regioselective).

PHOX ligands are highly versatile P,N bidentate ligands that have been used in a variety of Ni-catalyzed methodologies[54]. Their modular structure allows for the synthesis of a diverse library of ligands from simple starting materials, providing access to diverse substitution patterns at many different positions on the oxazoline ring, the linking benzene ring, and the diaryl phosphine fragment **(Figure 4a)**. Both synthetic routes used to synthesize PHOX ligands involve the coupling of three precursors: a benzonitrile, an aminoalcohol, and a chlorodiarylphosphine. Benzonitriles are cheap and abundant with diverse substitution patterns commercially available. Aminoalcohols are also abundant with many derived from the amino acid chiral pool, providing diverse substitution patterns and steric environments to the PHOX ligands that are made from them. Aminoalcohols bearing geminal disubstitution patterns can also be synthesized from amino esters

via Grignard addition to the carbonyl. Of the three coupling partners, the chlorodiarylphosphine is the most difficult to modify since few are commercially available, although chlorodiarylphosphines with various *ortho*-, *meta*-, and *para*-substitution patterns can be synthesized by treating secondary phosphine oxides with acetyl chloride[55] or by Grignard addition to $P(NEt_2)Cl_2$ followed by treatment with HCl[56]. Alternatively, PHOX ligands can be synthesized by a Cu-catalyzed cross-coupling protocol developed by the Stoltz group involving secondary phosphines and aryl bromides[57].

The PHOX ligands synthesized in-house were accessed via one of two synthetic routes in 2-4 steps. Route A **(Figure 4b)** starts with 2-bromobenzonitrile or a derivative thereof, which undergoes lithium-halogen exchange and is reacted with a chlorodiarylphosphine to form a triarylphosphine with a nitrile at the *ortho*-position of one of the arenes. This *ortho*-(diarylphosphino)benzonitrile is then condensed with an aminoalcohol in a $ZnCl_2$-catalyzed reaction to form a Zn(II)-PHOX complex. The PHOX ligand is finally liberated with just 0.99 eq. of bipyridine, which outcompetes the PHOX ligand for binding to Zn. Route B starts with a benzonitrile containing an *ortho*-hydrogen that is accessible for directed *ortho*-metalation in the second step. This benzonitrile is coupled with an aminoalcohol to

Figure 4: Modular PHOX ligand synthesis

a)

PHOX

b) **Route A**

1. lithium-halogen exchange

2.

ZnCl$_2$ (1 eq.)

(PHOX) ZnCl$_2$

bpy (1 eq.)

PHOX

Route B

cat. ZnCl$_2$

1. directed *ortho*-metalation

2.

PHOX

form the oxazoline ring via a ZnCl$_2$-catalyzed condensation reaction. The resulting oxazoline intermediate then undergoes directed *ortho*-metalation and the in situ-generated organolithium intermediate is treated with a chlorodiarylphosphine electrophile to afford the free PHOX ligand[58] **(Figure 4b)**. In some instances, the PHOX ligand was inadvertently oxidized to the corresponding phosphinoxide

during the final step, although these oxides could be reduced to the desired PHOX ligand by heating the PHOX ligand to 140 °C in the presence of excess diphenylsilane. The synthesis of PHOX ligands will be discussed in greater detail in Chapter 4.7.

A variety of PHOX ligands were synthesized or purchased and screened in the reaction between **1c** and **2g** under the optimal conditions **(Table 11)**. Starting with the previously optimal (*S*)-*i*-Pr-PHOX **(L7)** scaffold, substitution of the H atom *para*- to the oxazoline with an F atom **(L17)** produced identical regioselectivity but led to a dramatic increase in the yield of **3c** from 45% to 70% **(Table 11, entry 2)**. Replacing the -F group with -CF$_3$ **(L18)** produced a similar yield and r.r. When the same position had an -OMe group installed, the r.r. remained similar although yields plummeted to just 9% **(L19)**. **L20** bears a different substitution pattern, with a -Cl group *ortho*- to the oxazoline. This substitution pattern provided a slightly worse r.r. than obtained with the previously discussed *para*-substituted (*S*)-*i*-Pr-PHOX derivatives, but provided slightly higher yields than **L7 (Table 11, entry 5)**. Replacing the *i*-Pr group of **L7** with a *t*-Bu group **(L21)** led to a similar r.r. but a significantly improved yield **(Table 11, entry 6)**. Installation of three CF$_3$ groups *para*- to the P atom **(L22)** led to much lower yields and also a significantly worse regioselectivity. PHOX ligands bearing other alkyl groups on the oxazoline ring such as *i*-Bu **(L23)** or Bn **(L24)** produced much higher yields of **3c** than **L7**, although the regioselectivity of these ligands were not significantly different. When a -Ph group was present at this position **(L25)**, yields were slightly lower than with

L23 and **L24**, but the r.r. was significantly lower. When (*S,R*)-IndaPhox **(L26)** was

used, the highest yields of **3c** obtained thus far with a PHOX ligand were achieved

Table 11: PHOX ligand screening with substrate 1c

Entry	Ligand	Yield (*3c*, %)	r.r. (b:l)
1	**L7**	45	70:30
2	**L17**	70	70:30
3	**L18**	66	71:29
4	**L19**	9	72:28
5	**L20**	54	65:35
6	**L21**	78	70:30
7	**L22**	28	63:37
8	**L23**	73	69:31
9	**L24**	68	68:32
10	**L25**	62	61:39
11	**L26**	81	70:30
12	**L27**	56	72:28
13	**L28**	29	61:39

L7: R^1 = H; R^2 = H
L17: R^1 = F; R^2 = H
L18: R^1 = CF_3; R^2 = H
L19: R^1 = OMe; R^2 = H
L20: R^1 = H; R^2 = Cl

L21: Ar = Ph; R = H
L22: Ar = p-$C_6H_4CF_3$; R = CF_3

L23: R = *i*-Bu
L24: R = Bn
L25: R = Ph

L26: R = H
L27: R = F

(Table 11, entry 11). Although this yield was still similar to that achieved with the

simple and commercially cheap dppe ligand **(L6)**, the yield of **3c-b** was significantly

higher due to the improved (though still unsatisfactory) regioselectivity provided by

the PHOX scaffold. It was hypothesized that the installment of an F atom at the same position as in **L17** but on the IndaPHOX scaffold would lead to even further improved yields, as was the case when comparing **L7** with **L17**. Surprisingly, the fluorinated **L27** produced a much lower yield of **3a** than **L26**, although the regioselectivity did not change **(Table 11, entry 12)**. To probe whether a PHOX ligand bearing a sterically bulky disubstituted oxazoline would affect the regioselectivity, **L28** was also screened under the same conditions **(Table 11, entry 13)**. This ligand, bearing structural similarity to (*S*)-Ph-PHOX **(L25)** but with an extra -Ph group on the oxazoline ring, produced a similar r.r. to **L25**, but with a much lower yield.

Based on the data obtained thus far, contradictory trends emerge, although some key takeaways can be made. Varying the functional group present at the position *para*- to the oxazoline can have a great effect on the yield, but does not affect the regioselectivity. Installment of a fluorinated group *para*- to the oxazoline can have either a beneficial **(L17, L18)** or detrimental **(L27)** effect. In the single instance thus far where an electron-rich functional group was installed at this position **(L19)**, the yield suffers greatly. The major challenge of this rational ligand optimization campaign is that we have not yet identified a substitution pattern that produces a regioselectivity that is significantly different to that of our initial PHOX ligand **L7**. All PHOX ligands screened thus far produce regioselectivities within the narrow range of 6:4 and 7:3. Attempts to disturb the steric environment of the PHOX ligand in order to influence the regioselectivity of the reaction, either by the

installment of phenyl groups on the oxazoline ring (**L25** and **L28**), by *ortho*-substitution on the central aromatic ring **(L20)**, or by modifying the -PAr$_2$ group **(L22)** have only small negative effects in the observed regioselectivity.

Due to the modular nature of the PHOX ligand enabling access to diverse substitution patterns, there is still a large chemical space that we have not yet explored. We plan to synthesize PHOX ligands bearing diverse aryl and alkyl groups bonded to the central P atom, since we only have 1 entry so far **(L22)** that does not bear the -PPh$_2$ moiety. This will be a challenge since this fragment of the PHOX molecule is the most difficult to vary due to the limited commercial availability of chlorodiarylphosphines, chlorodialkylphosphines, and their precursors. Bulky aryl groups, such as *ortho*-tolyl, could produce a significantly different steric environment than the generic phenyl groups. PHOX ligands bearing diverse substitution patterns *ortho*- to the oxazoline ring will also be screened, since only 1 ligand bearing this substitution pattern **(L20)** has been made thus far. A functional group bulkier than a -Cl atom could impose a significant influence on the Ni-ligand complex conformation, although these are synthetically challenging to access due to side reactions during the lithiation step and difficulties in coupling bulky phosphine and oxazoline fragments. We also plan to synthesize PHOX ligands bearing geminal-dialkyl substitution patterns adjacent to the oxygen of the oxazoline ring. The necessary aminoalcohols to synthesize such ligands can easily be accessed via Grignard addition to aminoesters. PHOX ligand synthesis and optimization is ongoing.

4.5 Mechanistic hypothesis, supporting experiments, and future work

We have only just started to unravel the mechanism of this newly developed CPK ring-opening cyanation reaction. As discussed previously, there is substantial stoichiometric and catalytic evidence in the literature for Ni(0) undergoing oxidative addition into benzonitrile and CPKs. Therefore, a reasonable catalytic mechanism should invoke the intermediacy of Ni(II) aryl cyanide and Ni(II) oxanickelacycle species (generated from the oxidative ring-opening of the CPK).

Scheme 5: Control experiments and ^{19}F NMR reveal byproduct of ArCN activation
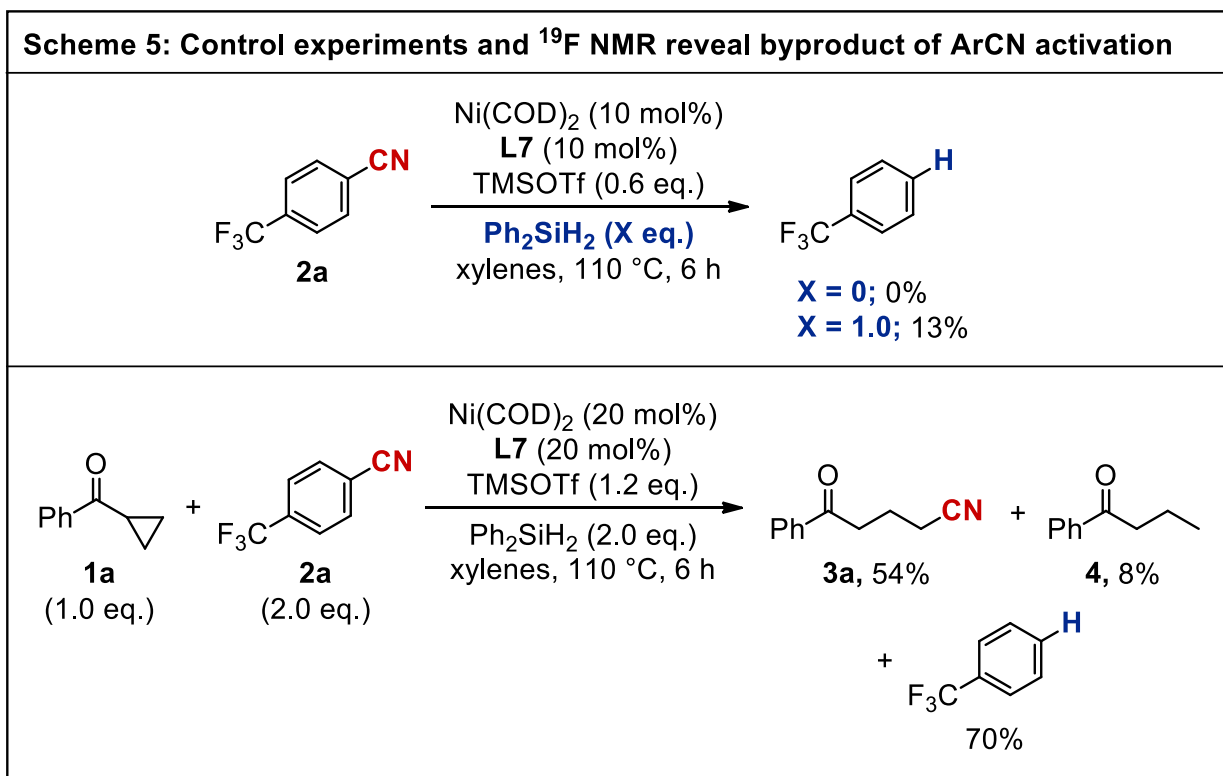
It is interesting that we have only ever observed cyanide transfer rather than aryl group transfer to the CPK substrate. This implies that the X-type aryl ligand resulting from oxidative addition into the benzonitrile must be removed from the Ni

211

catalyst in a way that does not incorporate it into the nitrile product in order to enable catalyst turnover. Since we had previously only achieved catalytic yields (>1 turnover) when silane additives were present in the reaction, it was of interest to identify the side product of ArCN activation in the absence of cyclopropyl phenyl ketone **(1a)**, both with and without added silane **(Scheme 5a)**. When 1.0 eq. of diphenylsilane is used, ^{19}F NMR spectroscopy reveals that 13% of **2a** is converted to PhCF$_3$. The absence of the formation of PhCF$_3$ in the absence of diphenylsilane is evidence for the replacement of the cyanide group of the benzonitrile with a hydride. We plan to further confirm this hypothesis using deuterated diphenylsilane. The catalytic CPK ring-opening cyanation reaction was also monitored by ^{19}F NMR **(Scheme 5b)**, demonstrating a much higher yield of PhCF$_3$ (70% with respect to the limiting reagent). Since the yield of **3a** in this reaction is 54%, the yield of PhCF$_3$ should be at least as high since at least 1 mmol of benzonitrile must be consumed per 1 mmol of **3a** generated. The observation of a significantly higher yield of PhCF$_3$ than **3a** indicates some degree of inefficiency between the benzonitrile activation and cyanide transfer steps.

Based on precedent from Weix and coworkers in which arylated or alkylated silyl enol ethers were formed from CPKs under similar Ni/LA conditions[22], we suspected that the cyanation reaction that we developed was actually forming silyl enol ethers that were being hydrolyzed before isolation of the product. This hydrolysis could happen in situ by trace HOTf (from the reaction of TMSOTf with trace moisture) or it could happen upon aqueous workup. Although we could not

observe the silyl enol ether in crude aliquots of the catalytic reaction taken in CDCl$_3$, we did observe partial incorporation of deuterium at the α-position of the ketone of **3a**, which is evidence for the intermediacy of a basic silyl enol ether or nickel enolate species.


Scheme 6: Preliminary result of a CPK ring-opening α,γ-difunctionalization reaction

---
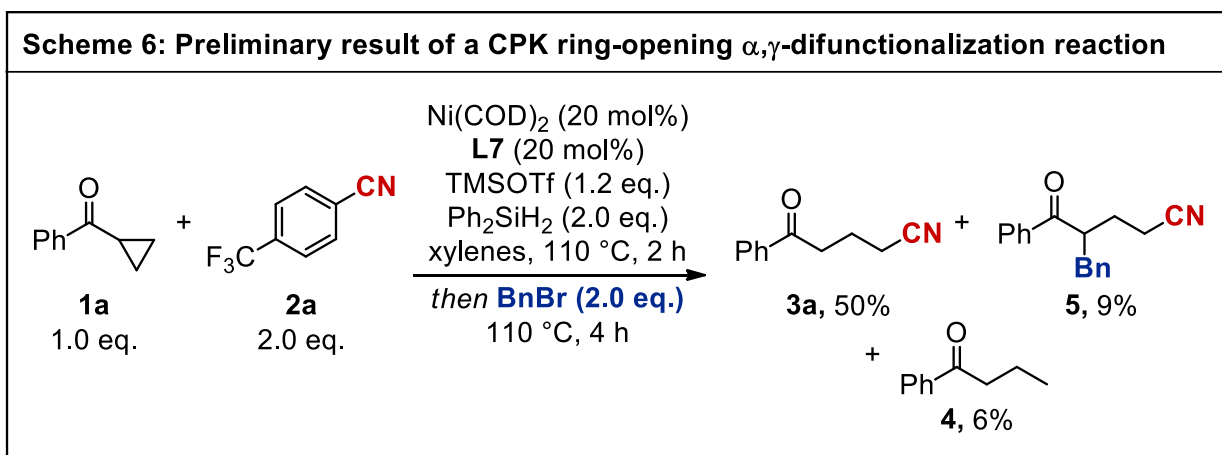
It was envisioned that a one-pot α,γ-difunctionalization reaction could be realized by the addition of a suitable electrophile to the in situ-generated silyl enol ether. To probe the feasibility of this, an experiment was conducted in which 2.0 eq. of benzyl bromide were added 2 hours after the catalytic ring-opening cyanation reaction of **1a** had begun **(Scheme 6)**. We were pleased to observe a low yield of the desired cyanoalkylation product **5**, in addition to a larger yield of the monofunctionalized nitrile product **3a**. When 2.0 eq. of benzyl bromide were added with the rest of the reagents at the beginning of the reaction, neither **3a** nor **5** were observed, but rather an open-chain alkyl bromide was formed in which a bromine atom is installed instead of a cyano group at the γ-position, with bibenzyl

formed as a byproduct. Efforts to enable the one-pot difunctionalization reaction to proceed with higher yields are ongoing.

Based on the insights obtained from these experiments along with the literature precedents supporting the viability of the proposed intermediates, we propose the catalytic cycle depicted in **Figure 5** as an initial mechanistic hypothesis. Starting from the Ni(0)-PHOX adduct **Ni-1**, Lewis acid-assisted oxidative addition with CPK **1** forms oxanickelacycle **Ni-2**. Since Ni(IV) is a highly unstable oxidation state and because of the already crowded steric environment of **Ni-2**, we propose a concurrent Lewis acid-assisted oxidative addition involving a second **Ni-1** complex, which activates benzonitrile **2** to form **Ni-3**. Mechanistic studies regarding the nature of the cyanide transfer event are ongoing, and gaps in our knowledge regarding this are reflected in the catalytic cycle, indicated by the dotted blue arrows. One possible explanation for the cyanide transfer step to form **Ni-4** is a direct transmetalation of the cyanide ligand from **Ni-3** to **Ni-2**. If there is not a direct transmetalation between these two species, the transfer of the cyanide ligand could be achieved through in situ formation of TMSCN or HCN. The Ni species resulting after the transfer of cyanide to form **Ni-4** is currently unknown, as well as the nature by which a benzene derivative, the byproduct of benzonitrile activation, is formed.

Figure 5: Initial mechanistic hypothesis for the Ni/LA-catalyzed CPK ring-opening cyanation reaction using benzonitrile as cyanide surrogate
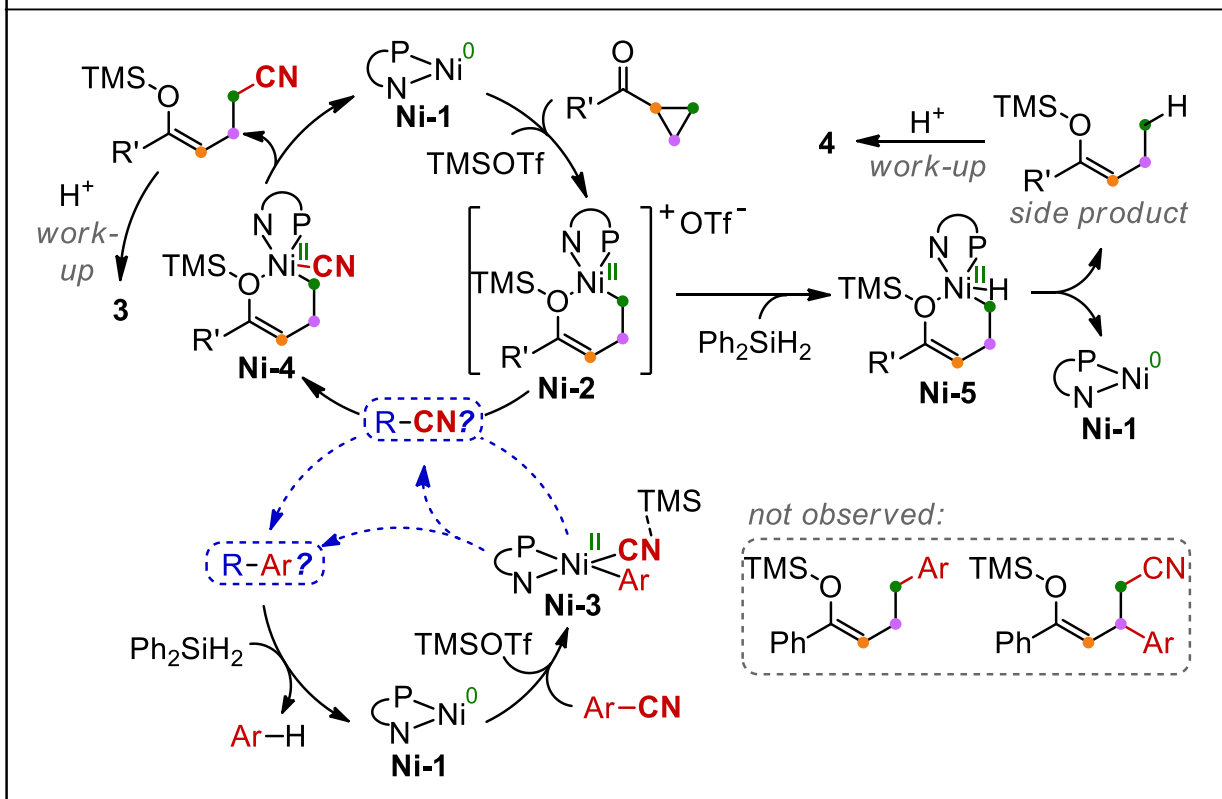
However, the mechanistic experiments discussed previously demonstrate that a competent silane as a hydride source is needed to form the benzene derivative byproduct. Additionally, catalytic control experiments demonstrated the necessity of diphenylsilane for catalyst turnover, as discussed in Chapter 4.2. Once **Ni-4** is formed, reductive elimination yields cyanated product **3** and also regenerates **Ni-1**. The formation of undesired side product **4** can be explained by the hydride transfer reaction of **Ni-2** with diphenylsilane occurring instead of cyanide transfer from **Ni-3**. This leads to complex **Ni-5**, which forms **4** after reductive elimination, regenerating **Ni-1**.

Experiments probing the mechanism of this cyanation reaction are ongoing, and we aim to fill in the gaps in our knowledge regarding this mechanistic puzzle. Perhaps the most enigmatic aspect of this mechanism is the nature of the cyanide transfer event. As discussed previously, the mechanism of cyanide transfer could involve either direct transmetalation between Ni species or the generation of some other CN-containing intermediate responsible for shuttling -CN ligands between metal centers. We plan to screen the catalytic reaction with TMSCN as the cyanide source instead of a benzonitrile derivative to probe whether TMSCN is a competent cyanide source for this chemistry. Such an experiment could only provide evidence against in situ formation of TMSCN and subsequent cyanide transfer; it could not provide evidence for it, since TMSCN could just be a competent alternative cyanide source (though far more toxic than benzonitriles). Stoichiometric experiments will be conducted to probe the feasibility of direct transmetalation of the cyanide ligand between the Ni(II) oxanickelacycle **(Ni-2)** and the Ni(II) aryl cyanide complex **(Ni-3)** by mixing these complexes together under a variety of reaction conditions (various stoichiometries of each complex, Lewis acid, and silane in addition to various temperatures and concentrations). Similar Ni(II) oxanickelacycles[21,33] and Ni(II) aryl cyanide complexes[43,44,47] have previously been synthesized, although most examples of isolable complexes bear a highly electron-rich trialkylphosphine or NHC ligand. Synthesis of these oxidative addition adducts could also inform whether elevated temperatures (needed for the catalytic ring-opening cyanation reaction) are required for either of the two oxidative additions, or if the high

temperature is instead only needed to promote reductive elimination. Ideally, we would be able to synthesize the PHOX or dppe analogs of these complexes, since we know these ligands are effective for the CPK ring-opening cyanation reaction. The generation of kinetic profiles for the catalytic reaction could also provide clues regarding the nature of the cyanide transfer step. If transmetalation of the cyanide ligand is the turnover-limiting step, the rate law would be expected to be second-order with respect to the initial Ni(0) loading. If the turnover-limiting step is unimolecular and involves a Ni complex intermediate (such as in reductive elimination), we should see first-order kinetics with respect to Ni(0) loading. The observation that choosing bulky bisphosphines (**L4**, **L5**, and **L16**) results in significant formation of **4** with negligible formation of **3a** provides support for the transmetalation hypothesis, since these bulky ligands might hinder the transmetalation of the -CN ligand, resulting in the decomposition of nickelacycle **Ni-2** by the pathway leading to the undesired product **4**.

As discussed in Chapter 4.4, it has proven very difficult to achieve high levels of regioselectivity for **3c** by modifying the structure of the PHOX ligands used, despite the successes attained in achieving higher yields from our PHOX ligand screening campaign. The nature of the regioselectivity-determining step is currently not understood, although it is most likely the oxidative addition with the CPK, since this will determine where the crucial $C(sp^3)$-$C(sp^3)$ bond disconnection occurs. It is unusual that the regioselectivities obtained with PHOX ligands of diverse steric and electronic parameters all fall within the narrow r.r. range of

approximately 6:4 to 7:3. In addition to the future plans to probe a broader chemical space of PHOX ligand steric environments, we are also interested in whether we can influence the regioselectivity by decreasing the temperature of the reaction or by employing a bulkier Lewis acid. When the optimal reaction conditions employing (S)-*i*-Pr-PHOX **(L7)** and cyclopropyl phenyl ketone **(1a)** were combined with triethylsilyl trifluoromethanesulfonate (TESOTf) as the Lewis acid instead of TMSOTf, a 63% yield of **3a** was obtained (accompanied by a 4% yield of **4**), which was lower than the 81% yield obtained with the slightly smaller Lewis acid TMSOTf, but still proves the feasibility of using larger Lewis acids for this cyanation chemistry. Adding steric bulk to the LA-ketone adduct could help differentiate the steric environments around the two $C(sp^3)$-$C(sp^3)$ bonds that Ni can oxidatively add into. Kinetic trials will reveal whether the r.r. changes over time.
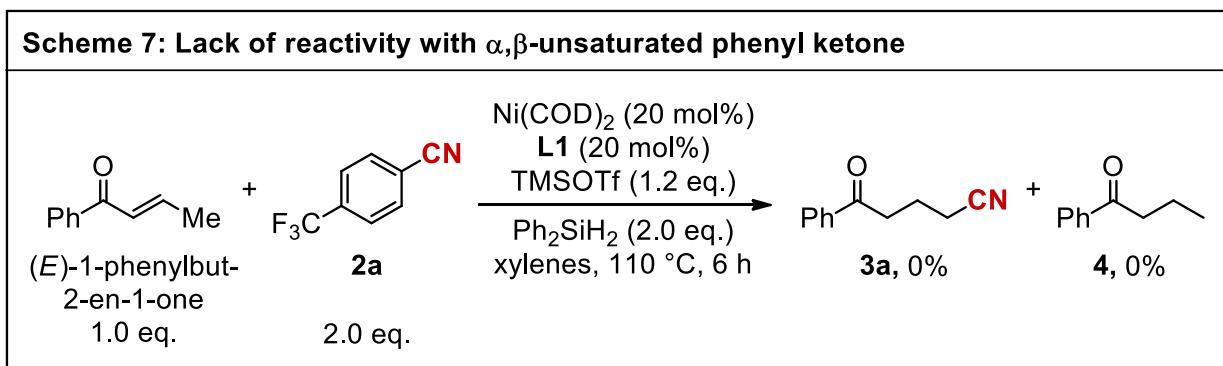
We also plan to probe the role of diphenylsilane in the cyanation reaction. Kinetics trials will be important for determining the rate dependence on initial silane loading, as well as any potential effects on product selectivity or regioselectivity. We know that the silane is necessary for catalytic turnover and that its presence leads to the formation of a benzene byproduct from the starting benzonitrile. The mechanism by which diphenylsilane converts ArCN to ArH is not currently understood, although stoichiometric studies should help to reveal it. Additionally, the formation of side product **4** from **1a** can be probed by stoichiometric experimentation by treating an analog of **Ni-2** with diphenylsilane under various conditions. Deuterated diphenylsilane will also be purchased, and would be very

helpful for determining if any H atoms in the nitrile product or benzene byproduct come from hydrides delivered by the silane rather than from protons delivered by acidic workup.

Kinetic studies are also expected to be helpful to determine the role of the Lewis acid in the dominant catalytic mechanism. As discussed previously, Lewis acids are known to promote oxidative additions of low-valent Ni into the C-C bonds of both CPKs and nitriles. However, many catalytic reactions involving such C-C bond activations proceed in the absence of Lewis acids[24–26,32]. Typically, CPK activation by Ni without Lewis acids can occur at lower temperatures and with weaker ligands than benzonitrile activation by Ni without Lewis acids, although this is not always the case. Alternatively, potential mechanistic steps such as reductive elimination, transmetalation, or in situ generation of TMSCN could be promoted by the Lewis acid. Because of this, it is not clear which mechanistic step(s) require substrate coordination to the Lewis acid. It is possible that many steps are concurrently being promoted by the Lewis acid. This hypothesis will be challenged by stoichiometric studies.

This reaction is unusual in that Ni engages two different C-C bond electrophiles in oxidative addition. One plausible hypothesis to explain why this is able to occur is that the rates of the two oxidative additions are on a similar order of magnitude. If one oxidative addition occurs much more rapidly than the other, then catalysis may be arrested due to the lack of available free Ni(0) for the activation of the other coupling partner. This could explain why some ligands

produce larger yields of side product **4**, which could be due to the oxidative addition of the CPK occurring much more rapidly to form **Ni-2**, which in the absence of **Ni-3** will undergo decomposition to form **4**. In this way, catalysis could be interrupted without the formation of off-cycle species. Catalyst deactivation may also be occurring by the formation of insoluble $Ni(CN)_2$ species, which are known off-cycle species that reduce catalytic efficiency in Ni-catalyzed olefin hydrocyanation reactions[42]. Such olefin hydrocyanation reactions have been shown to proceed through Ni(H)(CN) intermediates[30], which could also be present in the cyclopropane ring-opening cyanation reaction being studied. These Ni(H)(CN) species could be important catalytic intermediates if the cyclopropyl ketone was being converted to an α,β-unsaturated ketone in situ, although previously we had ruled out the intermediacy of such an α,β-unsaturated phenyl ketone due to the lack of reactivity observed when (*E*)-1-phenylbut-2-en-1-one was used instead of cyclopropyl phenyl ketone **1a (Scheme 7)**. It is still possible that such Ni(H)(CN) complexes are necessary intermediates for the CPK ring-opening cyanation reaction. We plan to conduct stoichiometric experiments to probe the feasibility of generating these Ni(H)(CN) species from Ni(0) in the presence of benzonitrile and diphenylsilane, and we will test whether mixing these Ni(H)(CN) complexes with oxanickelacycle **Ni-2** can afford the open-chain nitrile products **(3)**. It is also possible that Ni(H)(CN) species are off-cycle intermediates that hinder the desired catalysis, especially since we do not observe the desired cyanation reactivity when alkylnitriles are used with catalytic Ni loadings.

Scheme 7: Lack of reactivity with α,β-unsaturated phenyl ketone

Ni(COD)$_2$ (20 mol%)
L1 (20 mol%)
TMSOTf (1.2 eq.)
Ph$_2$SiH$_2$ (2.0 eq.)
xylenes, 110 °C, 6 h

(*E*)-1-phenylbut-2-en-1-one
1.0 eq.

2a
2.0 eq.

3a, 0%

4, 0%

Another enigmatic issue is the apparent lack of enantioselectivity despite the use of PHOX ligands, which are commonly employed in enantioselective transformations. The fact that we are seeing racemic products for each constitutional isomer of both **1c** and **1d** could mean many things. One explanation could be that the oxidative addition into the racemic disubstituted CPK starting material and the reductive elimination to form the nitrile product are both concerted and stereoretentive. In this case, the only available mechanism for enantioenrichment would be a kinetic resolution in the CPK opening where the catalyst would show a preference to react with only one enantiomer. This is not observed as both product and starting CPK remain racemic. Alternatively, asymmetric catalysis could also arise from equilibrium processes between diastereomeric substrate-Ni(PHOX) adducts. It is also possible that the enantiodetermining step(s) are not under the influence of the ligand due to a lack of proximity between PHOX ligand and substrate in the key intermediates, or because of a lack of conformational control from the asymmetric PHOX ligand.

4.6   Conclusion

This chapter has outlined an optimization campaign which has transformed a stoichiometric reaction forming trace yield of an unusual product into a high-yielding and catalytically efficient reaction. Interestingly, this process is able to cut and sew two different C-C bonds and circumvent the use of toxic cyanide sources for the synthesis of nitriles. Despite the advancements made, we still aim to further improve the yield, regioselectivity, and scope of this chemistry. Ligand optimization, mechanistic elucidation, and determination of the substrate scope are ongoing. The elucidation of this catalytic mechanism will provide insights into Ni/LA cooperative catalytic systems and their unusual ability to activate σ-C-C bonds. We hope to leverage these mechanistic insights to enable other types of catalytic cyanation reactions that use benzonitriles as low-toxicity HCN surrogates.

4.7   Experimental section

4.7.1   Synthesis of cyclopropyl ketones (1):

Cyclopropyl ketones **1a** and **1e** were purchased from commercial vendors. Cyclopropyl ketones **1b**, **1c**, and **1d** were synthesized according to the following procedures.
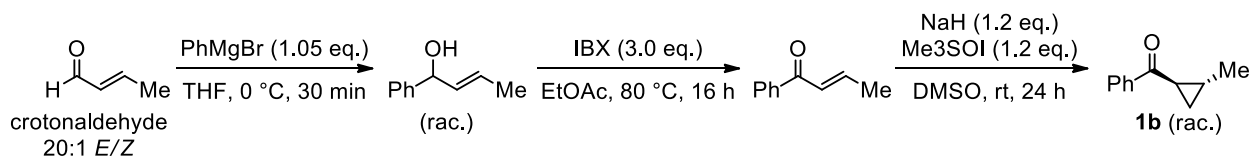
An oven-dried 100 mL 2-neck round bottom flask was charged with a magnetic stir bar and fitted with a 24/40 Suba-seal® septum. The flask was connected to a Schlenk line and the atmosphere in the reaction flask was replaced with nitrogen. Dry THF from a solvent purification system (21 mL) was injected into the reaction flask, then the flask was lowered into a brine/ice bath and stirred for 10 minutes to bring the solvent temperature down to 0 °C. PhMgBr (3.0 M in diethyl ether, 2.45 mL, 7.35 mmol) was then injected into the reaction flask. Next, crotonaldehyde (20:1 *E/Z*, 0.58 mL, 7.0 mmol) was injected dropwise with vigorous stirring. The reaction was stirred at 0 °C for 30 minutes then quenched with saturated aqueous ammonium chloride (5 mL). The crude mixture was partially evaporated to remove most of the THF and diethyl ether. After partial evaporation, the crude mixture was extracted with diethyl ether (2 x 20 mL). The combined organic extracts were washed with 1M HCl (2 x 10 mL) then brine (2 x 10 mL) and dried over sodium sulfate. The washed organic extract was evaporated to produce a yellow oil containing the benzylic alcohol intermediate, (*E*)-1-phenylbut-2-en-1-ol, which was isolated by column chromatography. Pure hexanes was used for making the silica slurry. The column was initially run in pure hexanes before gradually transitioning to 5% ethyl acetate in hexanes (**R**$_f$ = 0.10). The racemic product, (*E*)-1-phenylbut-

2-en-1-ol, was obtained as a colorless oil (655 mg, 63% yield). The *Z*-isomer of the product was not detected in the purified product by ^{1}H NMR. **^{1}H NMR** (500 MHz, CDCl$_3$) δ 7.40 – 7.32 (m, 4H), 7.28 (t, *J* = 6.7 Hz, 1H), 5.82 – 5.63 (m, 2H), 5.16 (d, *J* = 5.4 Hz, 1H), 1.88 (bs, 1H), 1.73 (d, *J* = 6.1 Hz, 3H). The product matched previously reported spectra.[59]

The next step of the synthesis used the oxidant IBX, which was synthesized according to a mild protocol reported in the literature[60].

The benzylic alcohol isolated in the previous step, (*E*)-1-phenylbut-2-en-1-ol (655 mg, 4.42 mmol), was dissolved in EtOAc (5 mL) in a 100 mL round bottom flask equipped with a magnetic stir bar and condenser, which was open to air. IBX (3.72 g, 13.3 mmol) was added to the reaction flask in one portion. The reaction was stirred at 80 °C for 16 hours. The crude mixture was filtered through a frit filter, then carefully evaporated to avoid the loss of the volatile ketone product. The ketone intermediate, (*E*)-1-phenylbut-2-en-1-one, was isolated by column chromatography. Pure hexanes was used for making the silica slurry. The column was initially run in pure hexanes before gradually transitioning to 5% ethyl acetate in hexanes (**R**$_f$ = 0.21). The product, (*E*)-1-phenylbut-2-en-1-one, was obtained as a colorless oil (304 mg, 47% yield). The *Z*-isomer of the product was not detected in the purified product by ^{1}H NMR. **^{1}H NMR** (500 MHz, CDCl$_3$) δ 7.93 (d, *J* = 7.8 Hz, 2H), 7.55 (t, *J* = 7.4 Hz, 1H), 7.47 (t, *J* = 7.7 Hz, 2H), 7.08 (dq, *J* = 15.0, 6.7

Hz, 1H), 6.91 (dq, J = 15.2, 1.6 Hz, 1H), 2.01 (d, J = 6.8 Hz, 3H). The product matched previously reported spectra[61].

An alternative oxidation reaction involving MnO_2 was also conducted according to a literature procedure[62], but poor yields of <10% were obtained and the yields reported in the literature could not be reproduced.

The cyclopropyl ketone product **1b** was synthesized from (*E*)-1-phenylbut-2-en-1-one via the Corey-Chaykovsky cyclopropanation reaction following a procedure adapted from the literature[63]. An oven-dried 2-neck round bottom flask equipped with a magnetic stir bar and fitted with a 24/40 vacuum adapter and 24/40 Suba-seal® septum. The reaction apparatus was attached to the Schlenk line and the atmosphere in the reaction flask was replaced with nitrogen. Sodium hydride (60% dispersion in mineral oil, 100 mg, 2.49 mmol) and trimethylsulfoxonium iodide (508 mg, 2.49 mmol) were added to the flask under nitrogen efflux, then the reactor was purged and refilled with nitrogen. The flask was charged with 5 mL of dry DMSO (added dropwise) at room temperature with stirring. Bubbles were observed, indicating the evolution of hydrogen gas. Once the evolution of hydrogen gas appeared to be complete, the reaction was stirred for an addition 15 minutes at room temperature. An oven-dried Schlenk flask fitted with a 14/20 Suba-seal® septum was charged with the α,β-unsaturated ketone starting material ((*E*)-1-phenylbut-2-en-1-one, 304 mg, 2.08 mmol), attached to the Schlenk line, and

purged and refilled with nitrogen gas. This Schlenk flask was charged with 2 mL of dry DMSO and manually swirled to dissolve the substrate. This solution was cannula transferred into the reaction flask containing the in situ-formed sulfur ylide, producing a bright red color (the color varies depending on the α,β-unsaturated ketone substrate). The reaction was stirred for 24 hours at room temperature. The reaction was quenched with 10 mL of deionized water and extracted with diethyl ether (3 x 15 mL). The combined organic extracts were dried over sodium sulfate, decanted, and the ether was evaporated to obtain the crude product. The cyclopropyl ketone product **1b** was isolated by column chromatography. Pure *n*-pentane was used for making the silica slurry. The column was initially run in pure *n*-pentane before gradually transitioning to 2.5% ethyl acetate in *n*-pentane (**R***f* = 0.25). The racemic product was obtained as a colorless oil (236 mg, 71% yield).

¹H NMR (400 MHz, CDCl₃) δ 7.99 (d, *J* = 6.9 Hz, 2H), 7.56 (t, *J* = 7.3 Hz, 1H), 7.47 (t, *J* = 7.4 Hz, 2H), 2.40 (dt, *J* = 8.2, 4.3 Hz, 1H), 1.62 (dqd, *J* = 8.6, 6.1, 3.9 Hz, 1H), 1.49 (ddd, *J* = 8.4, 4.6, 3.5 Hz, 1H), 1.23 (d, *J* = 6.0 Hz, 3H), 0.90 (ddd, *J* = 7.7, 6.4, 3.4 Hz, 1H). The product matched previously reported spectra[64].
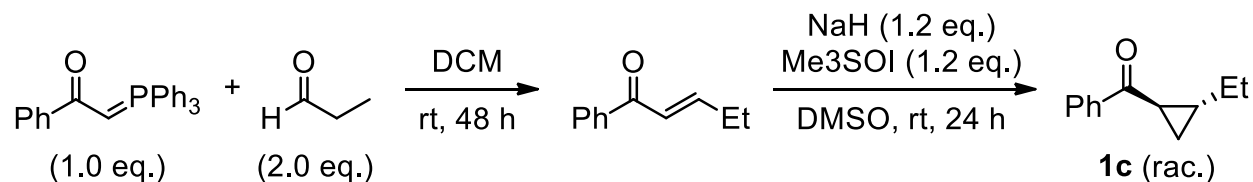
The α,β-unsaturated ketone intermediate, (E)-1-phenylpent-2-en-1-one, was synthesized via a Wittig reaction using a commercially available, stabilized phosphonium ylide according to a literature procedure[22]. An oven-dried, 100 mL 2-neck round bottom flask was equipped with a magnetic stir bar, 24/40 Suba-seal® septum, and 24/40 vacuum adapter. The reaction apparatus was quickly attached to the Schlenk line and the atmosphere in the flask was purged and refilled with nitrogen. Once the flask was cool to the touch, the solid phosphonium ylide 2-(triphenylphosphoranylidene)acetophenone (3.80 g, 10.0 mmol) was added to the reaction flask under nitrogen efflux, and the reactor was again purged and refilled with nitrogen. The reactor was charged with 25 mL of dry dichloromethane from a solvent purification system and stirred until the phosphonium ylide was completely dissolved. Propionaldehyde (1.43 mL, 20.0 mmol) was then injected dropwise, and the reaction was stirred at room temperature for 48 hours. Once the reaction was complete, the solvent was evaporated to yield the crude product. The α,β-unsaturated ketone, (E)-1-phenylpent-2-en-1-one, was isolated by column chromatography. Pure hexanes was used for making the silica slurry. The column was initially run in pure hexanes before gradually transitioning to 5% ethyl acetate

in hexanes (R_f = 0.23). The product was obtained as a colorless oil (1.39 g, 87% yield). **¹H NMR** (400 MHz, CDCl₃) δ 7.93 (d, *J* = 7.0 Hz, 2H), 7.55 (t, *J* = 7.4 Hz, 1H), 7.46 (t, *J* = 7.6 Hz, 2H), 7.11 (dt, *J* = 15.4, 6.4 Hz, 1H), 6.87 (dt, *J* = 15.4, 1.6 Hz, 1H), 2.43 – 2.25 (m, 2H), 1.15 (t, *J* = 7.4 Hz, 3H). The product matched previously reported spectra[65].

1c was synthesized from (E)-1-phenylpent-2-en-1-one following the Corey-Chaykovsky cyclopropanation procedure that was followed to synthesize **1b**. The cyclopropyl ketone product **1c** was isolated by column chromatography. Pure *n*-pentane was used for making the silica slurry. The column was initially run in pure *n*-pentane before gradually transitioning to 2.5% ethyl acetate in *n*-pentane (R_f = 0.25). A crude aliquot showed 77% conversion to product by ¹H NMR, but poor separation between starting material and product led to a lower isolated yield due to significant coelution. The pure racemic product was obtained as a colorless oil (509 mg, 34% yield). The fractions containing both starting material and product were saved (a second flash column could be conducted to isolate additional **1c**). **¹H NMR** (500 MHz, CDCl₃) δ 8.02 (d, *J* = 8.1 Hz, 2H), 7.58 (t, *J* = 7.3 Hz, 1H), 7.49 (t, *J* = 7.5 Hz, 2H), 2.46 (dt, *J* = 8.2, 4.2 Hz, 1H), 1.60 (dtd, *J* = 13.0, 6.6, 3.9 Hz, 1H), 1.53 – 1.41 (m, 3H), 1.04 (t, *J* = 7.4 Hz, 3H), 0.97 – 0.91 (m, 1H). The product matched previously reported spectra[22].
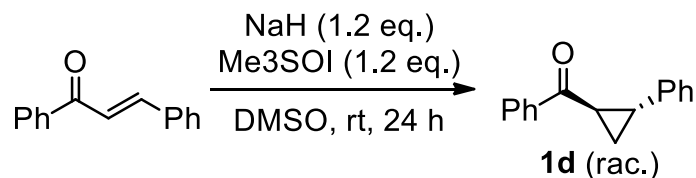
1d was synthesized from (*E*)-chalcone by Nathan Coddington following the Corey-Chaykovsky cyclopropanation procedure that was followed to synthesize **1b** and **1c**. Catalytic reactions involving **1d** were conducted by Nathan Coddington. The cyclopropyl ketone product **1d** was isolated by column chromatography. Pure *n*-pentane was used for making the silica slurry. The column was initially run in pure *n*-pentane before gradually transitioning to 5% ethyl acetate in *n*-pentane (**R**$_f$ = 0.20). The racemic product was obtained as a white solid (78.7 mg, 71% yield). **¹H NMR** (500 MHz, CDCl₃) δ 8.00 (d, *J* = 7.6 Hz, 2H), 7.56 (t, *J* = 7.4 Hz, 1H), 7.47 (t, *J* = 7.6 Hz, 2H), 7.32 (t, *J* = 7.5 Hz, 2H), 7.24 (t, *J* = 7.4 Hz, 1H), 7.19 (d, *J* = 7.5 Hz, 2H), 2.91 (dt, *J* = 8.9, 4.6 Hz, 1H), 2.71 (ddd, *J* = 10.1, 6.6, 4.0 Hz, 1H), 1.93 (dt, *J* = 9.3, 4.8 Hz, 1H), 1.57 (td, *J* = 7.3, 4.1 Hz, 1H). The product matched previously reported spectra[66].

## 4.7.2   Synthesis and characterization of γ-cyanoketones (3):

General procedure for the ring-opening cyanation of cyclopropyl ketones using benzonitriles as cyanide surrogates: The reactions were conducted in the glovebox in 20 mL scintillation vials bearing small stir bars. The reaction also works outside of the glovebox, but yields are lower and side product formation is higher. Xylenes

solvent was thoroughly degassed with 4 freeze-pump-thaw cycles outside of the glovebox followed by 10 minutes of sparging with N_2 inside the glovebox for the best and most reproducible results. A hot plate equipped with an aluminum hot block for 20 mL scintillation vials was preheated to 110 °C. All stock solutions were used within 1 hour of being prepared. Two stock solutions were made in the glovebox according to the following procedure:

Stock solution A: 14.9 mg (0.04 mmol) of (*S*)-*i*-Pr-PHOX **(L7)** or another bidentate ligand was weighed into a tared 1-dram vial. 4.0 mL of degassed/sparged xylenes were added to this 1-dram vial, which was capped and gently agitated to dissolve the ligand. 11.0 mg (0.04 mmol) of Ni(COD)$_2$ was weighed into a second tared 1-dram vial. The ligand solution was carefully transferred to the vial containing the solid Ni(COD)$_2$ via a glass Pasteur pipette, producing a color change from colorless to dark green upon coordination of the PHOX ligand to Ni(0). This solution was capped, shaken, and set aside while the other stock solution was being made.

Stock solution B (example using **1a**): 5.0 mL of degassed/sparged xylenes were added to a tared 20 mL scintillation vial. This was followed by the addition of 69 µL (0.5 mmol) of cyclopropyl phenyl ketone **(1a)**, 126 µL (0.75 mmol) of 3,5-bis(trifluoromethyl)benzonitrile **(2g)**, and 186 µL (1 mmol) of diphenylsilane. This solution was capped, shaken, and dispensed into the reaction vials soon after mixing.

The reaction vial (a 20 mL scintillation vial containing a small stir bar) was charged with 1.08 mL of stock solution B followed by 21.8 μL (0.12 mmol) of trimethylsilyl trifluoromethanesulfonate (TMSOTf). The reaction vial was immediately capped after addition of the Lewis acid and gently agitated for 15 seconds to ensure complete mixing of the reaction solution. The reaction vial was then quickly uncapped to add 0.5 mL of stock solution A, which immediately produced an orange or amber-colored solution. The reaction vial was capped, sealed with electrical tape, and placed on an aluminum hot block preheated to 110 °C and stirred at 450 rpm for 6 hours. The order of additions is important because the Ni complex decomposes when TMSOTf is added to it before being mixed with stock solution B. After the reaction was complete, it was allowed to cool and taken out of the glovebox, then exposed to air and quenched with ~1 mL of dichloromethane and 1 drop of deionized water. The crude mixture was stirred for 10 minutes at room temperature outside of the glovebox, then 4 to 5 mg of dimethyl fumarate was added as internal standard to the crude mixture, which was then shaken thoroughly to ensure that the internal standard fully dissolved. Acquisition of crude ^{1}H NMR spectra allows for quantification of the IS yield of all products. Nitrile products **3** were isolated by partial evaporation of the crude (to remove dichloromethane) followed by direct loading of the xylenes-containing mixture onto a silica column for flash chromatography.
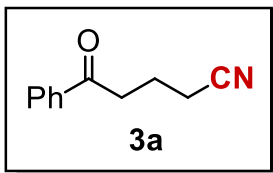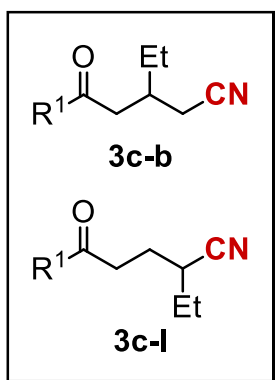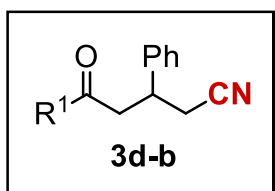
The γ-cyanoketone product **3a** was isolated by column chromatography. Pure *n*-pentane was used for making the silica slurry. The column was initially run in pure *n*-pentane before gradually transitioning to 20% ethyl acetate in *n*-pentane (**R$_f$** = 0.19). The racemic product was obtained as a white solid (14.0 mg, 81% yield using **L7**). **¹H NMR** (500 MHz, CDCl$_3$) δ 7.97 (d, *J* = 7.9 Hz, 2H), 7.59 (t, *J* = 7.4 Hz, 1H), 7.49 (t, *J* = 7.7 Hz, 2H), 3.19 (t, *J* = 6.8 Hz, 2H), 2.54 (t, *J* = 7.0 Hz, 2H), 2.13 (p, *J* = 6.9 Hz, 2H). The product matched previously reported spectra[67]. **HRMS** (ESI-TOF) *m/z* calculated for C$_{11}$H$_{10}$NO (M-H)$^-$: 172.0768, found 172.0776.
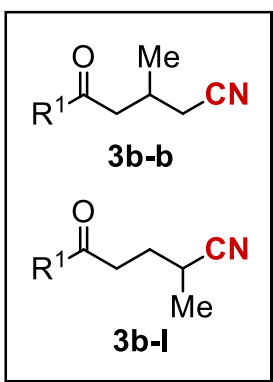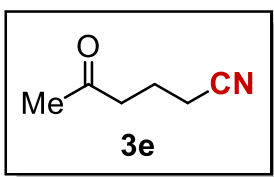
The γ-cyanoketone product **3b** was isolated by column chromatography. Pure *n*-pentane was used for making the silica slurry. The column was initially run in pure *n*-pentane before gradually transitioning to 10% ethyl acetate in *n*-pentane (**R$_f$** = 0.12). The product was obtained as a colorless oil (14.3 mg, 76% yield using **L6**; 55:45 **3b-b:3b-l**). **¹H NMR (3b-b)** (500 MHz, CDCl$_3$) δ 7.96 (d, *J* = 8.3 Hz, 2H), 7.59 (t, *J* = 7.4 Hz, 1H), 7.48 (t, *J* = 7.6 Hz, 2H), 3.12 (dd, *J* = 17.5, 7.4 Hz, 1H), 3.02 (dd, *J* = 17.6, 5.8 Hz, 1H), 2.62 (dq, *J* = 12.9, 6.4 Hz, 1H), 2.52 (d, *J* = 5.4 Hz, 2H), 1.20 (d, *J* = 6.8 Hz, 3H). **¹H NMR (3b-l)** (500 MHz, CDCl$_3$) δ 7.97 (d, *J* = 8.4 Hz, 3H), 7.59 (t, *J* = 7.3 Hz, 2H), 7.48 (t, *J* = 7.5 Hz, 4H), 3.29 – 3.15 (m, 2H), 2.88 – 2.77 (m, 1H), 2.11

(dq, J = 13.1, 7.5 Hz, 1H), 2.02 – 1.90 (m, 1H), 1.39 (d, J = 7.0 Hz, 3H). The product matched previously reported spectra[68].

The γ-cyanoketone product **3c** was isolated by column chromatography. Pure *n*-pentane was used for making the silica slurry. The column was initially run in pure *n*-pentane before gradually transitioning to 10% ethyl acetate in *n*-pentane (**R$_f$** = 0.15). The product was obtained as a colorless oil (16.6 mg, 83% yield using **L6**; 57:43 **3b-b:3b-l**). **¹H NMR (3c-b)** (500 MHz, CDCl₃) δ 7.96 (d, J = 7.6 Hz, 2H), 7.59 (t, J = 7.4 Hz, 1H), 7.48 (t, J = 7.6 Hz, 2H), 3.09 (d, J = 6.5 Hz, 2H), 2.63 – 2.50 (m, 2H), 2.39 (hept, J = 6.5 Hz, 1H), 1.58 (p, J = 7.3 Hz, 2H), 0.99 (t, J = 7.4 Hz, 3H). **¹H NMR (3c-l)** (500 MHz, CDCl₃) δ 7.98 (d, J = 7.6 Hz, 2H), 7.59 (t, J = 7.3 Hz, 1H), 7.48 (t, J = 7.6 Hz, 2H), 3.29 – 3.14 (m, 2H), 2.68 (ddt, J = 10.7, 7.7, 5.5 Hz, 1H), 2.18 – 2.06 (m, 1H), 1.95 (dddd, J = 13.4, 10.2, 7.5, 5.7 Hz, 1H), 1.71 (dqd, J = 13.7, 9.0, 8.2, 4.0 Hz, 2H), 1.12 (t, J = 7.4 Hz, 3H).


The γ-cyanoketone product **3d** was isolated by column chromatography. Both the reaction setup and product isolation were conducted by Nathan Coddington. Pure *n*-pentane was used for making the silica slurry. The column was initially run in pure *n*-pentane before gradually transitioning to 20% ethyl acetate in *n*-pentane (**R$_f$** =

0.31). The product was obtained as a pale-yellow oil (4.0 mg, 16% yield using **L6**; only the branched constitutional isomer **(3d-b)** was isolated; the linear constitutional isomer **(3d-l)** was not detected). **^{1}H NMR (3d-b)** (600 MHz, CDCl$_3$) δ 7.95 (d, *J* = 7.7 Hz, 2H), 7.59 (t, *J* = 7.3 Hz, 1H), 7.47 (t, *J* = 7.4 Hz, 2H), 7.39 – 7.32 (m, 4H), 7.29 (t, *J* = 6.7 Hz, 1H), 3.76 (p, *J* = 6.6 Hz, 1H), 3.54 (dd, *J* = 17.8, 8.2 Hz, 1H), 3.47 (dd, *J* = 17.7, 5.5 Hz, 1H), 2.91 – 2.77 (m, 2H). The product matched previously reported spectra[69].

3e

The γ-cyanoketone product **3e** was isolated by column chromatography. Both the reaction setup and product isolation were conducted by Nathan Coddington. Pure *n*-pentane was used for making the silica slurry. The column was initially run in pure *n*-pentane before gradually transitioning to 50% ethyl acetate in *n*-pentane (**R$_f$** = 0.40). The product was visualized with phosphomolybdic acid stain. The product was obtained as a colorless oil (0.3 mg, 3% yield using **L6**). **^{1}H NMR (3d-b)** (500 MHz, CDCl$_3$) δ 2.65 (t, *J* = 7.0 Hz, 2H), 2.43 (t, *J* = 7.0 Hz, 2H), 2.18 (s, 3H), 1.92 (p, *J* = 7.0 Hz, 2H). The product matched previously reported spectra[70].

### 4.7.3 Synthesis and characterization of α,γ-difunctionalized ketone (5):
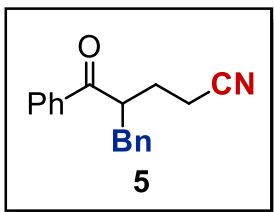
For the synthesis of the α,γ-difunctionalized ketone **(5)**, the general procedure for the ring-opening cyanation reaction was followed, with a slight modification. Stock solution A was made with dtbbpy **(L1)** at 4x concentration of ligand and Ni(COD)$_2$ in order to produce a 20 mol% Ni(ligand) stock solution. After 2 hours of stirring at 110 °C, benzyl bromide (2.0 eq.) was added in one portion and the reaction was stirred at 110 °C for an additional 4 hours. The product was isolated by column chromatography. Pure *n*-pentane was used for making the silica slurry. The column was initially run in pure *n*-pentane before gradually transitioning to 10% ethyl acetate in *n*-pentane (**R$_f$(5)** = 0.17, **R$_f$(3a)** = 0.10); this was to prevent the product from diffusing into the eluent during dry loading. The product **5** was obtained as a colorless oil (2.5 mg, 9% yield). The product **3a** was also isolated as a colorless oil (8.6 mg, 50% yield). **¹H NMR (5)** (400 MHz, CDCl$_3$) δ 7.94 (d, *J* = 7.1 Hz, 2H), 7.62 – 7.44 (m, 6H), 7.16 (d, *J* = 6.7 Hz, 2H), 4.01 – 3.87 (m, 1H), 3.12 (dd, *J* = 13.8, 6.3 Hz, 1H), 2.72 (dd, *J* = 13.8, 8.0 Hz, 1H), 2.42 – 2.15 (m, 4H). **HRMS (5)** (ESI-TOF) *m/z* calculated for C$_{18}$H$_{18}$NO (M+H)$^+$: 264.1383, found 264.1374.

### 4.7.4 Synthesis and characterization of PHOX ligands:

The following PHOX ligands were purchased from commercial vendors: **L7**, **L20**, **L21**, **L22**, **L23**, **L26**, and **L28**. The following PHOX ligands were synthesized by the author according to the procedures outlined in this section: **L17**, **L18**, **L19**, **L24**, **L25**, and **L27**. Both routes A and B were adapted from literature procedures[58].

Route A to synthesize PHOX ligands:
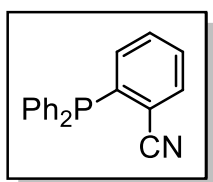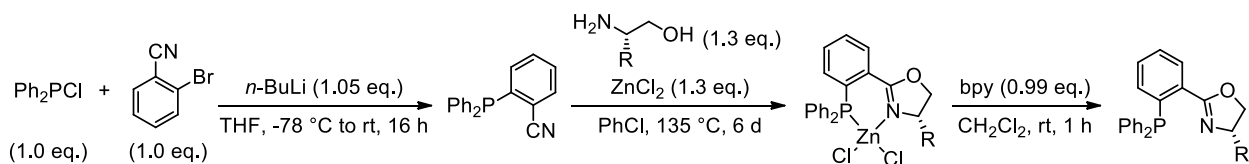
An oven-dried 250 mL Schlenk flask was charged with a magnetic stir bar, fitted with a 24/40 Suba-seal® septum, and put on the Schlenk line. The atmosphere inside the reaction flask was replaced with nitrogen. A chiller and acetone bath in a Dewar were assembled, and the chiller was set to -78 °C. 2-bromobenzonitrile (500 mg, 2.75 mmol) was added to the Schlenk flask through a weighing paper cone under nitrogen efflux. 37 mL of dry THF from a solvent purification system were injected into the Schlenk flask and stirred at room temperature until the 2-bromobenzonitrile was fully dissolved. Once dissolved, the reaction flask was lowered into the cold bath and stirred for 15 minutes to cool down the reaction mixture. Next, 1.19 mL of 2.38 M *n*-BuLi in hexanes was injected into the reaction flask, dropwise. The reaction was stirred at -78 °C for 10 minutes. During this time, a second oven-dried Schlenk

236

flask (10 mL size) was fitted with a 14/20 Suba-seal® septum and put on the Schlenk line. The atmosphere inside this second Schlenk flask was replaced with nitrogen. 2.5 mL of dry THF followed by 0.49 mL chlorodiphenylsilane were injected into this smaller Schlenk flask, which was gently stirred by hand until the chlorodiphenylsilane fully mixed with the THF solvent. This mixture was slowly cannula transferred to the reaction flask, dropwise. The reaction was stirred for 3 hours longer at -78 °C, then it was allowed to slowly warm to room temperature while stirring for 16 hours. The reaction was then uncapped and 15 mL of deionized water were added to quench the reaction. The reaction was poured into a 250 mL round-bottom flask and evaporated with a rotary evaporator to remove most of the THF solvent, leaving an aqueous layer with a thin organic layer containing the crude product, 2-(diphenylphosphino)benzonitrile. 40 mL of ethyl acetate were added to the round-bottom flask containing the crude product, then the heterogeneous mixture was poured into a separatory funnel, shaken, and the organic layer was collected. The aqueous layer was extracted with 20 mL of ethyl acetate. The organic extracts were combined, dried over sodium sulfate, decanted, and evaporated to yield the crude product. 2-(diphenylphosphino)benzonitrile was isolated by recrystallization from methanol (541 mg, 69% yield). **¹H NMR** (400 MHz, CDCl₃) δ 7.71 (ddd, *J* = 7.0, 2.8, 1.4 Hz, 1H), 7.47 (td, *J* = 7.7, 1.5 Hz, 1H), 7.44 – 7.36 (m, 7H), 7.34 – 7.29 (m, 4H), 7.04 (ddd, *J* = 7.6, 3.4, 1.0 Hz, 1H). **³¹P NMR** (243 MHz, CDCl₃) δ -8.5. The product matched previously reported spectra[71].
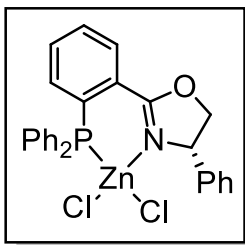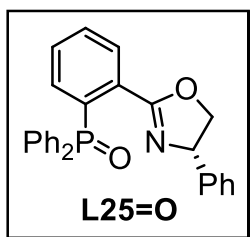
A 10 mL 2-neck round-bottom flask was charged with a stir bar and fitted with a 14/20 Suba-seal® septum and a 14/20 condenser. 2-(diphenylphosphino)benzonitrile (156 mg, 0.542 mmol) was added to the reaction flask, which was purged with nitrogen and kept under nitrogen pressure from the top of the condenser. $ZnCl_2$ (96 mg, 0.71 mmol) was quickly weighed (it is very hygroscopic and difficult to transfer once it becomes wet) and added under nitrogen efflux. Next, phenylglycinol (97 mg, 0.71 mmol) was added to the reaction flask under nitrogen efflux. 5 mL of chlorobenzene were injected into the reaction flask. The reaction was stirred at 135 °C for 6 days, adding additional chlorobenzene as needed to prevent the reaction from "drying up". Argon balloons were used to maintain an inert environment. After 6 days, the crude reaction mixture was evaporated. The product, ((S)-Ph-PHOX)ZnCl$_2$, was isolated by column chromatography. The column was initially run in 1:1 ethyl acetate:hexanes before gradually transitioning to 100% ethyl acetate (R_f = 0.40). The product was isolated as an orange crystalline solid (63.9 mg, 25% yield). The Zn complex was not characterized and the crude material was immediately brought to the next step.
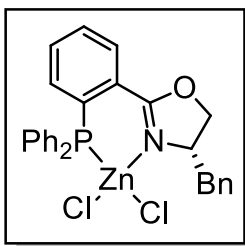

((S)-Bn-PHOX)ZnCl$_2$ was isolated following the same procedure that was followed for ((S)-Ph-PHOX)ZnCl$_2$. The aminoalcohol used was phenylalaninol (111 mg, 0.733 mmol,

1.3 eq.), and the reaction was run on a 0.564 mmol scale. The product, ((*S*)-Bn-PHOX)ZnCl$_2$, was isolated by column chromatography. The column was initially run in 1:1 ethyl acetate:hexanes before gradually transitioning to 100% ethyl acetate (**R***f* = 0.40). The product was isolated as a white crystalline solid (186 mg, 68% yield). The Zn complex was not characterized and the crude material was immediately brought to the next step.


L25=O

Unfortunately, route A to access PHOX ligands led to formation of undesired phosphinoxides for both of the ligands synthesized with this method. An oven-dried, 50 mL 2-neck round bottom flask was equipped with a magnetic stir bar, 14/20 Suba-seal® septum, and 14/20 vacuum adapter. The reaction apparatus was quickly attached to the Schlenk line and the atmosphere in the flask was purged and refilled with nitrogen. ((*S*)-Ph-PHOX)ZnCl$_2$ (63.9 mg, 0.135 mmol) and 2,2'-bipyridine (20.9 mg, 0.134 mmol) were added under nitrogen efflux, then 6 mL of dry dichloromethane were injected into the reaction flask. The reaction was stirred at room temperature for 1 hour. The reaction mixture was partially evaporated, then transferred directly onto a silica flash column. The column was run in 100% ethyl acetate (**R***f* = 0.13). The product, **L25=O**, was isolated as a white solid (34.5 mg, 60% yield). **^{1}H NMR** (400 MHz, CDCl$_3$) δ 8.03 (dd, *J* = 7.2, 3.6 Hz, 1H), 7.77 – 7.67 (m, 5H), 7.57 – 7.41 (m, 13H), 4.99 (t, *J* = 9.7 Hz, 1H), 4.30 (t, *J* = 9.3 Hz, 1H), 3.89 (t, *J* = 8.8 Hz, 1H). **^{31}P NMR** (162 MHz, CDCl$_3$) δ 29.8.
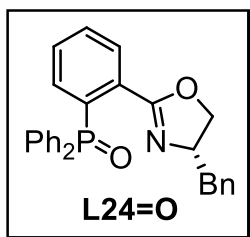
L24=O

L24=O was isolated using the same procedure used to isolate **L25=O**. The rxn was run in a 100 mL round-bottom flask with 24/40 fittings. The same equivalents of 2,2'-bipyridine (59.0 mg, 0.378 mmol, 0.99 eq.) were used, and the reaction was run on a 0.382 mmol scale. 18 mL of dry dichloromethane solvent were used. The column was run in 100% ethyl acetate (R_f = 0.15). The product, **L25=O**, was isolated as a white solid (117.8 mg, 70% yield). **^{1}H NMR** (600 MHz, CDCl$_3$) δ 7.90 (dd, J = 8.3, 3.7 Hz, 1H), 7.70 (ddd, J = 28.7, 11.9, 7.9 Hz, 4H), 7.59 (t, J = 7.5 Hz, 1H), 7.54 – 7.43 (m, 8H), 7.25 (t, J = 7.4 Hz, 2H), 7.19 (t, J = 7.4 Hz, 1H), 7.10 (d, J = 7.4 Hz, 2H), 4.21 – 4.11 (m, 1H), 3.81 (t, J = 8.8 Hz, 1H), 3.62 (t, J = 8.1 Hz, 1H), 2.99 (dd, J = 13.7, 5.5 Hz, 1H), 2.40 (dd, J = 13.8, 8.9 Hz, 1H). **^{31}P NMR** (243 MHz, CDCl$_3$) δ 29.5.

Route B to synthesize PHOX ligands:
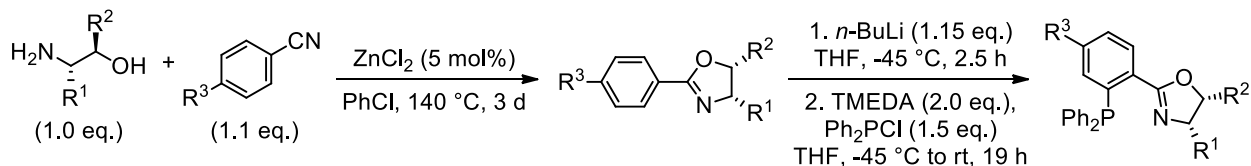
An oil bath was preheated to 140 °C. An oven-dried 25 mL round-bottom flask was charged with a magnetic stir bar and fitted with a 14/20 Suba-seal® septum and 14/20 condenser connected to the Schlenk line at the top. The reaction apparatus

was purged of air and refilled with nitrogen. $ZnCl_2$ (0.05 eq.) and *para*-substituted benzonitrile (1.1 eq.) were added to the reaction through a weighing paper cone under nitrogen efflux. Chlorobenzene (~1.0 M) was injected into the reaction, which was stirred at room temperature until the benzonitrile dissolved. Next, an aminoalcohol (1.0 eq.) was injected into the reaction apparatus in one portion, then the reaction was lowered onto the oil bath and stirred at 140 °C for 3 days. The 2-phenyl-2-oxazoline intermediates were isolated by column chromatography.

The 2-phenyl-2-oxazoline intermediates were used in a second step in which the PHOX products were accessed via directed *ortho*-metalation. An oven-dried 100 mL Schlenk flask was charged with a magnetic stir bar, fitted with a 24/40 Suba-seal® septum, and put on the Schlenk line. The atmosphere inside the reaction flask was replaced with nitrogen. A chiller and acetone bath in a Dewar were assembled, and the chiller was set to -45 °C. The 2-phenyl-2-oxazoline intermediate (1.0 eq.) was added to the Schlenk flask through a weighing paper cone under nitrogen efflux. Dry THF (0.1 M) from a solvent purification system was injected into the Schlenk flask and stirred at room temperature until the solid 2-phenyl-2-oxazoline intermediate was fully dissolved. Once dissolved, the reaction flask was lowered into the cold bath and stirred for 15 minutes to cool down the reaction mixture. Next, *n*-BuLi in hexanes (1.15 eq.) was injected into the reaction flask, dropwise. The reaction was stirred for 2.5 hours. During this time, a second oven-dried Schlenk flask (10 mL size) was fitted with a 14/20 Suba-seal® septum

and put on the Schlenk line. The atmosphere inside this second Schlenk flask was replaced with nitrogen. Dry THF (0.5 M) followed by chlorodiphenylsilane (1.5 eq.) were injected into this smaller Schlenk flask, which was gently stirred by hand until the chlorodiphenylsilane fully mixed with the THF solvent. At this point, TMEDA (2.0 eq.) was injected into the reaction flask, dropwise, at -45 °C. The reaction was stirred for 10 minutes at this temperature before slow cannula transfer of the contents of the Schlenk flask containing the chlorodiphenylsilane solution. The reaction was stirred for 19 hours longer and was allowed to slowly warm to room temperature while stirring under nitrogen or argon pressure. The reaction mixture was poured into a 250 mL round-bottom flask and evaporated with a rotary evaporator (at 30 °C to limit oxidation) to remove most of the solvent from the crude PHOX product. If the crude solidified, a small amount of dichloromethane was added to facilitate loading the column. Column chromatography was conducted less than 1 hour after exposing the crude mixture to air to limit oxidation of the PHOX ligand.
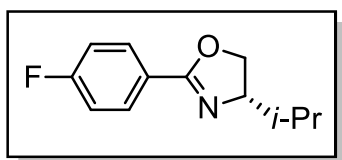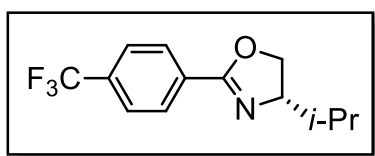

The reaction was run on a 3.95 mmol scale using L-valinol and 4-fluorobenzonitrile as starting materials. Pure hexanes was used for making the silica slurry. The column was initially run in pure hexanes before gradually transitioning to 5% ethyl acetate in hexanes ($\mathbf{R}_f$ = 0.16). The product ((S)-2-(4-fluorophenyl)-4-isopropyl-4,5-dihydrooxazole) was obtained as a colorless, crystalline solid (607 mg, 82%

yield). **¹H NMR** (600 MHz, CDCl₃) δ 8.00 (bs, 2H), 7.09 (t, *J* = 8.4 Hz, 2H), 4.44 (bs, 1H), 4.15 (bd, *J* = 28.9 Hz, 2H), 1.89 (bs, 1H), 1.03 (d, *J* = 6.8 Hz, 3H), 0.94 (d, *J* = 6.7 Hz, 3H). **¹⁹F NMR** (564 MHz, CDCl₃) δ -108.6. The product matched previously reported spectra[72].


L17
4-F(*S*)-*i*-Pr-PHOX
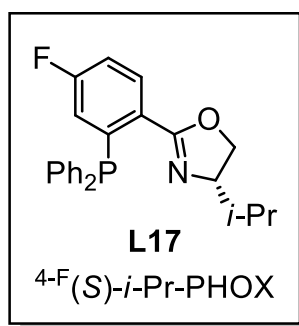
The reaction was run on a 2.93 mmol scale using (*S*)-2-(4-fluorophenyl)-4-isopropyl-4,5-dihydrooxazole as the oxazoline substrate. Pure *n*-pentane was used for making the silica slurry. The column was initially run in pure *n*-pentane before gradually transitioning to 5% ethyl acetate in *n*-pentane (**R*f*** = 0.13). The product (**L17**) was obtained as a pale-yellow oil (191 mg, 17% yield). **¹H NMR** (500 MHz, CDCl₃) δ 7.93 (ddd, *J* = 9.1, 5.7, 3.7 Hz, 1H), 7.30 (dd, *J* = 11.2, 3.8 Hz, 10H), 7.00 (td, *J* = 8.2, 2.6 Hz, 1H), 6.57 (dt, *J* = 9.9, 3.0 Hz, 1H), 4.16 – 4.10 (m, 1H), 3.91 – 3.77 (m, 2H), 1.45 (h, *J* = 6.6 Hz, 1H), 0.79 (d, *J* = 6.7 Hz, 3H), 0.68 (d, *J* = 6.7 Hz, 3H). **¹⁹F NMR** (376 MHz, CDCl₃) δ -109.9 (q, *J* = 8.0 Hz). **³¹P NMR** (162 MHz, CDCl₃) δ -5.1. The product matched previously reported spectra[73].
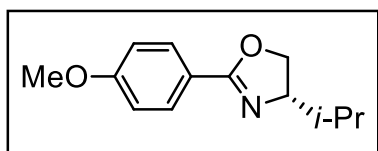

The reaction was run on a 3.95 mmol scale using L-valinol and 4-(trifluoromethyl)benzonitrile as starting materials. Pure hexanes was used for making the silica slurry. The column was initially run in pure hexanes before gradually

transitioning to 5% ethyl acetate in hexanes (R_f = 0.20). The product ((S)-4-isopropyl-2-(4-(trifluoromethyl)phenyl)-4,5-dihydrooxazole) was obtained as a colorless, crystalline solid (528 mg, 57% yield). **¹H NMR** (400 MHz, CDCl₃) δ 8.13 (bd, *J* = 4.3 Hz, 2H), 7.68 (d, *J* = 8.1 Hz, 2H), 4.50 (t, *J* = 7.8 Hz, 1H), 4.30 – 4.10 (m, 2H), 2.03 – 1.83 (m, 1H), 1.05 (d, *J* = 6.8 Hz, 4H), 0.95 (d, *J* = 6.7 Hz, 3H). **¹⁹F NMR** (376 MHz, CDCl₃) δ -64.3. The product matched previously reported spectra[74].
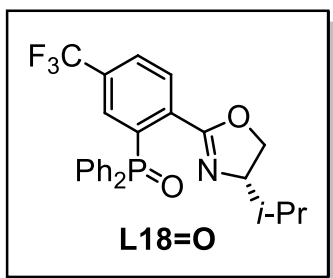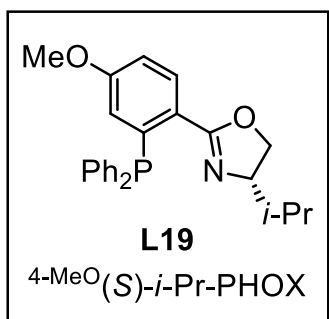

The reaction was run on a 2.05 mmol scale using (S)-4-isopropyl-2-(4-(trifluoromethyl)phenyl)-4,5-dihydrooxazole as the oxazoline substrate. The column was run in 100% ethyl acetate (R_f = 0.20). The product **(L18=O)** was obtained as a yellow oil (194 mg, 21% yield). **¹H NMR** (400 MHz, CDCl₃) δ 8.02 – 7.90 (m, 2H), 7.78 (d, *J* = 8.1 Hz, 1H), 7.72 – 7.59 (m, 4H), 7.47 – 7.37 (m, 6H), 3.79 (dd, *J* = 9.8, 8.3 Hz, 1H), 3.63 (t, *J* = 8.6 Hz, 1H), 3.49 – 3.38 (m, 1H), 1.53 – 1.39 (m, *J* = 6.7 Hz, 1H), 0.78 (d, *J* = 6.7 Hz, 3H), 0.69 (d, *J* = 6.7 Hz, 3H). **¹⁹F NMR** (376 MHz, CDCl₃) δ -64.4. **³¹P NMR** (162 MHz, CDCl₃) δ 29.4.
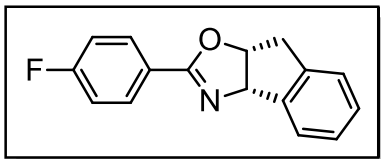

The reaction was run on a 7.18 mmol scale using L-valinol and 4-methoxybenzonitrile as starting materials. Pure hexanes was used for making the silica slurry. The column was initially run in pure hexanes before gradually

transitioning to 10% ethyl acetate in hexanes (**R***f* = 0.11). The product ((*S*)-4-isopropyl-2-(4-methoxyphenyl)-4,5-dihydrooxazole) was obtained as a white, foamy solid (664 mg, 45% yield). **^{1}H NMR** (400 MHz, CDCl$_3$) δ 7.94 (d, *J* = 8.4 Hz, 2H), 6.91 (d, *J* = 8.9 Hz, 2H), 4.41 (t, *J* = 8.3 Hz, 1H), 4.12 (dq, *J* = 16.9, 7.7 Hz, 2H), 3.85 (s, 3H), 1.96 – 1.83 (m, *J* = 6.7 Hz, 1H), 1.03 (d, *J* = 6.8 Hz, 3H), 0.93 (d, *J* = 6.8 Hz, 3H). The product matched previously reported spectra[73].

MeO

Ph$_2$P   N

*i*-Pr

L19

$^{4\text{-MeO}}$(*S*)-*i*-Pr-PHOX

The reaction was run on a 3.86 mmol scale using (*S*)-4-isopropyl-2-(4-methoxyphenyl)-4,5-dihydrooxazole as the oxazoline substrate. Pure *n*-pentane was used for making the silica slurry. The column was initially run in pure *n*-pentane before gradually transitioning to 10% ethyl acetate in *n*-pentane (**R***f* = 0.17). The product **(L19)** was obtained as a white solid (382 mg, 25% yield). **^{1}H NMR** (600 MHz, CDCl$_3$) δ 7.96 (bs, 1H), 7.36 – 7.29 (m, 10H), 6.88 (d, *J* = 8.7 Hz, 1H), 6.37 (s, 1H), 4.14 – 4.11 (m, 1H), 3.97 – 3.80 (m, 2H), 3.62 (s, 3H), 1.51 (bs, 1H), 0.81 (d, *J* = 6.4 Hz, 3H), 0.69 (d, *J* = 6.4 Hz, 3H). **^{31}P NMR** (243 MHz, CDCl$_3$) δ -4.4. The product matched previously reported spectra[73].

The reaction was run on a 7.0 mmol scale using (1*S*,2*R*)-1-amino-2,3-dihydro-1*H*-inden-2-ol and 4-fluorobenzonitrile as starting materials. Pure hexanes was used for making the silica slurry. The column was initially run in pure hexanes before gradually transitioning to 20% ethyl acetate in hexanes (**R**$_f$ = 0.24). The product ((3a*S*,8a*R*)-2-(4-fluorophenyl)-8,8a-dihydro-3a*H*-indeno[1,2-*d*]oxazole) was obtained as a white solid (910 mg, 51% yield). **¹H NMR** (400 MHz, CDCl₃) δ 8.00 (bs, 2H), 7.63 (bs, 1H), 7.33 – 7.27 (m, 3H), 7.07 (t, *J* = 8.7 Hz, 2H), 5.77 (d, *J* = 7.9 Hz, 1H), 5.56 (t, *J* = 7.2 Hz, 1H), 3.54 (dd, *J* = 18.0, 6.8 Hz, 1H), 3.39 (d, *J* = 18.5 Hz, 1H). **¹⁹F NMR** (376 MHz, CDCl₃) δ -106.0 (p, *J* = 8.3 Hz). The product matched previously reported spectra[75].
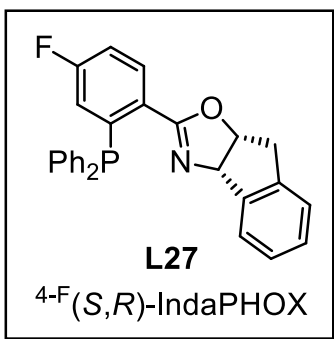
The reaction was run on a 3.60 mmol scale using (1*S*,2*R*)-1-amino-2,3-dihydro-1*H*-inden-2-ol as the oxazoline substrate. Pure *n*-pentane was used for making the silica slurry. The column was initially run in pure *n*-pentane before gradually transitioning to 5% ethyl acetate in toluene (**R**$_f$ = 0.39). The product **(L27)** was obtained as a white solid (286 mg, 18% yield). **¹H NMR** (400 MHz, CDCl₃) δ 7.96 (bs, 1H), 7.33 – 7.17 (m, 13H), 7.12 (t, *J* = 6.8 Hz, 1H), 7.00 (td, *J* = 8.2, 2.6 Hz, 1H), 6.50 (dt, *J* = 9.8, 3.0 Hz, 1H), 5.54 (d, *J* = 7.9 Hz, 1H), 5.20 (t, *J* = 7.4 Hz, 1H), 3.30 (dd, *J* = 18.0,

6.9 Hz, 1H), 3.05 (d, J = 17.9 Hz, 1H). **¹⁹F NMR** (376 MHz, CDCl₃) δ -109.7. **³¹P**

NMR (162 MHz, CDCl₃) δ -4.3.

Procedure for the reduction of PHOX oxides:
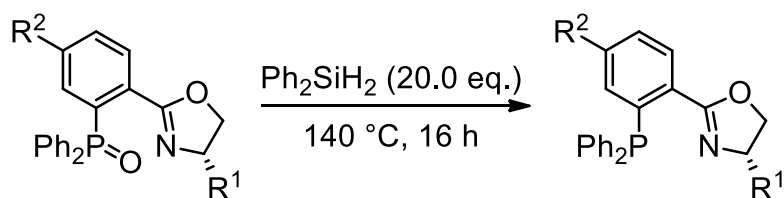
Some PHOX ligands were prone to oxidation and were isolated as the phosphinoxide. Fortunately, these phosphinoxides could be cleanly converted to the desired P(III) PHOX compounds by reduction with diphenylsilane following a procedure adapted from the literature[58]. An oil bath was preheated to 140 °C. An oven-dried Schlenk bomb was charged with a magnetic stir bar and the PHOX-oxide starting material and connected to the Schlenk line. The atmosphere was replaced with nitrogen. Diphenylsilane (20.0 eq.) was added to the reaction under nitrogen efflux. The reaction was sealed off from the Schlenk line before it was lowered into the oil bath. Two blast shields were placed on either side of the oil bath to protect the user and the Schlenk line from a potential explosion due to pressure buildup. After 16 hours of stirring at 140 °C, the reaction was lifted off the hot oil bath and allowed to cool to room temperature. The crude reaction mixture was loaded directly onto a silica column for purification by flash chromatography.

L24
(*S*)-Bn-PHOX

The reaction was run on a 0.269 mmol scale using **L24=O** as the PHOX-oxide substrate. Pure *n*-pentane was used for making the silica slurry. The column was initially run in pure *n*-pentane be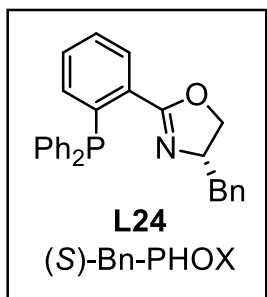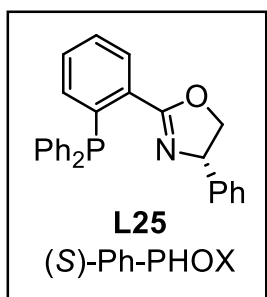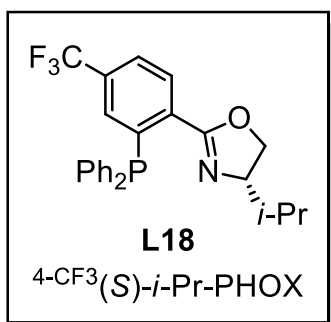fore gradually transitioning to 15% ethyl acetate in *n*-pentane (**R$_f$** = 0.27). The product **(L24)** was obtained as a colorless oil (96.1 mg, 85% yield). **^{1}H NMR** (400 MHz, CDCl$_3$) δ 7.91 (ddd, *J* = 7.6, 3.5, 1.6 Hz, 1H), 7.68 (d, *J* = 7.7 Hz, 1H), 7.45 – 7.36 (m, 11H), 7.29 (t, *J* = 7.3 Hz, 2H), 7.22 (t, *J* = 7.3 Hz, 1H), 7.11 (d, *J* = 7.0 Hz, 2H), 6.92 (ddd, *J* = 7.7, 4.4, 1.5 Hz, 1H), 4.38 (tdd, *J* = 9.3, 7.4, 5.0 Hz, 1H), 4.06 (t, *J* = 8.9 Hz, 1H), 3.81 (t, *J* = 7.9 Hz, 1H), 2.97 (dd, *J* = 13.8, 5.0 Hz, 1H), 2.15 (dd, *J* = 13.8, 9.3 Hz, 1H). **^{31}P NMR** (162 MHz, CDCl$_3$) δ -4.6. The product matched previously reported spectra[58].

L25
(*S*)-Ph-PHOX

The reaction was run on a 0.082 mmol scale using **L25=O** as the PHOX-oxide substrate. Pure *n*-pentane was used for making the silica slurry. The column was initially run in pure *n*-pentane before gradually transitioning to 10% ethyl acetate in *n*-pentane (**R$_f$** = 0.21). The product **(L25)** was obtained as a colorless oil (20.5 mg, 62% yield). **^{1}H NMR** (600 MHz, CDCl$_3$) δ 8.09 – 8.00 (m, 1H), 7.69 – 7.63 (m, 3H), 7.43 – 7.35 (m, 9H), 7.24 (s, 3H), 6.96 (s, 3H),

5.24 (t, J = 9.5 Hz, 1H), 4.58 (t, J = 9.3 Hz, 1H), 3.98 (t, J = 8.5 Hz, 1H). **³¹P NMR**

(243 MHz, CDCl₃) δ -5.3. The product matched previously reported spectra[58].

F₃C
Ph₂P
O
N
i-Pr
L18
4-CF3(*S*)-*i*-Pr-PHOX

The reaction was run on a 3.60 mmol scale using (1*S*,2*R*)-1-amino-2,3-dihydro-1*H*-inden-2-ol as the oxazoline substrate. Pure *n*-pentane was used for making the silica slurry. The column was initially run in pure *n*-pentane before gradually transitioning to 5%

ethyl acetate in toluene (**R*f*** = 0.39). The product **(L27)** was obtained as a white

solid (286 mg, 18% yield). **¹H NMR** (400 MHz, CDCl₃) δ 8.16 (bdd, J = 7.8, 3.1 Hz,

1H), 7.63 (d, J = 8.6 Hz, 1H), 7.39 – 7.26 (m, 11H), 7.11 (s, 1H), 4.24 (bs, 1H), 3.96

(bs, 2H), 1.59 (bs, 1H), 0.85 (d, J = 6.7 Hz, 3H), 0.74 (d, J = 6.8 Hz, 3H). **¹⁹F NMR**

(376 MHz, CDCl₃) δ -64.6. **³¹P NMR** (162 MHz, CDCl₃) δ -4.3. The product matched

previously reported spectra[76].

4.8   References

(1)   Mann, J. B.; Meek, T. L.; Knight, E. T.; Capitani, J. F.; Allen, L. C. Configuration Energies of the D-Block Elements. *J. Am. Chem. Soc.* **2000**, *122* (21), 5132–5137. https://doi.org/10.1021/ja9928677.

(2)   Tasker, S. Z.; Standley, E. A.; Jamison, T. F. Recent Advances in Homogeneous Nickel Catalysis. *Nature* **2014**, *509* (7500), 299–309. https://doi.org/10.1038/nature13274.

(3)   Batsanov, S. S. Van Der Waals Radii of Elements. *Inorg. Mater.* **2001**, *37*, 871–885.

(4)   Chen, P. H.; Billett, B. A.; Tsukamoto, T.; Dong, G. Cut and Sew Transformations via Transition-Metal-Catalyzed Carbon-Carbon Bond Activation. *ACS Catal.* **2017**, *7* (2), 1340–1360. https://doi.org/10.1021/acscatal.6b03210.

(5)   Zhao, T. T.; Xu, W. H.; Zheng, Z. J.; Xu, P. F.; Wei, H. Directed Decarbonylation of Unstrained Aryl Ketones via Nickel-Catalyzed C - C Bond Cleavage. *J. Am. Chem. Soc.* **2018**, *140* (2), 586–589. https://doi.org/10.1021/jacs.7b11591.

(6)   Morioka, T.; Nishizawa, A.; Furukawa, T.; Tobisu, M.; Chatani, N. Nickel-Mediated Decarbonylation of Simple Unstrained Ketones through the Cleavage of Carbon-Carbon Bonds. *J. Am. Chem. Soc.* **2017**, *139* (4), 1416–1419. https://doi.org/10.1021/jacs.6b12293.

(7)   Jiang, C.; Lu, H.; Xu, W. H.; Wu, J.; Yu, T. Y.; Xu, P. F.; Wei, H. Ni-Catalyzed 1,2-Acyl Migration Reactions Triggered by C-C Bond Activation of Ketones. *ACS Catal.* **2020**, *10* (3), 1947–1953. https://doi.org/10.1021/acscatal.9b04112.

(8)   Nakai, K.; Kurahashi, T.; Matsubara, S. Nickel-Catalyzed Cycloaddition of o -Arylcarboxybenzonitriles and Alkynes via Cleavage of Two Carbon - Carbon σ Bonds. *J. Am. Chem. Soc.* **2011**, *133* (29), 11066–11068. https://doi.org/10.1021/ja203829j.

(9)   Saya, L.; Fernández, I.; López, F.; Mascareñas, J. L. Nickel-Catalyzed Intramolecular [3 + 2 + 2] Cycloadditions of Alkylidenecyclopropanes. A Straightforward Entry to Fused 6,7,5-Tricyclic Systems. *Org. Lett.* **2014**, *16* (19), 5008–5011. https://doi.org/10.1021/ol502288x.

(10)   Saito, S.; Masuda, M.; Komagawa, S. Nickel-Catalyzed Intermolecular [3 + 2 + 2] Cocyclization of Ethyl Cyclopropylideneacetate and Alkynes. *J. Am.*

Chem. Soc. **2004**, *126* (34), 10540–10541.
https://doi.org/10.1021/ja0494306.

(11)   Yao, B.; Li, Y.; Liang, Z.; Zhang, Y. Ni-Catalyzed Intramolecular
Cycloaddition of Methylenecyclopropanes to Alkynes. *Org. Lett.* **2011**, *13*
(4), 640–643. https://doi.org/10.1021/ol1028628.

(12)   Saya, L.; Bhargava, G.; Navarro, M. A.; Gulías, M.; López, F.; Fernández,
I.; Castedo, L.; Mascareñas, J. L. Nickel-Catalyzed [3+2+2] Cycloadditions
between Alkynylidenecyclopropanes and Activated Alkenes. *Angew. Chem.
Int. Ed.* **2010**, *49* (51), 9886–9890. https://doi.org/10.1002/anie.201004438.

(13)   Komagawa, S.; Saito, S. Nickel-Catalyzed Three-Component [3+2+2]
Cocyclization of Ethyl Cyclopropylideneacetate and Alkynes - Selective
Synthesis of Multisubstituted Cycloheptadienes. *Angew. Chem. Int. Ed.*
2006, *45* (15), 2446–2449. https://doi.org/10.1002/anie.200504050.

(14)   Komagawa, S.; Takeuchi, K.; Sotome, I.; Azumaya, I.; Masu, H.; Yamasaki,
R.; Saito, S. Synthesis of Vinylcycloheptadienes by the Nickel-Catalyzed
Three-Component [3 + 2 + 2] Cocyclization. Application to the Synthesis of
Polycyclic Compounds. *J. Org. Chem.* **2009**, *74* (9), 3323–3329.
https://doi.org/10.1021/jo900189g.

(15)   Juliá-Hernández, F.; Ziadi, A.; Nishimura, A.; Martin, R. Nickel-Catalyzed
Chemo-, Regio- and Diastereoselective Bond Formation through Proximal
C◻C Cleavage of Benzocyclobutenones. *Angew. Chem. Int. Ed.* **2015**, *127*
(33), 9673–9677. https://doi.org/10.1002/ange.201503461.

(16)   Auvinet, A. L.; Harrity, J. P. A. A Nickel-Catalyzed Benzannulation Approach
to Aromatic Boronic Esters. *Angew. Chem. Int. Ed.* **2011**, *50* (12), 2769–
2772. https://doi.org/10.1002/anie.201007598.

(17)   Fan, C.; Lv, X. Y.; Xiao, L. J.; Xie, J. H.; Zhou, Q. L. Alkenyl Exchange of
Allylamines via Nickel(0)-Catalyzed C-C Bond Cleavage. *J. Am. Chem.
Soc.* **2019**, *141* (7), 2889–2893. https://doi.org/10.1021/jacs.8b13251.

(18)   Irifune, K.; Yamazaki, K.; Nakamuro, T.; Murakami, M.; Miura, T. Ligand-
Controlled Regiodivergence in Nickel-Catalyzed Vinylcyclopropane
Rearrangement. *Angew. Chem. Int. Ed.* **2023**, *62* (33).
https://doi.org/10.1002/anie.202307826.

(19)   Tombe, R.; Kurahashi, T.; Matsubara, S. Nickel-Catalyzed Cycloaddition of
Vinylcyclopropanes to Imines. *Org. Lett.* **2013**, *15* (8), 1791–1793.
https://doi.org/10.1021/ol4005068.

(20)   Bowman, R. K.; Johnson, J. S. Nickel-Catalyzed Rearrangement of 1-Acyl-2-Vinylcyclopropanes. A Mild Synthesis of Substituted Dihydrofurans. *Org. Lett.* **2006**, *8* (4), 573–576. https://doi.org/10.1021/ol052700k.

(21)   Ogoshi, S.; Nagata, M.; Kurosawa, H. Formation of Nickeladihydropyran by Oxidative Addition of Cyclopropyl Ketone. Key Intermediate in Nickel-Catalyzed Cycloaddition. *J. Am. Chem. Soc.* **2006**, *128* (16), 5350–5351. https://doi.org/10.1021/ja060220y.

(22)   Gilbert, M. M.; Trenerry, M. J.; Longley, V. R.; Castro, A. J.; Berry, J. F.; Weix, D. J. Ligand-Metal Cooperation Enables Net Ring-Opening C-C Activation/Difunctionalization of Cyclopropyl Ketones. *ACS Catal.* **2023**, *13* (17), 11277–11290. https://doi.org/10.1021/acscatal.3c02643.

(23)   Liu, L.; Montgomery, J. Dimerization of Cyclopropyl Ketones and Crossed Reactions of Cyclopropyl Ketones with Enones as an Entry to Five-Membered Rings. *J. Am. Chem. Soc.* **2006**, *128* (16), 5348–5349. https://doi.org/10.1021/ja0602187.

(24)   Sumida, Y.; Yorimitsu, H.; Oshima, K. Nickel-Catalyzed Borylation of Aryl Cyclopropyl Ketones with Bis(Pinacolato)Diboron to Synthesize 4-Oxoalkylboronates. *J. Org. Chem.* **2009**, *74* (8), 3196–3198. https://doi.org/10.1021/jo900071m.

(25)   Yuan, B.; Ding, D.; Wang, C. Nickel-Catalyzed Regioselective Reductive Ring Opening of Aryl Cyclopropyl Ketones with Alkyl Bromides. *ACS Catal.* **2022**, *12* (8), 4261–4267. https://doi.org/10.1021/acscatal.2c00677.

(26)   Wang, Z. Y.; Liu, S. Z.; Guo, C.; Cheng, Y. Z.; Li, Q.; Dou, J.; Li, D. Nickel-Catalyzed γ-Alkylation of Cyclopropyl Ketones with Unactivated Primary Alkyl Chlorides: Balancing Reactivity and Selectivity via Halide Exchange. *RSC Adv.* **2024**, *14* (18), 12883–12887. https://doi.org/10.1039/d4ra02616k.

(27)   Tamaki, T.; Ohashi, M.; Ogoshi, S. [3+2] Cycloaddition Reaction of Cyclopropyl Ketones with Alkynes Catalyzed by Nickel/Dimethylaluminum Chloride. *Angew. Chem. Int. Ed.* **2011**, *50* (50), 12067–12070. https://doi.org/10.1002/anie.201106174.

(28)   Liu, L.; Montgomery, J. [3+2] Cycloaddition Reactions of Cyclopropyl Imines with Enones. *Org. Lett.* **2007**, *9* (20), 3885–3887. https://doi.org/10.1021/ol071376l.

(29)   Sumida, Y.; Hayashi, S.; Hirano, K.; Yorimitsu, H.; Oshima, K. Nickel-Catalyzed Allylation of Allyl Carbonates with Homoallyl Alcohols via Retro-

Allylation Providing 1,5-Hexadienes. *Org. Lett.* **2008**, *10* (8), 1629–1632. https://doi.org/10.1021/ol800335v.

(30) Fang, X.; Yu, P.; Morandi, B. Catalytic Reversible Alkene-Nitrile Interconversion through Controllable Transfer Hydrocyanation. *Science* **2016**, *351* (6275), 832–836.

(31) Reisenbauer, J. C.; Finkelstein, P.; Ebert, M. O.; Morandi, B. Mechanistic Investigation of the Nickel-Catalyzed Transfer Hydrocyanation of Alkynes. *ACS Catal.* **2023**, *13* (17), 11548–11555. https://doi.org/10.1021/acscatal.3c02977.

(32) Nakao, Y. Metal-Mediated C-CN Bond Activation in Organic Synthesis. *Chem. Rev.* **2021**, *121* (1), 327–344. https://doi.org/10.1021/acs.chemrev.0c00301.

(33) Tamaki, T.; Nagata, M.; Ohashi, M.; Ogoshi, S. Synthesis and Reactivity of Six-Membered Oxa-Nickelacycles: A Ring-Opening Reaction of Cyclopropyl Ketones. *Chem. Eur. J.* **2009**, *15* (39), 10083–10091. https://doi.org/10.1002/chem.200900929.

(34) Groutas, W. C.; Jin, Z.; Zhang, H. Cyanotrimethylsilane. In *Encyclopedia of Reagents for Organic Synthesis*; John Wiley & Sons, Ltd, 2011. https://doi.org/10.1002/047084289x.rc276.pub2.

(35) Liu, J.; Liu, X. P.; Wu, H.; Wei, Y.; Lu, F. D.; Guo, K. R.; Cheng, Y.; Xiao, W. J. Visible-Light-Induced Triple Catalysis for a Ring-Opening Cyanation of Cyclopropyl Ketones. *Chem. Commun.* **2020**, *56* (77), 11508–11511. https://doi.org/10.1039/d0cc05167e.

(36) Chen, H.; Sun, S.; Liu, Y. A.; Liao, X. Nickel-Catalyzed Cyanation of Aryl Halides and Hydrocyanation of Alkynes via C-CN Bond Cleavage and Cyano Transfer. *ACS Catal.* **2020**, *10* (2), 1397–1405. https://doi.org/10.1021/acscatal.9b04586.

(37) Takise, R.; Itami, K.; Yamaguchi, J. Cyanation of Phenol Derivatives with Aminoacetonitriles by Nickel Catalysis. *Org. Lett.* **2016**, *18* (17), 4428–4431. https://doi.org/10.1021/acs.orglett.6b02265.

(38) Mills, L. R.; Graham, J. M.; Patel, P.; Rousseaux, S. A. L. Ni-Catalyzed Reductive Cyanation of Aryl Halides and Phenol Derivatives via Transnitrilation. *J. Am. Chem. Soc.* **2019**, *141* (49), 19257–19262. https://doi.org/10.1021/jacs.9b11208.

(39)   Ueda, Y.; Tsujimoto, N.; Yurino, T.; Tsurugi, H.; Mashima, K. Nickel-Catalyzed Cyanation of Aryl Halides and Triflates Using Acetonitrile: Via C-CN Bond Cleavage Assisted by 1,4-Bis(Trimethylsilyl)-2,3,5,6-Tetramethyl-1,4-Dihydropyrazine. *Chem. Sci.* **2019**, *10* (4), 994–999. https://doi.org/10.1039/c8sc04437f.

(40)   Yu, P.; Morandi, B. Nickel-Catalyzed Cyanation of Aryl Chlorides and Triflates Using Butyronitrile: Merging Retro-hydrocyanation with Cross-Coupling. *Angew. Chem. Int. Ed.* **2017**, *129* (49), 15899–15903. https://doi.org/10.1002/ange.201707517.

(41)   Tolman, C. A.; Seidel, W. C.; Druliner, J. D.; Domaille, P. J. Catalytic Hydrocyanation of Olefins by Nickel(0) Phosphite Complexes - Effects of Lewis Acids. *Organometallics* **1984**, *3* (1), 2350.

(42)   Bini, L.; Müller, C.; Vogt, D. Ligand Development in the Ni-Catalyzed Hydrocyanation of Alkenes. *Chem. Commun.* **2010**, *46* (44), 8325–8334. https://doi.org/10.1039/c0cc01452d.

(43)   Lachaize, S.; Gallegos, D. C.; Antonio, J. J.; Atesin, A. C.; Ateşin, T. A.; Jones, W. D. Ortho-Fluoro Effect on the C-C Bond Activation of Benzonitrile Using Zerovalent Nickel. *Organometallics* **2023**, *42* (15), 2134–2147. https://doi.org/10.1021/acs.organomet.3c00275.

(44)   Jones, W. D. Reversible Cleavage of Carbon-Carbon Bonds in Benzonitrile Using Nickel(0). *Organometallics* **2000**, *19* (26), 5544–5545. https://doi.org/10.1021/om0008474.

(45)   Gao, H.; Hu, L.; Hu, Y.; Lv, X.; Wu, Y. B.; Lu, G. Origins of Lewis Acid Acceleration in Nickel-Catalysed C-H, C-C and C-O Bond Cleavage. *Catal. Sci. Technol.* **2021**, *11* (13), 4417–4428. https://doi.org/10.1039/d1cy00660f.

(46)   Ren, H.; Du, G. F.; Zhu, B.; Yang, G. C.; Yao, L. S.; Guan, W.; Su, Z. M. Theoretical Mechanistic Study of Nickel(0)/Lewis Acid Catalyzed Polyfluoroarylcyanation of Alkynes: Origin of Selectivity for C-CN Bond Activation. *Organometallics* **2018**, *37* (15), 2591–2601. https://doi.org/10.1021/acs.organomet.8b00338.

(47)   Garcia, J. J.; Brunkan, N. M.; Jones, W. D. Cleavage of Carbon-Carbon Bonds in Aromatic Nitriles Using Nickel(0). *J. Am. Chem. Soc.* **2002**, *124* (32), 9547–9555. https://doi.org/10.1021/ja0204933.

(48) Marco Foà; Luigi Cassar. Oxidative Addition of Aryl Halides to Tris(Triphenylphosphine)Nickel(0). *J. Chem. Soc., Dalton Trans.* **1975**, No. 23, 2572–2576.

(49) Bajo, S.; Laidlaw, G.; Kennedy, A. R.; Sproules, S.; Nelson, D. J. Oxidative Addition of Aryl Electrophiles to a Prototypical Nickel(0) Complex: Mechanism and Structure/Reactivity Relationships. *Organometallics* **2017**, *36* (8), 1662–1672. https://doi.org/10.1021/acs.organomet.7b00208.

(50) Ting, S. I.; Williams, W. L.; Doyle, A. G. Oxidative Addition of Aryl Halides to a Ni(I)-Bipyridine Complex. *J. Am. Chem. Soc.* **2022**, *144* (12), 5575–5582. https://doi.org/10.1021/jacs.2c00462.

(51) Yang, T. P.; Li, Q.; Lin, J. H.; Xiao, J. C. Boron-Trihalide-Promoted Regioselective Ring-Opening Reactions of Gem-Difluorocyclopropyl Ketones. *Chem. Commun.* **2014**, *50* (9), 1077–1079. https://doi.org/10.1039/c3cc47879c.

(52) Dolbier, W. R.; Cornett, E.; Martinez, H.; Xu, W. Friedel-Crafts Reactions of 2,2-Difluorocyclopropanecarbonyl Chloride: Unexpected Ring-Opening Chemistry. *J. Org. Chem.* **2011**, *76* (9), 3450–3456. https://doi.org/10.1021/jo200423y.

(53) Holmberg-Douglas, N.; Nicewicz, D. A. Photoredox-Catalyzed C–H Functionalization Reactions. *Chem. Rev.* **2022**, *122* (2), 1925–2016. https://doi.org/10.1021/acs.chemrev.1c00311.

(54) Bae, J.; Cho, E. J. P,N Ligand in Ni-Catalyzed Cross-Coupling Reactions: A Promising Tool for π-Functionalization. *ACS Catal.* **2023**, *13* (20), 13540–13560. https://doi.org/10.1021/acscatal.3c03851.

(55) Zhang, J. Q.; Yang, S.; Han, L. B. Facial Conversion of Secondary Phosphine Oxides R1R2P(O)H to Chlorophosphines R1R2PCl by Acetyl Chloride. *Tetrahedron Lett.* **2020**, *61* (10). https://doi.org/10.1016/j.tetlet.2019.151556.

(56) Li, H.; Cheng, L.; Li, G.; Xu, T.; Zhang, S.; Zeng, F. Copper-Catalyzed Asymmetric Boroprotonation of Phosphinylallenes. *Org. Lett.* **2023**, *25* (3), 488–493. https://doi.org/10.1021/acs.orglett.2c04180.

(57) Tani, K.; Behenna, D. C.; McFadden, R. M.; Stoltz, B. M. A Facile and Modular Synthesis of Phosphinooxazoline Ligands. *Org. Lett.* **2007**, *9* (13), 2529–2531. https://doi.org/10.1021/ol070884s.

(58) Koch, G.; Lloyd-Jones, G. C.; Loiseleur, O.; Pfaltz, A.; Prctgt, R.; Schaffner, S.; Schnider, P.; Von Matt, P. Synthesis of Chiral (Phosphinoaryl) Oxazolines, a Versatile Class of Ligands for Asymmetric Catalysis. *Recl. Trav. Chim. Pays-Bas* **1995**, *114*, 206–210.

(59) Fuchter, M. J.; Levy, J. N. One-Pot Formation of Allylic Chlorides from Carbonyl Derivatives. *Org. Lett.* **2008**, *10* (21), 4919–4922. https://doi.org/10.1021/ol802026u.

(60) Frigerio, M.; Santagostino, M.; Sputore, S. A User-Friendly Entry to 2-Iodoxybenzoic Acid (IBX). *J. Org. Chem.* **1999**, *64* (12), 4537–4538. https://doi.org/10.1021/jo9824596.

(61) Gualandi, A.; Mazzarella, D.; Ortega-Martínez, A.; Mengozzi, L.; Calcinelli, F.; Matteucci, E.; Monti, F.; Armaroli, N.; Sambri, L.; Cozzi, P. G. Photocatalytic Radical Alkylation of Electrophilic Olefins by Benzylic and Alkylic Zinc-Sulfinates. *ACS Catal.* **2017**, *7* (8), 5357–5362. https://doi.org/10.1021/acscatal.7b01669.

(62) Wu, D.; O'Shea, D. F. Synthesis and Properties of BF2-3,3′-Dimethyldiarylazadipyrromethene near-Infrared Fluorophores. *Org. Lett.* **2013**, *15* (13), 3392–3395. https://doi.org/10.1021/ol401434c.

(63) Amador, A. G.; Sherbrook, E. M.; Yoon, T. P. Enantioselective Photocatalytic [3 + 2] Cycloadditions of Aryl Cyclopropyl Ketones. *J. Am. Chem. Soc.* **2016**, *138* (14), 4722–4725. https://doi.org/10.1021/jacs.6b01728.

(64) Xu, J.; Samsuri, N. B.; Duong, H. A. Nickel-Catalysed Cyclopropanation of Electron-Deficient Alkenes with Diiodomethane and Diethylzinc. *Chem. Commun.* **2016**, *52* (16), 3372–3375. https://doi.org/10.1039/c5cc10296k.

(65) Garapati, V. K. R.; Gravel, M. Oxazolium Salts as Organocatalysts for the Umpolung of Aldehydes. *Org. Lett.* **2018**, *20* (20), 6372–6375. https://doi.org/10.1021/acs.orglett.8b02636.

(66) Zhou, Y.; Uyeda, C. Reductive Cyclopropanations Catalyzed by Dinuclear Nickel Complexes. *Angew. Chem. Int. Ed.* **2016**, *128* (9), 3223–3227. https://doi.org/10.1002/ange.201511271.

(67) Ren, R.; Wu, Z.; Xu, Y.; Zhu, C. C−C Bond-Forming Strategy by Manganese-Catalyzed Oxidative Ring-Opening Cyanation and Ethynylation of Cyclobutanol Derivatives. *Angew. Chem. Int. Ed.* **2016**, *128* (8), 2916–2919. https://doi.org/10.1002/ange.201510973.

(68)   Gaspar, B.; Carreira, E. M. Mild Cobalt-Catalyzed Hydrocyanation of Olefins with Tosyl Cyanide. *Angew. Chem. Int. Ed.* **2007**, *46* (24), 4519–4522. https://doi.org/10.1002/anie.200700575.

(69)   Ren, R.; Wu, Z.; Xu, Y.; Zhu, C. C−C Bond-Forming Strategy by Manganese-Catalyzed Oxidative Ring-Opening Cyanation and Ethynylation of Cyclobutanol Derivatives. *Angew. Chem. Int. Ed.* **2016**, *128* (8), 2916–2919. https://doi.org/10.1002/ange.201510973.

(70)   Gilissen, P. J.; Blanco-Ania, D.; Rutjes, F. P. J. T. Oxidation of Secondary Methyl Ethers to Ketones. *J. Org. Chem.* **2017**, *82* (13), 6671–6679. https://doi.org/10.1021/acs.joc.7b00632.

(71)   Zhao, Y. L.; Wu, G. J.; Li, Y.; Gao, L. X.; Han, F. S. [NiCl 2(Dppp)]-Catalyzed Cross-Coupling of Aryl Halides with Dialkyl Phosphite, Diphenylphosphine Oxide, and Diphenylphosphine. *Chem. Eur. J.* **2012**, *18* (31), 9622–9627. https://doi.org/10.1002/chem.201103723.

(72)   Constantine, R. N.; Kim, N.; Bunt, R. C. Hammett Studies of Enantiocontrol by PHOX Ligands in Pd-Catalyzed Allylic Substitution Reactions. *Org. Lett.* **2003**, *5* (13), 2279–2282. https://doi.org/10.1021/ol034610q.

(73)   Constantine, R. N.; Kim, N.; Bunt, R. C. Hammett Studies of Enantiocontrol by PHOX Ligands in Pd-Catalyzed Allylic Substitution Reactions. *Org. Lett.* **2003**, *5* (13), 2279–2282. https://doi.org/10.1021/ol034610q.

(74)   Soleymani Movahed, F.; Foo, S. W.; Mori, S.; Ogawa, S.; Saito, S. Phosphorus-Based Organocatalysis for the Dehydrative Cyclization of N-(2-Hydroxyethyl)Amides into 2-Oxazolines. *J. Org. Chem.* **2022**, *87* (1), 243–257. https://doi.org/10.1021/acs.joc.1c02318.

(75)   Deng, H.; Wang, J.; He, W.; Ye, Y.; Bai, R.; Zhang, X.; Ye, X. Y.; Xie, T.; Hui, Z. Microwave-Assisted Rapid Synthesis of Chiral Oxazolines. *Org. Biomol. Chem.* **2023**, *21* (11), 2312–2319. https://doi.org/10.1039/d2ob02192g.

(76)   Armstrong, P. B.; Dembicer, E. A.; Desbois, A. J.; Fitzgerald, J. T.; Gehrmann, J. K.; Nelson, N. C.; Noble, A. L.; Bunt, R. C. Investigation of the Electronic Origin of Asymmetric Induction in Palladium-Catalyzed Allylic Substitutions with Phosphinooxazoline (PHOX) Ligands by Hammett and Swain-Lupton Analysis of the 13C NMR Chemical Shifts of the (π-Allyl)Palladium Intermediates. *Organometallics* **2012**, *31* (19), 6933–6946. https://doi.org/10.1021/om3007163.